Helsinki University of Technology Control Engineering Laboratory

Espoo 2005 Report 146

MODELLING AND CONTROL OF PRINTING PAPER SURFACE WINDING

Jari Paanasalo

TEKNILLINEN KORKEAKOULU
TEKNISKA HÖGSKOLAN
HELSINKI UNIVERSITY OF TECHNOLOGY
TECHNISCHE UNIVERSITÄT HELSINKI
UNIVERSITE DE TECHNOLOGIE D´HELSINKI

Helsinki University of Technology Control Engineering Laboratory

Espoo June 2005 Report 146

MODELLING AND CONTROL OF PRINTING PAPER SURFACE WINDING

Jari Paanasalo

Dissertation for the degree of Doctor of Science in Technology to be presented with due permission of the Department of Automation and Systems Technology, for public examination and debate in Auditorium AS1 at Helsinki University of Technology (Espoo, Finland) on the 19th of August, 2005, at 12 noon.

Helsinki University of Technology

Department of Automation and Systems Technology

Control Engineering Laboratory

Distribution:
Helsinki University of Technology
Control Engineering Laboratory
P.O. Box 5500
FIN-02015 HUT, Finland
Tel. +358-9-451 5201
Fax. +358-9-451 5208
E-mail: control.engineering@hut.fi
http://www.control.hut.fi/

ISBN 951-22-7749-2 (printed)
ISBN 951-22-7750-6 (pdf)
ISSN 0356-0872

Cover photo courtesy of Metso Paper, Inc.

Picaset Oy
Helsinki 2005

Available on net at http://lib.tkk.fi/Diss/2005/isbn9512277506

HELSINKI UNIVERSITY OF TECHNOLOGY P.O. BOX 1000, FI-02015 TKK http://www.tkk.fi	ABSTRACT OF DOCTORAL DISSERTATION

Author Jari Paanasalo

Name of the dissertation

MODELLING AND CONTROL OF PRINTING PAPER SURFACE WINDING

Date of manuscript June 7, 2005	Date of the dissertation August 19, 2005
☑ Monograph	☐ Article dissertation (summary + original articles)

Department	Automation and Systems Technology
Laboratory	Control Engineering Laboratory
Field of research	Control Engineering
Opponent(s)	Professor Pentti Lautala, Professor Raimo von Hertzen
Supervisor	Professor Heikki Koivo, AS-74
(Instructor)	Dr. Kai Zenger, AS-74

Abstract

Feasibility and construction of closed loop winding tightness controller was studied. Both basic PI-controller and LQR state feedback controller were applied. The controllers were tuned and tested in winding simulations and in pilot winder trial runs. The chosen feedback variable was the web thickness or strain in the roll radial direction measured by means of the density measurement. The controller output was the Wound On Tension, which was converted to the winder control variables, nip load, web tension and winding force, by means of the inverted nip model. The nip model was constructed as the experimental response surface model. The nip model data was measured in the pilot winder with several different winder reference values and web speeds and the response surface model was fitted to the data by means of the least squares method. The experimental nip model was inverted and used as a component in winding control and simulation. Two theoretical nip models were reviewed and compared to the experimental nip model. The density measurement was implemented with a novel algorithm based on the time varying least squares method. The Wound On Tension measurement was done by means of the indirect method, which uses the roll deformation data from the density measurement and the wound roll stress model. The method was improved compared to the earlier implementations by using the large deformations total stress version of the wound roll model augmented with the viscoelastic material model and the centrifugal forces. A new method for indirect web calliper measurement was introduced based on the roll model and radial deformation data. The various versions of the wound roll stress models were implemented and their results compared. The total stress version was found to be suited for the Wound On Tension measurement from the radial deformation measurement data. The algorithms were tested with pilot winder trial runs with two printing paper grades, the LWC paper and the Newsprint paper. The computed radial pressures were verified with the direct pressure measurements.

Keywords winding, paper, roll, tightness, calliper, control, tension, stress

Number of pages	159	ISBN (printed)	951-22-7749-2
ISBN (pdf)	951-22-7750-6	ISBN (others)	
ISSN (printed)	0356-0872	ISSN (pdf)	

Publisher Helsinki University of Technology, Control Engineering Laboratory

Print distribution Helsinki University of Technology, Control Engineering Laboratory

☑ The dissertation can be read at http://lib.tkk.fi/Diss/

PREFACE

My work was inspired by the David Roisum's 1989 thesis "The Measurement of Web Stresses during Roll Winding". The last sentence of Roisum's preface called "I sincerely hope that this work will be extended by others to include alternative methods of caliper and radii measurement, new winding models and most importantly, application of the closed loop control of the winding process."

On my behalf I hope that I succeeded to reach the objectives David Roisum had in his mind when writing those words. During my 20 years career in Metso Paper, Inc. (former Wärtsilä and Valmet) all the winders built in the Järvenpää factory have been equipped with the density measurement system. I had always been intrigued to know how well the density analyser was able to detect the small variations in the wound roll tightness and what limitations it had. The final push to fulfil this work was given by my colleaque Marko Jorkama, who himself finished his thesis on nip modelling in 2001. The practical and material conditions to carry out the research work were finally provided when the new Metso Paper Winding Technology Centre was started in Järvenpää in April, 2002. The work has been fully financed by Metso Paper.

I wish to express my gratitude to all people who assisted me in this work including my thesis advisors Dr. Kai Zenger and professor Heikki Koivo. My colleagues in the Winding Technology Centre, Jarmo Malmi, Jari Pelkonen, Arto Leskinen and Sami Marttinen, were a great help in carrying out the extensive trial program. I wish to specially thank Arto Leskinen, whose great skills in mechanical and electrical instrumentation made possible the special measurements needed. I wish also to thank Marko Jorkama of giving the inspiration to theoretical work and my boss Pauli Koutonen of his patience to let me work on this subject. And the final thanks go to my family, Satu, Minna and Ville, for their support and belief on me.

Järvenpää, May 2005 Jari Paanasalo

SYMBOLS AND ABBREVIATIONS

A Coefficient matrix in state-space representation
a System pole parameter
a_1,a_2,a_3 Stress-strain curve parameters
a_{ij} Response surface model quadratic term coefficients
B Coefficient matrix in state-space representation
b basis weight of the web
bl buffer length of the time varying least squares algorithm
b_i Response surface model linear term coefficients
C Coefficient matrix in state-space representation
C_0,C_1,C_2 Polynomial coefficients for the radial modulus curve
c_0, c_1, c_2 Viscoelastic difference equation coefficients
CD Cross direction = width-wise direction in the roll
D Roll diameter
D Coefficient matrix in state-space representation
DCS Distributed Control System
D_0 Core diameter
dl Density measurement diameter layer
$\delta\sigma_r,\delta\sigma_t$ Incremental radial and circumferential stress
E_C Core elastic modulus
E_r,E_t Radial (z-direction) and tangential (machine direction) elastic moduli
E_{r0},E_{r1} Polynomial coefficients for the Pfeiffer radial modulus curve
E_{t0},E_{t1} Polynomial coefficients for the tangential modulus curve
$\varepsilon_r,\varepsilon_t$ Radial and circumferential strain
$FIFO$ First in – First out buffer
FSR Force sensitive resistor
F_1, F_2, F_3 Two-drum winder nip forces
Φ Least squares regressor matrix
G Coefficient matrix in state-space representation
G Gravitational force
G_{rt} Radial-tangential shear modulus
h Web thickness
h_i,h_0 Web calliper = undeformed thickness under zero pressure
i Layer index in the large deformations model
l Roll width
K Controller gain in state feedback control
K PI controller gain
K_d Roll compliance coefficient
L Web length in the roll
L Observer gain
LQG Linear quadratic Gaussian controller
LQR Linear quadratic regulator
LWC Light weight coated paper
λ Time varying least squares forgetting factor

MD Machine direction = tangential direction in the roll
N Total number of layers in the roll
NIT Nip induced tension
NL Nip loading
n Time index
nm nanometers = 10^{-9} meters
ν_{rt}, ν_{tr} Poisson ratios
ω angular speed of the roll
PI Proportional-Integral controller
PID Proportional-Integral-Derivative controller
PLC Programmable logic controller
P Recursive least squares "covariance" matrix
q LQ control tuning parameter
Q LQ control state variable weight matrix
R Roll outer radius
R LQ control input variable weight matrix
R_0 Core outer radius
r_0 Layer radius at the imaginary unstressed state in the roll
r_{out} Roll outer diameter during the winding
r Radial position inside the roll
ρ Density of the web in the roll
S Web speed
SC Supercalendered paper
S_r, S_t Radial (z-direction) and tangential (machine direction) stress-strain functions
ST Surface traction
s_e Least squares error variance
s_θ Least squares estimate variance
σ_r, σ_t Radial and circumferential stress
T Web tension
T_i PI controller integration time
θ Least squares parameter vector
u Radial displacement
u_k Linear system input vector at time k
um micrometers = 10^{-6} meters
v Web speed
v_k Linear system measurement noise vector at time k
WF Winding force
w_k Linear system process noise vector at time k
WOT Wound On Tension
x_k Linear system state vector at time k
Y Least squares response matrix
y_k Linear system output vector at time k
z z-direction = radial direction in the roll
z z-transform variable

CONTENTS

1 INTRODUCTION

1.1 Scope and goal

Is closed loop winding tightness control possible? And if it is, is it feasible in the paper mill production environment? What would be the controlled process variable and how it would be measured? What kind of controller would be sufficient to close the control loop, and what are the requirements for good winding control?

The web winding unit operation has not been usually recognized as a process in the same meaning as the complex chemical and physical reactions occurring in the paper machine wet end or the drying process in the huge paper machine drying section. The winding process has been run blindly with fixed reference values and slow feedback from manual off-line roll tightness measurements. No measured web material properties have been utilized in the winding control design and no winding process models have been used.

The complexity of the winding process prohibits answering all the questions in the winding control and modelling in a single thesis work. This work has been limited rather conventionally in one-dimensional wound roll and nip models and measurements. The roll is modelled and measured with only one space variable, the roll radius. The roll is considered perfectly axisymmetric, all tightness and web thickness variations in the circumferential and cross machine directions are neglected. The limitation is however quite practical, since the out-of-roundness control would require acting several times faster than the roll is rotating, and there is no method to measure on-line the cross machine variations within one roll (Lee and Wickert 2002). The work has also been restricted to the winding of thin printing papers and surface or hybrid winding. The printing paper winding has become more demanding since roll sizes have grown and winder speeds increased to close to 3000 m/min. Two basic printing paper grades were chosen for closer inspection, the Newsprint and LWC paper grades.

More than 300 trial and measurement winding runs were made with the two chosen paper grades to test the models and algorithms. There were 5 test rolls used, about 800 mm wide and 1000-1200 mm in diameter. The pilot winder

was a full size single drum winder. The highest winding speed tested was 2000 m/min. Both a hard steel winding drum and a resilient soft covered winding drum were used in the pilot winder. A material testing device was built for the measuring of the paper material properties. The testing device can do both stack press test and sheet pull test. The device is used to measure the non-linear paper stress-strain curves both in the z-direction and in the machine direction and also the viscoelastic creep and relaxation curves in both directions (Pfeiffer 1996).

The roll internal radial pressures were measured with force sensitive resistors (Fikes 1990). The pressure measurements were not used to derive any computed roll tightness measures like the Wound On Tension, but they served only as a means of cross checking and validation of the roll tightness (Good et al. 1999). The relative accuracy of the force sensitive resistor sensors in the paper winding application can hardly be better than 10% of the reading. The hardness and thickness variations cause large variations at different roll radial locations and also on both sides of the roll, especially with the LWC paper. The sensing area is small, so the sensor measures only a local pressure. The thickness of the sensor causes it to measure force over a larger effective area than the resistor area itself, so a calibration in the stack testing machine is required to correct the readings to megapascals. Also the paper viscoelastic deformation around the sensors causes the calibration to be lost over longer exposure to the roll internal pressure. In any case a large number of sensors must be used in the roll and still only an average roll pressure can be measured at a better accuracy.

The force sensitive resistors can only serve as a replacement for other manual measurements, like the pull tabs or the Cameron test or more exotic ones as the ultrasonic measurement (Pfeiffer 1966). The direct Wound On Tension measurement by means of the WOT measuring roller has been deemed to measure only a fraction of the true Wound On Tension (Pfeiffer 1977), (Good et al. 1999). The pilot winder was equipped with a WOT roller, but it was not used in the trial runs. The reason for this was that the WOT roller did not produce consistent measurements. The direct WOT measurement is in any case not practical in the production environment. The only on-line roll tightness measurement left is the density measurement (Komulainen 1982), (Roisum 1990). The density measurement can measure the web thickness in the roll with enough accuracy and resolution for closed loop control. This is an essential finding in this work. The thickness accuracy is in the range of 10-100 nanometers, 1000 to 10000 more accurate than the roll diameter measurement, which is the basis for the density measurement. The density measurement in this work was implemented with a new time varying least squares based algorithm patented by the author. The new method contains an automatic procedure to update the least squares forgetting factor in order to maintain the accuracy in terms of the thickness confidence limit. The density measurement alone has been demonstrated not to be enough to indicate the roll tightness (Roisum 1990), but the free web calliper is needed to convert it to the z-direction

strain. The pilot winder had no calliper measurement device. This problem was overcome with a novel method of the web calliper indirect measurement based on the wound roll stress model and centre wound thickness data.

The use of thickness or strain as the feedback variable instead of tension means shifting the focus from stresses to deformations. Both have their advantages and weaknesses as roll tightness measures. The strain can be converted to stress by means of the stress strain curve and the wound roll stress model. If the paper elasticity varies, the same strain will produce different amounts of stress. On the other hand the internal roll stresses with the same Wound On Tension depend on the web elasticity. The indirect web thickness measurement by means of the density measurement is in any case the only on-line measurement available.

The closed loop control with the density measurement feedback can be done without any winding models. However, the outcome of surface winding with a winding nip depends on the web tension, nip load, surface traction and the web speed in an unknown manner. The controller design requires knowledge of this dependency. The controller must use the winding parameters in a reasonable way not only to achieve the correct tightness, but at the same time avoid damaging the web or hitting the winder reference value limitations. The nip model was used to close the gap between the controller output and the winder reference values.

There is not many work published on the winding nip model. Two models were reviewed, the simpler OSU model (Good et al. 1999) and the more comprehensive JvH model (Jorkama 2001). The chosen model for further study was however the experimental nip model, the theoretical models were not found to be suitable for control purposes. The experimental nip model that was constructed as a quadratic Response Surface Model, is simple to program and is inverted without difficulty. The use of the inverse nip model for both closed loop control and winding tuning and control scheme planning was demonstrated with simulations and trial runs. The inverse nip model is a new tool for winding tuning, and it is especially efficient in the more complicated winding geometry of the two-rum winder.

The experimental nip model can be constructed on any of the directly measured or derived roll tightness measures. If the directly measured z-direction strain is chosen as the output variable, the model fit to the data can be done without the need to use the wound roll stress model. This would be sufficient also for the control purposes, and then both the controller input and output are web thickness or strain. Other suitable output variables for the inverse nip model are the interlayer stress or the Wound On Tension. These can be derived from the measured radial strain by means of the wound roll stress model (Roisum 1990). The computed radial stress value can then be compared to the stress measured by the force sensitive resistor sensors.

The wound roll stress model was implemented in its original linearized incremental stress version (Hakiel 1987) augmented with the centrifugal forces (Olsen 1996) as well as in the non-linear total stress version (Benson 1995). The

model was also supplemented with the viscoleastic material model (Qualls 1995). The outer boundary condition was selected as either the Hakiel-style "no tension loss" version and as the "tension loss" condition (Good and Pfeiffer 1992). Solution method for the "tension loss" version was improved compared to (Good and Pfeiffer 1992) as no iteration was needed. The different model versions and their predictions were compared. In most cases the viscoelastic stress relaxation was found to be small enough to be neglected. Substantial part of the relaxation has occurred already during winding and the rest relaxes the radial stress about 15-20 % during the next days. Also the "tension loss" outer boundary condition was found to lower the roll stresses only by a few per cent, and can be neglected for the printing papers. The main finding from the model version comparisons was that the linearized incremental stress version is not as accurate in predicting the deformations and the stresses in the deformed roll as the total stress version. This is important in the application where the stresses are computed back from the measured deformations. The use of the more complicated and CPU time consuming total stress model is well justified by the improved accuracy. The preceding work by Roisum (Roisum 1990) used the incremental stress version of the wound roll model. The solution method was also slightly improved compared to this earlier work by noting that no iterative solver is needed in the incremental stress version for the Wound On Tension computation and the same non-linear Newton solver is enough for the total stress version.

The new method of indirect calliper measurement is a modified version of the Wound On Tension computation from the wound roll stress model. The model has $2N$ unknown stresses where N is the number of layers in the model. When either the Wound On Tension or the web calliper is unknown, there are $2N+1$ unknowns and one extra equation is needed to complete the system. This extra equation is the roll radius deformation equation, which links together the measured outer roll radius and the Wound On Tension and the calliper. When the roll is centrewound, the Wound On Tension equals to the known web tension and the calliper can be solved. The pilot winder was equipped with a special reverse winding mode, where the roll was wound backwards to the unwind stand with nipless centre winding.

The nip model data was measured for Newsprint and LWC paper and with both the hard and resilient winding drums. Wide range of nip load, winding force, web tension and web speed values were used and the measurement windings spanned over most of the roll in each run. A reverse run for web calliper measurement preceded each Wound On Tension measurement run. This eliminated the error caused by the bulk loss when the same roll was used over and over again. The extensive nip model data is documented and the experimental models fitted to it. The data is used to compare the hard and resilient winding drums, and the latter was found to produce more Wound On Tension at higher nip loads, a significant effect in two drum winders and large roll diameters. The effect of the web speed on the nip induced tension was found to be small up to 2000 m/min speeds. The data was

compared to the only known earlier published work by Good (Good et al. 1999). Good used the pressure method to compute the Wound On Tension without the density measurement. Even though Roisum (Roisum 1990) was the first to present the Wound On Tension measurement based on the density measurement and the wound roll stress model, he gives only few samples of actual measurement runs. The CPU time demand for a single run could exceed 100 hours with the computers at that time giving a hint why no more measurements were made.

The final goal of the work was reached when a successful winding tightness controller was designed and tuned. The feedback variable was chosen to be the measured thickness or strain and the controller output was the Wound On Tension. The standard linear control technique methods were sufficient when the non-linearity of the winding nip was hidden into the inverted nip model. The controller performance was tested with simulations and trial winding runs.

Two basic controller types were used in the trials, the PI controller and the state feedback regulator. Both were tuned with pole placement and the latter also with the LQG optimal control design. The state feedback regulator was modified to give zero steady state error, which leads to a controller structure equivalent to a PI controller when a simple first order system model is used. Analogously the LQR design can be used to tune the standard PI controller. The controllers were tuned first in the winding simulation system made of the nip model and the wound roll stress model. The tuning parameter values found in simulation were adequate also in real winding trials in most cases. The closed loop winding control trials prove the competence of the inverted nip model in a real control task. The resulting winder reference values behaved smoothly and the thickness error was small. The inverted nip model was also tested in open loop winding trials with predetermined Wound On Tension or radial pressure reference curve.

The closed loop winding control was proved to be possible and even feasible technique in real paper winding. The most important prerequisite is that the web calliper is measured at the winder or at the preceding machine in the paper making line. The presented procedure to measure the nip model is straightforward to accomplish at a laboratory winder.

1.2 Contributions

The contributions of this thesis are listed below:

- Successful winding tightness controller was presented with a few alternative structures and tuning methods. There is no earlier published work on closed loop winding control except that the Beloit Technologies Inc. has the patent of “Closed Loop Control For A Web Winding Machine”, WO 93/15008.

- The inverted nip model was presented as a component for both open and closed loop winding control.

- A new method to implement the density measurement was presented and patented by the author. The method includes a new way of adjusting the forgetting factor of the time varying least squares algorithm. The accuracy of the density measurement was shown to be more than enough for the indirect Wound On Tension measurement and closed loop winding control.

- Substantial amount of nip model data was measured and documented for the Newsprint and LWC paper surface winding.

- A new method to indirectly measure the web calliper by means of the density measurement and the wound roll stress model from centrewound data was presented.

- An improved method to compute the Wound On Tension by means of the wound roll stress model and the density measurement was presented. The method's accuracy was improved by using the total stress version of the wound roll stress model and including the viscoelastic material model and the centrifugal forces in the model.

- A new total stress version of the wound roll stress model was presented and compared to a number of earlier implementations. The version was based on an earlier displacement type realisation, but the unknowns were retained as stresses for the sake of clarity. The viscoelastic material model was included in the total stress model and the creep strain behaviour measured for the paper materials. The total stress model was shown to be superior in accuracy over the incremental stress model especially when the displacements were concerned. The computation time of the total stress model was still reasonable, about one minute for a winding run.

1.3 Basic concepts

The main computational tool used in the work is the wound roll stress model. The elementary form of the wound roll stress model is a simplified one-dimensional description how the input of the model, the Wound On Tension, produces the final radial and tangential stress distributions over the radial direction in the roll, FIGURE 1:

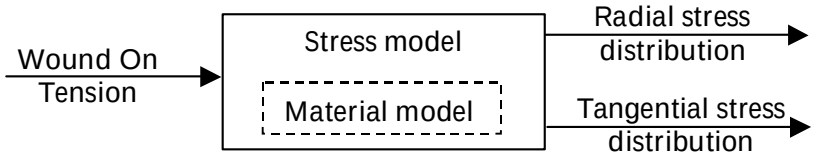

FIGURE 1 Basic wound roll stress model input/output diagram.

The input to the model, the Wound On Tension (sometimes also called as Wound In Tension), is defined as the tension of the outermost web layer of the roll as it enters the roll. The model outputs the radial and tangential stresses for every web layer in the roll. The roll is built up layer by layer and the model is recomputed for every layer added to the roll. The material model is part of the roll model, and it describes the web's elasticity in the radial and tangential directions.

The model can be extended to include the strain or deformation computations, FIGURE 2:

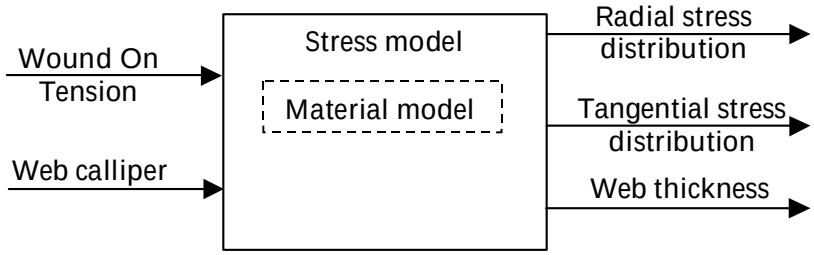

FIGURE 2 Basic roll model extended to strain computations.

The radial stresses and the material model give the radial strain. When the web calliper (the thickness under zero radial stress) is known, the radial strain can be converted to web thickness in the roll. Both the Wound On Tension and the web calliper can vary from layer to layer.

This "normal" form of the wound roll stress model is useful only for simulation purposes. However, it can be inverted so that the output variable web thickness is moved to input and the input variable Wound On Tension is moved to output, FIGURE 3:

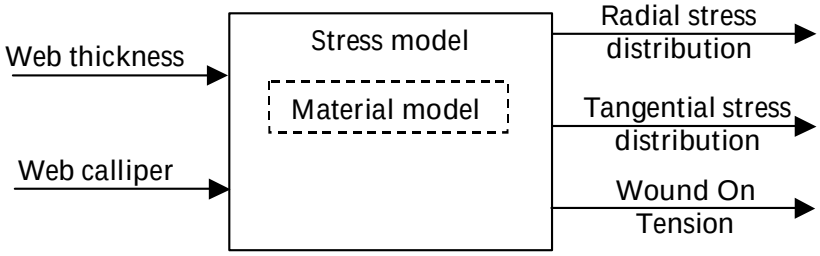

FIGURE 3 The inverted roll model with Wound On Tension as output.

This version of the wound roll model is the real workhorse of this work, which is used to produce all the computed Wound On Tension values presented later.

Yet another form of the roll model exists that outputs the web calliper if the Wound On Tension is known, FIGURE 4:

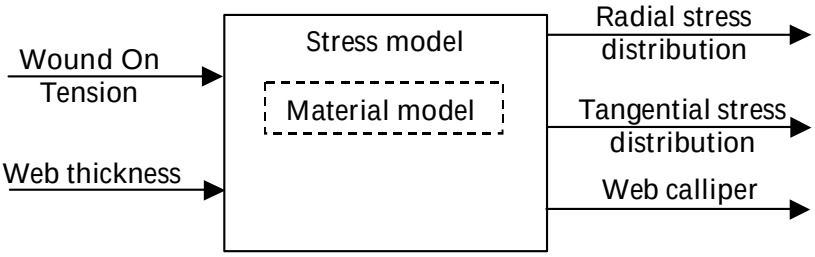

FIGURE 4 The inverted roll model with web calliper as output.

The web calliper indirectly measured with the wound roll stress model was not calibrated to produce same results as the laboratory instruments or TAPPI T-411 standard. It should be noted that the result is the average calliper over the width of the roll, and the radial location of the sample for the laboratory measurement should also be accounted for. However, the calliper measured by means of the roll model is best suited for the Wound On Tension measurement made also by means of the roll model.

The other input to the Wound On Tension indirect measurement in FIGURE 3, the web thickness, was measured by means of the density measurement. The name "density measurement" has become industry and literature standard for the indirect measurement of the web thickness in the roll (Roisum (Roisum 1990) uses the term Density Analyzer meaning the system used for density measurement). The thickness is usually converted to density by means of the assumed basis weight. Real density measurement would require actual measured basis weight to be used. The web thickness is indirectly measured from the measured web length and roll diameter, FIGURE 5:

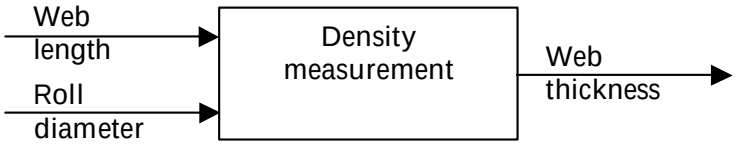

FIGURE 5 The Density measurement input / output diagram.

The basic function of the density measurement is to differentiate and filter the measured roll diameter to give the web thickness. The web length is used to improve the accuracy of the result.

Finally the models and processes in FIGURE 3, FIGURE 4 and FIGURE 5 are combined to the Wound On Tension measurement system in FIGURE 6. This procedure for Wound On Tension measurement eliminates the need for separate instrumentation for web calliper measurement. The method requires two winding runs for each Wound On Tension measurement made: first the web calliper measurement with direct Wound On Tension measurement (with special winding equipment allowing for direct WOT measurement) and then

the actual WOT measurement winding run with the target winding configuration.

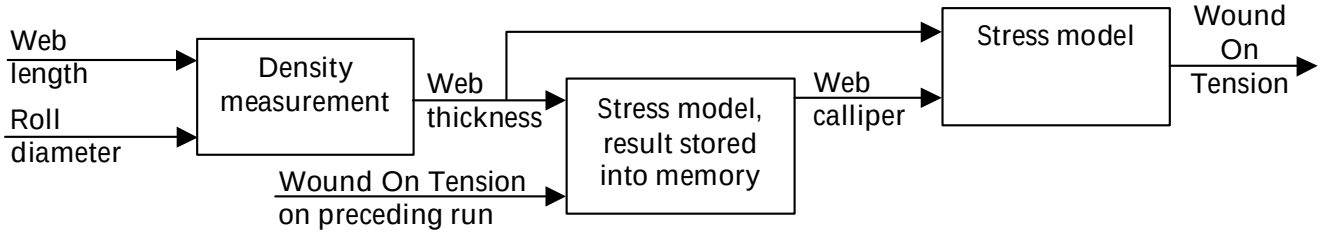

FIGURE 6 Aggregate Wound On Tension measurement system consisting of web thickness, web calliper and Wound On Tension indirect measurements. The direct physical measurements are the web length and roll diameter measurements. The first wound roll stress model outputs the web calliper, which is stored into memory to be used in the subsequent winding run for the Wound On Tension computation. The web calliper measurement winding run requires that the Wound On Tension can be directly measured.

The basic winding configuration and the winding parameters are depicted in FIGURE 7, (Jorkama 2001):

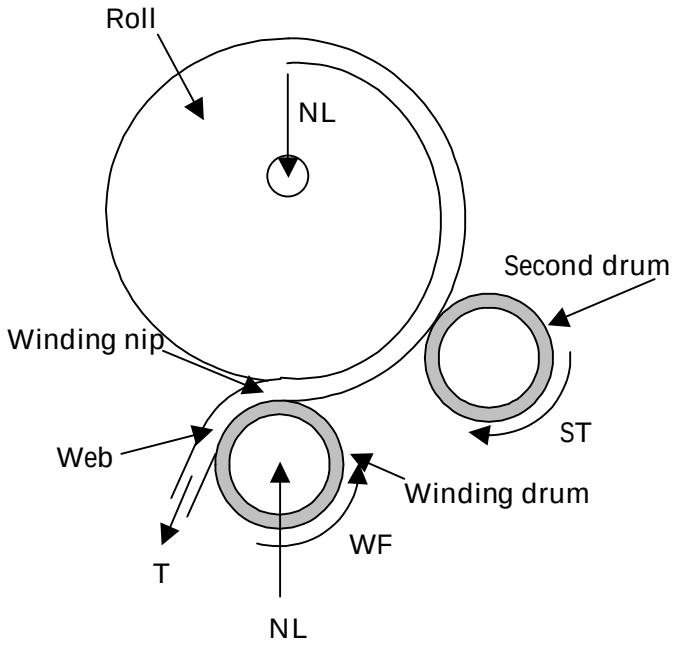

FIGURE 7 Winding configuration and the winding parameters.

The winding parameters are those winder process variables that affect the roll tightness. They include the winding nip load NL, the web tension T and the winding nip surface traction called the Winding Force WF. Sometimes the surface traction ST of the auxiliary drum is used instead of the Winding Force. The connection between them is WF=ST-T if roll inertia forces are neglected. All these variables are measured in SI units as Newtons per meter.

1.4 Outline

Chapter 2 presents various alternative wound roll stress models and justifies why the so-called "total stress" version of the models is most accurate when the web deformations must be accounted for. The differences in the model outcomes are graphically demonstrated. The chapter also describes how the model is inverted for the Wound On Tension and web calliper computations.

Chapter 3 deals with the material models. Several different elastic model structures have been presented earlier in the literature and the chosen model is logarithmic stress to strain curve leading to second order polynomial for the elastic modulus. The model is shown to be fitting well to the experimental data both in Z- and MD-directions for printing papers. The viscoelastic creep is modelled with second order time difference equation, and again the fit is good for printing paper creep test experimental data.

Chapter 4 describes the density measurement. Instead of the conventional differentation and moving average filtering of the roll diameter the measurement is implemented by means of time varying least squares algorithm. The accuracy of the algorithm is estimated and means to reduce the initial transient effect are presented.

Chapter 5 discusses the theoretical winding nip models. Two alternative theoretical nip models are studied, but instead the experimental nip model is chosen for control purposes. Measured Wound On Tension data is presented for Newsprint and LWC paper rolls and the Response Surface Models are fitted to the data. The models are compared to the earlier nip model data and also validated by means of direct Wound On Tension measurement. The viscoelastic effects are shown to be negligible in winding nip modelling.

Chapter 6 presents a new paradigm for winding control by means of the inverted winding nip model. The use of the model is demonstrated with simulation and experimental data examples. The use of the inverted nip model is also discussed in two-drum winding control, where the more complicated winding geometry makes it even more useful winding control tool.

Chapter 7 finally achieves the goal of the closed loop winding control. The feedback variable is the web thickness in the roll as measured by means of the density measurement. The reference value for the controller must account for the inevitable web calliper variations, at least for the LWC paper. The control loop is closed by the inverted nip model, and the controller output is the Wound On Tension driving the inverted nip model.

2 WOUND ROLL STRESS MODELS

The wound roll stress models are a very well known field of the web handling theory. The standard representation is the one dimensional Hakiel model (Blaedel 1974),(Hakiel 1987). In this model the roll stresses are computed in cylindrical coordinates and the stresses are constant in the z (cross machine) and in the θ (the circumferential direction around the roll periphery) so the stresses need to be solved only in the r (roll radius) direction. The model is solved for both the radial and tangential (θ) stresses and strains. The cross machine strains induced by the other strains could also be solved, if the appropriate Poisson ratios would be known (the plane stress assumption Hakiel made actually does not hold for wide paper rolls, which are closer to plane strain condition). This model requires that the Wound On Tension be known, as it is the driving input value for the model. Thus the model can be directly applied only on centre winding, where the WOT is the web tension. The model also neglects circumferential and cross machine material and load variations, which are important in real winding. However, the model is the basis of wound roll stress analysis, and it can be applied to any web material wound onto rolls or to thin concentric cylinders tensioned onto each other or even to a solid cylinder with thick wall and compressed on the outer or inner surface. The Wound On Tension needs not to be constant during winding, but can vary from layer to layer as can the material parameters. The Hakiel version of the wound roll stress model is known as the first "nonlinear" development. Hakiel claimed it to be nonlinear since it used nonlinear radial direction (z direction in the stack) elastic modulus curve instead of a constant elastic modulus. However, in the normal mathematical meaning it still was a linear model, since the basically nonlinear equations (stemming from the nonlinear stress strain curves) were linearized and the numerical solution method was a linear one.

Hakiel itself didn't care to compute the strains and displacements. Neglecting the displacements causes error in the outermost layer hoop stress equation, where the roll radius is not correctly summed up from the compressed web layers. This error is small for the incremental strains but

accumulates for large roll radii. More importantly, the Hakiel version cannot give correct strains and deformations, especially for soft materials like paper, which can compress up to 10 % in a roll. The version introduced by Benson (Benson 1995) is a true nonlinear wound roll stress model, as in his formulation the nonlinear equations were not linearized before numerical solution, but instead nonlinear equation numerical solution method was used. Benson formulation is actually solved in terms of radial displacements and thus strains and the stresses are derived from these by means of the measured stress strain curves. The wound roll model equations can be as easily written with the strains as unknowns as with the stresses as unknowns (Roisum 1990). There exists one early stress formulation by Willet and Poesch (Willet and Poesch 1988), which uses nonlinear radial stress strain curve (polynomial fit) and nonlinear numerical solver. Unfortunately their results are difficult to compare since they do not give numerical values for the stress strain curve used. The Benson formulation was selected as the basis for this work because of its better accuracy in computing the strains, but the stresses were retained as unknowns to maintain more similarity compared with the majority of wound roll model formulations presented during the last 20 years.

The reason why better strain and deformation accuracy is needed is that this work uses the measured radial deformations as input to the wound roll model and the Wound On Tension is got as an output of the model. This is the second known attempt to do such a measurement; Roisum was the first to present it in his thesis (Roisum 1990). Roisum used the Hakiel version of the wound roll model, which gives different results compared to the Benson formulation as is later seen.

The model versions differ also in how they incorporate the Wound On Tension into the equations. The most common way is to show it only in the outer boundary condition, which is the hoop stress equation for the outermost layer in the roll. This is natural in the incremental linearized model, where the other layers Wound On Tensions do not appear and the stresses solved are the increments caused by the last layer. On the other hand it may be confusing, since a more elegant outer boundary condition would be to set the radial pressure at the roll surface to zero. In the Benson formulation the Wound On Tension can be put in the right place into the force equilibrium equation along with the other forces acting on the web layer. Now all layers have their Wound On Tensions visible in the equations and the unknowns are always the total stresses, not the incremental stresses due to adding the last layer to the roll. As well the WOT can be put in the geometrical conditions of the Benson formulation, which leads to slightly different equations but exactly the same solutions. Actually the Hakiel hoop stress outer boundary condition can be stated alternatively as keeping the last layer incremental tangential stress zero, which means that the last layer does not shrink with the roll when it is fit onto the roll. This means a different physical interpretation, which implies that the roll is first compressed to the correct incremental strain by the hoop stress, and

after that the last layer is added to it with perfect fit. This will be elaborated in the subsequent chapter on the so-called "tension loss" model.

The wound roll stress model is quite heavy in its CPU time demand, since the model equations must be set up and solved for each layer added to the roll. This feature is called the accretive nature of the wound roll modelling. It would be tempting to find a shortcut so that the whole roll with the final number of layers in it could be processed as a one entity. There are at least two known attempts to present such a model, Burns (Burns *et al.* 1999) and (Piper 1995). Even though such a model could be mathematically correct, it does not model a wound roll in a physically meaningful way. Basically the problem is caused by the fact that the equation for the linear strain in the radial direction in cylindrical coordinates defined as the derivative of the displacement with respect of the radius does hold only for the layers already in the roll. In other words this means that to correctly calculate the displacements and strains one must know the intermediate roll radii at each layer added to the roll. And this means that the model must be solved for each layer to compute the radial displacement for it. Although this sounds something you could neglect, the small displacements eventually pile up and cause large errors. This error is inadvertently averted in the Hakiel formulation, since the stresses are solved incrementally layer-wise. The total stress versions like the Benson formulation could allow building the roll from pretensioned cylinders, which simultaneously shrink and find the equilibrium. But this solution does not correspond to a real wound roll.

2.1 The basic stress model

All subsequent model development assumes that the roll is built by placing tensioned hoops of web onto the roll. One might argue on how much this theoretical process differs from the real winding, whether centre-winding without a winding nip or surface winding with a nip. However, every modelling requires idealisations to be made, and the final judgement of the validity of the model is based on measurements.

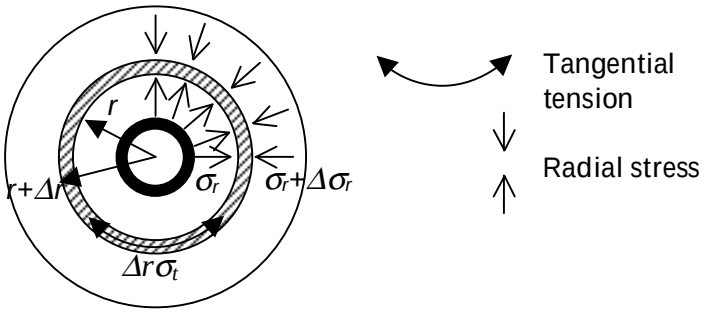

FIGURE 8 Web layer's force equilibrium in the roll. The outer surface force is $(\sigma_r+\Delta\sigma_r)2\pi(r+\Delta r)$ and the inner surface force is $-(\sigma_r+\Delta r\sigma_t/r)\,2\pi r$ and their sum is zero in the equilibrium for small Δr (Roisum 1990).

The first condition for the model is the force equilibrium, all parts of the roll lay in rest or move at a constant speed and all forces balance each other. In a rotating roll there exists centrifugal accelerations, which later on will be added to the force equilibrium equation. When winding stops, these accelerations and inertia forces vanish, and the roll will be left in a different equilibrium state than it would have been if the winding would have been done without rotating the roll. The pure stress equilibrium without body forces can be immediately written as the equilibrium equation for plane stress in cylindrical coordinates in the absence of shear as Hakiel notes. It is also easily derived by considering the forces acting on a cylindrical web layer's internal and external surfaces and the hoop stress caused by its tangential stress, see FIGURE 8:

$$r\frac{\partial \delta\sigma_r}{\partial r} + \delta\sigma_r - \delta\sigma_t = 0 \tag{1}$$

The stresses are here the incremental radial $\delta\sigma_r$ and tangential $\delta\sigma_t$ stresses caused by the addition of the last layer in the roll, but the equation holds equally well for the total stresses, which also must be in equilibrium at any time during the winding. If the radial stress is almost constant in some radial range, then the radial and tangential stresses are almost equal. Some materials like paper have such properties that create rather large constant stress range in the midrange of the roll, which is called the "plateau area" (the requirement is that the tangential elastic modulus is much larger than the radial elastic modulus). Since the radial stress is always negative (that is compressive pressure), the tangential stress is also negative in the plateau area. So the web is under compression in both directions.

2.1.1 Wound On Tension and the outer boundary condition

The Hakiel style incremental model and the Benson style total stress model differ in how they treat the pretension of the web hoops. In the incremental version only the last layer Wound On Tension appears, since the unknown stresses are the increments caused by the addition of the last layer on the roll. In the total stress version the WOT and the hoop stress caused by it must appear in the force equilibrium for every layer, not only in the outer boundary condition.

The most common outer boundary condition in the incremental model is the hoop stress equation for the last layer:

$$\delta\sigma_r(R) = \frac{WOT}{R} \tag{2}$$

This outer boundary condition assumes that the last layer does not loose any of it pretension=WOT when it is placed onto the roll. This means that the incremental tangential stress is zero for the last layer, which would be the other choice for the outer boundary condition. On the other hand then the

incremental tangential strain must also be zero for the last layer, and it cannot shrink with the rest of the roll, when the hoop stress caused by it compresses the roll. So it can become part of the solid roll formed by the other web hoop layers only after the roll is first deformed to the outer radius to fit with its inner radius. Note that this outer boundary condition is not in contradiction with the requirement that the radial stress must be zero at the roll's outer surface, since the last layer's hoop stress acts on the inner surface of the layer, and the stress decreases to zero inside the last layer.

The hoop stress is inversely proportional to the hoop radius. One could jump to the conclusion that also the radial stress in the roll would decrease inversely proportionally with the radial position inside the roll. This contradicts with the notion that typically in paper rolls the stresses are fairly constant over a large radial range. Also measurements and models confirm that the radial displacement caused by the layer-wise hoop stress is almost constant for constant WOT. For example LWC paper roll shrinks radially 2-5 micrometers depending on the tension for every added layer. This can be understood by noting that the total force caused by the last layer is constant even though the stress decreases and that the roll's compliance does not depend on the radius. Constant radial displacement leads to decreasing tangential strains due to the circular geometry and so the incremental tangential stresses are also smaller. This means that the layers relax their tension over longer radial range at larger radii, and these opposing factors cause the smaller incremental hoop stresses to accumulate to almost constant total radial stress.

In any case, the radial stress must approach zero close to the roll surface and the tangential stress must be equal to or slightly less than the stress by the Wound On Tension (how much less it could be is shown later on).

2.1.2 Core stiffness and the inner boundary condition

Rolls without a winding core, which is stiffer than the roll itself, would have radial stress zero at the inner surface as a boundary condition. Such a roll would have very soft bottom and possibly collapse except in case of steel coils (Li and Cao 2001). Stiff core will decrease the radial stress (increase pressure) and increase the tangential stress since it decreases the radial and thus tangential strains near the core. The inner boundary condition can be written by equating the radial displacements at the core-roll surface:

$$\varepsilon_t(R_0) = \frac{u}{R_0} = \frac{\delta\sigma_r}{E_C} = \frac{\delta\sigma_t}{E_t} - \nu_{rt}\frac{\delta\sigma_r}{E_r} \tag{3}$$

where the first equation is a consequence of the axisymmetric conditions, second equation assumes constant core radial compliance $1/E_c$ and the last equation uses the linearized small incremental stress material model. The tangential and radial elastic moduli can be functions of stress, but in the large displacement total stress formulation fully nonlinear material model should be

used. The core elastic modulus E_c can be derived from the core material and geometrical parameters (Roisum 1990), (Ilomäki 2004).

An alternative way to handle the core would be to include it in the model as a part of the roll, which has different material parameters and no pretension. Then the inner boundary condition would be simply to set the radial pressure to zero at the core inner surface. The core wall would have to be discretized at suitable intervals for numerical solution. For homogeneous materials analytical solution is also available.

Until now the inner boundary condition is the only place the web and core material parameters were needed. If the equations would have only one stress as unknowns, the problem would have been already defined and ready to be solved.

2.1.3 Geometric conditions in the axisymmetric roll

The radial and tangential stresses in the roll are connected together by the circular geometry of the web hoops. The radial hoop stress induced by the tangential stress was already one consequence of this geometry. Second consequence is the link between radial displacements and tangential strains:

$$\varepsilon_t = \frac{u}{r} \tag{4}$$

Third geometrical condition is the strain compatibility in the radial direction, which states that the radial strain of each web layer and the radial displacements of adjoining layers must conform to each other. In other words, the radial displacement field must be unambiguous, continuous and differentiable. There must not be gaps or overlapping between layers. With this condition holding, the radial strain can be written:

$$\varepsilon_r = \frac{\partial u}{\partial r} \tag{5}$$

This condition can only hold for the layers already in the roll. The other layers do not even exist and their radius is indefinite. This was the reason why wound roll stresses must be solved separately for each layer added to the roll.

The last two conditions can be combined to the so-called strain compatibility equation:

$$\begin{aligned} &\varepsilon_t = \frac{u}{r} \Rightarrow \frac{\partial \varepsilon_t}{\partial r} = \frac{1}{r}\frac{\partial u}{\partial r} - \frac{u}{r^2} = \frac{\varepsilon_r - \varepsilon_t}{r} \Rightarrow \\ &r\frac{\partial \varepsilon_t}{\partial r} - \varepsilon_r + \varepsilon_t = 0 \end{aligned} \tag{6}$$

Note that this equation is not valid for the last layer with the normal outer boundary condition, since the last layer does not shrink with the rest of the roll and so its radial displacement is not defined.

In order that this equation can be used in the stress model, the strains must be replaced by stresses. This is the point where the equations describing the material elastic properties are needed.

2.1.4 The material model

When the incremental stresses and strains are small, the measured nonlinear stress-strain curves can be replaced by the linearized versions:

$$\varepsilon_r = \frac{\delta\sigma_r}{E_r} - \nu_{tr}\frac{\delta\sigma_t}{E_t} \tag{7}$$

$$\varepsilon_t = \frac{\delta\sigma_t}{E_t} - \nu_{rt}\frac{\delta\sigma_r}{E_r} \tag{8}$$

This is an oversimplification for paper material, since its stress-strain curves are very nonlinear and they have hysteresis and viscoelastic behavior. The non-linearity can be handled if the elastic moduli are written as functions of the total stress. The model is also optimistic, since the Poisson ratios are very difficult if impossible to measure. However, it is useful to retain they in the model parameters to be able to experiment their effect. Usually the other Poisson ratio is eliminated by means of the Maxwell strain energy condition:

$$\frac{\nu_{tr}}{E_r} = \frac{\nu_{rt}}{E_t} \tag{9}$$

But as Benson notes (Benson 1995) this condition cannot hold for materials like paper, which have high hysteresis. The condition is nevertheless not necessary in the model development.

The constitutive equations can now be used to replace the strains with stresses in the strain compatibility equation:

$$r\frac{\partial\delta\sigma_t}{\partial r} + \left(\nu_{tr} - \nu_{rt}\frac{E_t}{E_r} + 1\right)\delta\sigma_t + \left(\frac{\nu_{rt}r}{E_r}\frac{\partial E_r}{\partial\sigma_r}\frac{\partial\sigma_r}{\partial r} - 1\right)\frac{E_t}{E_r}\delta\sigma_r = 0 \tag{10}$$

where the derivative of the radial strain is eliminated by means of the stress equilibrium equation. If the Poisson ratios are set to zero this simplifies to:

$$r\frac{\partial\delta\sigma_t}{\partial r} + \delta\sigma_t - \frac{E_t}{E_r}\delta\sigma_r = 0 \tag{11}$$

The material elastic properties appear in the model only as the ratio of the tangential to the radial elastic modulus. The term

$$\frac{\nu_{rt} r}{E_r} \frac{\partial E_r}{\partial \sigma_r} \frac{\partial \sigma_r}{\partial r} \tag{12}$$

is usually neglected and simulation confirms that it is insignificant in paper rolls.

2.1.5 The wound roll stress boundary value problem

Now the preceding equations can be combined into the incremental stress two-point boundary value problem, which is linear with respect to its unknowns, the stresses:

$$r \frac{\partial \delta\sigma_r}{\partial r} + \delta\sigma_r - \delta\sigma_t = 0 \tag{13}$$

$$r \frac{\partial \delta\sigma_t}{\partial r} + \left(\nu_{tr} - \nu_{rt} \frac{E_t}{E_r} + 1 \right) \delta\sigma_t - \frac{E_t}{E_r} \delta\sigma_r = 0 \tag{14}$$

$$\delta\sigma_r(R) = \frac{WOT}{R} \tag{15}$$

$$\frac{\delta\sigma_r}{E_C} = \frac{\delta\sigma_t}{E_t} - \nu_{rt} \frac{\delta\sigma_r}{E_r} \tag{16}$$

This boundary value problem can be easily solved by first discretizing it leading to linear system of equations. The discretizing grid steps need not to be exact multiples of the web thickness, and best compromise between speed and accuracy is acquired with 1-3 web layers steps for printing papers. The linear system is tridiagonal, which is very fast to solve and the CPU time demand grows only linearly with problem size. Usually the tangential stress is removed from the equations and a second order differential equation for the radial stress is solved instead. This conversion halves the linear system size. But since only 10-20 % of the CPU time is spent in the tridiagonal equation solver, the speed gain is not essential. The solutions of the boundary value problem are incremental stresses caused by each layer added to the roll. The total stresses are computed by summing up these incremental stresses until the whole roll is wound, FIGURE 10.

There is an additional advantage in not eliminating the tangential stress from the boundary value problem. Debugging this kind of complex computational program is not easy. One way is to compare the results from linear material parameters with the analytical solution. Hakiel and others computed the tangential stress from the final total radial stress by means of the stress equilibrium equation. The present method gives both stresses as solutions

of the model and the stress equilibrium equation is available for checking the total stresses, since they must satisfy it too, see FIGURE 11. More about error checking follows in a later chapter.

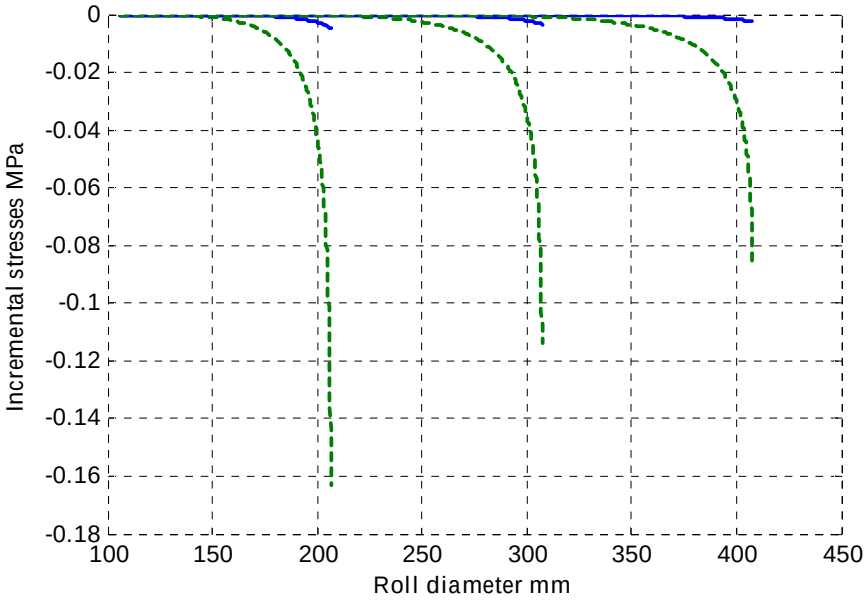

FIGURE 9 Computed incremental stresses at three different roll radii for a typical paper roll. Solid line = radial stress, dashed line = tangential stress. Wound On Tension was 500 N/m = 9.9 MPa. The decreasing of stresses with increasing radius is clear. The last layer's effect on stresses extend 25-50 mm inside the roll surface.

The displacements where not included in the model computations, but they are implicitly present in the strain compatibility equation. How much the accuracy of the model is compromised when displacements are not updated and the last layer does not shrink with the roll? Measured typical paper roll surface displacement is about 5 or less micrometers for every layer added to the roll. In a 1000 layer roll with 100 mm radius this means 5 mm error in radius and 5% error in the last layer hoop stress. The missing relaxation in the last layer tangential stress is immediately seen from FIGURE 9 incremental tangential stress, it is about -0.16 Mpa at the 100 mm radius, less than 2 % of the WOT stress.

2.2 The "tension loss" model

Good and Pfeiffer present (Good and Pfeiffer 1992) a model they describe as solving the discrepancy between measured and modeled stresses in a centrewound roll. They had better agreement between measured and computed pressures when the roll was wound with an undriven nip. They used quite low web tensions 140 – 460 N/m and the resulting roll radial stresses where low 0.03-0.2 MPa. They corrected the Hakiel model by estimating the radial displacement at the roll surface due to the last layer by means of the previous layer displacements.

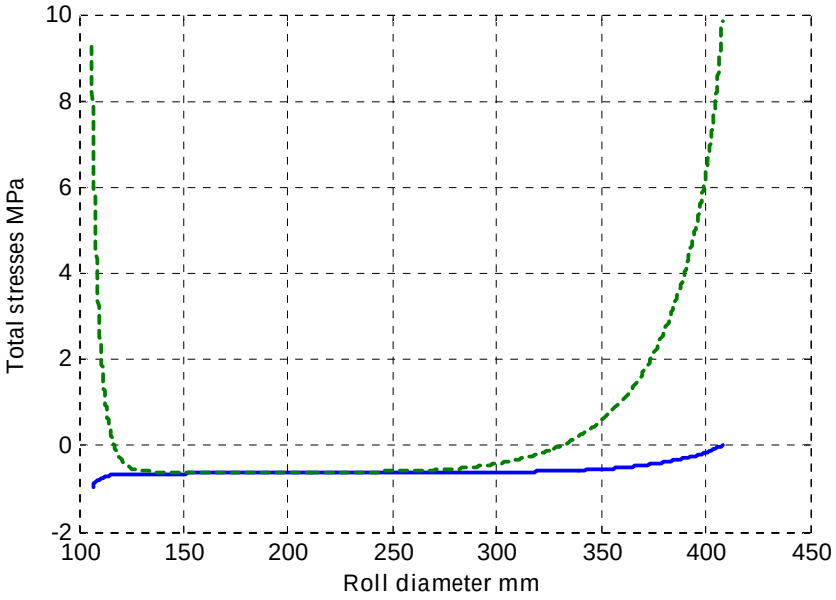

FIGURE 10 Computed total stresses resulting from the incremental stresses of the FIGURE 9. At the roll surface the tangential stress is equal to the wound on stress and radial stress is zero. The plateau area is large and the stresses there are about –0.6 MPa. The web has also retained almost all its tangential stress at the core due to the small radial displacement at the stiff core.

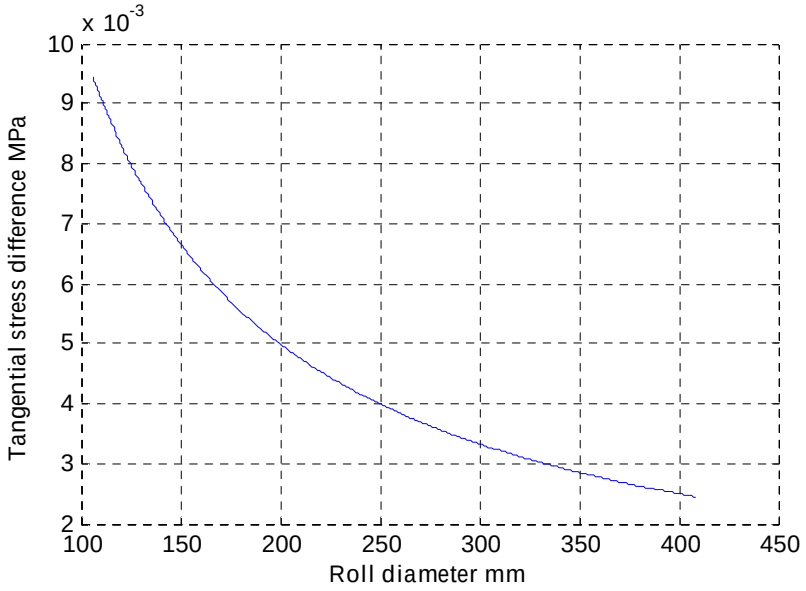

FIGURE 11 Difference in the tangential stress as computed directly from the model versus computed from the stress equilibrium equation and the final radial stress. The maximum difference is less than 10 KPa. The difference in the plateau area is reasonably less than 1 % of the plateau tangential stress.

However, the model can be easily modified to account for this last layer tension loss or relaxation. The last layer tension loss is nothing else but the incremental tangential stress at this layer, if it is modeled the same way as every

other layer in the roll. Then the relaxed tension of the last layer is got directly from the boundary value problem solution and no extra computation is needed.

As mentioned earlier, the normal Hakiel outer boundary condition implicitly assumes that the last layer does not shrink with the roll. The modified model handles the last layer equally with the other layers, so the strain compatibility equation will hold for it too and the outer boundary condition is simply:

$$\delta\sigma_r(R) = 0 \tag{17}$$

Since the Wound On Tension disappears from the outer boundary condition, it will be moved to the stress equilibrium equation for the last layer.

The difference between the radial stresses from these two model versions in the typical paper roll wound at 500 N/m is between 0.01-0.03 MPa, which is 2-5% of the –0.6 MPa plateau stress, FIGURE 11 and FIGURE 13. Good and Pfeiffer warn that the tension loss can be so great to completely loosen the outermost layer. However, this would require the roll being extremely soft, so that very small hoop stress would still compress it. In normal cases the roll is hard enough so that the loss is few percent of the WOT.

The accuracy of the pressure measurements, either with pull tabs or with pressure sensitive resistors, is not good enough to decide which one of the models better describe centre wound rolls. In normal conditions of paper winding, there is no such big difference found between measured and modeled pressures as Good and Pfeiffer report. However, in nipless centre winding the outermost layer will retain its WOT tension if its slips on the roll. Since the hoop stress under the last layer is WOT/R and the area is 2πR the total force (per width unit) is 2πWOT. If the static paper to paper friction coefficient is less than $1/2\pi$, the last layer will slip and retain its tension. Normal friction coefficients are greater than that, so the last layer will be partly slipping, and the true tension loss is somewhere in between what the two models predict.

This calculation also implies that the high tension loss of the outermost layer would be very instable condition in nipless centre winding, where each web layer must be able to transfer the torque from the centre of the roll to the surface. Where would be the stick region to withstand this torque? It is not reasonable to think that there would be a high stress stick area just after the point where the web enters the roll and after this area the tension loss would decrease the WOT in the last layer. This stick area would be forced to slip, since it would not shrink with the roll under it. More realistic view is to have a no tension loss slipping area first which at some point at the roll periphery ends and after that the roll can be modelled as a solid object.

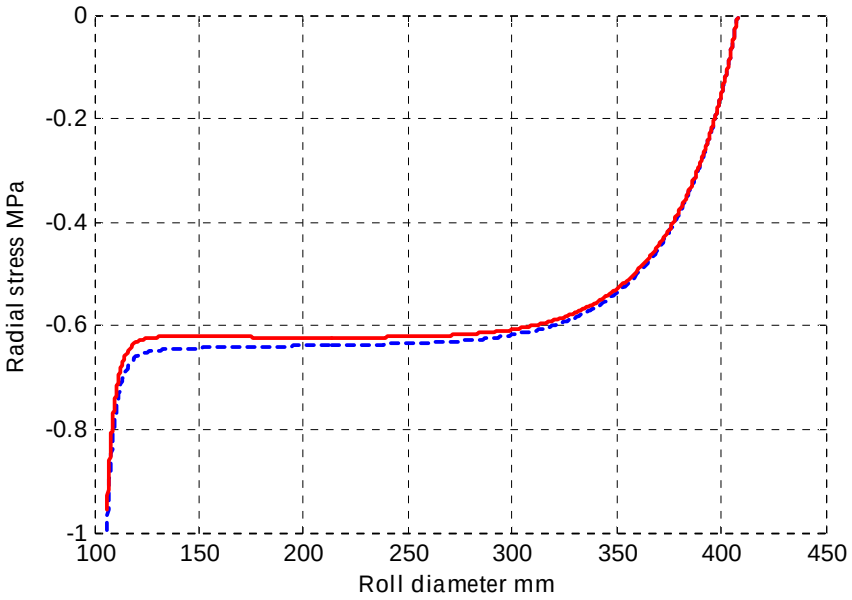

FIGURE 12 Comparison of the "Tension loss" and "No tension loss" versions of the incremental stress wound roll models. Radial stress with no tension loss in the outer layer = dashed line and radial stress with tension loss = solid line. Wound On Tension was 500 N / m.

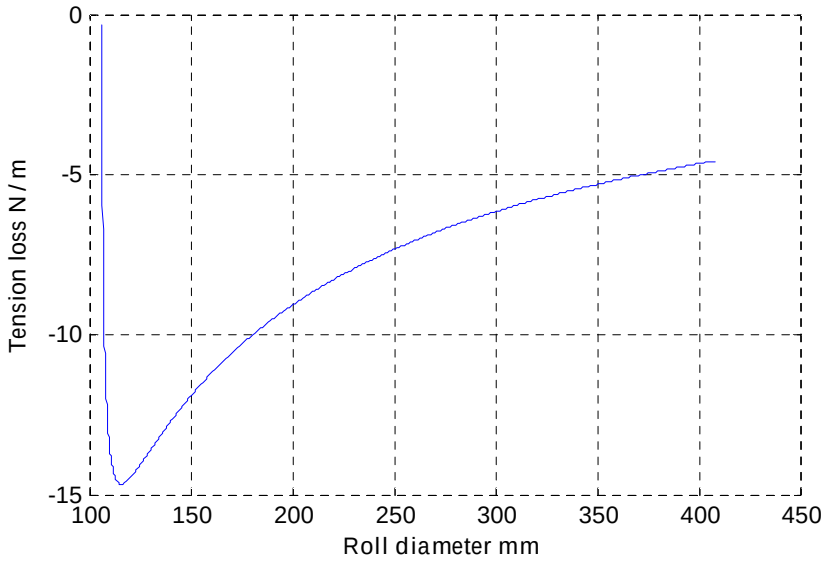

FIGURE 13 Comparison of the "Tension loss" and "No tension loss" versions of the incremental stress wound roll models. Simulated tension loss in the paper roll wound at 500 N / m. Near the core the tension loss is small due to the stiff core. The tension loss decreases with diameter since the radial displacement is almost constant and the tangential displacement decreases with increasing diameter ε_t=u / r.

Table 1 Discretized linear system, columns 1-8 represent the coefficient matrix to be inverted by the tridiagonal solver, column 9 is the unknown vector and column 10 is the input vector. The system matrix is highly sparse tridiagonal matrix, the width of the diagonal band is 3. The outer boundary condition is here written as $\delta\sigma_{tR}=0$ and the Wound

On Tension appears in the stress equilibrium for the last layer. The differential equations where discretized with forward and backward differences to keep the system tridiagonal. The terms including Poisson ratios are not written in the table to keep it more readable. The total number of columns and rows in the system matrix is 2N, indexed from 0 to 2N-1. When N=1 keep the last two rows of the table.

$-E_t/E_c$	1	...	0	0	...	0	0	$\delta\sigma_{r,0}$	0
$1-r_1/(r_1-r_0)$	-1	$r_1/(r_1-r_0)$	0	0	...	0	0	$\delta\sigma_{t,0}$	0
...	...	...	...	...	...	...	...	...	...
0	0	$-r_i/(r_i-r_{i-1})$	$-E_t/E_r$	$1+r_i/(r_i-r_{i-1})$	...	0	0	$\delta\sigma_{r,i}$	0
		...	$1-r_{i+1}/(r_{i+1}-r_i)$	-1	$r_{i+1}/(r_{i+1}-r_i)$	0	0	$\delta\sigma_{t,i}$	0
...	...	...	...	...	...	...	...	...	...
0	0	...	0	0	...	1	0	$\delta\sigma_{r,N-1}$	$-WOT_{N-1}/r_{N-1}$
0	0	...	0	0	...	0	1	$\delta\sigma_{t,N-1}$	0

Table 2 Discretized linear system for the tension loss version of the model. The table is otherwise the same as the previous table except for the last two rows. The last row is the stress equilibrium for the last layer and the previous row is the compatibility condition for the last layer, and the outer boundary condition is implicitly present as $\delta\sigma_{rN}=0$. When N=1, keep the first and last rows of the table.

$-E_t/E_c$	1	...	0	0	...	0	0	$\delta\sigma_{r,0}$	0
$-r_1/(r_1-r_0)$	$-E_t/E_r$	$1+r_1/(r_1-r_0)$	0	0	...	0	0	$\delta\sigma_{t,0}$	0
...	...	...	...	...	...	...	...	...	...
0	0	$-r_i/(r_i-r_{i-1})$	$-E_t/E_r$	$1+r_i/(r_i-r_{i-1})$	...	0	0	$\delta\sigma_{r,i}$	0
		...	$1-r_{i+1}/(r_{i+1}-r_i)$	-1	$r_{i+1}/(r_{i+1}-r_i)$	0	0	$\delta\sigma_{t,i}$	0
...	...	...	...	...	...	...	...	...	...
0	0	...	0	0	$-r_{N-1}/(r_{N-1}-r_{N-2})$	$-E_t/E_r$	$1+r_{N-1}/(r_{N-1}-r_{N-2})$	$\delta\sigma_{r,N-1}$	0
0	0	...	0	0	...	1	$(r_N-r_{N-1})/r_{N-1}$	$\delta\sigma_{t,N-1}$	$-WOT_{N-1}/r_{N-1}$

2.3 Centrifugal forces

The centrifugal forces are body forces acting on every layer on the roll (Olsen 1996). The centrifugal stress on the last layer in the roll of mass *m* and radius *r* counteracting the hoop stress is

$$\frac{mv^2}{r2\pi rl} = \rho 2\pi rlh\frac{v^2}{r^2 2\pi l} = \rho\omega^2 h \tag{18}$$

For typical LWC paper roll parameters, density 1000 kg/m^3, radius 0.5m, thickness 50 micrometers and web speed 40 m/s this would be about 30 % of the hoop stress caused by 500 N/m Wound On Tension. The centrifugal forces cannot clearly be neglected and they can be very easily added to the incremental stress model. What is needed is adding the above stress term in the rows where WOT appears in Table 1 and Table 2 in the last column. For the sake of accuracy every other row representing the stress equilibrium needs the term $\rho\left(\omega_N^2 - \omega_{N-1}^2\right)h$, which is the difference in the centrifugal stress when layer N is added to the roll (if Poisson ratios are present, they cause more terms to appear). It is interesting to note that the stresses will not be the same as without the centrifugal terms even though the roll is stopped rotating at the end of winding. This is true even with the simplest model, which does not calculate and update displacements. If the roll would be one solid elastic object, it would return to the same stress state where it was before the rotating started, FIGURE 14.

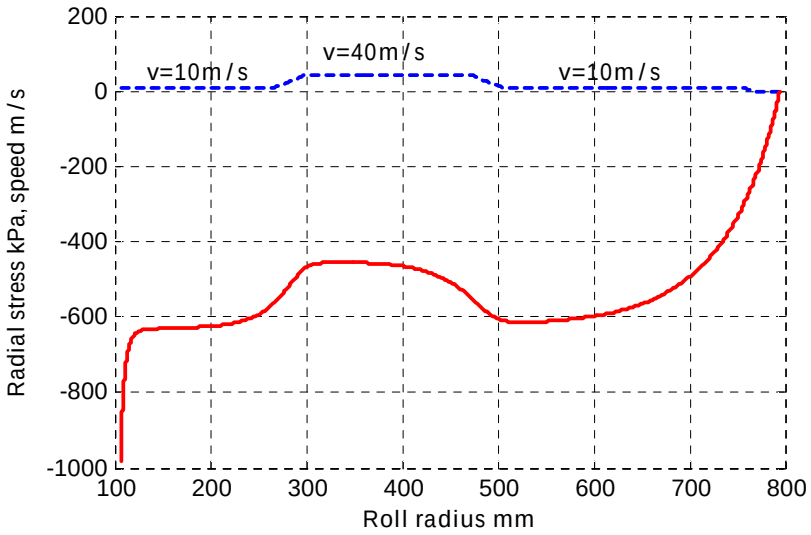

FIGURE 14 Speed changes during simulated winding causing stress changes when centrifugal force terms are added to the model. Solid line = radial stress, dashed line = web speed.

2.3.1 Thermal, hygroscopic and viscoelastic effects

Other stress inducing effects acting inside the roll as it is being wound and after it are the thermal, hygroscopic and viscoelastic effects (Qualls 1995). These

effects appear in the model through the material model, which gets time dependent terms. Since these processes are slow taking hours if days to change the stresses (viscoelasticity is perhaps an exception), they are most easily modelled separately from the winding. Most paper grades are quite viscoelastic, so it must be included in a proper winding stress treatment. The thermal and hygroscopic effects can be eliminated by keeping the roll in constant ambient conditions. The viscoelastic wound roll stress model will be later presented as a modification of the total stress version of the model.

2.4 Including the displacements

Until now the displacements did not explicitly appear in the wound roll stress model. The roll radius was updated by summing up the original unstrained web thickness. This model can fairly well predict the stresses in the roll, but fails to say nothing about the density changes in it. For a typical LWC paper roll, the radial strain can be up to 10%, so it really cannot be neglected. And if the measured radial displacements are to be used with the model to measure the Wound On Tension, they must be included in the model.

The non-linear material model constitutive equations are

$$\varepsilon_r = S_r(\sigma_r) - \nu_{tr} S_t(\sigma_t), \varepsilon_t = S_t(\sigma_t) - \nu_{rt} S_r(\sigma_r) \tag{19}$$

The functions S_r and S_t are chosen to be easy to program and fast to compute and to have few experimentally determined parameters. The choice can be made so that

$$\frac{\partial S_r}{\partial \sigma_r} = \frac{1}{C_0 + C_1\sigma_r + C_2\sigma_r^2} = \frac{1}{E_r(\sigma_r)} \tag{20}$$

and the polynomial for the radial modulus E_r is the same as used in the incremental "non-linear" model. The polynomial for E_t can be of first order, since typically for paper the tangential stretch stress-strain curve is not as non-linear as the z-direction curve.

The displacements in the incremental wound roll model are updated after the total radial stresses are solved at each layer added to the roll. First the modulus is updated on the total stress and then it is used in the linear constitutive equation to give the incremental radial strain. Then the incremental strain is used to solve the new layer thickness and finally the web layer radial positions are got from the cumulative sum of the strained layer thickness, FIGURE 16.

2.5 Wound roll stress model error checking

The displacements and strains give two more ways to compute error terms to check the validity and error in the program in addition to the stress equilibrium error term mentioned earlier. The error terms are:

$$ERRSTRESS_i = r_i \frac{\Delta\sigma_{r,i}}{\Delta r} + \sigma_{r,i} - \sigma_{t,i} \tag{21}$$

$$ERRSTRAINR_i = \sigma_{r,i} - S_r^{-1}\left(\varepsilon_{r,i}\right) \tag{22}$$

$$ERRSTRAINT_i = \sigma_{t,i} - S_t^{-1}\left(\varepsilon_{t,i}\right) \tag{23}$$

The term *ERRSTRESS* indicates how well the stress equilibrium holds for the total stresses, which were cumulative sums of the incremental stresses, *ERRSTRAINR* is a measure of radial strain compatibility expressed as stress to be easier to compare with the total stresses and *ERRSTRAINT* is the same for the tangential strain (Poisson terms not shown). The tangential strain is computed as

$$\varepsilon_{t,i} = \frac{r_i - r_{out,i}}{r_{out,i}} \tag{24}$$

where $r_{out,i}$ is the radius of the roll when layer *i* was added to it. The term *ERRSTRAINR* vanishes if the nonlinear constitutive equation is used to compute the radial displacement, but still the two other terms are nonzero for the incremental stress model, FIGURE 15.

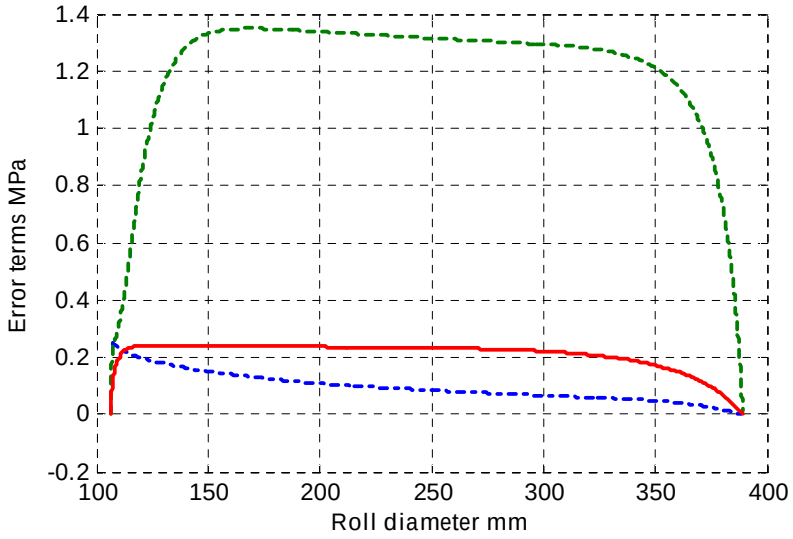

FIGURE 15 The error terms *ERRSTRESS* solid line, *ERRSTAINR* dash-dot line and *ERRSTRAINT* dashed line. The model and parameters are the same as in FIGURE 10 except that now the displacements are updated. The error stresses are large compared to the plateau stress of –0.6 MPa. The *ERRSTRESS* term is about 20 times bigger than in the FIGURE 11, when the displacements were not updated in the model.

2.6 The total stress model

The total stress model is solved in the same layer by layer manner as the incremental stress model, but now the non-linear stress strain curves are not linearized but instead a non-linear numerical solver is applied. The layer-wise boundary value problem is solved for the total stresses σ_r and σ_t caused by all layers ' Wound On Tensions and the strains are exactly solved from the non-linear material model. The total stress model is not meaningful to solve without updating the displacements, since its accuracy on stresses and on strains is based on exact modelling of the displacements and it can handle also large deformations. The total stresses at each radial position are got directly as the solution of the layer-wise boundary value problem, not as a cumulative sum of the incremental stresses solved for each layer added to the roll. The difference of the successive solutions is the incremental stress added by the last web layer. The cost of the more accurate solution is increased computing effort and a more complex program. The non-linear numerical solver needs to take 2-4 iteration steps for each layer-wise boundary value problem and the computing time is increased accordingly.

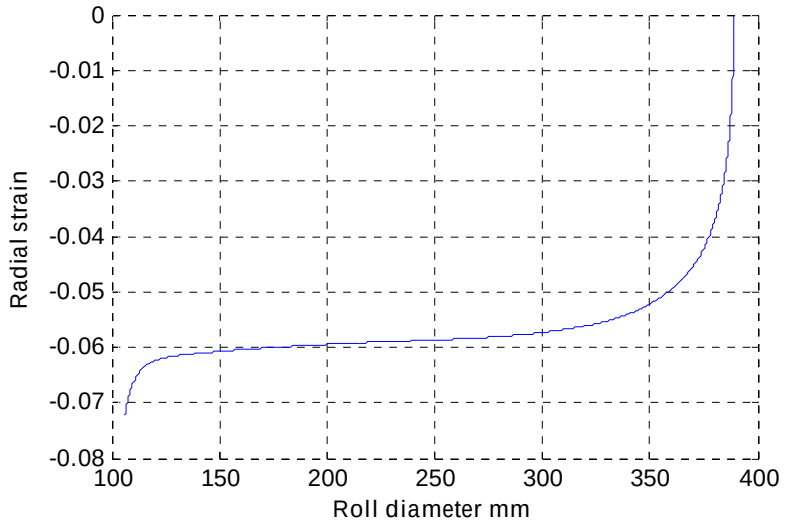

FIGURE 16 Simulated radial strain of the typical LWC paper roll wound at 500 N/m Wound On Tension. The strain is computed with the incremental stress model.

The Benson formulation (Benson 1995) was written as a displacement model, where the deformed layer radius was the unknown to be solved. However, the equations can be equally well written for the stresses, as is done in what follows, and the solution will be the same. Benson stated that the deformed layer radius or radial position in the deformed roll cannot be used as an independent variable of the problem, since it depends on the problem solution. However, if the equations are written for the unknown stresses, this is not true, since the stress equilibrium and other conditions must hold for the deformed state of the roll after it has found the equilibrium. Benson used the

layer index as the independent variable, as will be used here too, since a dimensionless independent variable makes more evident that the layer radii will be part of the solution.

There are two alternative but equal ways to get the Wound On Tension into the equations of the total stress model. The more obvious way is to show it explicitly in the stress equilibrium equation as a kind of external force applied on every web layer. Then the tangential stress variable represents only partial layer's tangential stress, namely how much the original Wound On Tension has been relaxed in the roll. This component of the tangential stress is always negative, and the total tangential stress is got as a sum of it and the Wound On Tension. The other way is to write the Wound On Tension into the geometric strain condition as the radius of the layer where the tangential stress would be relaxed to zero. This is the way Benson adopted, which was natural in his radial displacement equations. In this case the tangential stress solution is the total stress, and the Wound On Tension does not appear explicitly in the equations anywhere except in the equation for the relaxation radius r_0 for each layer.

The stress equilibrium equation is essentially untouched except for the change of the independent variable:

$$r\frac{\frac{\partial \sigma_r}{\partial i}}{\frac{\partial r}{\partial i}} + \sigma_r - \sigma_t = \frac{WOT - br_{out} r\omega^2}{\frac{\partial r}{\partial i}} \tag{25}$$

This equation shows the Wound On Tension explicitly, so the tangential stress σ_t is the (negative) change in the layer's tension since it got into the roll. If the WOT would not be visible, it would be implicitly included in the σ_t variable. The centrifugal force term is now written by means of the web's basis weight b to anticipate the fact that the density is changing when layer thickness deforms. Actually the same thing affects the WOT stress, which could be constant by dividing the WOT by the constant (in the deformation process) original layer thickness instead of the variable layer thickness. The term dr/di is the deformed layer thickness in the roll. All variables in the equation are functions of the layer index i except for the roll rotational speed ω, which is a function of the total number of layers N in the roll.

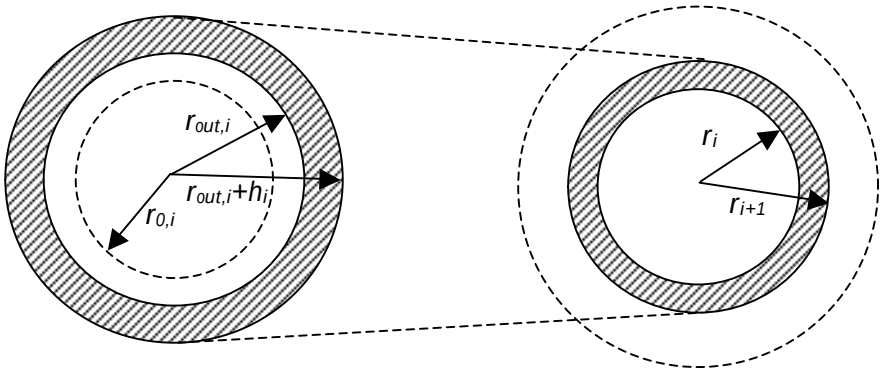

Figure 17 The roll just after the layer i was added to it on the left and after some more layers were added on the right. This picture represents the "tension loss" outer boundary condition, where the outermost layer shrinks with the roll and relaxes its tangential stress in the deformation caused by it, so the layer starts its radial displacement from the radius r_{out}.

2.6.1 The geometric conditions revised

The geometric conditions used in the incremental stress model were based on the small displacements assumption, where the radial displacement field variable *u* could be used without explicitly expressing the original undeformed position of each material location. When the displacements are not small the undeformed position of each web layer must be defined and expressed in the equations. This fact changes the equations how strains and displacements were related to each other:

$$\varepsilon_r = \frac{\partial u}{\partial r}, \varepsilon_t = \frac{u}{r} \tag{26}$$

where the displacement for the radial strain is found not to be the same as for the tangential strain. First the equation for the tangential stress is rewritten, which can be done in three alternative ways each representing one possible version of the model.

$$\varepsilon_{t,i} = \frac{u_i}{r_{0,i}} = \frac{r_i - r_{out,i-1} - h_i}{r_{0,i}} \tag{27}$$

The above equation holds for the "tension loss" version where the outermost layer of the roll also relaxed some of its tension, see Figure 17. The second version holds for the "no tension loss" version of the model:

$$\varepsilon_{t,i} = \frac{u_i}{r_{0,i}} = \frac{r_i - r_{out,i}}{r_{0,i}} \tag{28}$$

Note that $r_{out,i-1}+h_i>r_{out,i}$ so the "tension loss" model gives larger radial displacements and larger tangential strains than the "no tension loss" model. Both of the above versions require that the WOT is visible in the stress equilibrium, since the zero point for the radial displacements is at the radius, where the layer has all its original WOT stress before displacements and relaxations occur in the roll. The third version of the tangential strain equation holds if the WOT stress is not visible in the stress equilibrium equation but it is implicitly included in the tangential strain variable:

$$\varepsilon_{t,i} = \frac{u_i}{r_{0,i}} = \frac{r_i - r_{0,i}}{r_{0,i}} \tag{29}$$

This version gives the same solutions as the two earlier versions when the outer boundary condition is selected according to the "tension loss" or "no tension loss" choice. In all three cases the nominator could be also r_i, but since the strain in the pull test is defined as the length change divided by the original length of the sample, the relaxation radius r_0 nominator is more compatible with the strain in the pull test. The relaxation radius is got with the nonlinear material model as

$$r_0 = \frac{r_{out}}{S_t\left(\frac{WOT}{h_i}\right)+1} \tag{30}$$

In all three cases the displacement difference Δu is not equal to Δr-h_i, which would be required to have

$$\varepsilon_r = \lim_{\Delta r \to 0} \frac{\Delta u}{\Delta r} \tag{31}$$

but instead the radial strain is defined to be

$$\varepsilon_{r,i} = \frac{\frac{\partial r_i}{\partial i} - h_i}{h_i} \tag{32}$$

again in compliance with the strain definition used when the stress strain curve is measured in the stack testing machine. The strain compatibility equation is now rewritten for the three cases as:

$$\frac{\partial r_i}{\partial i} = h_i \varepsilon_{r,i} + h_i = \frac{\partial\left(r_{0,i}\varepsilon_{t,i} + r_{out,i-1} + h_i\right)}{\partial i} \tag{33}$$

$$\frac{\partial r_i}{\partial i} = h_i \varepsilon_{r,i} + h_i = \frac{\partial\left(r_{0,i}\varepsilon_{t,i} + r_{out,i}\right)}{\partial i} \tag{34}$$

$$\frac{\partial r_i}{\partial i} = h_i \varepsilon_{r,i} + h_i = \frac{\partial\left(r_{0,i}\varepsilon_{t,i} + r_{0,i}\right)}{\partial i} \tag{35}$$

This equation can be immediately used to write the program and no need to change the unknowns to stresses exist. The equation is simply discretized and the strains are computed from stresses by means of the non-linear material model. The non-linear numerical solver needs the partial derivatives with respect of the stresses, which are also easily derived from these equations by means of the derivative chain rule and the derivatives of the non-linear material model equations. This approach to writing the program keeps its simpler as unnecessary terms are avoided and the original form of the equations is visible.

2.6.2 The boundary conditions

The core boundary condition is the strain compatibility equation for the core-web surface where the radial displacements of the core surface and the first web layer must be equal:

$$\varepsilon_{t,0} = \frac{r_0 - r_{out,0}}{r_{0,0}} \tag{36}$$

$$\varepsilon_{t,core} = \frac{\sigma_{r,0}}{E_c} = \frac{r_0 - r_{out,0}}{r_{out,0}} \tag{37}$$

and the final core boundary condition is got by equating the first layer radius r_0 got from the two above equations:

$$r_{0,0}\varepsilon_{t,0} + r_{out,0} = r_{out,0}\frac{\sigma_{r,0}}{E_c} + r_{out,0} \tag{38}$$

This is again the case where the WOT stress is explicit in the stress equilibrium equation, and the other choice is got by replacing the core original radius $r_{out,0}$ by the first layer relaxation radius $r_{0,0}$ in the first equation.

The outer boundary condition is very simple in all cases:

$$\sigma_{t,N-1} = 0 \tag{39}$$

for the "no tension loss" case and the same if WOT stress is implicit:

$$\sigma_{t,N-1} = \frac{WOT}{h_{N-1}} \tag{40}$$

and finally the "tension loss" version:

$$\sigma_{r,N} = 0 \tag{41}$$

2.6.3 The numerical solver for the non-linear boundary value problem

The stress equilibrium and strain compatibility differential equations are first discretized by means of forward and backward differences, which leads to a non-linear vector valued function $\bar{f}$, whose zero point is to be found:

$$\bar{f}\left(\bar{\sigma}\right) = 0 \tag{42}$$

where the unknown vector is

$$\bar{\sigma} = \begin{bmatrix} . \\ \sigma_{r,i} \\ \sigma_{t,i} \\ . \end{bmatrix} \tag{43}$$

and the nonlinear function is

$$\bar{f}(\bar{\sigma}) = \begin{bmatrix} r_{0,0}\varepsilon_{t,0} + r_{out,0} - r_{out,0}\dfrac{\sigma_{r,0}}{E_c} - r_{out,0} \\ . \\ h_i\varepsilon_{r,i} + h_i - r_{0,i}\varepsilon_{t,i} - r_{out,i-1} + h_i + r_{0,i-1}\varepsilon_{t,i-1} + r_{out,i-2} + h_{i-1} \\ r_i\dfrac{\sigma_{r,i+1} - \sigma_{r,i}}{r_{i+1} - r_i} + \sigma_{r,i} - \sigma_{t,i} + \dfrac{br_{out,i}r_i\omega_{N-1}^2 - WOT_i}{r_{i+1} - r_i} \\ . \\ r_{N-1}\dfrac{0 - \sigma_{r,N-1}}{r_N - r_{N-1}} + \sigma_{r,N-1} - \sigma_{t,N-1} + \dfrac{br_{out,N-1}r_{N-1}\omega_{N-1}^2 - WOT_{N-1}}{r_N - r_{N-1}} \end{bmatrix} \tag{44}$$

which holds for the "tension loss" model. The outer boundary condition is used in the last equation, which is the stress equilibrium equation for the last layer in the roll, whose index is N-1. The discretizing grid points are under the web layers, so $\sigma_{r,N-1}$ is the stress under the last layer and $\sigma_{r,N}$ is the stress above it, which is of course zero. The WOT stress can be hidden in the relaxation radii without altering the solution:

$$\bar{f}(\bar{\sigma}) = \begin{bmatrix} r_{0,0}\varepsilon_{t,0} + r_{0,0} - r_{out,0}\dfrac{\sigma_{r,0}}{E_c} - r_{out,0} \\ . \\ h_i\varepsilon_{r,i} + h_i - r_{0,i}\varepsilon_{t,i} - r_{0,i-1} + r_{0,i-1}\varepsilon_{t,i-1} + r_{0,i-1} \\ r_i\dfrac{\sigma_{r,i+1} - \sigma_{r,i}}{r_{i+1} - r_i} + \sigma_{r,i} - \sigma_{t,i} + \dfrac{br_{out,i}r_i\omega_{N-1}^2}{r_{i+1} - r_i} \\ . \\ r_{N-1}\dfrac{0 - \sigma_{r,N-1}}{r_N - r_{N-1}} + \sigma_{r,N-1} - \sigma_{t,N-1} + \dfrac{br_{out,N-1}r_{N-1}\omega_{N-1}^2}{r_N - r_{N-1}} \end{bmatrix} \tag{45}$$

In this case the Wound On Tensions are only used to compute the relaxation radii $r_{0,i}$ for each layer when it is added to the roll. The roll outer radii r_i and the relaxation radii $r_{0,i}$ are constant in the subsequent computations, but the layer radii inside the roll are updated by means of the non-linear material model:

$$r_i = r_{i-1} + \left(1 + S_r(\sigma_{r,i}) - \nu_{tr}S_t(\sigma_{t,i})\right)h_i \tag{46}$$

The "no tension loss" version keeps the last layer tangential stress equal to the WOT stress:

$$\bar{f}\left(\overline{\sigma}\right)=\begin{bmatrix} r_{0,0}\varepsilon_{t,0}+r_{out,0}-r_{out,0}\dfrac{\sigma_{r,0}}{E_c}-r_{out,0} \\ \vdots \\ h_i\varepsilon_{r,i}+h_i-r_{0,i}\varepsilon_{t,i}-r_{out,i-1}+h_i+r_{0,i-1}\varepsilon_{t,i-1}+r_{out,i-2}+h_{i-1} \\ r_i\dfrac{\sigma_{r,i+1}-\sigma_{r,i}}{r_{i+1}-r_i}+\sigma_{r,i}-\sigma_{t,i}+\dfrac{br_{out,i}r_i\omega_{N-1}^2-WOT_i}{r_{i+1}-r_i} \\ \vdots \\ r_{N-1}\dfrac{0-\sigma_{r,N-1}}{r_N-r_{N-1}}+\sigma_{r,N-1}-0+\dfrac{br_{out,N-1}r_{N-1}\omega_{N-1}^2-WOT_{N-1}}{r_N-r_{N-1}} \\ \sigma_{t,N-1} \end{bmatrix} \tag{47}$$

which can also be written without explicitly showing the WOT stress as the previous equation except for the last equation:

$$\bar{f}\left(\overline{\sigma}\right)=\begin{bmatrix} r_{0,0}\varepsilon_{t,0}+r_{0,0}-r_{out,0}\dfrac{\sigma_{r,0}}{E_c}-r_{out,0} \\ \vdots \\ h_i\varepsilon_{r,i}+h_i-r_{0,i}\varepsilon_{t,i}-r_{0,i}+r_{0,i-1}\varepsilon_{t,i-1}+r_{0,i-1} \\ r_i\dfrac{\sigma_{r,i+1}-\sigma_{r,i}}{r_{i+1}-r_i}+\sigma_{r,i}-\sigma_{t,i}+\dfrac{br_{out,i}r_i\omega_{N-1}^2}{r_{i+1}-r_i} \\ \vdots \\ r_{N-1}\dfrac{0-\sigma_{r,N-1}}{r_N-r_{N-1}}+\sigma_{r,N-1}-\sigma_{t,N-1}+\dfrac{br_{out,N-1}r_{N-1}\omega_{N-1}^2}{r_N-r_{N-1}} \\ \sigma_{t,N-1}-\dfrac{WOT_{N-1}}{r_N-r_{N-1}} \end{bmatrix} \tag{48}$$

The non-linear system of equations can be easily solved by means of the Newton method, since the Jacobian matrix is easily computed and inverted and the previous solution is a good initial guess for the next iteration as one more layer is added to the roll.

$$\Delta\overline{\sigma}_k=-J\left(\overline{\sigma_k}\right)^{-1}\overline{f}\left(\overline{\sigma_k}\right) \tag{49}$$

where *k* is the iteration index and *J* is the Jacobian matrix

$$J\left(\overline{\sigma_k}\right)=\frac{\partial\bar{f}\left(\overline{\sigma_k}\right)}{\partial\sigma_j} \tag{50}$$

where σ_j is the *j*th component of the σ-vector. Normally 2-4 iteration steps give excellent accuracy and the iteration can be stopped when the relative norm of the iteration step falls under some limit. The following table shows the Jacobian matrix in detail for the "tension loss" version of the model.

Table 3 The numerical solver structure for the "no tension loss" version of the total stress model. The terms including the Poisson ratios are left out for clarity. There are 2N rows in the table and the index i runs from 0 to N-1. If N=1 keep two last rows of the table. The first 8 columns of the table represent the Jacobian matrix of the *f* vector function, 9th column is the iteration step vector and the last column is the residual vector. The Jacobian matrix is computed, inverted and the σ-vector is updated until the step size or the residual vectors are small enough.

$-r_{out,0}/E_c$	$r_{0,0}/E_{t,0}$	...	0	0	...	0	0	$\Delta\sigma_{r,0}$	$-f_0$
$1-r_0/(r_1-r_0)$	-1	$r_0/(r_1-r_0)$	0	0	...	0	0	$\Delta\sigma_{t,0}$	$-f_1$
...	...	...	...	...	...	...	...	...	...
0	0	$r_{0,i-1}/E_{t,i-1}$	$h_i/E_{r,i}$	$-r_{0,i}/E_{t,i}$	...	0	0	$\Delta\sigma_{r,i}$	$-f_{2i}$
		...	$1-r_i/(r_{i+1}-r_i)$	-1	$r_i/(r_{i+1}-r_i)$	0	0	$\Delta\sigma_{t,i}$	$-f_{2i+1}$
...	...	...	...	...	...	...	...	...	...
0	0	...	0	0	...	$1-r_{N-1}/(r_N-r_{N-1})$	0	$\Delta\sigma_{r,N-1}$	$-f_{2N-2}$
0	0	...	0	0	...	0	1	$\Delta\sigma_{t,N-1}$	$-f_{2N-1}$

As with the incremental stress model, the matrix to be inverted is tridiagonal and easily inverted. Most of the computing time is spent in updating the elastic moduli E_t and E_r and computing the nonlinear stress strain curves S_t and S_r, so they should be as simple functions as possible to fit with the experimental data.

2.7 Comparison of the incremental and total stress models

It should be immediately clear that the total stress model is superior to the incremental stress model in predicting the deformations and specifically the density or web thickness in the roll. The total stress model is a kind of "closed loop" system compared to the "open loop" incremental stress model. The total stress model is solved for every roll layer for the governing equations, which hold for the total stresses and displacements caused by all the forces acting on the roll. On the other hand the final solution of the incremental stress model is got as a large cumulative sum of the layer-wise incremental stresses, and every intermediate solution is vulnerable to the possibly cumulative errors in all preceding solutions. Solving the displacements by means of the linearized material model from the sum of the incremental strains causes even more error compared to the total strain solved from the nonlinear material model and the total stress. The only benefit of the incremental stress model is its faster execution time. The program for the total stress model is only slightly more complex needing one more outer loop for the nonlinear solver iteration and computing the residuals of the nonlinear equations.

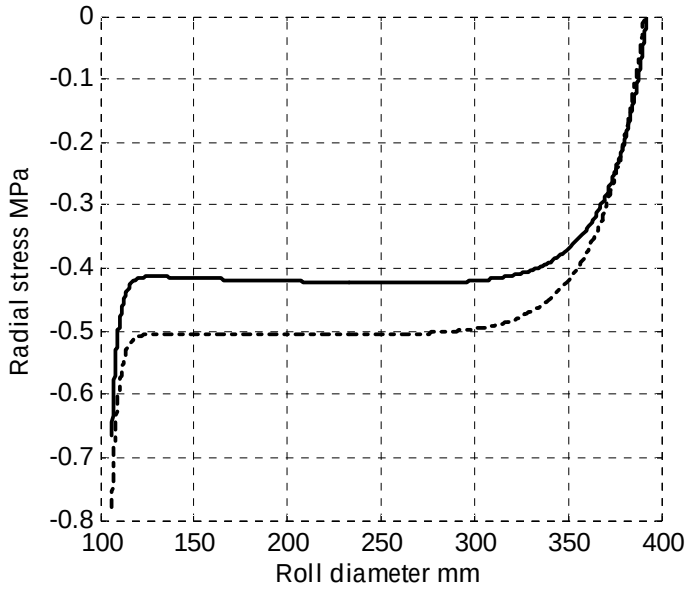

Figure 18 Comparison of the radial stresses computed with the total and incremental stress models. Wound On Tension was 500 N / m. The "tension loss" version of the models was used for both models and the displacements were updated for the incremental stress model. The incremental stress model gives higher pressure for this LWC paper simulation.

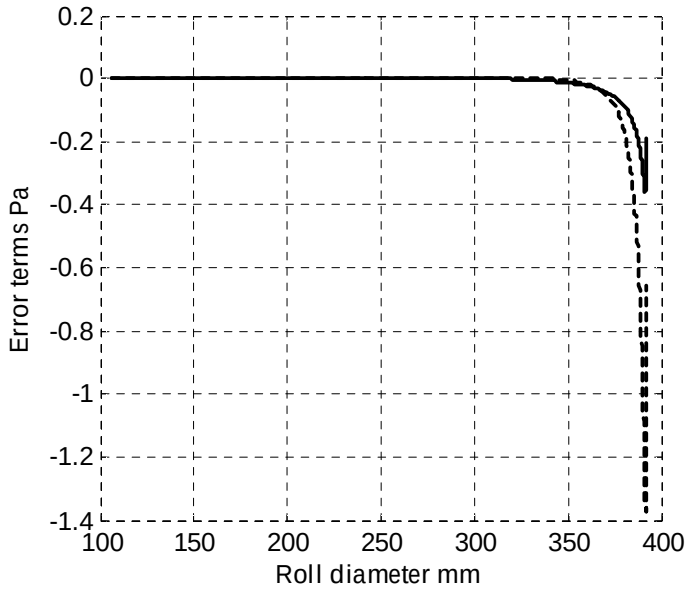

FIGURE 19 The error terms *ERRSTRAINT* = solid line and *ERRSTRESS* = dashed line for the total stress model. The maximum of the error term *ERRSTRAINR* is 4×10^{-9} Pa, so it is not drawn.

The accuracy of the total stress model is readily assured in terms of the governing equations and the material model by checking the residuals of the governing equations and the error terms *ERRSTRESS*, *ERRSTRAINR* and *ERRSTRAINT*, see FIGURE 19. The incremental stress model gives higher radial stresses than the total stress model for typical paper properties, Figure 18. The

absolute difference in tangential stresses is about the same as in radial stresses, Figure 20, but the incremental stress model gives less tangential stress. This violates the stress equilibrium equation in the plateau area, where the two stresses should be about the same.

There is about 0.22 MPa difference in the plateau area stresses in the incremental stress model whereas the difference is only 0.017 MPa in the total stress model. This error goes unnoticed if the incremental model is solved as a second order differential equation for the radial stress and the tangential stress is solved from the final total radial stress by means of the stress equilibrium equation. The error vanishes though if the displacements are not updated, but then the model is useless for computing web densities or thickness in the roll.

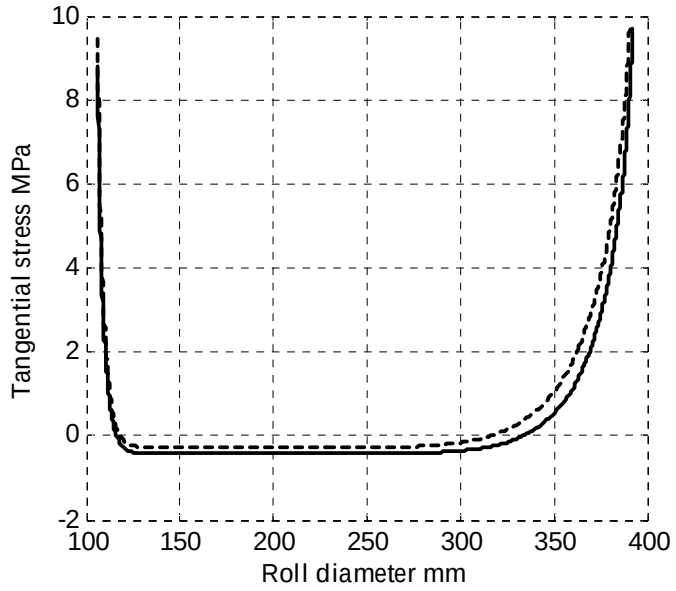

Figure 20 Comparison of the tangential stresses computed with the total and incremental stress models. Wound On Tension was 500 N / m and other parameters the same as in the previous pictures. The difference in the tangential stresses is about the same as in the radial stresses, but the incremental stress model gives less tangential stress.

The computed web thickness show clear difference between the total and incremental stress models, FIGURE 21 and FIGURE 22. The incremental model predicted web thickness is less than for the total stress model, in compliance with the higher radial stress of the incremental stress model. The dashed lines in the pictures show the difference of the successive outer diameters of the roll, which is what can be measured by the density measurement. This thickness is almost constant throughout the roll for constant WOT except near the core, where the stiff core makes it rise. On the other hand the true thickness has the same curve form as the radial strain, with thickest web at the roll surface and most compressed web near the core.

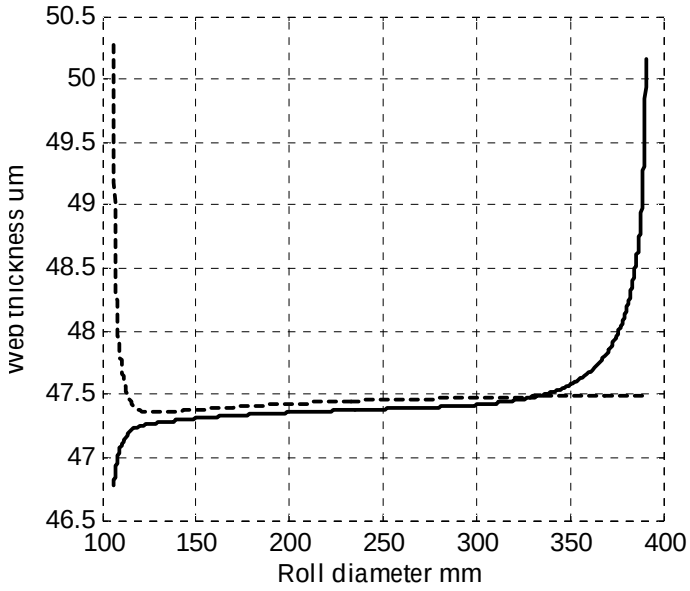

FIGURE 21 Web thickness in the roll as computed from the incremental stress model. Solid line = true thickness = r_{i+1}-r_i and dashed line = web thickness that can be measured by the measured roll diameter differences = $r_{out,i+1}$-$r_{out,i}$. The web calliper was 50.3 micrometers.

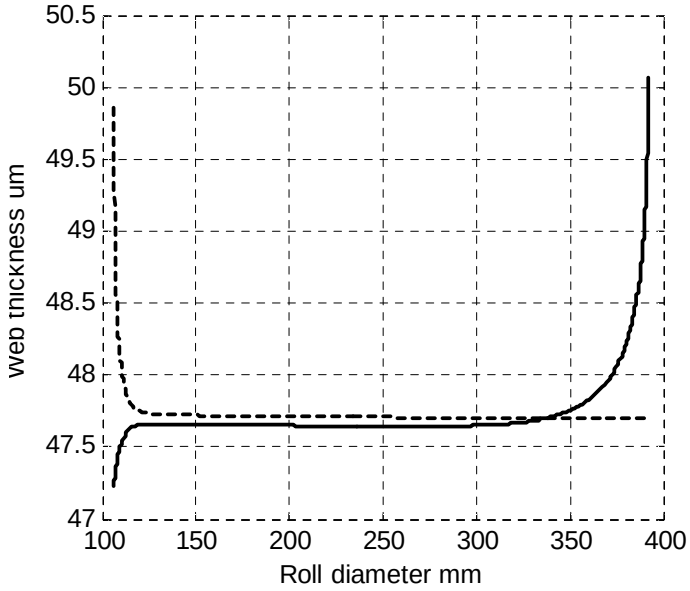

FIGURE 22 Web thickness in the roll as computed from the total stress model. Solid line = true thickness = r_{i+1}-r_i and dashed line = web thickness that can be measured by the measured roll diameter differences = $r_{out,i+1}$-$r_{out,i}$.

2.7.1 Numerical values

The simulated numerical outputs from the incremental and total stress wound roll model versions are compared in Table 4. The Wound On Tension was constant 1000 N / m and the total number of laps in the simulations was 3000.

The radial modulus polynomial was E_r=0.8152-71.50*σ_r-30.12*σ_r^2 MPa and the tangential modulus polynomial E_t=8730-76.46*σ_t MPa. The core modulus was 10000 MPa. The web calliper was 50.32 micrometers. No centrifugal forces were present. There are four simulation results in the table numbered as: 1=incremental stress model with no tension loss and displacements were not updated, 2=same as 1 but with tension loss, 3= same as 2 but with displacements updated and 4= total stress version with tension loss and with displacements updated. The length and diameter values were taken from simulation number 1. The discrepancy in the incremental stress model with respect to the force equilibrium in the plateau area is clear in the stresses of the simulation number 3. The stresses of the simulation number 2 and 4 are quite close to each other, meaning that if the incremental stress model is run without updating the displacements, it gives correct stresses as compared to the total stress model.

Table 4 Numerical comparison of the incremental and total stress versions of the wound roll model. Columns are: N=number of laps, Length = web length in m, Diameter = roll diameter in mm, σ_{rn} and σ_{tn} = radial and tangential stresses in MPa in four simulations where n is the run number.

N	Length	Diameter	σ_{r1}	σ_{t1}	σ_{r2}	σ_{t2}	σ_{r3}	σ_{t3}	σ_{r4}	σ_{t4}
10	0	106	-2.1758	18.3057	-2.1350	18.3217	-2.2824	21.1411	-2.0367	18.3900
160	54	121	-1.4093	-0.8020	-1.3739	-0.7793	-1.4833	-0.1069	-1.3529	-0.8681
310	115	136	-1.3881	-1.3358	-1.3553	-1.3314	-1.4599	-0.8079	-1.3412	-1.3584
460	182	151	-1.3854	-1.3515	-1.3556	-1.3496	-1.4588	-0.8332	-1.3436	-1.3687
610	257	166	-1.3836	-1.3530	-1.3563	-1.3515	-1.4583	-0.8397	-1.3457	-1.3688
760	339	181	-1.3820	-1.3536	-1.3568	-1.3523	-1.4579	-0.8444	-1.3476	-1.3684
910	428	197	-1.3807	-1.3536	-1.3573	-1.3524	-1.4575	-0.8478	-1.3491	-1.3678
1060	524	212	-1.3794	-1.3523	-1.3576	-1.3512	-1.4571	-0.8492	-1.3503	-1.3660
1210	628	227	-1.3781	-1.3483	-1.3577	-1.3473	-1.4565	-0.8472	-1.3512	-1.3617
1360	738	242	-1.3765	-1.3383	-1.3573	-1.3375	-1.4555	-0.8384	-1.3516	-1.3517
1510	856	257	-1.3741	-1.3161	-1.3560	-1.3154	-1.4536	-0.8162	-1.3510	-1.3300
1660	980	272	-1.3702	-1.2695	-1.3531	-1.2692	-1.4499	-0.7677	-1.3488	-1.2848
1810	1 112	287	-1.3631	-1.1763	-1.3469	-1.1768	-1.4427	-0.6697	-1.3435	-1.1942
1960	1 251	302	-1.3502	-0.9973	-1.3348	-0.9993	-1.4292	-0.4810	-1.3325	-1.0192
2110	1 397	317	-1.3266	-0.6653	-1.3121	-0.6704	-1.4042	-0.1316	-1.3113	-0.6924
2260	1 550	332	-1.2847	-0.0696	-1.2712	-0.0808	-1.3596	0.4929	-1.2721	-0.1020
2410	1 710	348	-1.2118	0.9657	-1.1996	0.9439	-1.2819	1.5728	-1.2026	0.9307
2560	1 878	363	-1.0883	2.7137	-1.0779	2.6745	-1.1504	3.3828	-1.0830	2.6815
2710	2 052	378	-0.8840	5.6009	-0.8760	5.5360	-0.9335	6.3419	-0.8828	5.5734
2860	2 234	393	-0.5515	10.3914	-0.5469	10.2924	-0.5818	11.1719	-0.5539	10.3359

2.8 The viscoelastic wound roll model as an extension of the total stress model

Viscoelasticity is one of the phenomena that introduce time dependency into the wound roll stress models. It can be modelled basically the same way as

thermal expansion was modelled in (Willet and Poesch, 1988). Viscoelasticity is easily modelled with time dependent material model laws:

$$\varepsilon_r = S_r(\sigma_r, t) - \nu_{tr} S_t(\sigma_t, t), \varepsilon_r = S_t(\sigma_t, t) - \nu_{rt} S_r(\sigma_r, t) \tag{51}$$

where the strain functions S_r and S_t need not to be given in closed form but instead they can be computed by means of linear time independent difference equations. It is natural to use difference equations instead of differential equations since the computations are anyway done in discrete time and finding the difference equation coefficients from the experimental stress strain data is basically a simple system identification task. The strain functions can be divided into the non-linear elastic S and the linear time dependent part:

$$\varepsilon_n = c_0 \varepsilon_{n-1} + c_1 \varepsilon_{n-2} + c\sigma, \varepsilon = \varepsilon_n + S(\sigma), \varepsilon_0 = 0 \tag{52}$$

where n is the discrete time index. For typical paper materials second order difference system is enough to fit with the experimental data both in tangential and radial strains. This model corresponds to the generalized Maxwell model with two viscous components and thus two time constants. The typical parameter values for LWC paper are T_1=152s and T_2=2672s and ε_∞=1,9% for the radial strain, FIGURE 23, and T_1=77s and T_2=1128s and ε_∞=0.001% for the tangential strain at 1MPa step input. The model could further be elaborated to include also the hysteresis of the nonlinear stress strain curve S, FIGURE 24. This can be accomplished by modelling the stress strain curve parameters with similar time difference equations as the creep strain was done (Austrel, 1997), (Lif, 2003).

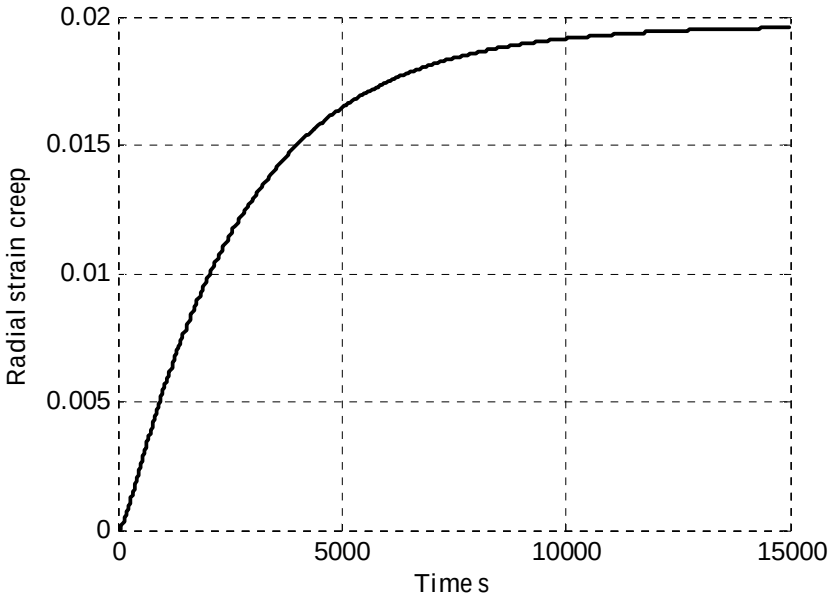

FIGURE 23 Typical simulated radial strain creep curve for LWC paper.

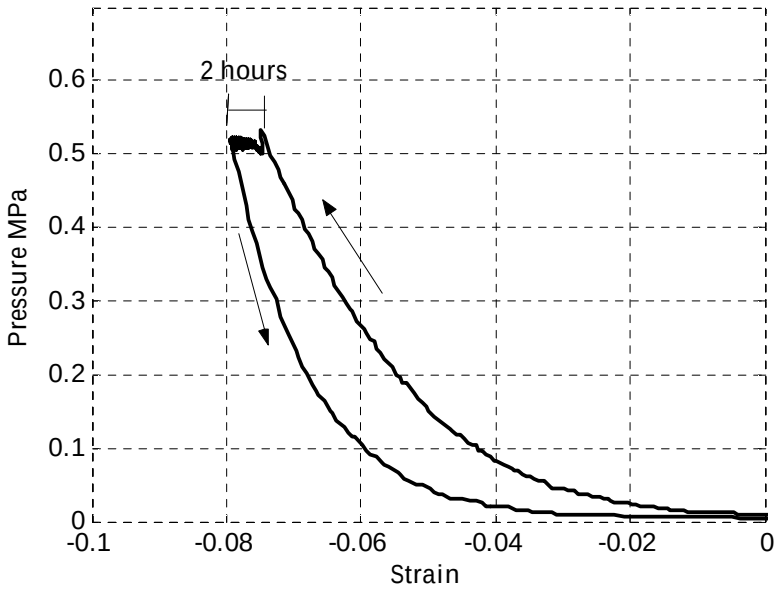

FIGURE 24 Typical stack test data for two hours creep at 0.5 MPa pressure, LWC paper. The curve shows the hysteresis in the stress curve.

The viscoelastic total stress model equations and program are otherwise the same as earlier except for the material model equations, which now exhibit the time dependence. Some complications in the program structure are caused by the need to keep track on each layer relaxation history individually, since the residence time in the roll and stress history is different for every layer.

Under steady state conditions after very long relaxation time the viscoelastic behaviour can be modelled as a linearly elastic element in series with the nonlinear material model with the elastic modulus:

$$E_\infty = \frac{c}{1 - c_0 - c_1} \tag{53}$$

where the coefficients c,c_0 and c_1 are from the viscoelastic difference equation.

The smaller viscoelastic relaxation time constant is short compared with the winding time in the laboratory winder for typical paper material, which can be something from 15 minutes to one hour. So at least part if not most of the relaxation has already occurred during the winding before the roll pressures are measured. The modelling can take this into account by running the vicoelastic model for each layer wound with the winding time of the layer. After the winding is ready the viscoelastic model is run with the stresses inside the roll and then the non-linear solver for the stress model is run again for the whole roll. This must be repeated a few times until the stresses and strains have converged to steady values, FIGURE 25.

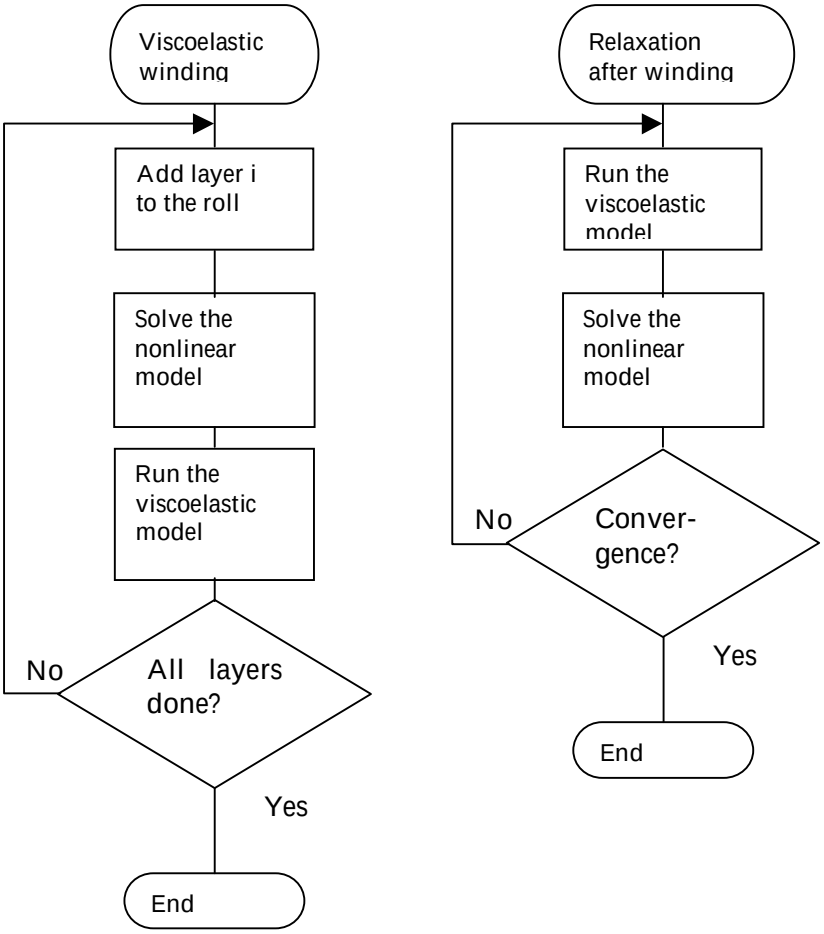

FIGURE 25 Two version of the viscoelastic model computation routine. The viscoelastic creep model can be run at every web layer added to the roll, on the left, or after winding is ready and the whole roll relaxes as a solid object, on the right.

The following figures depict the simulation results how viscoelastic relaxation during winding and after it affect the stresses and strains in a LWC paper roll. FIGURE 26 shows the radial stresses where more than half of the final radial stress relaxation has occurred already during winding time, which was rather long, 3700s. The relaxation has decreased the radial stress most of all near the core, where the stress is normally highest. This results that with highly viscoelastic paper grades and less stiff cores it is difficult to wind very tight roll bottoms. FIGURE 27 shows how much viscoelastic creep has added to the radial strains, which is less than one percent. The creep is zero at the roll surface since the stress is also zero there. FIGURE 28 shows the tangential creep strain. The final stretching of the surface layers has occurred after winding, since the residence time for these layers is very short during winding.

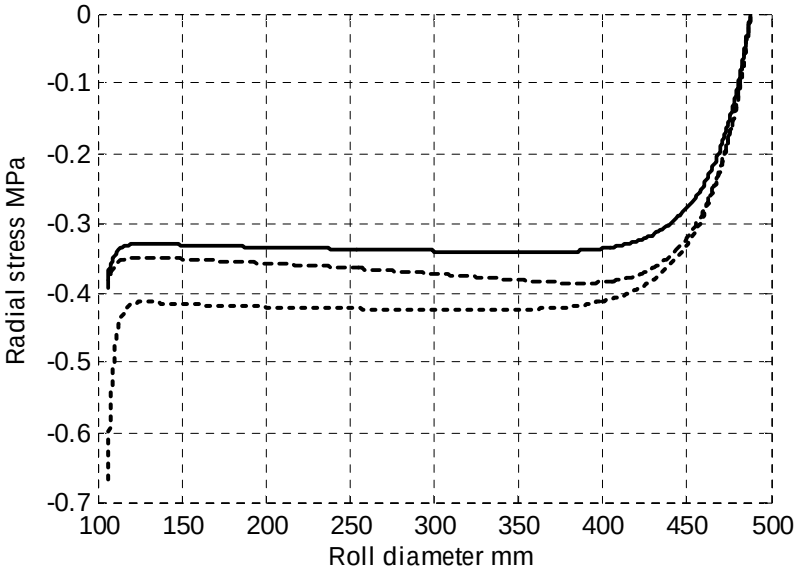

FIGURE 26 Stresses in a LWC paper roll model when viscoelasticity is accounted for. Dotted line = radial stress without viscoelastic relaxation, dashed line = radial stress after 3700 s long winding with relaxation and solid line = final relaxed radial stress at T=10000s.

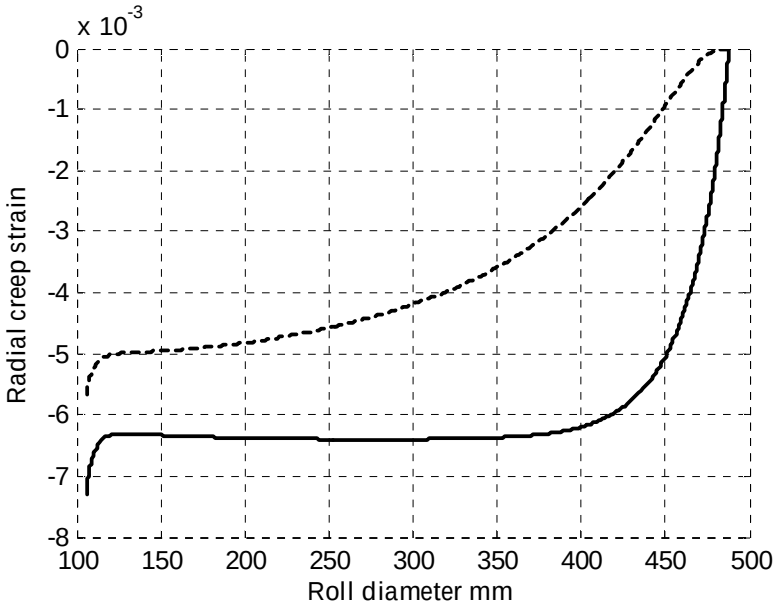

FIGURE 27 Viscolelastic creep radial strains for the previous picture roll just after winding = dashed line and at T=10000s = solid line. Comparison to FIGURE 16 reveals that the viscoelastic creep has added the radial strain about 10%.

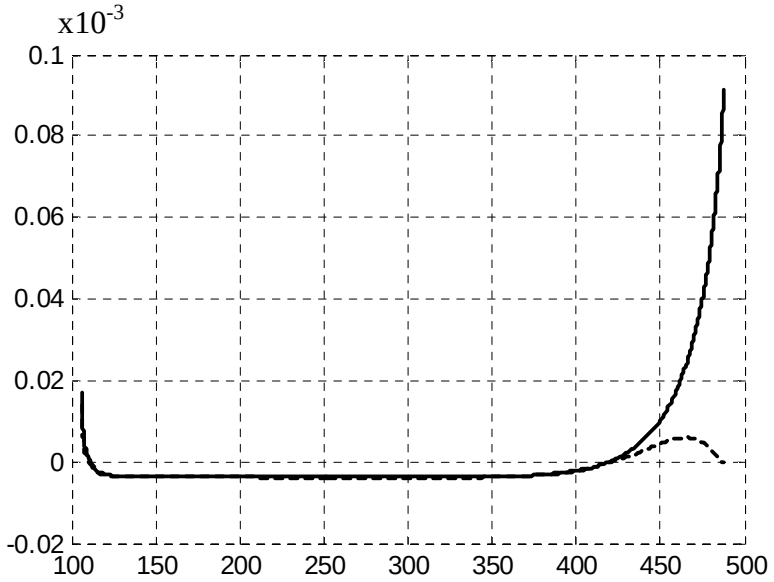

FIGURE 28 Viscoelastic tangential creep strains for the previous picture roll just after winding = dashed line and at T=10000s = solid line.

FIGURE 29 shows the radial displacements that have occurred in the roll after winding due to the viscoelastic creep. Roll outer radius has shrunk 15 micrometers and the outer surface layers have moved to smaller diameters, but inner parts of the roll have moved to slightly larger diameters.

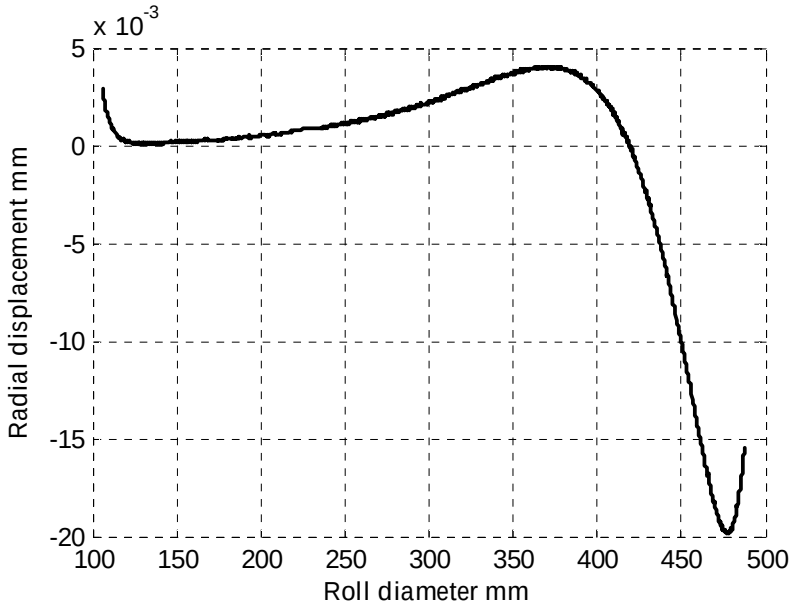

FIGURE 29 Radial displacements inside the roll after winding till T=10000s.

2.9 Non-accretive models

The accretive nature of the winding models leads to rather long program execution time, since the governing boundary value problem must be set up

and solved for every layer added to the roll. It would be tempting to find a fast track to the final solution for the whole roll as one entity. One of the recent attempts to present such a model is in (Burns *et al.*, 1999) and (Debesis and Burns, 2003). Non-accretive model can be mathematically flawless, but does not accurately model a real wound roll. The problem lies in the geometric strain conditions. If the roll is modelled to be initially composed of pretensioned hoops of the original web thickness h_i and of the radii $r_{0,i+1}=r_{0,i}+h_i$, then the radial and tangential stresses fulfil the incremental stress model strain equations exactly:

$$\varepsilon_{r,i} = \frac{\Delta u_i}{\Delta r_i} = \frac{r_{i+1} - r_{0,i+1} - \left(r_i - r_{0,i}\right)}{r_{i+1} - r_i} = 1 - \frac{h_i}{r_{i+1} - r_i} \tag{54}$$

$$\varepsilon_{t,i} = \frac{u_i}{r_i} = \frac{r_i - r_{0,i}}{r_i} \tag{55}$$

This initial pretensioned roll is then modelled to relax and find its equilibrium as one solid body.

The total stress model can be readily modified to allow this kind of "once for all" modelling: the radii tables are initiated according to the above equations and then the nonlinear solver is run once for the whole roll. The results are shown in FIGURE 30 and FIGURE 31, which where created with the same material parameter values as in (Debesis and Burns, 2003) Table 1 and Figure 1. They call their models "Clamped On Stress" and "Wound On Strain" models. What is immediately clear from the figures, is that the WOS version, that gives results close to the non-accretive version in this work, has very high tangential stress relaxation near the roll surface and consequently lower radial stresses too. On the other hand the COS model is very close to the present work accretive model. With typical paper material parameters, the non-accretive model gives extremely low stresses.

The higher tangential strain in the non-accretive model is caused by the fact that every layer's radial displacement is a result of all inner layers' radial strain sum. On the other hand, in the non-accretive model, only that part of the inner layers' radial strain causes radial displacement in the layer above them, that is present only after the layer was added to the roll.

Debesis and Burns try to explain the differences in the "COS" and "WOS" model results resulting from the differences of the outer boundary condition. This is the same argument as was used in (Good and Pfeiffer, 1992) for the "tension loss" version of the model.

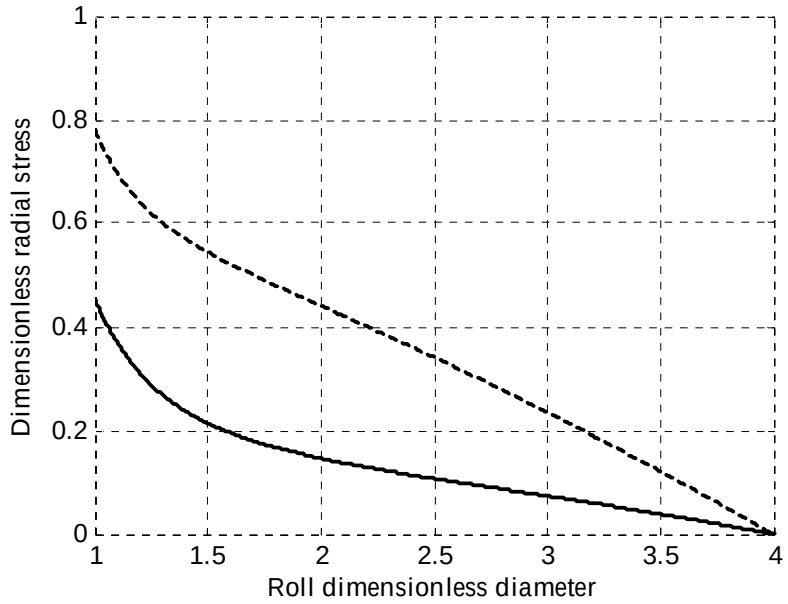

FIGURE 30 Radial stresses from the non-accretive model, solid line and the normal accretive model, dashed line. The stresses are made dimensionless by dividing them with the web tension and the roll diameter by dividing with the core diameter.

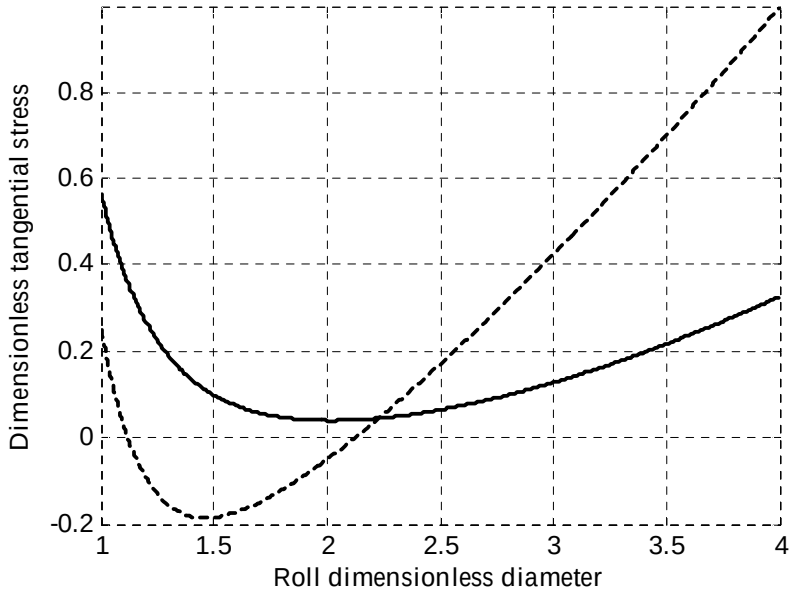

FIGURE 31 Tangential stresses from the non-accretive model, solid line and the normal accretive model, dashed line.

However, results of the "tension loss" and "no tension loss" outer boundary condition versions of the model do not explain such a great difference in the results. Even the difference between the incremental stress and total stress versions with these material parameters is insignificant. The large outermost layer tangential stress relaxation of about 70% that Debesis and

Burns show in their figures cannot be explained by the outer boundary condition alone, but must be a consequence of the model structure where the radial displacements are much larger than in the accretive models.

2.10 Solving the Wound On Stress from the wound roll stress model

Since the Wound On Tension was one of the input parameters of the wound roll stress model, some extra data is needed if the WOT is to be solved from the stress model. The layer to layer pressure can be easily measured and suits well to be the extra data for the computation. If the web material properties are such that long constant radial strain plateau area exists in the middle parts of the roll, it is enough to take the mean value of the pressure samples in the plateau area. This of course means that only the average value of the WOT could be measured. The most straightforward way to do this computation is to run the stress model with different WOT values to find out the dependence between WOT and the mean radial stress and to use this curve to solve the WOT from the experimental data (Good et al. 1999). If it is possible to centre wind the same roll, this pressure to WOT curve can also be found with experiments alone without running the stress model at all. Any of the model versions could be used for the WOT computations, but they give slightly different results.

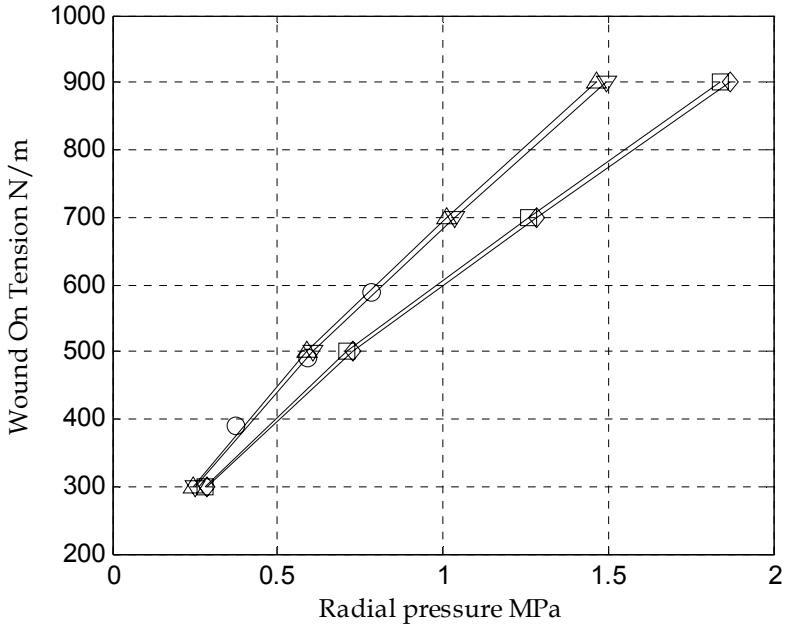

FIGURE 32 The Wound On Tension to radial pressure curves for the four wound roll stress models and three measured points with centre winding. The curves are marked Δ = total stress "tension loss" model, ∇ = total stress "no tension loss" model, □ = incremental stress "tension loss" model and ◊ = incremental stress "no tension loss" model. The measured values are marked with circles.

The results for LWC paper roll are shown in FIGURE 32. The total stress model gives more WOT for the same pressure than the incremental stress model and fits very well with the measured values. The differences between the "tension loss" and the "no tension loss" versions of the models are insignificant. For example if the measured mean interlayer pressure would be 0.7 MPa, the incremental stress model would interpolate to 496 N / m, the total stress model to 553 N / m and the measured value to 546 N / m.

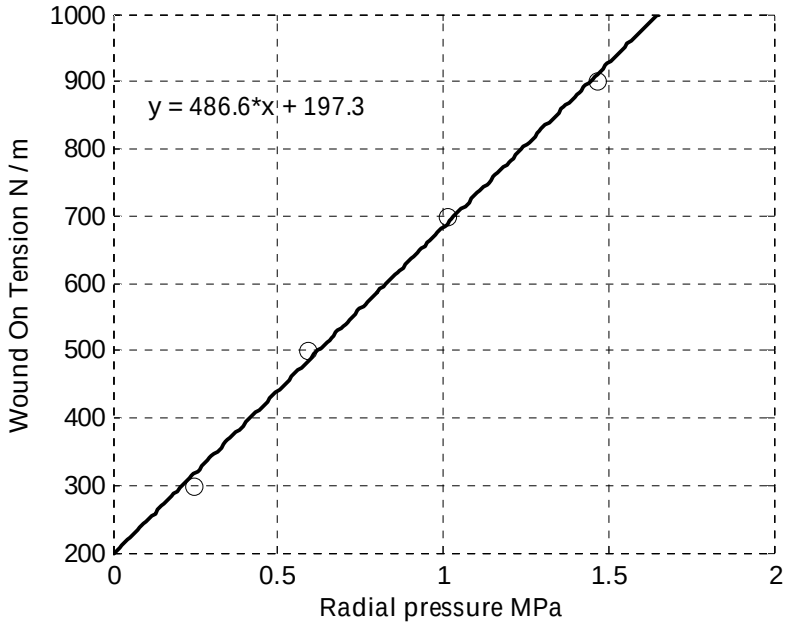

FIGURE 33 Curve fit to the total stress model radial pressure to WOT curve. The data points are marked with circles and the linear fit with solid line.

The curves can be interpolated to give the Wound On Tension from the measured roll interlayer pressure. However, the curves are linear enough so that a straight line can be curve fitted to them, FIGURE 33. The measured interlayer pressure seems to be a sensitive measure for the WOT at least in case of LWC paper rolls. However, it is only applicable in laboratory winders as an off-line measurement done after winding. There is also a great deal of variation between individual pressure measurements and also between both sides of the roll due to profile and other differences in the web with harder paper grades. So the pressure measurement is only accurate in giving an overall mean tightness value for the whole roll.

2.10.1 Solving WOT from the measured web thickness

The web thickness in the roll can also be used as the input data to the computation of the Wound On Tension. The source of the web thickness data can be the density measurement. Alternatively to the web thickness the measured roll outer radii can also be used as input data.

As the web thickness curves in FIGURE 22 show, the web thickness, which is got as the differences of the measured roll outer radii, does not give the true web thickness in the roll, but it still is very close to the true value in the middle part of the roll. The radial stress strain curve gives a known one-to-one correspondence between the web thickness and the radial stress, except for hysteresis and viscoelasticity:

$$\sigma_{r,i} = S_r^{-1}\left(\varepsilon_{r,i} + \nu_{tr} S_t\left(\sigma_{t,i}\right)\right) = S_r^{-1}\left(\frac{\frac{\partial r}{\partial i} - h_i}{h_i} + \nu_{tr} S_t\left(\sigma_{t,i}\right)\right) \tag{56}$$

This known dependence can be used to derive the radial stress if the free web calliper h_i is measured. Then the previous correlation curve from the radial pressure to WOT can be used to compute the Wound On Tension, at least in the middle part of the roll. The weakness of this method is that the web calliper is not usually known to any useful accuracy. The error in pressure with respect to error in calliper is

$$\Delta\sigma_r = E_r\left(\sigma_r\right)\Delta\varepsilon_r = -E_r\left(\sigma_r\right)\frac{\frac{\partial r}{\partial i}}{h_i^{\,2}}\Delta h_i \approx -E_r\left(\sigma_r\right)\frac{\Delta h}{h_i} \tag{57}$$

so when typical LWC paper radial modulus at 1 MPa is 40-60 MPa and calliper 50 micrometers, even modest 0.5 micrometer error in calliper causes 0.5 MPa error in pressure, which can be 50 % of the true pressure.

The pressure and Wound On Tension curves in the FIGURE 34 and in the FIGURE 35 show the calibration problem in this measurement method. The variation in the WOT pressure and curve measured from the measured web thickness in the roll is caused by the web calliper variation. For example LWC paper calliper variation within the 20000 meters wound into one roll can be 0.2 −0.3 micrometers, which can cause 50 to 150 N / m error in the computed WOT.

2.10.2 Solving WOT from the wound roll stress model

The method of inverting the wound roll stress model to have the measured web thickness or radial displacements as inputs and the Wound On Stress as output has been described in (Roisum 1990). This method is much more complicated and CPU time consuming than the previous methods but provide some extra benefits. For example, the radial and tangential stresses are got as a side product and viscoelasticity can be accounted for too. The method requires that both radial and tangential stress strain curve parameters are known in addition to the web calliper. And if the viscoelastic calculations are to be made, also the parameters characterising it will be needed too. The number of required material parameter values is much higher than in the simpler methods risking possible overfitting the results to data.

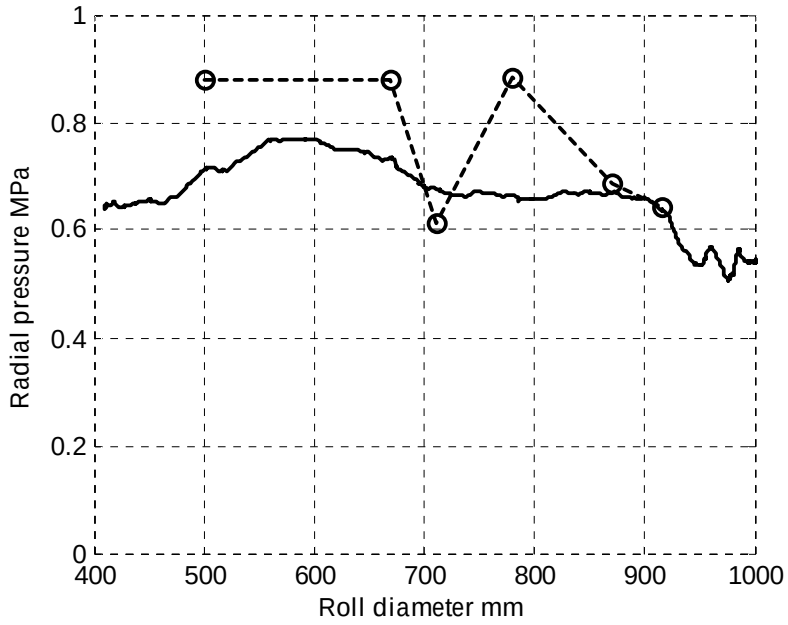

FIGURE 34 Centre wound LWC paper roll measured radial pressures = dashed line with circles at the measurement points and computed radial pressure from the measured web thickness = solid line.

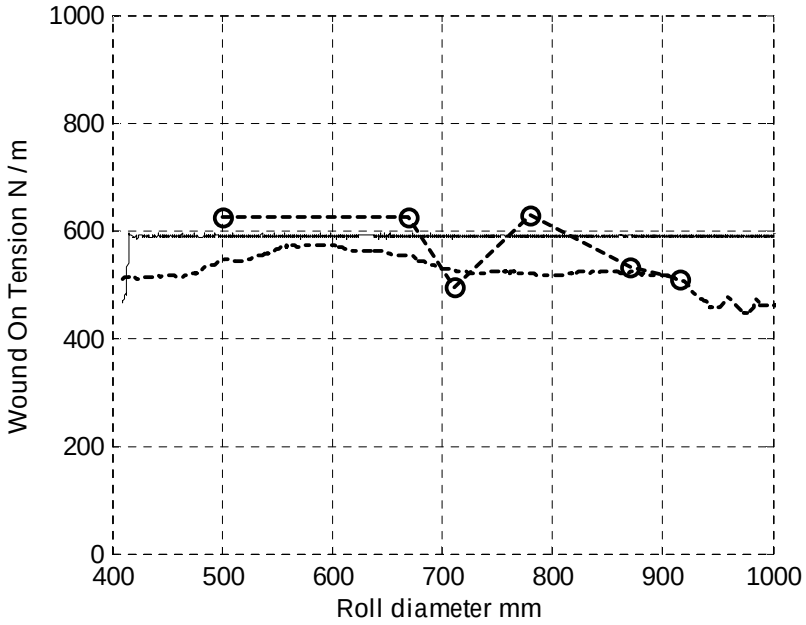

FIGURE 35 Centre wound LWC paper roll actual Wound On Tension = solid line,WOT computed from actual measured pressures = dashed line with circles at the measurement points and computed WOT from the measured web thickness = dash-dot line.

Both the incremental and total stress versions of the wound roll stress models can be solved for the WOT in a straightforward manner. As the WOT for the last layer added to the roll is unknown, one more algebraic equation is

needed to solve the ambiguity in the boundary value problem. This extra equation is got from the update equation for the deformed radius for the last layer. If this displacement equation would be simply added to the 2N size linear equation system, the new 2N+1 system of equations would not be anymore tridiagonal and the fast tridiagonal equation solver speed would be lost. This obstacle can be overcome by utilizing the fact that the stresses solved from the linear system of equations are directly proportional to the WOT. The linear system of equations can first be solved for WOT value one, and the resulting stress vector is used in the displacement equation in solving the WOT.

$$A\overline{\delta\sigma}_{WOT} = \overline{B}\times WOT_{N-1} + \overline{C} \Rightarrow \overline{\delta\sigma}_{WOT} = A^{-1}\overline{B}\times WOT_{N-1} + A^{-1}\overline{C} \tag{58}$$

for the incremental stress model, where WOT_{N-1} is the scalar last layer unknown Wound On Tension, A is the linear system coefficient matrix in columns 1 to 8 in Table 1, vector $B\times WOT_{N-1}+C$ is the last column in the table, and $\delta\sigma_{WOT}$ is the vector of stress increments. If Poisson ratios are zero and no centrifugal forces are present, then the vector C vanishes. The incremental radial displacement is

$$\delta u = r_{out,N} - r_{out,N-1} - h_{N-1} = \frac{\delta\sigma_{r,0}}{E_c} r_{out,0} + \sum_{i=0}^{N-1}\left(\frac{\delta\sigma_{r,i}}{E_r(\sigma_r)} - \nu_{tr}\frac{\delta\sigma_{t,i}}{E_t(\sigma_t)} \right) h_{0,i} \tag{59}$$

from where the Wound On Tension for the last layer can be solved in terms of the incremental stresses for WOT value one. This solution requires no iteration loops to be run and the program structure is almost unchanged from the normal incremental stress model. The roll outer radii $r_{out,i}$ as well as the web calliper h_i are measured values. Finally the incremental stresses are multiplied with the Wound On Tension.

The total stress model is modified similarly, but the WOT for the last layer is iterated in the Newton algorithm along with the stresses:

$$A\overline{\Delta\sigma}_{WOT} = \overline{B}\times \Delta WOT_{N-1} + \overline{C} \Rightarrow \overline{\Delta\sigma}_{WOT} = A^{-1}\overline{B}\times \Delta WOT_{N-1} + A^{-1}\overline{C} \tag{60}$$

where A is now the Jacobian matrix and vector $B\times\Delta WOT_{N-1}+C$ the residual vector partitioned into terms containing the WOT and the other terms. The update step for the WOT is solved at every Newton iteration step from the displacement equation

$$\Delta u_{N-1} = r_{out,N} - r_{N-1} - h_{N-1} = \frac{\Delta\sigma_{r,0}}{E_c} r_{out,0} + \sum_{i=0}^{N-1}\left(\frac{\Delta\sigma_{r,i}}{E_r(\sigma_r)} - \nu_{tr}\frac{\Delta\sigma_{t,i}}{E_t(\sigma_t)} \right) h_{0,i} \tag{61}$$

where the displacement step Δu_{N-1} eventually converges to zero when the layer radius r_{N-1} is updated at every iteration step:

$$r_{N-1} = \left(1 + \frac{\sigma_{r,0}}{E_c}\right) r_{out,0} + \sum_{0}^{N-2} \left(1 + S_r\left(\sigma_{r,i}\right) - \nu_{tr} S_t\left(\sigma_{t,i}\right)\right) h_i \tag{62}$$

Again the program structure is almost unchanged compared to the normal total stress model except for the above equations to solve the WOT inside the Newton iteration. The iteration may take some extra steps to converge, which increases the execution time.

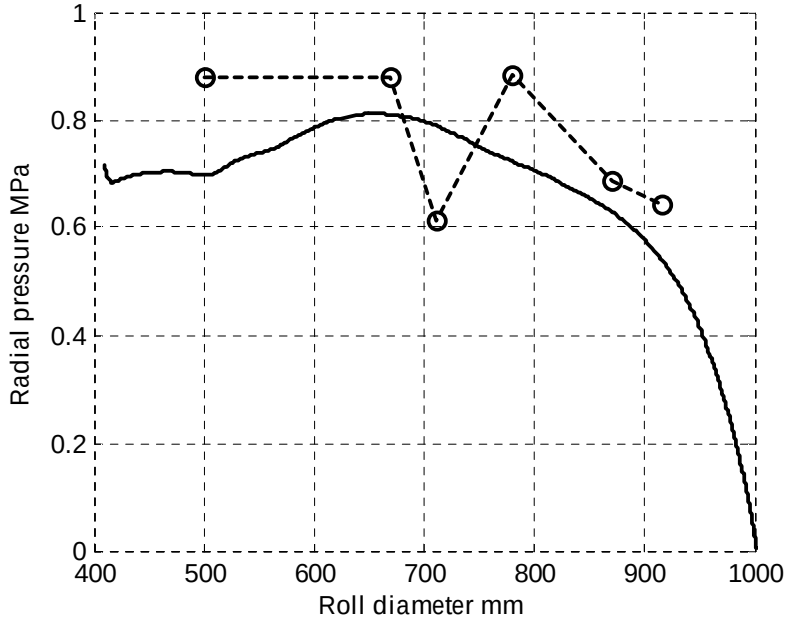

FIGURE 36 Centre wound LWC paper roll measured radial pressures = dashed line with circles at the measurement points and computed radial pressure from the measured web thickness = solid line.

The results from a centre wound LWC paper roll are in FIGURE 36 and FIGURE 37, which were computed with the total stress model and constant web calliper of 50.3 micrometers. The results clearly lack accuracy, mainly due to the inaccurate web calliper value, the same problem that also plagued the simpler method presented in the previous chapter.

Clearly an accurate on-line calliper measurement is needed to improve the accuracy of the Wound On Tension measurement, as was mentioned in (Roisum 1990). The commercial paper calliper measurement devices typically provide resolution if not accuracy about 1 micrometer, which is not enough for typical printing papers like LWC and Newsprint in the 40-80 micrometers range. To overcome this problem a replacement for the direct calliper measurement was devised for this work suitable for laboratory winding, which will be explained in the next chapter.

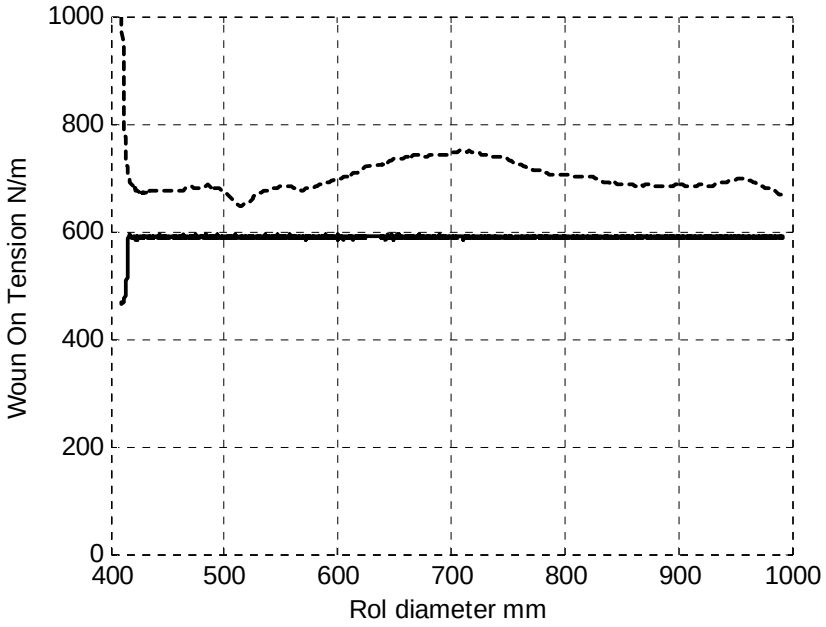

FIGURE 37 Centre wound LWC paper roll actual Wound On Tension = solid line and computed WOT from the measured web thickness = dashed line.

2.10.3 Solving the web calliper from the wound roll stress model.

In centre winding the Wound On Tension is known, that is the web tension. This opens the possibility to solve the wound roll stress model for the unknown web calliper instead of the Wound On Tension as was done in the previous chapter. This method is even easier to implement than the WOT algorithm and the modifications required to the wound roll stress model are minor. The diameter of the new layer just added to the roll is updated from the diameter measurement. The web calliper is computed as a difference of this outer diameter $r_{out,N-1}$ and the deformed previous layer diameter r_{N-2}, which is got from the model:

$$h_{N-1} = r_{out,N-1} - r_{N-2} \tag{63}$$

Otherwise the model structure and program remains the same, both for the incremental and total stress versions. The web calliper measured from a LWC paper roll with this method is shown in the FIGURE 38. The calliper measured in the stack testing machine was 50.3 micrometers. The reason why the calliper in the stack testing machine was higher is mostly due to the bulk loss when the roll was run several times after the sample for the stack testing machine was taken from it.

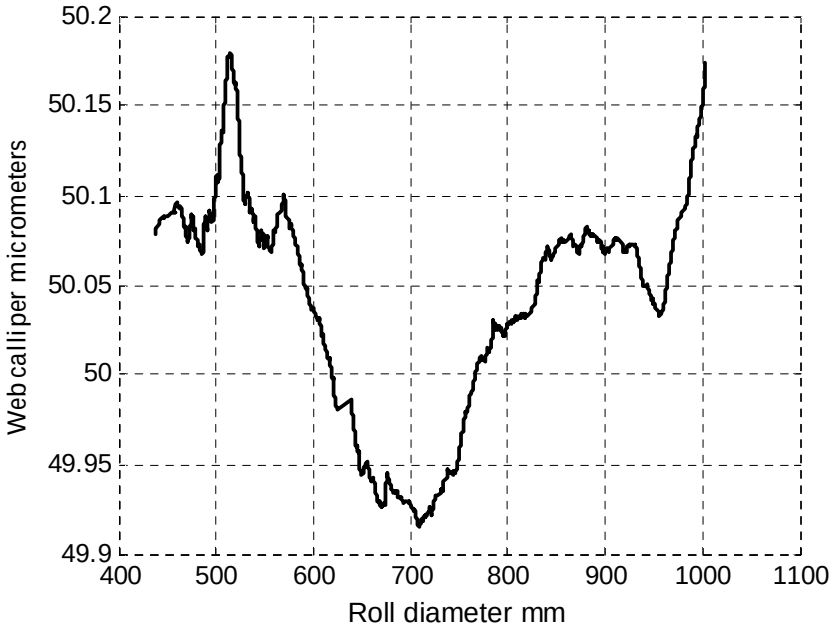

FIGURE 38 Indirectly measured web calliper by means of the wound roll model from a centre wound LWC paper roll. The calliper measured in the stack testing machine was 50.3 micrometers.

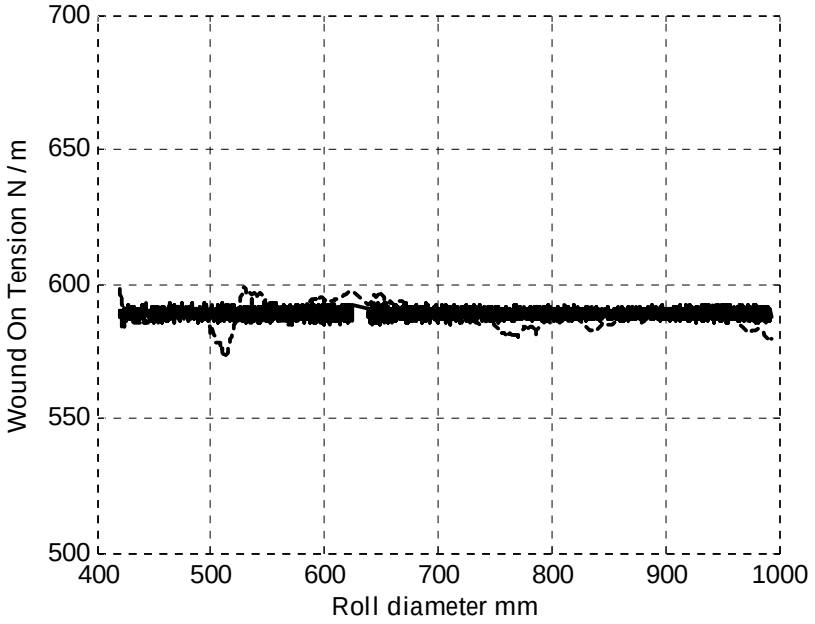

FIGURE 39 Actual and computed Wound On Tension in a LWC paper roll, when the web calliper was measured with the stress model. Solid line = actual web tension, dashed line = computed Wound On Tension.

The Wound On Tension curves in FIGURE 39 show excellent agreement, which is not surprising, since the computations for both the calliper and the WOT was done on the data got from the same centre winding run, so it merely

tests the program. The usefulness of the method is seen when the roll is first centre wound for calliper measurement and then again surface wound for WOT measurement.

2.10.4 Wound On Tension measurement for surface winding

The Wound On Tension measurement method presented in the previous chapter is an efficient way for WOT measurement in a laboratory winder. Two winders are needed, one for surface winding and another for centre winding, or only one if the same winder is capable of doing both centre and surface winding. Even better is a set up, where the centre and surface winding can be done without taking the roll out of the winder between them. This can be done, if the winder can wind the roll in both directions, that is the direction of rotation of winding drums and the rolls are reversed and the other end of the winder works as a centre winder and the other end as a surface winder, FIGURE 40.

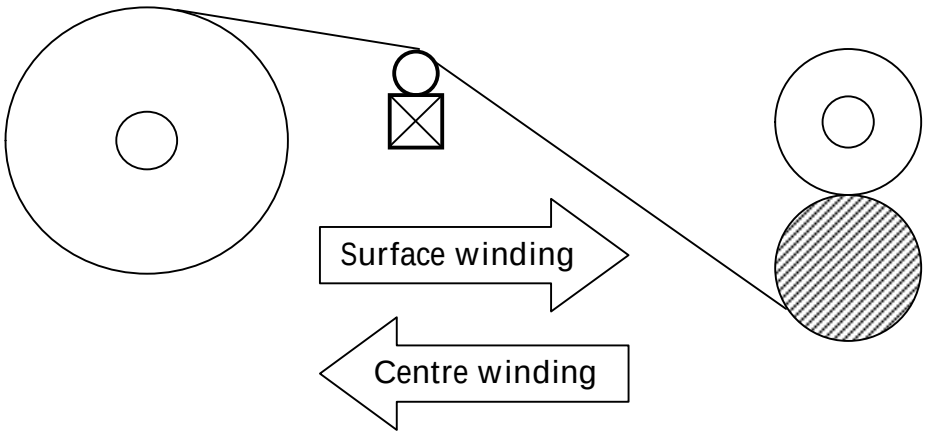

FIGURE 40 Laboratory winder with reversible winding capable of doing both centre winding on the left and surface winding on the right.

The web calliper measurement is done on every centre winding before every surface winding. This arrangement makes it possible to measure the bulk loss at every surface winding and has the additional benefit that the roll is wound to the same tightness before each surface winding.

The method was applied to a LWC paper roll, which was surface wound at 8000 N / m nip loading, 650 N / m web tension and 800 m / min web speed. No winding torque or surface traction was applied on the roll. The results are shown in FIGURE 41-FIGURE 43. The measured Wound On Tension varied from 1000 to 1070 N / m except for the first 50 mm of winding. The radial pressure computed with the total stress model and with pressure sensitive resistors coincide well, and the highest pressure is 1.64 MPa. The lower pressure area at roll surface extends deep into the roll, about 200 mm in diameter. The measured caliper varied in between 49.95 to 50.40 micrometers, and the web thickness in the roll is about 3.3 micrometers less than the free web caliper and the radial strain is about 6.6-6.7 %. This example shows why the

simpler methods presented in the earlier chapters cannot be used with very tight rolls, where the plateau area of constant stress is short. It also demonstrates how the paper calliper in a typical LWC roll varies and would cause error in the WOT measurement if the calliper variation would not have been compensated with the calliper measurement.

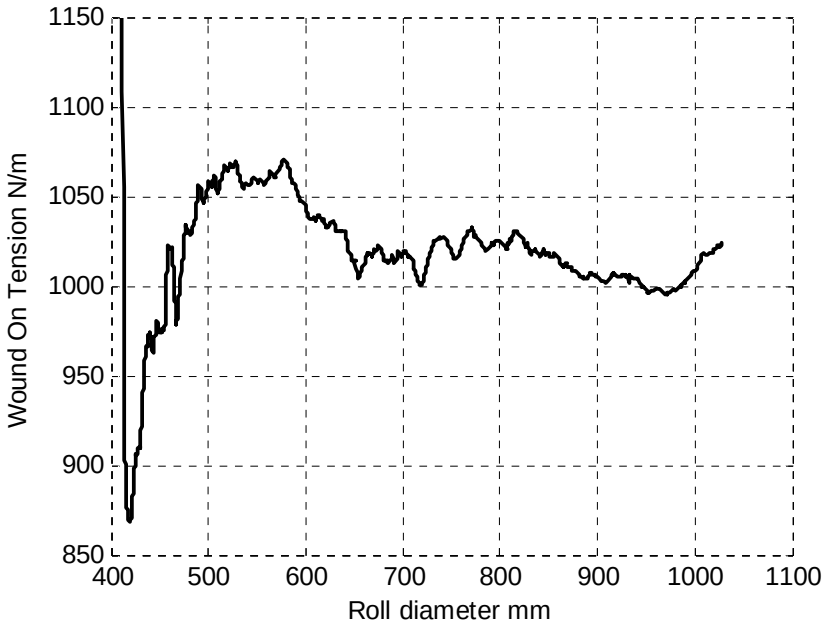

FIGURE 41 LWC paper roll was surface wound with 8000 N / m nip loading, 650 N / m web tension, 800 m / min web speed and with no winding torque. The curve shown is the indirectly measured Wound On Tension with the web calliper variations compensated by means of the indirect calliper measurement.

The comparison of the measured pressures to the computed pressure is a means of cross checking the results of the WOT measurement. If the WOT would be computed by adjusting the wound roll stress output to the measured stress, this check would be lost. The method provides a way to link together two independent measurements, the web thickness measurement and the pressure measurement. The measured Wound On Tension value relies on the information from both of these measurements. The measured WOT can be checked also by means of the unwind web thickness measurement in FIGURE 43. The previous centre winding in the reverse direction was wound at web tension of 700 N / m, which accounts for the higher web thickness in the unwound roll.

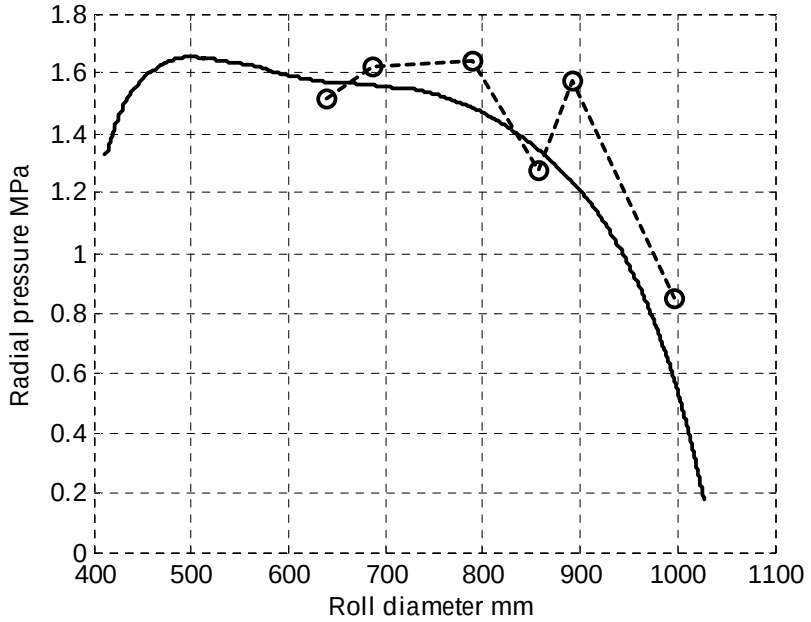

FIGURE 42 LWC paper roll measured radial pressure = dashed line with circles in the measurement points, solid line = computed pressure.

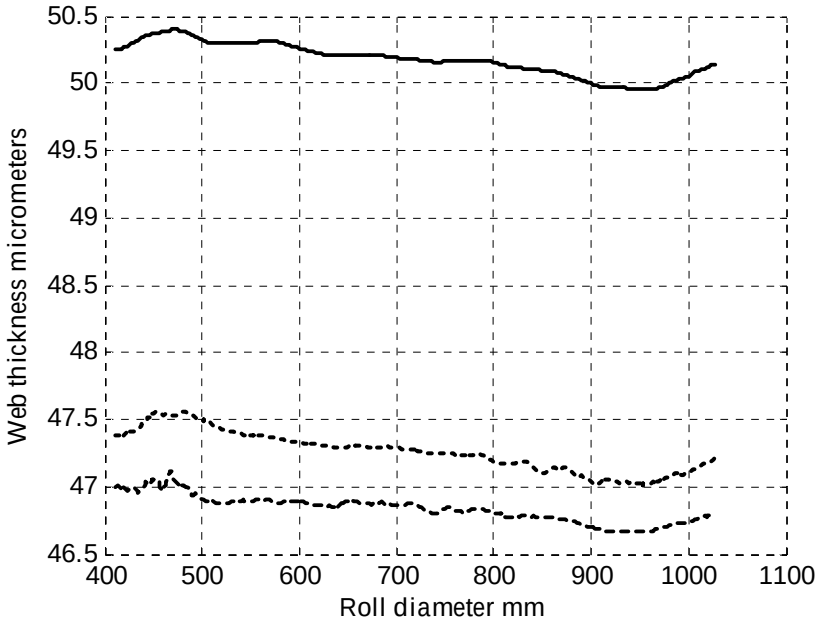

FIGURE 43 LWC paper roll computed web calliper = solid line, measured windup web thickness = dashed line and measured unwind web thickness = dotted line.

2.11 Summary

The two basic variants of the wound roll stress models, the incremental stress and the total stress versions were presented and compared. The incremental stress model can be seen as an approximation of the total stress model. The approximation is done by means of linearizing the non-linear material model equations, so that the boundary value problem equations (13)-(16) are linear with respect to the unknown stresses. Thus the equations can be solved with faster linear problem numerical solvers.

The total stress version on the other hand uses the non-linear material model equations (19) and (20) instead of the linearized equations (7) and (8), so the boundary value problem consisting of equations (25), (33)-(35), (38) and (39)-(41) is also non-linear.

The longer CPU time demand of the total stress version is compensated by better accuracy, especially when large deformations are accounted for. The better accuracy of the total stress version is not a consequence of the numerical solver performance or for example the discretizing grid size, but it stems from the non-linear model equations. The three residual error terms in equations (21)-(23) can be made arbitrary small by letting the non-linear solver to iterate to smaller residuals at every web layer. This means that the solution will fulfill the governing equations, the force equilibrium and the non-linear material model equations, to the required precision. The same is not true for the incremental stress version, but the residual errors cannot be made to vanish for example by decreasing the discretizing grid step.

Both model versions can be modified for the inverted Wound On Tension and web calliper computations, but again the total stress version works with better accuracy. The total stress version of the wound roll stress model has the advantage over the incremental stress version that the viscoelastic material model fits the model structure without extra pain.

The Wound On Tension computation by means of the wound roll stress model can be done with two alternative ways. The simpler method is to start from the measured roll radial pressures, and iteratively find the WOT that produces the same plateau pressure from the model that was measured in the roll. The more complicated method uses the measured web thickness values and the inverted roll model for WOT computation. The advantage of the simpler pressure method is that it is not as sensitive to web calliper variations, but on the other hand it can only produce average WOT value over the whole roll diameter and cannot account for viscoelasticity. And since it depends on the more inaccurate pressure measurements compared to the web thickness measurement, it is inevitably less accurate.

The more complex web thickness to WOT computation needs the measured web calliper in order to get accurate results. The web caliper within one LWC paper roll can vary about 0.2-0.3 micrometers, which could cause several hundred N/m error in the computed WOT. This problem can be overcome by means of the presented web calliper computation. The method has also the advantage that its results can be validated by comparing the computed radial stresses to the measured stresses.

3 NONLINEAR VISCOELASTIC PAPER PROPERTIES

The elastic properties of paper are the most important paper characteristics affecting winding. As this work handles only the one-dimensional winding (radial direction only), the paper elastic properties need to be determined only in the machine direction MD = tangential direction in the roll and in the z-direction = radial direction in the roll.

The usual elastic material model parameters are the elastic moduli, Poisson ratios and the shear moduli arranged in the constitutive matrix *C* .The three dimensional stress-strain relation can the be written in the compact form (Persson, 1991):

$$\bar{\varepsilon} = \bar{C}\bar{\sigma} \qquad 64$$

where the stress and strain vectors have six components for the normal and shear stresses and strains. As the one dimensional winding model is developed based on the plane stress assumption and axisymmetric condition, the shear and cross-machine stresses vanish. The only stresses appearing in the roll's cylindrical coordinates are the radial and tangential stresses, which are directly linked together by the geometric conditions.

However, this usual linear elastic description is not valid for paper material, which is highly non-linear at least in the z-direction and also has viscoelastic if not viscoplastic properties, which cannot be neglected in real winding. The non-linear wound roll model used in this work is based on the machine and z-direction stress to strain curves and the elastic moduli are needed only in the numerical solver. In this case most emphasis is put on finding parametric curves that best fit to the measured stress strain curves and are easy to compute.

There have been several suggestions for the stress strain curves in the past literature. Few examples of the functions have been collected in the following table along with their inverse functions and derivatives. The inverse function,

which gives stress as a function of strain, is not actually needed in the wound roll stress model except for error checking.

Table 5: Different forms of parametric functions that can be fitted to the stress strain measurement data. The first column in the table shows the stress to strain function, the second column its inverse function, either analytical or curve fit and the third column the elastic modulus as a function of the stress. The first line is the Pfeiffer exponential function, (Pfeiffer 1996), the second line the Hakiel second order modulus, (Hakiel 1987), the third line the polynomial function fit presented in (Willet & Poesch 1988), the fourth line the exponential strain function presented in (Piper 1995), and the last line is the hyperbolic function (Persson 1991). The modulus can in all cases be computed as a polynomial of stress or the exponential function of stress. The relation between the parameters on line 2 are:

$$a_1 = \frac{1}{\sqrt{C_1^2 - 4C_0C_2}}, a_2 = \frac{C_1a_1 + 1}{C_0a_1 2}, a_3 = \frac{C_1a_1 - 1}{C_0a_1 2}$$

	Stress to strain	Strain to stress	Elastic modulus
1)	$\varepsilon(\sigma) = \frac{\ln\left(C_1\frac{\sigma}{C_0}+1\right)}{C_1}$	$\sigma(\varepsilon) = \frac{C_0}{C_1}\left(\exp(C_1\varepsilon)-1\right)$	$\frac{\partial\sigma}{\partial\varepsilon}(\sigma) = C_1\sigma + C_0$
2)	$\varepsilon(\sigma) = a_1\ln\left(\frac{a_2\sigma+1}{a_3\sigma+1}\right)$	$\sigma(\varepsilon) = \frac{1-\exp\left(\frac{\varepsilon}{a_1}\right)}{\left(a_3\exp\left(\frac{\varepsilon}{a_1}\right)-a_2\right)}$	$\frac{\partial\sigma}{\partial\varepsilon}(\sigma) = C_2\sigma + C_1\sigma + C_0$
3)	$\varepsilon(\sigma) = \sum_{n=0}^{N} C_n\sigma^n$	$\sigma(\varepsilon) = \sum_{n=0}^{N} A_n\varepsilon^n$	$\frac{\partial\sigma}{\partial\varepsilon}(\sigma) = \sum_{n=0}^{M} B_n\sigma^n$
4)	$\varepsilon(\sigma) = C_0\sigma - \sum_{n=1}^{N} C_n\left(1-\exp(C_{n+1}\sigma)\right)$	---	$\frac{\partial\sigma}{\partial\varepsilon}(\sigma) = \sum_{n=1}^{N} C_nC_{n+1}\exp(C_{n+1}\sigma) + C_0$
5)	$\varepsilon(\sigma) = \frac{C_0\sigma}{1-C_1\sigma}$	$\sigma(\varepsilon) = \frac{\varepsilon}{C_1\varepsilon + C_0}$	$\frac{\partial\sigma}{\partial\varepsilon}(\sigma) = \frac{(1-C_1\sigma)^2}{C_0}$

The measured stress to strain data is fitted to the functions in the Table 5 by means of the least squares algorithm to find values for the free parameters. Most of the functions are non-linear in terms of the parameters, so the more complicated non-linear least squares algorithm is needed. On the other hand most of the modulus functions are linear in terms of the parameters, so the simpler linear least squares can be used to fit them to the differentiated

measurement data. The parameter values found with the linear least squares can be used as initial values for the non-linear least squares iterative solver to get better fit for the stress to strain curve.

3.1 Z-direction stress strain measurement and least squares fit

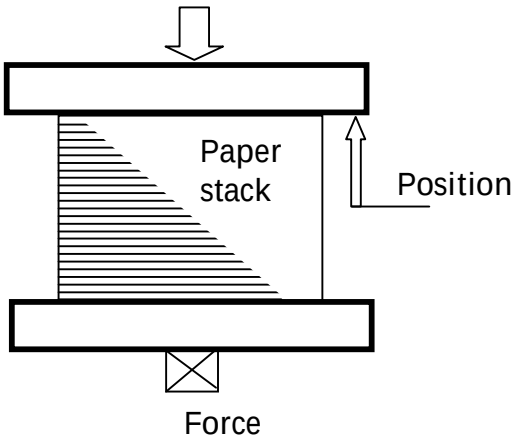

FIGURE 44 Stack testing machine. The stack size is 70x70 mm = 4900 mm^2. The force measurement range is 0 –50000N = 0 –10 MPa and the position measurement accuracy is 1 micrometer. The upper and lower steel plates are pivoted so that no torque is applied on the sample stack or on the force sensor. The position sensors as arranged so that inclination does not cause position measurement error.

The z-direction stress strain measurement is done in the stack testing machine, FIGURE 44. The square sample is 70 mm wide and 30-40 mm high containing 400-1000 sheets of paper. It is pressed in the machine to the highest pressure it will undergo during winding with constant strain rate and then released with the same speed. This measurement cycle is then repeated 2-3 times and the second or third rising curve is used to fit the stress strain function. The paper calliper is measured from the same sample if the number of sheets is known from the stack height where the force rises above a limit. The viscoelastic tests are done in the same machine. The creep test is done under constant pressure and the position creep is logged over long period of time. The relaxation test is done in the same way but under constant position and the pressure relaxation is measured.

The reason to use the second rising curve for the curve fit is, that the web is put under a rising pressure cycle when it is wound into the roll and that the web was stored under pressure in a roll prior it was again wound. The SC paper compresses about 3 micrometers or 7 % under the 1.6 MPa pressure. The lowering curves are “harder ” than the rising curves, that is they rise sharper. The hysteresis is clear and the curves are very nonlinear, FIGURE 45.

The second order polynomial elastic modulus fit is shown in FIGURE 46. The data is visibly nonlinear with respect to stress, so second order polynomial is justified even though first order line could also have been fitted. Since the data was collected at samples evenly spaced in strain, they are more densely

populated at low pressures, which gives more weight for the low pressure samples in the least squares fit. This could have been corrected with resampling.

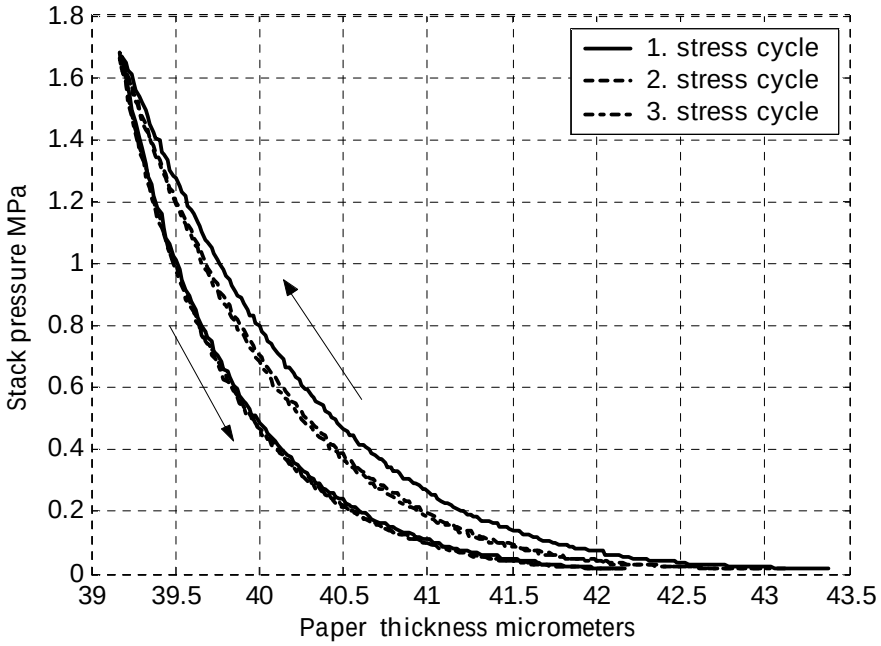

FIGURE 45 SC paper stack testing data. The stack was pressed three times with 0.2 %/s strain rate up to 1.6 MPa pressure. The paper calliper was measured as 43.38, 42.97 and 43.12 micrometers respectively. The threshold pressure to detect the press plate impact with the stack was set to 0.014 MPa. The curves start with very low slope so the measured calliper is sensitive to the threshold pressure. The first rising curve is offset from the other rising curves but rest of the rising and lowering curves coincide.

The goodness of the fit can be compared in FIGURE 47, where two stress strain curve fits are compared. The function fitted is in both cases the second order elastic modulus polynomial on line two in Table 5. The curve parameters for curve 1 are got from the linear least squares fit in FIGURE 46, whereas the curve 2 is directly adjusted to the stress strain data with non-linear least squares. The second curve fits much better to the measurement data, the error in strain would be largest at low pressures if curve 1 would be used in the wound roll stress model computations. The goodness of the fit can be more precisely compared with the "root mean squared" error norm:

$$RMSerror = \sqrt{\frac{\sum_{n=1}^{N} (\varepsilon_n - \varepsilon(\sigma_n))^2}{N}} \qquad 65$$

where ε_n and σ_n are measured data and $\varepsilon(\sigma)$ is the fitted curve. The value of this error norm is 0.0059 for the curve 1 and 0.0010 for curve 2.

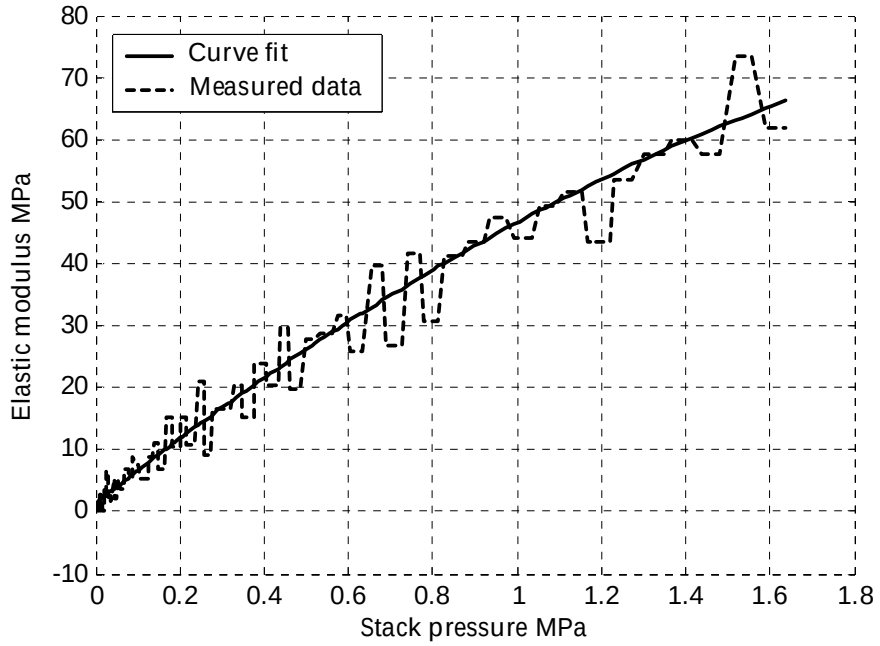

FIGURE 46 Curve fit to the differentiated stress strain data. The fitted curve is a second order polynomial in stress.

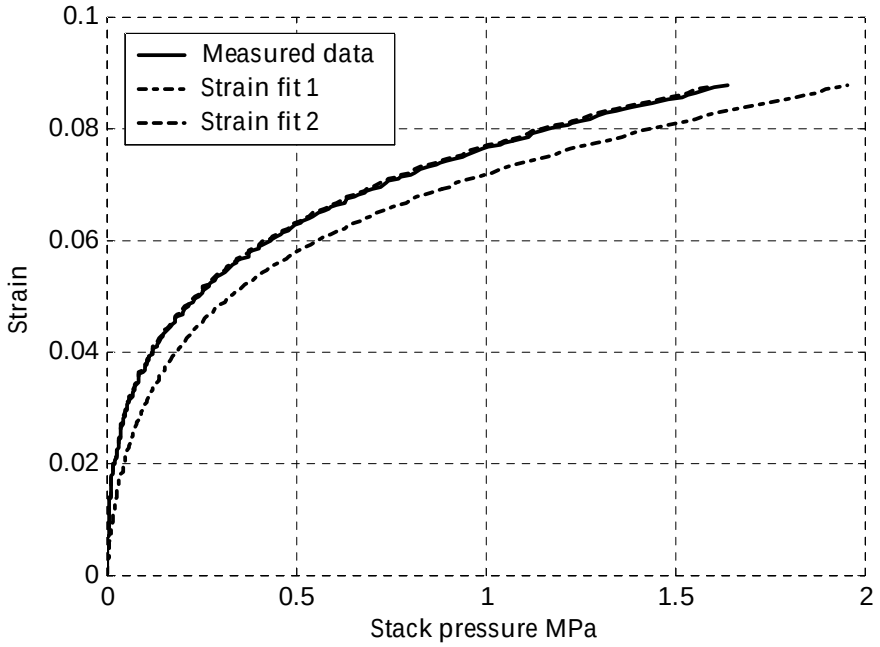

FIGURE 47 Curve fit to the stress strain data. Curve fit 1 parameters are got from the second order elastic modulus polynomial in FIGURE 46 and curve fit 2 is fitted with nonlinear least squares.

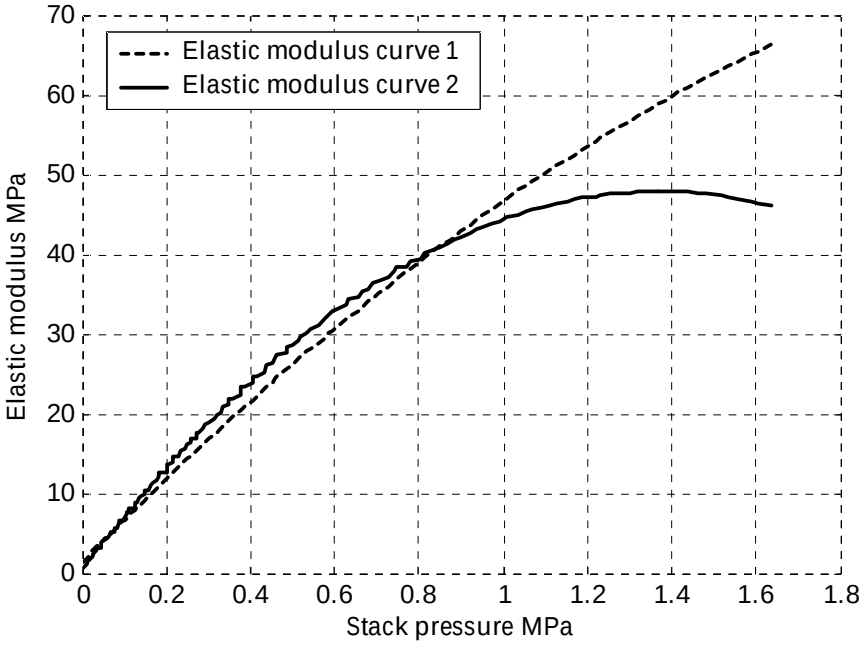

FIGURE 48 The elastic modulus curves got from the previous data as linear least squares fit to the differentiated measurement data = curve 1 and wit nonlinear least squares fit to the stress strain data = curve 2.

The elastic modulus curve in FIGURE 48 for the nonlinearly fitted stress strain curve does not look as "good" as the curve that was got with the linear fit to the differentiated data. This shows that the logarithmic curve does not perfectly fit with the data at higher pressures. But the overall good fit shown in FIGURE 47 is more important than the not perfect fit for the elastic modulus, at least when the total stress wound roll model is used. And the elastic modulus curve is an auxiliary function that is needed only for the numerical solver of the total stress model. The accuracy of the solution depends on the accuracy of the stress strain curve, not on the elastic modulus curve. The elastic modulus curve does not go through the origin, which means that the paper has some stiffness also at zero stress. On the other hand, all the stress strain curves in Table 5 do go through the origin, including the polynomial curve if C_0 is forced to zero. This is physically reasonable, since the strain should be zero at zero stress according to the definition.

3.2 MD-direction stress strain measurement and least squares fit

The machine direction stress strain data was measured in a similar manner to the Z-direction data in the pull test machine, FIGURE 49. The main difference is that now only a single 205 times 50 mm sheet of paper can be tested at a time. To get a more reliable estimate several measurements of samples taken from different CD positions from the roll should be averaged. The CD stress strain measurement was done on the first pull cycle lowering stress curve. This is justified because the web is stretched to the maximum tension before it enters

the roll and the tension is relaxed while winding. And the web was mostly under negative tension in the roll from where it was unwound.

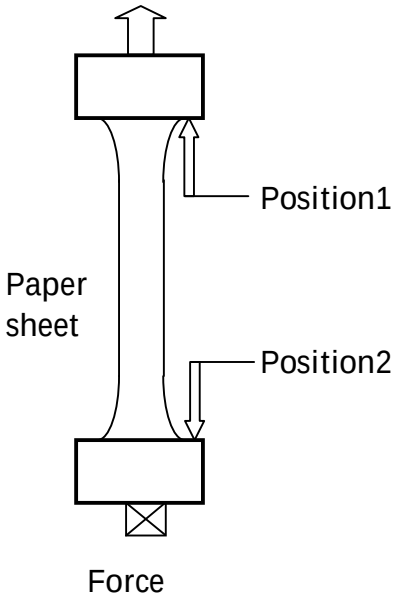

FIGURE 49 Pull test machine. The sheet is 50 mm wide and 205 mm long strip of paper. The force measurement range is 0 –100 N = 0 –40 MPa depending on paper thickness. The upper and lower clamp positions are measured with two laser displacement sensors with 1 micrometer accuracy.

The raw pull test data from a SC paper sample is in FIGURE 50. The curve fit chosen was the linear elastic modulus simple logarithm in line 1 in Table 5. The fit was done with nonlinear least squares and the result is shown in FIGURE 51. The fit is very good and the *RMSerror* is 1.68e-005. The resulting elastic modulus function, which is in this case a straight line, is shown in FIGURE 52. The elastic modulus is almost two times higher at normal winding tensions as it is at zero tension, so the nonlinear nature of the stress strain data cannot be neglected also in the machine direction.

3.3 Z-direction creep test

The viscoelasticity parameters were measured with creep test, where the sample is put under constant stress and the creep in stack height is logged under long period of time. The pressure used should be close to the pressure in the roll and the testing time long enough to find out the longest time constants.

The system model chosen is a linear time invariant differential or difference equation, so standard system identification tools could be used, like those found in Matlab. The system identification can also be done by nonlinear least squares fit of the step response function to the creep test data. For a second order system with two time constants the step response function for strain is:

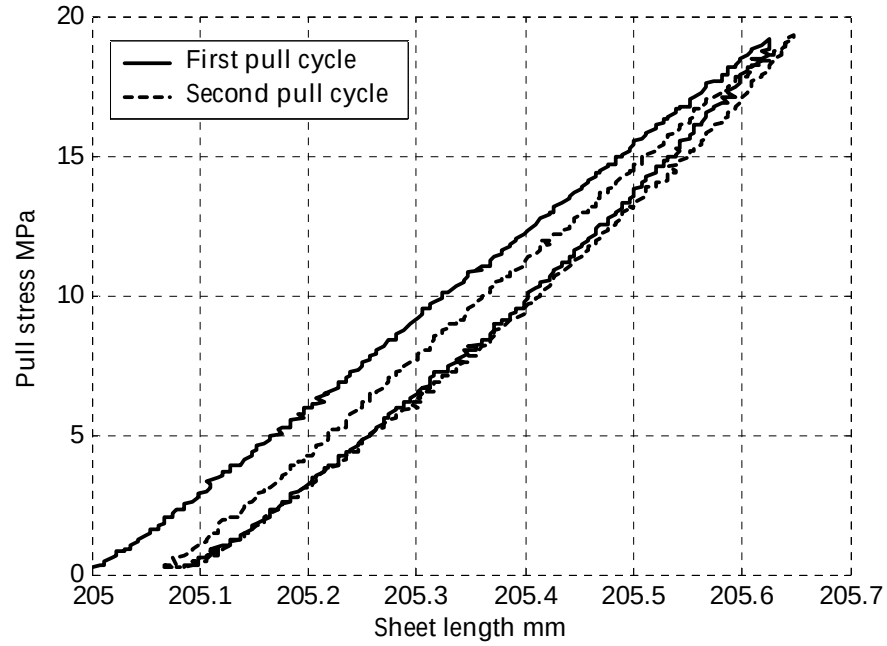

FIGURE 50 SC paper pull test data. The sheet remains stretched 0.066 mm after the first pull and the hysteresis is clear. The threshold stress was set to 0.2 MPa to detect when the clamps start to tension the sheet.

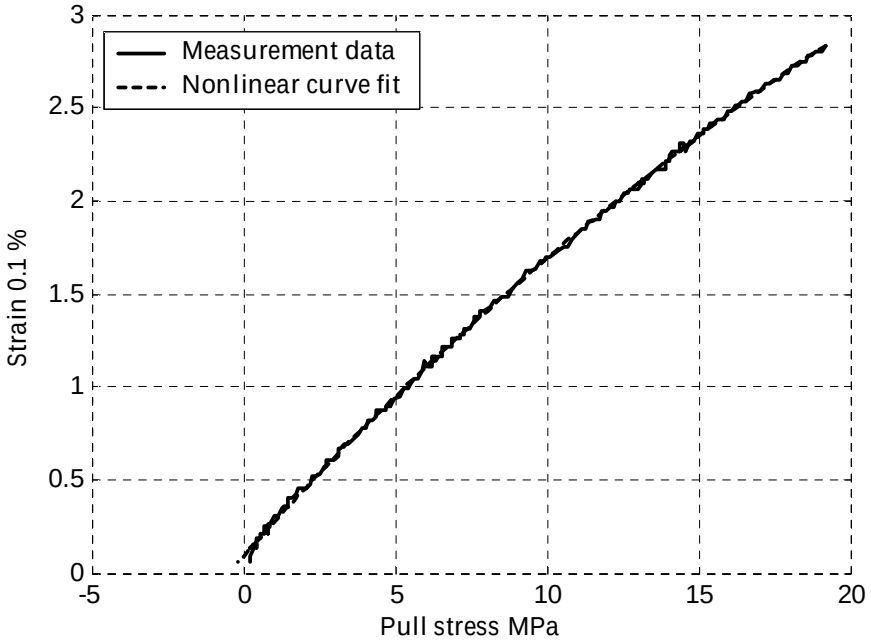

FIGURE 51 Non-linear stress strain curve fit to the pull test data.

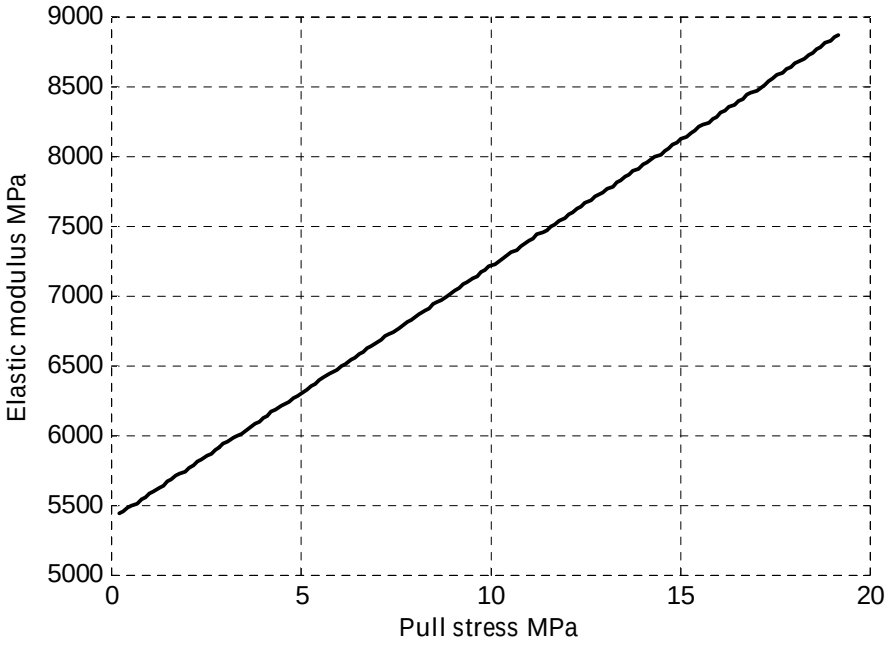

FIGURE 52 The MD direction elastic modulus for SC paper as a function of stress.

$$\varepsilon_n = a_0 a_2^n + a_1 a_3^n + a_4 \tag{66}$$

where n is the time step index and a_0-a_4 are the unknown parameters to be found. The parameters a_2 and a_3 are less than one, so at infinity the strain has crept to the steady state value a_4. The difference equation for this step response function without any input filter is

$$\varepsilon_n = -c_0 \varepsilon_{n-1} - c_1 \varepsilon_{n-2} + c\sigma_n \tag{67}$$

for a stress input, strain output second order system. The parameters in these two equations are connected together by the relations:

$$c_0 = -(a_2 + a_3), c_1 = a_2 a_3, c = -\frac{(a_0 + a_1)(1 + c_0 + c_1)}{\sigma_\infty} \tag{68}$$

for the step input σ_∞. Sample measurement data for SC paper is seen in FIGURE 53. The paper has lost 0.22 micrometers of its thickness in 3 hours under 1 MPa pressure. The step response function fit to the data is seen on the same figure. The fit is very good already with two time constant function. The time constants for this data are 258 and 6876 seconds and the steady state sheet thickness is 39.30 micrometers, which means -0.58 % total creep strain. The smaller time constant is shorter than normal winding time, so viscoelastic relaxation will occur already during winding time and will continue after it.

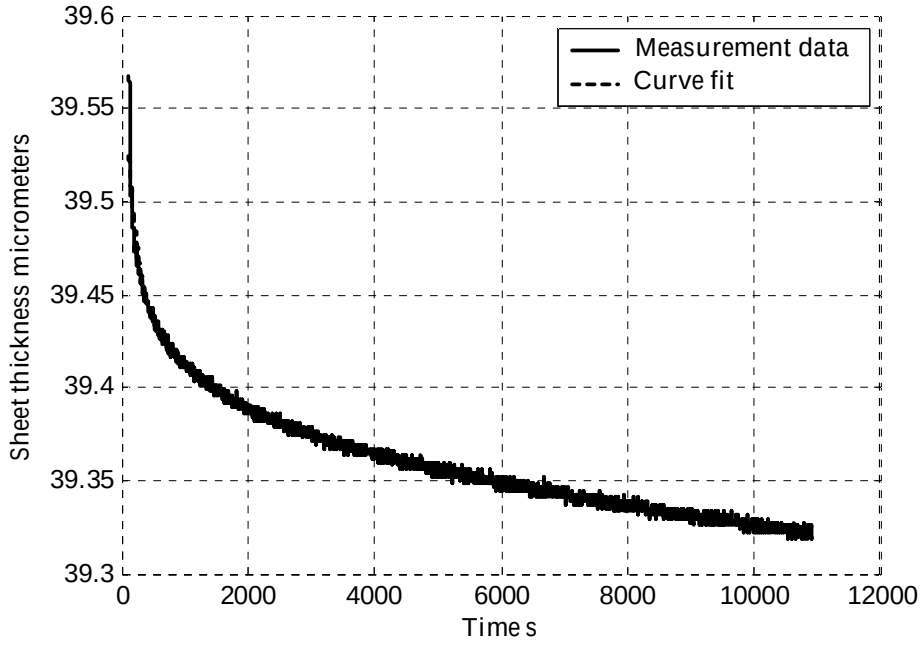

FIGURE 53 Step response function nonlinear least squares fit to the SC paper creep test data.

3.4 MD-direction creep test

The MD-direction creep test is done in the pull test machine by keeping the test sample under constant tension and logging the length creep of the specimen. The problem of this test is the same as the MD-direction stress strain measurement, that only small sample can be tested at a time and several measurements and averaging is needed to get mean values over the width and length of the roll. Sample data for SC paper pull test creep data is shown in FIGURE 54. The sample was two hours under 18.7 MPa tensile stress and its length crept 0.105 mm during this time. The curve fit was done for the same second order system step response function as for the Z-direction data, and the fit is again very good with only two time constants. The measured time constants were 30 and 2100 seconds and the steady state sheet length at inifinte time is 205,704 mm, which is in other words 0.054 % total creep strain.

Both the Z-direction and MD-direction viscoelastic creep have shortest time constant well under the normal winding times. This first time constant accounts for about 50% of the total creep, which was -0.58 for Z- and 0.054 % for MD-direction. So significant part of the viscoelastic relaxation has already occurred when the roll is ready and out of the winder and the pressures inside the roll can be measured. The Z-direction creep strain is about 10 times greater than the MD-direction creep strain, which is about the same ratio as with the normal strains at the stresses in the roll.

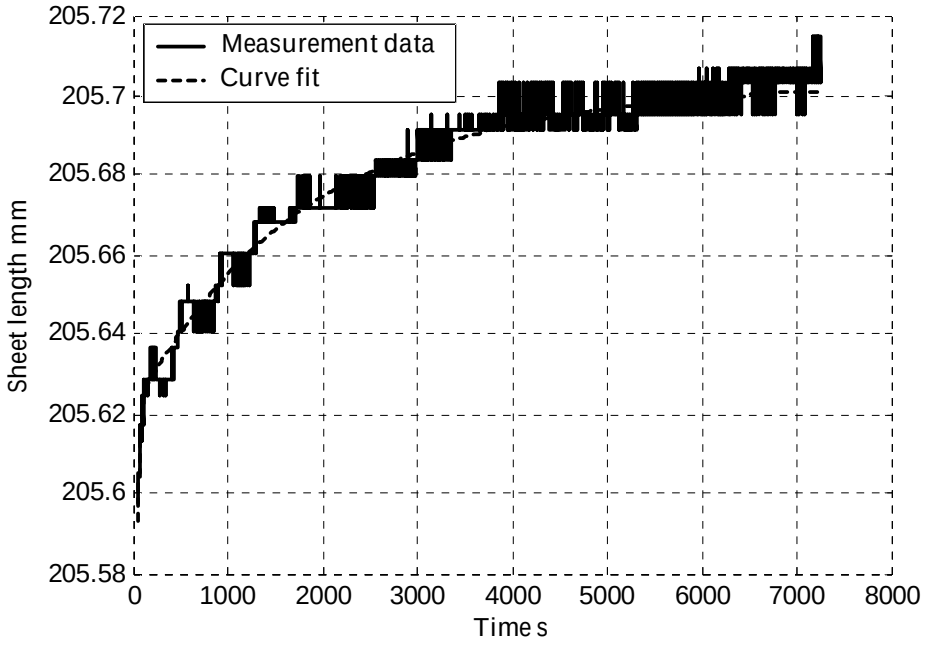

FIGURE 54 SC paper pull test creep data and nonlinear least squares curve fit to it.

3.5 Summary

The SC printing paper elastic properties were measured to be highly non-linear for both machine and z-directions. The LWC and Newsprint papers also have non-linear elastic characteristics. The choice of the parametric curve for the stress-strain data is based on the computational cost and the goodness of fit. The cost to compute the curve is important, since most of the CPU time demand of the wound roll stress models is caused by the computing time of the stress strain functions.

The viscoelastic creep behaviour was modeled with second order constant coefficient time difference equations. Second order equation with two time constants gives reasonable fit over few hours creep data, but to better fit over longer creep periods, third or fourth order equation would be needed. However, it is difficult to maintain constant roll temperature and humidity over long relaxation periods of several days, so viscoelastic relaxation will be mixed with other factors causing pressure drops or increases.

4 DENSITY MEASUREMENT

4.1 Density versus thickness

The density inside the roll can only be measured as an average value over the whole volume of the roll. This can be done by first measuring the outer dimensions of the roll and its weight and then the density is computed as weight divided by volume. The average web thickness h_{ave} in the roll can also be measured if the length of the web L in the roll is known:

$$h_{ave} = \frac{\pi\left(D_{out}^2 - D_{in}^2\right)}{4L} \tag{69}$$

This formula is derived by considering the end surface area of the roll and expressing it either by means of the inner D_{in} and outer D_{out} diameters or as length times web thickness. The diameter range can cover any smaller portion of the roll volume, if the length inside that portion is known, and the density got is the average over that smaller diameter range. All density measurement installations presented are based on the web thickness measurement and the output ρ is simply rescaled to density scale by the relation:

$$\rho = \frac{b}{h} \tag{70}$$

where the basis weight b is just a scaling factor and does not affect the accuracy or resolution of the result.

Paper thickness and density vary according to the paper grade. Papers that have same web thickness may have different density and vice versa. Since this work deals with stresses and strains in the wound roll, it is more natural to display the thickness as the principal measured value, not the density. The callipers of various paper grades are typically LWC 50 micrometers, SC 40 micrometers, Newsprint 85 micrometers and WFC 70 micrometers.

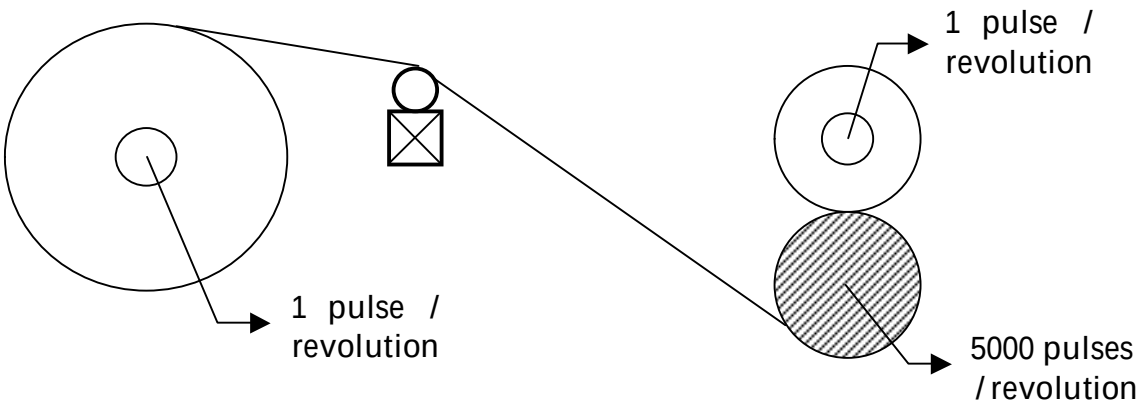

FIGURE 55 Winder instrumentation for diameter and length measurement.

4.2 Density measurement by pulse counting

The schematic instrumentation to measure the roll diameters and web length are shown in FIGURE 55. The instruments are pulse encoders to log the roll and winding drum rotations. Detailed description of the measurement principles is found for example in (Roisum 1990). The 5000 pulses per revolution sensor on the winding drum counts the web length and the one pulse revolution sensors on the windup and unwind core chucks count the roll revolutions. The web length L is got from the counted drum pulses pp_{tot} and the drum diameter D_d as

$$L = \frac{pp_{tot}}{5000} D_d \tag{71}$$

and the roll diameter D as

$$D = \frac{pp}{5000} D_d \tag{72}$$

where the pulse count pp in the latter equation is the number of pulses counted during one roll revolution, which is done by means of the core chuck pulse encoder. In the previous equation the pp_{tot} is the total number of pulses since winding started.

The equation that is used as the basis for density calculation has not been traditionally equation (69) but instead a bit simpler one:

$$h_{ave} = \frac{D_i - D_k}{2N_{i\_k}} \tag{73}$$

for any diameter range D_i to D_k and N_{i_k} roll revolutions in between them.

4.3 Noise reduction in density measurement

The basic principle of density or thickness measurement is very simple. Basically it means differentiating the measured diameter. This operation is known to amplify high frequency noise. Noise can be kept small by keeping the number of roll revolutions in the averaging range large enough. The measurement can however be updated at every roll revolution. Better noise reduction still can be achieved by first looking at what are the sources of noise in the pulse counting measurements.

The number of pulses per revolution in the drum pulse encoder, which was here chosen to be 5000, is limited by the maximum pulse frequency. It cannot be much higher than 5000 to be practical in industrial applications, even though the final pulse number can be easily multiplied by quadrature pulses and pulse multipliers.

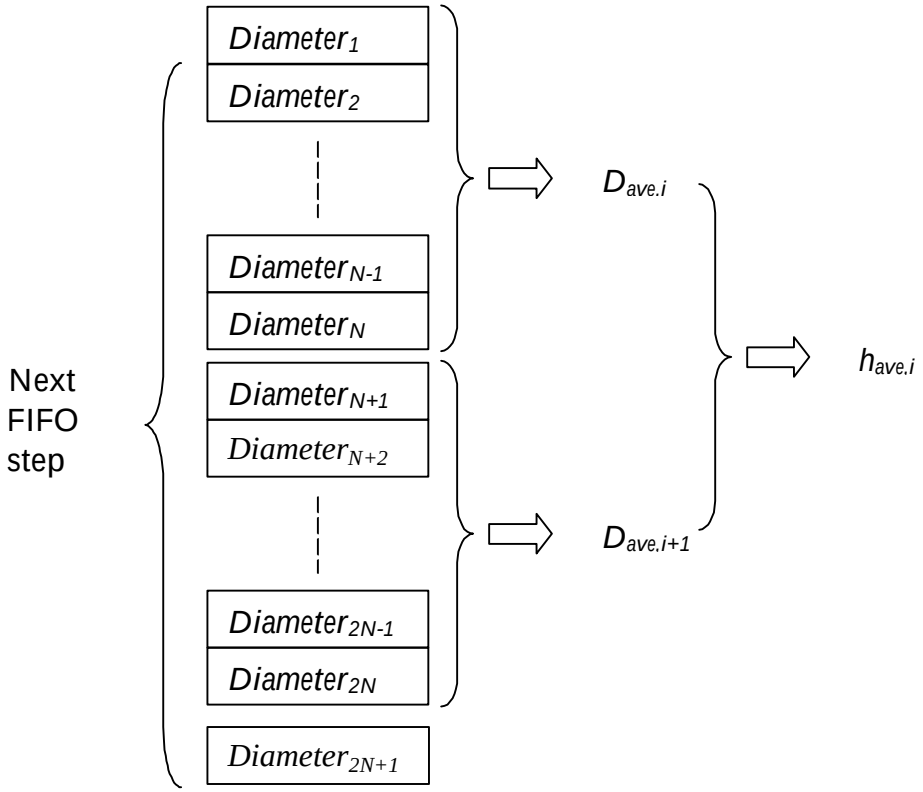

FIGURE 56 Pulse counting density measurement floating average computing FIFO.

The dominant error in the diameter measurement is the jitter or random fluctuation in the core chuck pulse encoder to detect the exact moment when the roll has made another full revolution. Every measured diameter is affected by the jitter error e_i of the previous and the current core chuck pulse $D_i=D_{i,true}-e_{i-1}+e_i$. If the drum pulse count can be logged exactly on every roll revolution and these are summed to the average diameter, all other jitter errors except the first and last in the range cancel out. And if the thickness is computed from the difference of the consecutive average diameters, the error is reduced by the square of the number of roll revolutions in the average. This method thus requires pulse counting hardware that can keep in pace with the roll rotating at

full speed. The result can again be updated at every roll revolution by computing the moving averages at every revolution. The pulse counts must be kept in a First In –First Out memory.

The usual FIFO length has been around N=100, which has been considered to give reasonable measurement accuracy at least if simple low pass filtering is added as post processing, see (Roisum 1990) for thorough analysis.

4.4 Density measurement by means of least squares

The equation (69) leads to a different but more flexible algorithm to compute the web thickness. It can be seen as an equation of defining a line in the coordinate system, where the x-axis is length and y-axis is diameter squared. The task of finding the web thickness from the measured length and diameter L_i, D_i data is that of fitting a straight line to the data. The method of least squares is simple to apply and fast to compute and effectively removes noise. The normal least squares algorithm is able to give the average thickness in the diameter range between the smallest and largest diameter value D_{in} and D_{out}, which could also be directly computed from equation (69). The least squares method is more accurate as it uses the information in all the measurement points, not only the end points. The result's units are micrometers if web length is measured in meters and roll diameter in millimeters.

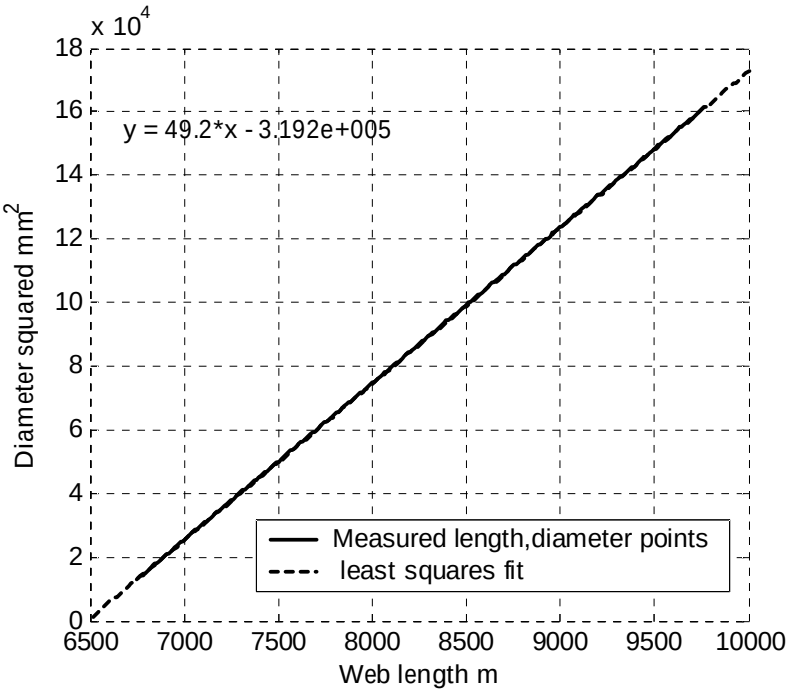

FIGURE 57 Least squares line fit to the length, diameter data from a LWC paper roll. The average paper thickness in the data range was found to be 49.2 micrometers.

The least squares algorithm for density measurement is more flexible than the direct pulse counting algorithm in that the measurement sample times need not to be exactly synchronized to roll revolutions. The density calculation can

be even done in a remote PC, which gets the data points from the winder control system through a relatively slow communication link. The data sample times need not to be fixed or evenly spaced in time. There might even be breaks in data collection without total break in density measurement.

The diameter measurement need not to be done with the pulse counting method, but any method to measure the roll diameter can do, if the accuracy is good enough. This makes savings in the complex pulse counting hardware capable of fast synchronized counting.

4.4.1 Time-varying least squares

The time-varying form of the least squares algorithm is even better suited for density measurement, where the web thickness profile instead of the average thickness is desired. The time-varying least squares algorithm in the recursive form requires little memory and is simple to program and fast to compute. The normal least squares algorithm to find the parameter vector θ is written in matrix form as (Johansson 1993):

$$\theta = \left(\Phi^T \Phi\right)^{-1} \Phi^T Y \tag{74}$$

where the regressor matrix Φ and the response matrix Y are in this case

$$\Phi = \begin{bmatrix} L_N & 1 \\ . & . \\ L_1 & 1 \end{bmatrix}, Y = \begin{bmatrix} \frac{\pi}{4} D_N^2 \\ . \\ \frac{\pi}{4} D_1^2 \end{bmatrix} \tag{75}$$

and web thickness is the first component of the θ vector. The solution to the least squares algorithm minimizes the sum of error squares *SSE*:

$$SSE = \left(Y - \Phi\theta\right)^T \left(Y - \Phi\theta\right) \tag{76}$$

The equation (73) can be partitioned into

$$\theta_N = \left(\Phi_N^T \Phi_N\right)^{-1} \left(\Phi_N Y_N\right) = \begin{bmatrix} \sum_{n=1}^{N} L_n^2 & \sum_{n=1}^{N} L_n \\ \sum_{n=1}^{N} L_n & N \end{bmatrix}^{-1} \begin{bmatrix} \frac{\pi}{4} \sum_{n=1}^{N} L_n D_n^2 \\ \frac{\pi}{4} \sum_{n=1}^{N} D_n^2 \end{bmatrix} \tag{77}$$

$$= \left(\begin{bmatrix} L_N^2 & L_N \\ L_N & 1 \end{bmatrix} + \begin{bmatrix} \sum_{n=1}^{N-1} L_n^2 & \sum_{n=1}^{N-1} L_n \\ \sum_{n=1}^{N-1} L_n & N-1 \end{bmatrix} \right)^{-1} \left(\begin{bmatrix} \frac{\pi}{4} L_N D_N^2 \\ \frac{\pi}{4} D_N^2 \end{bmatrix} + \begin{bmatrix} \frac{\pi}{4} \sum_{n=1}^{N-1} L_n D_n^2 \\ \frac{\pi}{4} \sum_{n=1}^{N-1} D_n^2 \end{bmatrix} \right) \tag{78}$$

$$= \left(\begin{bmatrix} L_N \\ 1 \end{bmatrix} \begin{bmatrix} L_N & 1 \end{bmatrix} + \Phi_{N-1}^T \Phi_{N-1} \right)^{-1} \left(\frac{\pi}{4} \begin{bmatrix} L_N \\ 1 \end{bmatrix} D_N^2 + \Phi_{N-1} Y_{N-1} \right) \tag{79}$$

where *N* is the number of data points. This format is the least squares algorithm in a recursive form and it can be immediately turned into time varying form by introducing the forgetting factor λ:

$$\theta_N = \left(\begin{bmatrix} L_N \\ 1 \end{bmatrix} \begin{bmatrix} L_N & 1 \end{bmatrix} + \lambda \Phi_{N-1}^T \Phi_{N-1} \right)^{-1} \left(\frac{\pi}{4} \begin{bmatrix} L_N \\ 1 \end{bmatrix} D_N^2 + \lambda \Phi_{N-1} Y_{N-1} \right) \tag{80}$$

The usual textbook versions of the time-varying least squares avoid the matrix inversion by utilizing the matrix inversion lemma, but in this case the matrix to be inverted is 2x2, so inverting it is not a big task. The time-varying least squares minimizes weighted sum of squares, where the data points are weighted by $\lambda^{(N-n)/2}$, which shows that the forgetting factor λ should be less than one. The forgetting factor λ has similar meaning to the filter coefficient in a first order IIR low pas filter. The closer the factor is to 1 the tighter is the "filtering" built into the time-varying least squares algorithm. Normal values are in the range 0.99-0.999. It might be hard to find the best value for λ, as it should be chosen according to the frequency contents of the noise and the density profile. Too high value makes the response slow and causes large delay and may hide useful information in the signal.

4.4.2 Noise rejection and the forgetting factor

The forgetting factor λ can be replaced by another parameter that better reflects the information content of the density signal and from where the value for λ can be computed. This new parameter is a statistical parameter that determines the variance or the confidence limit for the measured density or web thickness. The variance of the least squares estimate s_θ can be expressed by means of the error variance s_e and the regression correlation matrix *R* (Pindyck and Rubinfeld) as

$$s_\theta^2 = s_e^2 R^{-1} = \frac{(Y - \Phi\theta)^T (Y - \Phi\theta)}{N - 2} \left(\Phi^T \Phi \right)^{-1} \tag{81}$$

This can be written out in the recursive time-varying format for the web thickness, which was the first component of the θ-vector:

$$s_{\theta,N}^2 = \left(k \left(\frac{\pi}{4} D_N^2 - \begin{bmatrix} L_n & 1 \end{bmatrix} \theta_N \right)^2 + (1-k) s_{e,N-1}^2 \right) \left(\begin{bmatrix} L_N^2 & L_N \\ L_N & 1 \end{bmatrix} + \lambda \begin{bmatrix} \sum_{n=1}^{N-1} L_n^2 & \sum_{n=1}^{N-1} L_n \\ \sum_{n=1}^{N-1} L_n & N-1 \end{bmatrix} \right)^{-1} \tag{82}$$

whose diagonal elements are the variances of the least square estimates. The square root of the first component is the standard deviation for the web thickness, and *N* is the number of measurement data points. If the error is not zero-mean, the square of the error mean estimate should be subtracted from s_e^2. This standard deviation estimate can be changed to the 95% confidence limit by multiplying it with the t-distribution 5% critical value since the least squares estimate is t-distributed (Pindyck and Rubinfeld). The standard deviation and the confidence limit are values expressed in micrometers and their meaning is easily understood. The confidence limit gives the range around the measured web thickness, where the "true" web thickness lies with 95% likelihood

The forgetting factor λ can be expressed in another form that also is much better to understand, that is the "buffer length" *bl*:

$$bl = \frac{1}{1-\lambda} \tag{83}$$

and conversely

$$\lambda = \frac{bl-1}{bl} \tag{84}$$

The buffer length has similar meaning as the FIFO buffer length has in the pulse counting density measurement. It is the average number of past samples that still has some weight in the time-varying least squares algorithm, even though the weighting decreases exponentially. It can be turned into an even more descriptive parameter by multiplying it with the measured web thickness *h*:

$$dl = bl * h \tag{85}$$

which gives the approximate layer thickness *dl* on the roll surface, over which the measured web thickness is averaged. For example if the web thickness is 50 micrometers and the buffer length is 200, then the result is an average over 10 millimeter layer on the roll surface.

Practical values for the buffer length are in the range 100 to 200 for a 95% confidence limit of $0.05 - 0.1$ micrometers. The adjustment of the buffer length parameter can be automated so that the target confidence limit is given. The buffer length is then continuously adjusted by a "controller" in order to keep the actual confidence limit close to the target value.

The pulse counting and the time-varying least squares density measurements are compared in FIGURE 58 and FIGURE 59. The pulse counting density was not postprocessed with a filter to give a clearer view of the better accuracy of the least squares density measurement.

4.5 Accuracy of the density measurement

It follows from the equation (69) that the average relative error in the web thickness is the same as the average relative error in the measured diameter, if the length measurement error is assumed zero and the diameter error is zero-mean:

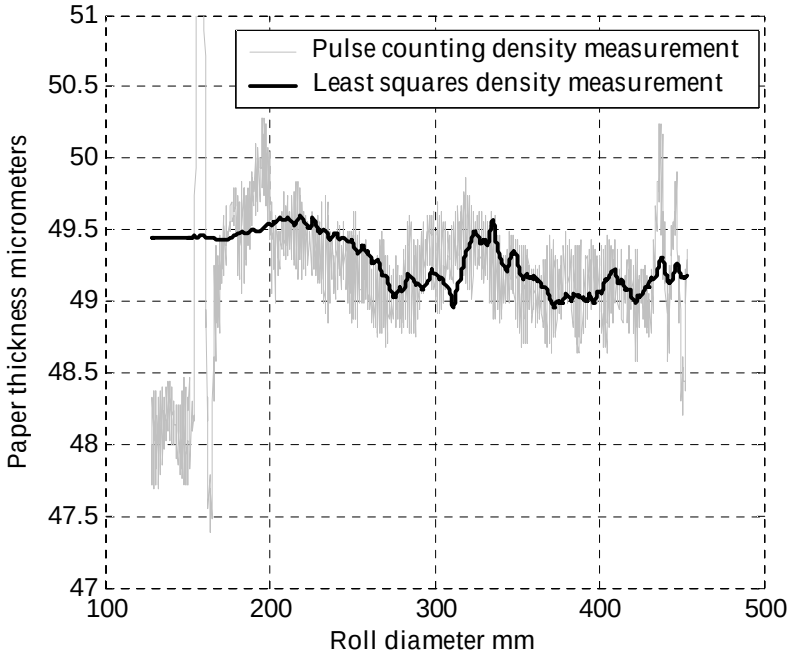

FIGURE 58 LWC roll density measurement with least squares and pulse counting algorithms. The pulse counting FIFO length was set to 2x50 and the least squares buffer length was also 50.

$$\frac{\overline{h_e}}{h} = \frac{\overline{D_e}}{D} \tag{86}$$

where h_e and D_e are the thickness and diameter errors. The accuracy of the diameter measurement is better than 0.1 millimeters for pulse counting measurement. The resulting relative error in web thickness is then 0.1 −0.01 % for normal roll sizes. This is 5 to 50 nanometers for 50 micrometer paper. The relative error decreases inversely proportional to diameter. The least squares algorithm can effectively reduce zero-mean random error and can easily keep the confidence limit of thickness below 50 nanometers. Systematic non zero-mean error in diameter measurement is much more difficult to eliminate from the measurement. The most important systematic error in the diameter measurement in the windup is the core chuck slippage. If the core chuck pulse encoder is synchronized to the core chuck rotation, it is sensitive to the slippage. The slippage is almost unavoidable in the single-drum multistation winders, where the core chuck loading is high. This error can be avoided if the

roll revolutions are logged by a photoswitch reading pulses from reflective tape attached to the core itself.

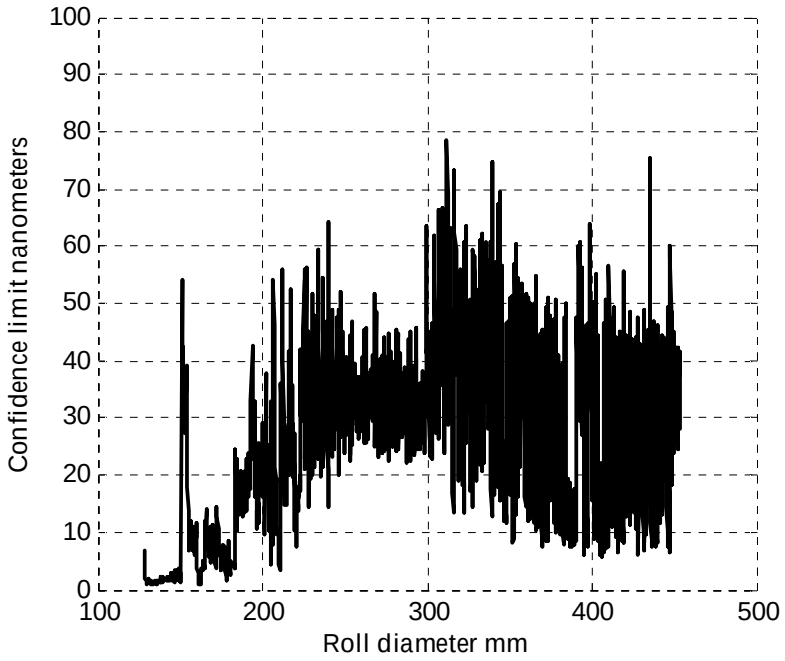

FIGURE 59 Web thickness confidence limit for the least squares density measurement in FIGURE 58.

There is a special error source in the unwind density measurement. The unwind density measurement has own pulse encoder in the unwind core chuck, but uses the same windup length measurement than the windup density measurement. The web length is measured by means of counting the winding drum revolutions in FIGURE 55. There is perhaps 15 meters long web path between the unwind and windup. When the web tension is changed, it causes stretch change in this web path and this causes error in the measured unwind diameter and web thickness.

The effect of changing the confidence limit target value for the confidence limit "controller" is shown in FIGURE 60 and FIGURE 61. The web thickness curve for the 50 nanometers confidence limit is clearly noisier than the 5 nanometers curve. The buffer length for the 50 nanometers confidence limit has been around 50 and for the 5 nanometers confidence limit it has risen up to 250.

4.5.1 Initializing the least squares algorithm

The pulse counting algorithm does not need any special initialisation, but as soon as the roll has made enough revolutions to fill up the FIFO buffers, the measurement has stabilized. On the other hand, the least squares algorithm needs more careful initialisation, since the possible bad data at the winder startup may cause long initial transient. The basic difference in the algorithm is

that the pulse counting density measurement is "finite impulse response" and the least squares algorithm "infinite impulse response" type systems. The confidence limit controller may prolong the transient if it increases the buffer length and fixes the system to bad data. Several initialisation schemes can be used to make the transient shorter and catch up faster the new good data, FIGURE 62.

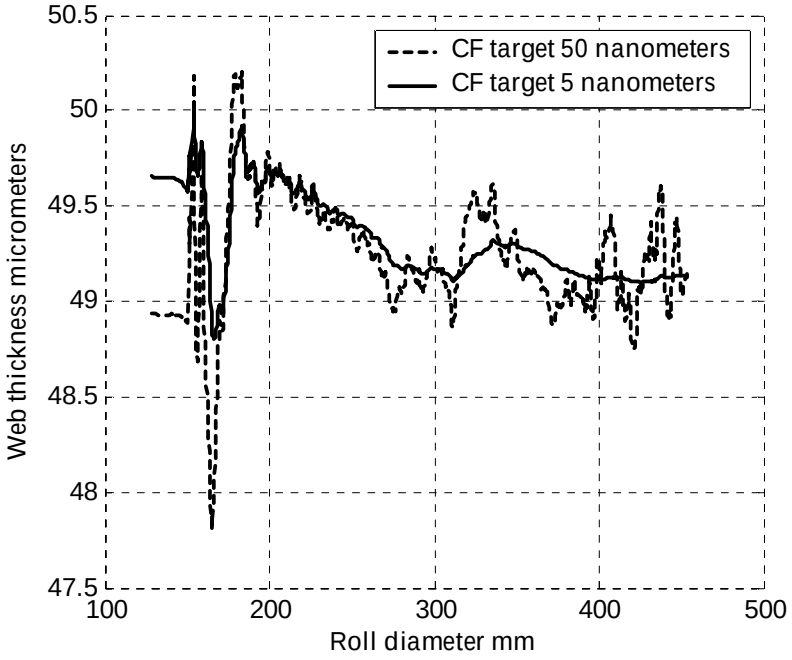

FIGURE 60 Least squares density measurements with two different confidence limit targets, 50 and 5 nanometers.

The simplest way to initialise the density measurement is not to initialise it at all. The measurement simply goes on from where it was left at the end of the previous roll. This works well if the web thickness does not change a lot from the roll end to the next roll beginning. The transient can be speeded up by means of resetting the buffer length to a minimum.

If the web thickness does change much between rolls and the thickness early in the roll bottom is interesting, the initialisation can be done on new data. This cannot be done on-line, but after a few hundred meters is wound and the web thickness has settled to the new value. Then the initialisation is done on this new data.

Another simple initialisation is done if the internal variables are resetted to zero and the measurement starts from clean table.

4.6 Summary

The accuracy of the web thickness measurement is crucial for the accuracy of the Wound On Tension measurement method used in this work. Zero-mean

noise reduction is simple to achieve, basic low-pass filtering or data averaging is enough. More important is to avoid possible systematic errors. The most important systematic error source in the measurement data is the error in the diameter measurement. The relative error in the web thickness is directly proportional to the relative error in the measured diameter. Checking diameter measurement accuracy is not easy, since the final roll is not necessarily exactly round, and manual measurement accuracy is hardly better than 1 millimeter. There might also be difference in diameter measured on both ends of the roll.

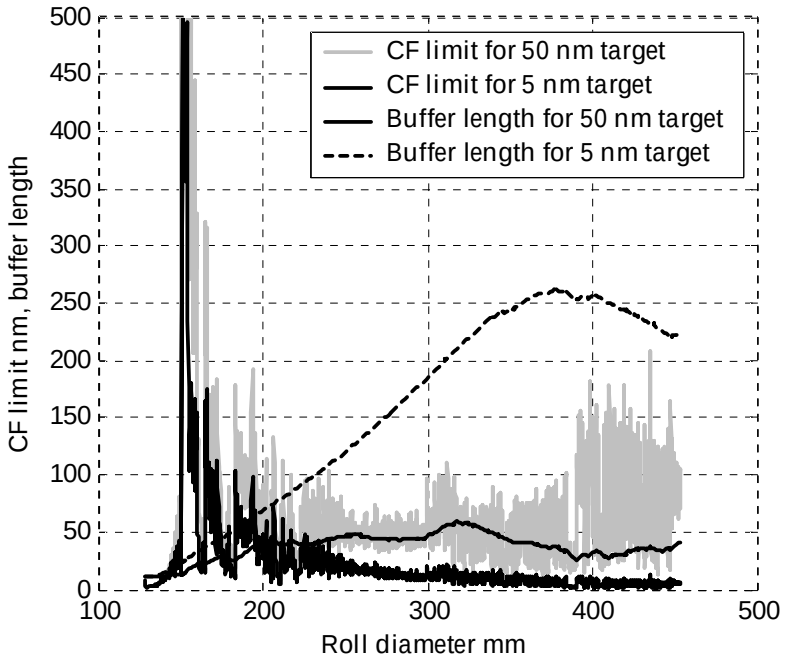

FIGURE 61 Actual confidence limits and buffer lengths for the two least square density measurements in FIGURE 60.

The 50 micrometer thick printing paper compresses under the pressure in the roll about 1 – 5 micrometers. The resolution and accuracy of the web thickness measurement must be better than 0.1 micrometers to be able to detect the variations in the thickness caused by winding tightness variations.

Two filtering algorithms for the web thickness measurement were presented. Both methods, the moving average filter and the time-varying least squares filter produce estimate of the mean web thickness over a definite diameter range on the roll surface. Compared to basic low pass filters, whose tuning is based on selecting a cut-off frequency value, these methods have the advantage that the averaging layer thickness is known.

The moving average filter has the extra advantage, that it can utilize the known error correlation, if every web layers diameter is counted. This advantage is compensated by the flexibility and simplicity of the time-varying least squares algorithm.

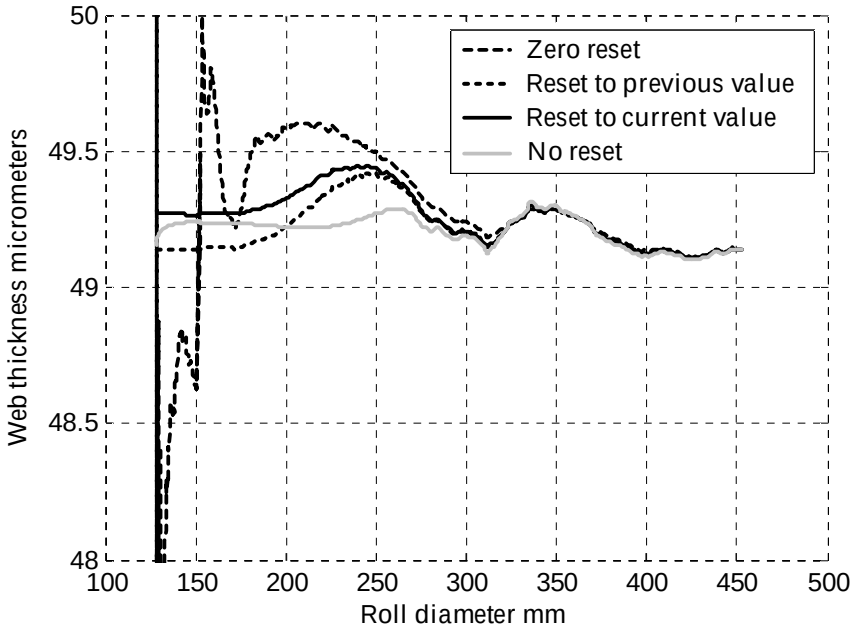

FIGURE 62 Different ways to initialise the least squares algorithm. The fastest initialisation is by means of resetting the measurement to the current value. It can only be done by recomputing the thickness curve after good data has been got for initialisation. Until then the computation can be done without resetting.

5 NIP MODELS

The winding nip is the first windup nip where the web enters the roll. The winding nip model describes how the Wound On Tension is produced in the winding nip as a sum of the Nip Induced Tension and the web tension *T*:

$$WOT = T + NIT \tag{87}$$

This model implies that the NIT can also be negative for the cases when the WOT is less than the original web tension. The theoretical winding nip models assume that the significant portion of the NIT is present already when the web has passed first time the winding nip and the possible tension changes occurring in the other nips and also in the winding nip after the first pass can be neglected. Also the possible tension changes occurring in the web wrap over the winding drum before the nip are modelled as being part of the NIT. According to Jorkama (Jorkama and von Hertzen 2001) the tension change in the wrap is negligible at least for hard winding drums.

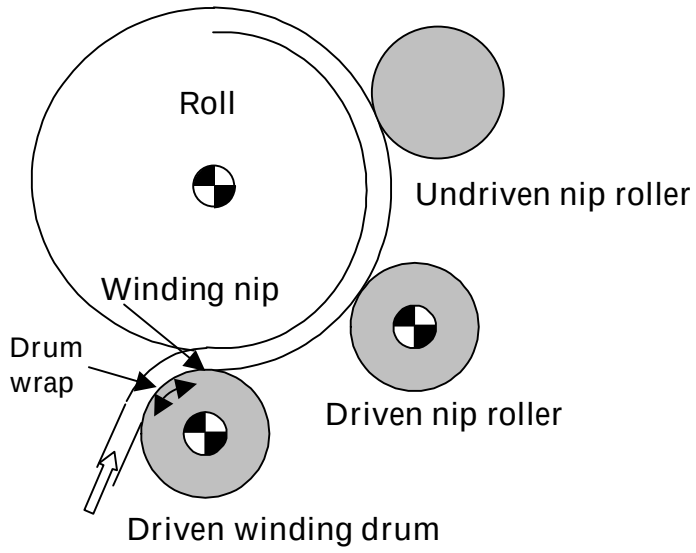

FIGURE 63 Winding configuration and winding and other nips on the roll.

If the necessary torque to withstand the pull caused by the web tension is produced by the winding drum alone in FIGURE 63, the winding configuration is said to be *surface winding*. But if the roll itself or the other nip rollers are driven instead, the configuration is *centre winding*. In this case the nip rollers including the winding nip can be absent and the roll is supported and driven on its centre. In paper winding the configuration is in most cases *hybrid winding*, where there is more than one drive units at the nip rollers and/or the roll centre. Nip loading against the winding drum is produced by the roll weight and relief/loading on the roll centre or other nip rollers. It is assumed that the Nip Induced Tension is a function of the nip loading, web tension and the surface traction in the winding nip. If the winding drum is rotating at constant speed, the surface traction depends only on the torque of the winding drum. Experiments (Good et al. 1999) have verified the following upper limits for the WOT for web tension T and nip loading NL and paper to paper friction coefficient μ:

$$\begin{aligned} WOT_{\max imum} &= T + \mu NL, center winding \\ WOT_{\max imum} &= \mu NL, surface winding \end{aligned} \tag{88}$$

The methods used in this work to measure the deformations and stresses in the wound roll do not allow to separate the Wound On Tension into nip induced tension components at every nip roller and web layer. The wound roll stress models assume that the web has already got all the WOT when it enters the roll. The density measurement can only measure the net radial deformations caused by all the strain changes in the roll surface layer. However, these restrictions do not hamper the goal to measure the final stress state of the roll.

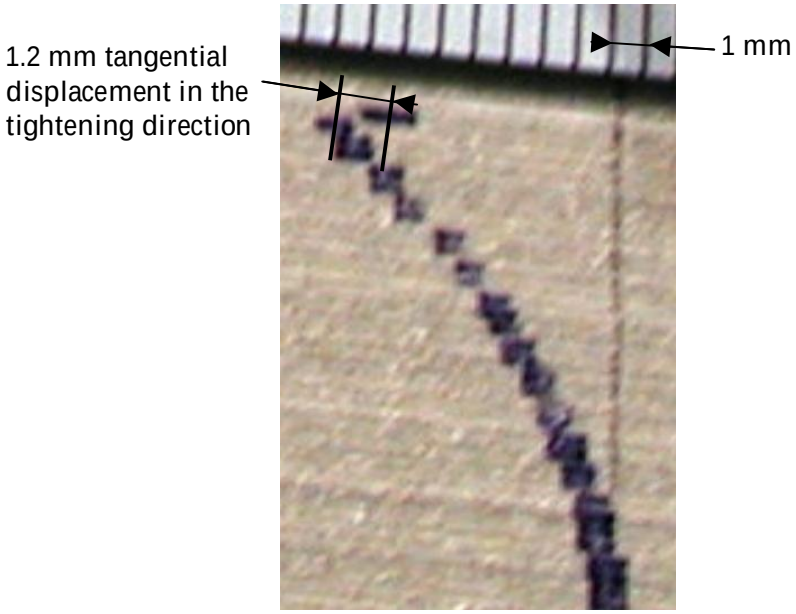

FIGURE 64 The J-line measured on a paperboard roll. In most cases the layers have moved in pairs two layers stuck together. The roll diameter was 1.9 m and the web thickness 0.4 mm.

5.1 The J-line

The well-known J-line method is a means to measure the tangential displacements of the web layers after the first pass through the winding nip. The J-line is shot at the rotating roll edge by means of an inked string. The line will bend when more and more layers are wound onto the roll. The line can bend either to the direction indicating web tightening in the roll or to the loosening direction. The direction depends on the web properties and winding parameters. The bending ends eventually when the J-line is deep enough in the roll indicating that the nip effect has certain penetrating depth into the roll. The J-line can only measure the sum displacements of all nips, but it is a way to see how large displacements and stress changes occur beneath the surface layer of the roll. The tangential displacements are read as the distances of the successive layer marks in the J-line.

The tip of the J-line is often bent to the tightening direction even when the rest of the line is bent to the loosening direction, as in FIGURE 64, indicating that these layers have gained more tangential strain after the J-line was struck on the roll. Only the topmost layer in the J-line has collected all the displacements into the J-line it got when it was inside the nip effect depth (the layers deeper in the J-line already had done part of the passes through the nip area when the line was struck). The other layers have moved to the loosening direction only because the line does not show all the displacements for them. This means that all layers will gain some more tension also after the first pass through the nip. The displacement in FIGURE 64 is 1.2 mm, which is $1.2/(\pi 1900)=0.02\%$ in strain. If the modulus is 5000 MPa, this would be equivalent to 1 MPa stress = 400 N/m tension. For a 50 μm thick paper the per layer displacement is possibly less than this, which means for a 1 m diameter roll max $1.2/(\pi 1000)=0.04\%$ strain and 1.9 MPa stress, which is 95 N/m tension change. So the web gains some more tension also beneath the surface layer in the roll, which however will be modeled as though the final WOT was reached already after the first pass through the winding nip (Güldenberg 2000), (Güldenberg and Welp, 2001),(Pfeiffer 1968).

5.2 Proper dimensioning of the winding modeling problem

In many cases the NIT measurement results have been acquired with laboratory winders that run with much lower web tensions, torques and nip loads that is usual in full size paper and board winding. Also the roll size is often a fraction of paper mill roll size and the resulting stresses and strains in the roll are very low. This makes it difficult to compare the results to real life winding and some effects like viscoelasticity are not properly accounted for. Also the measurement and modeling accuracy are poor since the small NIT and pressure values are close to the resolution of the measurement equipment.

To fulfill these requirements the roll size should be in the range 0.5 to 1.5 meters, web tension from 300 to 1500 N/m (lower if only paper is studied) and

nip loadings from 1000 N/m up to 15000 N/m for compliant drums. The resulting WOT is assumed to be somewhere in the range 200 to 2000 N/m for paper with tensile strength of 2500-3000 N/m and even more for board grades. The radial pressure in the roll should be around 0.1 – 2 MPa. The maximum winding speed should be over 3000 m/min and the roll width several meters to get the air penetration and other speed related effects to show their full potential.

The model and measurements to verify it should not be limited to only pure centre or surface winding, but a range of surface traction from 0 to over the web tension should be used.

5.3 The OSU nip model

The OSU nip model (Good and Wu 1993),(Good 2001) is derived in a somewhat heuristic manner without rigorous treatment of the deformations and stresses in the nip area. The nip induced tension in the model is the consequence of the Poisson effect and radial stress increase in the nip causing increase in the tangential stress. The roll-web surface in the nip area is partly slipping and the point where the slippage ends is determined by the "traction capacity" function. The model ignores the effect of the surface traction in the nip so it can be applied only to pure centre winding. The model considers slip/stick behaviour only on the web/roll surface and ignores the web/drum surface.

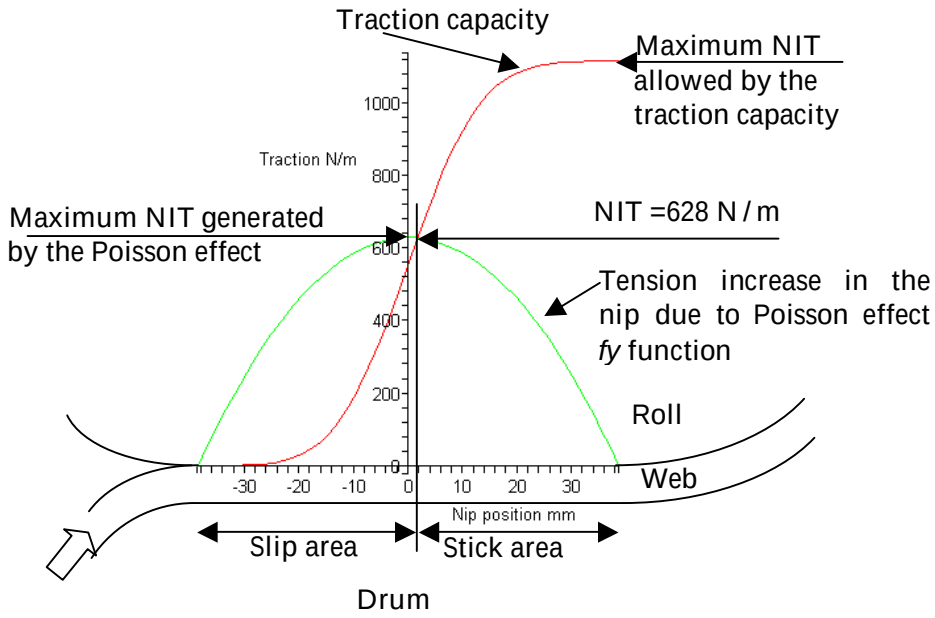

FIGURE 65 The OSU nip model tension inducing mechanism. The example is calculated with LWC paper parameters for 8000 N/m nip loading, 800 mm diameter roll and 800 mm diameter winding drum. The nip width is 2x39 mm. The web-roll contact slips until the traction capacity has increased to overcome the tension increase in the nip after which point the web is locked on the roll and the increase in the web tension is maintained. Nothing is said about the web-drum contact. The drum is assumed not to be deforming.

The OSU nip model uses heuristic roll indentation equation:

$$\varepsilon = \frac{3\pi}{16\mathrm{aR}}\left(\mathrm{a}^2 - y^2\right) \tag{89}$$

where *a* is the nip half-width, *y* is the position coordinate in the nip and *R* is the combined radius:

$$R = \frac{1}{\frac{1}{R_1} + \frac{1}{R_2}} \tag{90}$$

and R_1 is the roll radius and R_2 the drum radius. The radial stress due to the indentation strain is got by using the Pfeiffer version of the stress-strain curve:

$$\sigma = \left(e^{\frac{3\pi}{16aR}\left(a^2 - y^2\right)E_{r1}} - 1 \right)\frac{\mathrm{E_{r0}}}{E_{r1}} \tag{91}$$

where E_{r0} and E_{r1} are the radial elastic modulus parameters:

$$E_r\left(\sigma_r\right) = E_{r0} + E_{r1}\sigma_r \tag{92}$$

The nip load is got as an integral:

$$Pfun = \int_{-a}^{a} \sigma dy = \frac{2E_{r0}}{E_{r1}}\left(\frac{2e^{\frac{3\pi aE_{r1}}{16R}} erf\left(\sqrt{\frac{3\pi aE_{r1}}{16R}}\right)}{\sqrt{\frac{3E_{r1}}{aR}}} - a \right) \tag{93}$$

from where the nip width can be solved when the nip load is known. The traction capacity is defined as the integral of the nip stress multiplied with the paper to paper friction coefficient μ:

$$Tcap\left(yy\right) = \mu\int_{-a}^{yy} \sigma dy =$$
$$\frac{\mu E_{r0}}{E_{r1}}\left(\frac{2e^{\frac{3\pi aE_{r1}}{16R}} erf\left(\sqrt{\frac{3\pi E_{r1}}{16aR}}\, yy\right)}{\sqrt{\frac{3E_{r1}}{aR}}} - yy \right) + \frac{\mu E_{r0}}{E_{r1}}\left(\frac{2e^{\frac{3\pi aE_{r1}}{16R}} erf\left(\sqrt{\frac{3\pi aE_{r1}}{16R}}\right)}{\sqrt{\frac{3E_{r1}}{aR}}} - a \right) \tag{94}$$

The last equation needed in the model is the NIT function *fy* which explains the basic NIT generating mechanism to be the Poisson effect:

$$\mathrm{fy}(\mathrm{yy}) = \nu_{rt} \frac{3\pi}{16} \mathrm{E_t} \frac{\left(\mathrm{a}^2 - yy^2\right)}{\mathrm{aR}} \mathrm{h} \tag{95}$$

where h is the web thickness and ν_{rt} is the Poisson ratio. This function is the "source" of the NIT and the traction capacity function determines how much of the NIT is finally locked into the roll and at which yy value the slip area ends and the web sticks to the roll. This happens at the intersection of the two curves.

5.3.1 Fitting the OSU nip model to data

The OSU nip model can be easily fitted to centre winding experimental NIT data. The friction coefficient and the Poisson ratio can be used as free parameters to fit the model to two data points. The values for the friction coefficient and Poisson ratio are got from this fit. Surprisingly this method gives reasonable values to them and the resulting NIT curve as a function of nip loading fits rather well to the measurement data, at least in two cases.

The fit was done to Newsprint and LWC paper WOT measurement data. The data points were chosen from the centre winding curve for web tension = 500 N / m (winding drum at zero torque). The fit points were at 1000 and 8000 N / m nip loads, were the NIT was 153 and 851 N / m for Newsprint and 139 and 628 N / m for LWC. The paper parameters were then:

	E_{r0} MPa	E_{r1}	E_t MPa	h mm	μ	ν_{rt}
Newsprint	0.8451	24.02	5800	0.085	0.156	0.0205
LWC	0.0206	59.58	8730	0.054	0.139	0.0117

The friction coefficients are little low but not unreasonable, and the lower value for LWC is as expected. Measured values for the static coefficients of friction were found to be 0.28 for Newsprint and 0.21 for LWC and dynamic coefficients 0.24 for Newsprint and 0.20 for LWC. These are rather low friction paper grades. The friction coefficients can be 0.3 – 0.4 for coated papers and 0.5 – 0.6 for DIP Newsprint papers. The Poisson ratio values are close to what Good (Good 2001) used for Newsprint.

The result of the fit is shown in FIGURE 66. The fit is excellent for the Newsprint, the maximum error is 11 N / m. For LWC the fit is not as perfect, but the maximum error is still only 43 N / m. The friction limit $Tcap_{max} = \mu NL$ is drawn for both papers.

The nip widths resulting from the model are shown in FIGURE 67. The model predicts rather long nips. The LWC nip is longer than Newsprint nip, what is contrary that would be expected. The reason might be the low value of E_{r0} for the LWC.

5.4 The Jorkama – von Hertzen nip model

The JvH nip model presents a much more detailed description than the OSU model of the events in the winding nip causing the accumulation of the Nip Induced Tension (Jorkama and von Hertzen, 1999), (Jorkama, 2001) and (Jorkama and von Hertzen, 2001), (Jorkama and von Hertzen, 2002). The JvH model contains a full solution by means of Fourier series for the linear, elastic, orthotropic cylinder surface displacements under the pressure and tangential traction distributions in the nip area.

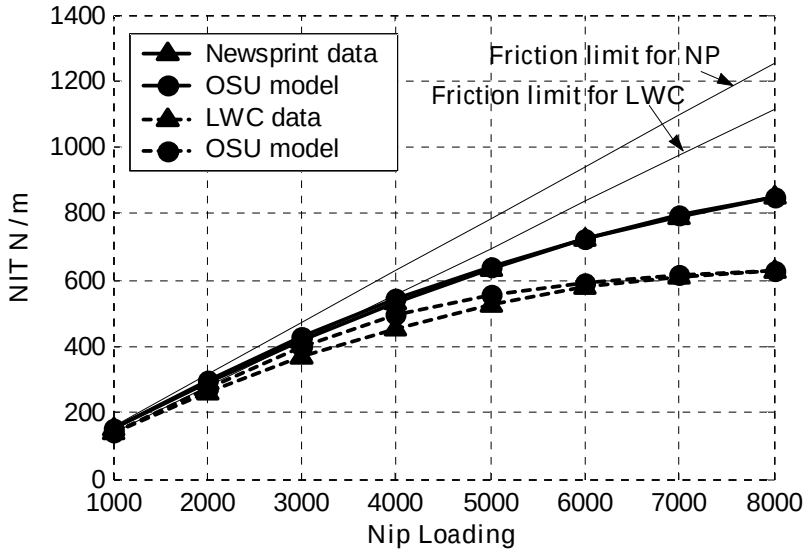

FIGURE 66 Comparison of the OSU nip model to measurement data for Newsprint and LWC papers centre wound at 500 N / m web tension and various nip loadings.

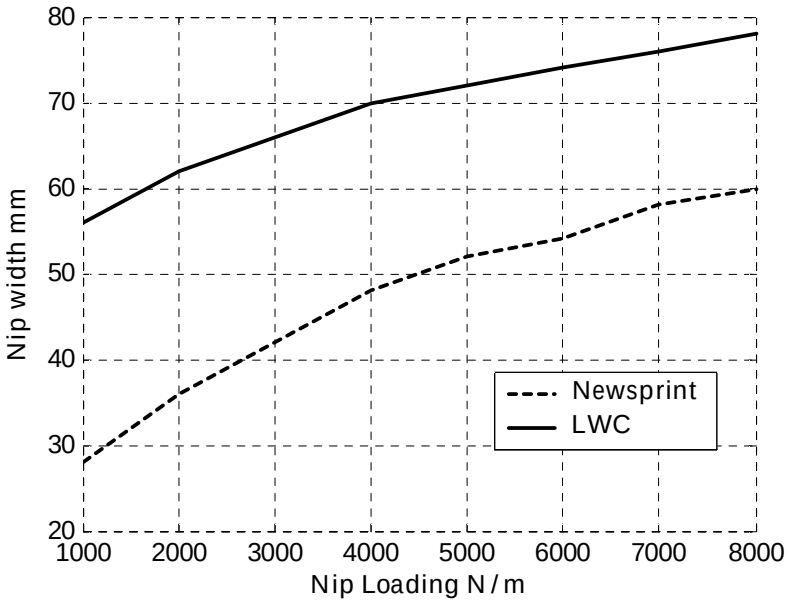

FIGURE 67 Nip widths for LWC and Newsprint papers for various nip loadings as predicted by the OSU nip model. Roll and drum diameters are 800 mm.

The linear material model is a limitation, since paper is known to be nonlinearly elastic material in the z-direction. Also similar treatment is given for the incoming web section within the nip area. The pressure and tangential traction distributions are handled on both sides of the web in the nip. The winding drum is also allowed to deform under the nip loading. The deformations, stresses and stick/slip conditions for the web-roll winding contact problem are presented in a general way, with the "Wound-On-Condition" stating that the web becomes part of the solid roll after the nip. In other words it is assumed that there is no more slipping occurring in the layers beneath the surface layer. Numerical solution to the winding contact problem is implemented by means of the so-called "modified Panagiotopoulos" process.

Jorkama defines (Jorkama 2001) the *Winding Force* to be the surface traction of the winding drum. The definition was changed in (Jorkama and von Hertzen, 2001) to the surface traction of the driven nip roller. The earlier definition is used in what follows, FIGURE 68:

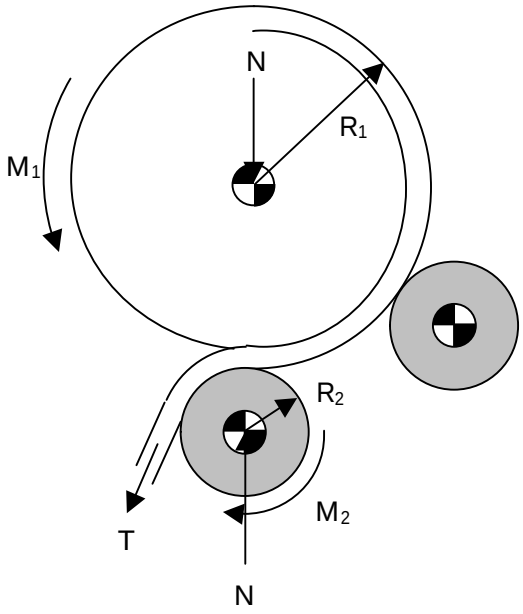

FIGURE 68 The Winding configuration with the forces acting on the roll and winding drum. The Winding Force is defined to be $WF = -\frac{M_2}{R_2} = \frac{M_1}{R_1} - T$. The torque M_1 can be produced by the roll centre drive or by the driven nip roller. The torque needed to accelerate/decelerate the roll inertia does not change the Winding Force if it is provided by the centre or nip roller drives and the winding drum torque remains constant (the torque needed to accelerate/decelerate the drum itself is not included in M_2).

Jorkama also proofs the "Winding theorem" which states that the NIT can be written as a function of the nip load and the Winding Force alone:

$$WOT = T + NIT(N, WF) \tag{96}$$

For centre winding *WF=0* and NIT should depend on the nip load only. For surface winding *WF=-T* and no clear linear dependence of WOT on web tension should appear.

The more detailed nature of the JvH model compared to the OSU model is clear in FIGURE 69. The JvH model outputs both the tractions on the web-roll contact (q^+, solid line on the left) and web-drum contact (q^-, dashed line on the left). The friction limits for both contacts are drawn with grey background shading. The relative tangential speed differences are shown on the right for web-roll v^+ (solid line) and web-drum v^- (dashed line) and the web tension (dash-dotted line). The web-roll contact is in stick between the points A to B and the web-drum contact is in stick from the start of the contact to the point C. From point C to the trailing edge of the nip both contacts are slipping and this is the area where the web tension increases. Jorkama notes that in the web-drum stick area from the leading edge till point C the rigid steel winding drum prevents tangential strain changes in the web. This is a very different description from the OSU model.

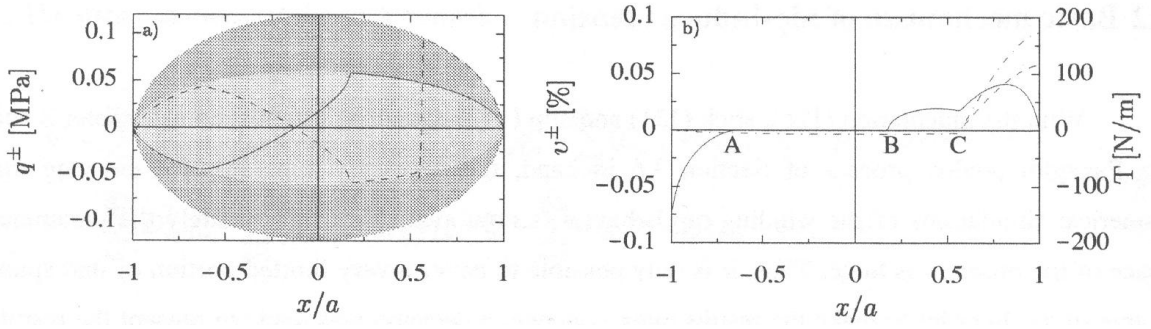

FIGURE 69 Tangential tractions on the left and relative speed differences with web tension on the right. This is a copy of Figure 15 in (Jorkama 2001).

The JvH model claims that the value of the cross Poisson ratio ν_{rt} has little influence on the NIT. On the other hand it replaces the Poisson ratio with another parameter whose value is difficult to measure for paper material, namely the shear modulus. The JvH model also shows that in most cases the NIT decreases with increasing paper to paper friction coefficient.

5.5 Comparison of the OSU and Jorkama – von Hertzen nip models

Both Good (Good 2001) and Jorkama (Jorkama 2001) compare their theoretical results on the same experimental data from (Good et al. 1999). The data is got from Newsprint paper centre winding trials and the WOT is measured with an indirect method. The method is based on measuring the roll layer-wise pressure by means of pull tabs and then adjusting the WOT into the incremental stress wound roll model (Hakiel version) until the pressure from the model fits with the measurement. Good claims that the direct WOT measurement method with the WOT measurement roller (Pfeiffer 1977)

measures only a fraction of the true WOT due to slippage in the first wrap after the nip, FIGURE 70. He explains this is due to the tension loss in the web wrap around the roll after the nip and before it is extracted to the WOT measurement roller. Another explanation for the alleged measurement error is that the web achieves more WOT in the subsequent passes through the nip as shown earlier with the J-line.

Nevertheless the data is redrawn here (FIGURE 71), even though it cannot be directly compared to the data presented later on in this work since there are differences in the paper properties. The Newsprint centre winding data in (Good et al. 1999) and (Good 2001) seem to be the same, even though the paper parameters in the two reports differ from each other. The parameter comparison for Jorkama and Good is given in Table 6. The parameters are not the same, even though both claim to get a good fit to the same measurement data with them.

Table 6 Comparison of the paper parameters used by Jorkama (Jorkama 2001) and Good (Good 2001) to fit their theory to the measurement data in (Good et al. 1999).

	E_{r0}	E_{r1}	E_t	μ	h	ν_{rt}	G_{rt}	$\mu_{paper-drum}$
Jorkama	27 MPa	0	3380 MPa	0.19	0.066 mm	0.0015	10 MPa	0.2
Good	0.59 MPa	24.49	5140 MPa	0.19	0.071 mm	0.016	-	-

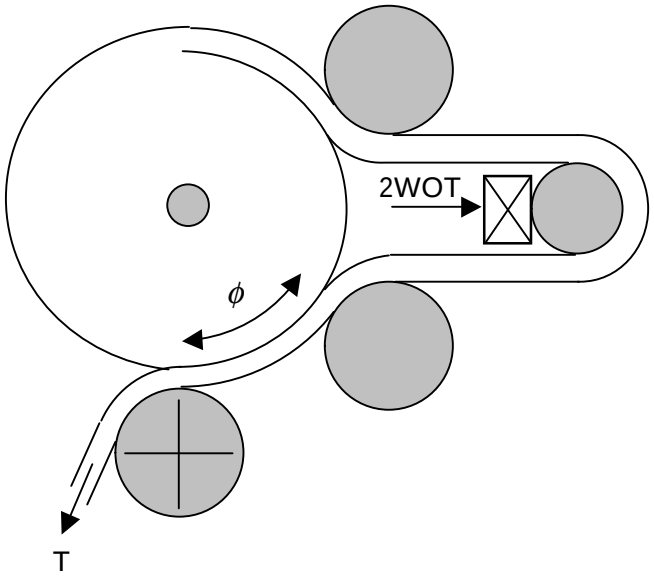

FIGURE 70 Direct WOT measurement configuration with a WOT roller (Pfeiffer 1977) and (Pfeiffer 1977). Good claims (Good et al. 1999) that the WOT measurement roller can measure only a fraction of the true WOT: $WOT_{measured} = \frac{WOT}{e^{\mu\phi}}$ where ϕ is the wrap angle shown in the figure and μ is the paper to paper friction coefficient.

The differences in the OSU and JvH nip models are fundamental, and still both succeed in explaining the same measurement data, perhaps because both have enough freedom to choose the unknown paper parameters appropriately. The JvH model's method to solve the nip indentation is more exact (maybe only FEM model can do better) than that of OSU model, and it can also handle compliant winding drum cover. The JvH model accounts for stick/slippage on both contact surfaces on the web in the nip, whereas the OSU model only considers the web-roll surface. The JvH model does not make a priori assumptions on the mechanism, which creates the NIT, but the winding contact problem is solved in a general way. The OSU model uses the Poisson effect as the source of web tension in the nip, and uses a heuristic method to solve the nip strains and stresses. And finally the JvH model has no problem to include the Winding Force in the solution.

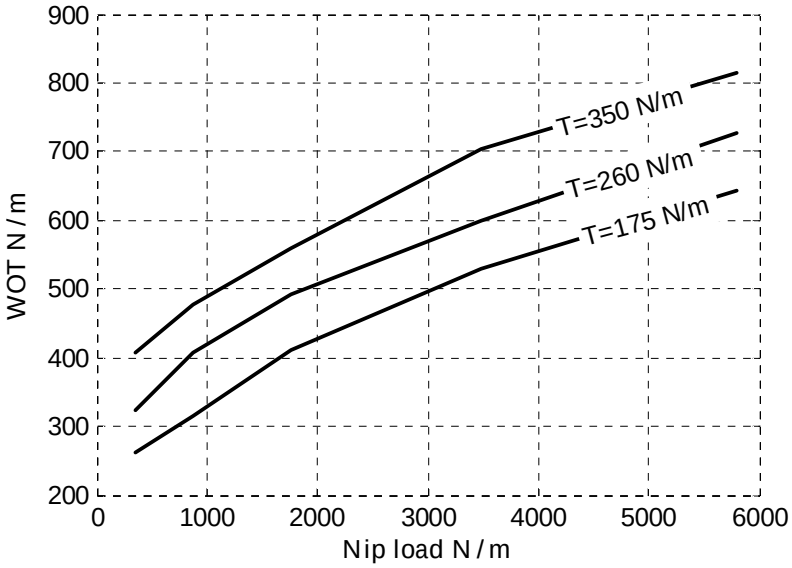

FIGURE 71 WOT measurement data for centre wound Newsprint (Good et al. 1999). The measurement was repeated three times for web tensions 175, 260 and 350 N/m each with several values of nip loading. The Nip Induced Tension *NIT=WOT-T* does not depend on web tension as both OSU and JvH nip models agree.

The OSU model's explanatory power is weaker, but it is much simpler and easier to compute than the JvH model. It can be easily fitted to the measurement data, if the resulting values for the coefficient of friction and Poisson ratio can be accepted. The JvH model is more general and fundamental, and it can be tested more comprehensively with hybrid winding measurement data. On the other hand, it also relies on hard to find paper parameter values, which make the results somewhat arbitrary. The JvH model could be improved by replacing the linear orthotropic material model with a non-linear orthotropic material model.

5.6 Experimental nip modeling

The nip model is an essential tool to accomplish the control and optimization of the winding process, the goal of this work. The available theoretical nip models lack either field of applicability, or are very laborious to program and overload the available CPU capacity. To overcome these obstacles, a fully experimental nip model is instead implemented as a replacement. The WOT measurement method described earlier is used, which is based on the density measurement and the total stress version of the wound roll stress model. The roll radial pressure measurements are used only as a reference to see that the pressures got from the wound roll stress model are reasonable.

The modeling is done as extensively as possible, not only centre or surface winding, but also as hybrid winding. The nip loading, web tension, winding force and web speed are used in a broad range. The roll size is close to paper mill size, and the measurements are recorded over a wide diameter range. The model has been measured for two paper grades, Newsprint paper of 55 gsm and 85 micrometers thick and 57 gsm LWC paper of 53 micrometers thick. The Newsprint is non-calendered and non-coated soft and bulky paper. The LWC is lightly coated (5 gsm on both sides) and calendered paper, much harder in the z-direction than the Newsprint. The resulting pressures in the LWC rolls are higher than in the Newsprint rolls. The reverse run to measure the paper caliper was done for each measurement run to check the possible caliper loss due to calendering in the winding nip. The measurement series for both grades were run for both steel winding drum and a soft covered compliant winding drum. The total period of time over which the measurements were run was 7 months, so some variation in the environmental conditions and the test rolls were possible over time. The climatic conditions in the pilot plant were not controlled, but they were recorded.

5.6.1 The pilot winder

The pilot winder is depicted in FIGURE 72. The maximum roll size is 1800 mm in diameter and 2800 mm in width. The maximum web speed is 3500 m/min and web tension up to 1500 N/m. The winding drum diameter is 800 mm.

The pilot winder is of single-drum type, with only one winding drum and the roll is core supported. The nip loading on the winding nip can be completely controlled by loading or relieving the roll by means of the core support. The rider rolls can be used as extra loading and relieving element especially for wide rolls to avoid excessive loads at the core. The rider rolls provide also a means to draw the roll at its periphery to make possible winding force control. The winding force can be controlled from pure surface winding through centre winding up to positive winding force.

The pilot winder drive control system is specially programmed to allow running the winder in both directions. In normal mode the web is unwound from the roll on the left in FIGURE 72. The winding direction can be reversed at any roll size so that the web is unwound from the “windup” roll on the right and running direction is to the left. The web tension, winding force and nip

loading controls work as normal in the reversed running mode. The unwind stand on the left, which works as windup in the reverse running mode, winds the roll in pure nipless centre winding mode. The Wound On Tension is then equal to the web tension and no special WOT measurement is needed in the reverse running mode.

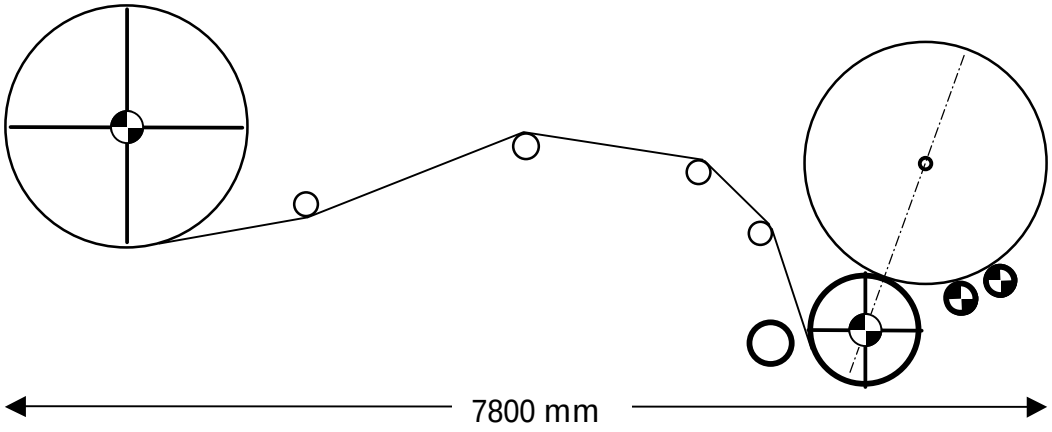

FIGURE 72 The pilot winder. The unwind roll is on the left and the windup roll is on the right. The roll is centre supported, and the nip loading at the winding nip is partially controlled by means of loading/relieving at the core centre, and partially by loading or supporting with the driven rider roll system. The winding drum, rider rolls and the unwind drum are driven. The rider roll system is equipped with drives for winding force control. The winding drum is speed controlled, and the rider roll and unwind drives torque controlled. The winder can be run in both directions, normally from left to right and in reversed mode from right to left.

The winder has standard measurement equipment: web tension measurement roller with three load cells, nip loading measurement by load cells at the roll centre support and winding force measurement from the drive system torque measurements. The web length is measured by means of a 5000 pulse encoder on the winding drum. The roll diameter is measured with pulse counting equipment, which uses the winding drum pulses and photocell that detects the roll revolutions from a reflective tape on the roll centre.

5.6.2 The pressure measurements

The pressure measurements were done with the Flexiforce™ force sensitive resistor instruments (Tekscan Inc.), FIGURE 73.

The total length of the sensor is 203 mm and the centre of the sensing area is about 167 mm from the roll edge inside the roll. The diameter of the sensing head is 9.53 mm and the area is 71.3 square millimeters. The sensor thickness is 0.127 mm, which is about 2-3 times the paper thickness. The sensor comes in various force measurement ranges. At first the 'M'-type sensors were used, which have $0 - 111$ N range, or $0 - 1.5$ MPa in pressure. The sensors can be overloaded to about twice the nominal range, so LWC paper roll pressures can

also be measured. However, it was found, that the 'M'-type sensors did not sustain the higher load peaks in the nip, but eventually would break down. Even worse, before they failed completely they lost their calibration and gave false readings. The sensors were replaced with the higher load 'H'-types in the course of the test series, which have poorer resolution but did last better in the winding environment. The 'H'-type sensors have 0 - 444 N range, or 0 – 6 MPa in pressure. Each sensor used needed individual calibration with a dead weight.

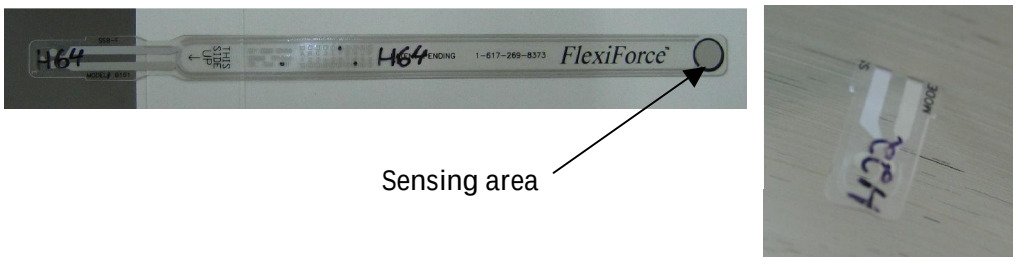

FIGURE 73 The pressure measurement sensor on the roll (left), and the sensor connector head sticking out of the roll edge (right).

The force sensitive resistors are a replacement for the simple pull tabs, but both are actually force sensors. And to give precise pressure readings, they need to be calibrated with known pressures. This was done in the stack testing machine, where the sensors could be loaded with a series of known pressures inside a stack of paper. The need to make the pressure calibration paper grade specifically is caused by the thickness of the sensor and the different hardness of the paper grades, FIGURE 74.

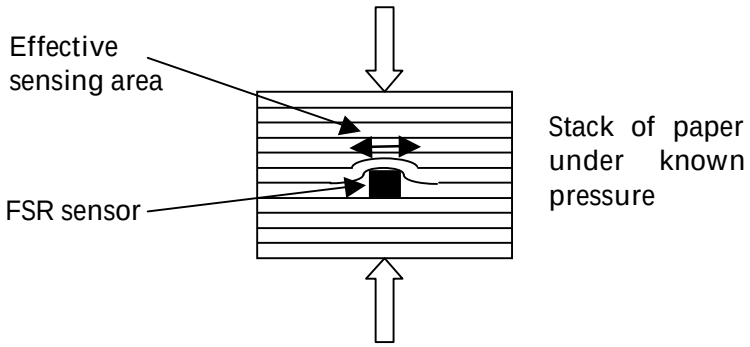

FIGURE 74 Calibration of the force sensitive sensors in the stack testing machine. The same calibration is required for the pull tabs, if absolute pressure values are measured.

The calibration curves for LWC and Newsprint papers are shown in FIGURE 75. The linear fit gives the calibration parameters:

	Multiplier	Offset MPa
LWC	0.626	-0.0604
Newsprint	0.669	-0.138

Viscoelasticity causes extra trouble to the sensor calibration, especially with the softer Newsprint paper. When the sensors are in the stack or in the roll over longer periods of time under pressure, the paper layers close to the sensor conform to it and cause less load to be carried by the sensor. The calibration must be checked so that the sensor is not removed from the layers but they are cut out from the roll together and taken to the stack testing machine. This problem is valid for pull tabs too, but they are not normally kept in the roll any longer time before they are pulled out of it.

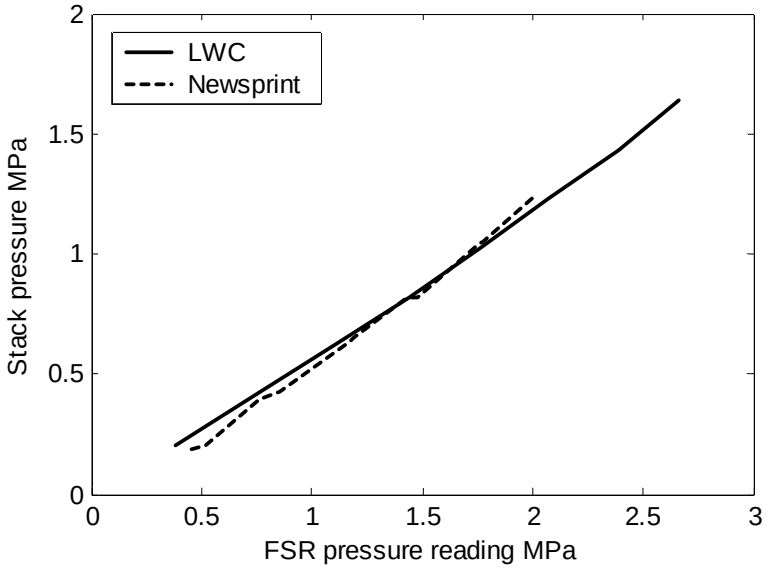

FIGURE 75 FSR sensor calibration curves for LWC and Newsprint papers.

5.6.3 Model structure

The a prori information of the nip model suggest that the Nip Induced Tension is not a very non-linear function of nip loading and winding force, see FIGURE 71. Therefore simple second order polynomials are sufficient to give reasonable interpolation accuracy. The chosen modelling method would then be the Response Surface Method (RSM) with up to second order terms. This is reasonable also because there is no simple theoretical parametric curve available that could be fitted to the data. The form of the quadratic response function is

$$\begin{aligned} WOT = {} & a_{11}NL^2 + a_{12}NL*T + a_{13}NL*ST + a_{14}NL*S + a_{21}T^2 + \\ & a_{22}T*ST + a_{23}T*S + a_{31}ST^2 + a_{32}ST*S + a_{41}S^2 + \\ & b_1NL + b_2T + b_3ST + b_4S + c_1 \end{aligned} \tag{97}$$

where NL is the nip load, T is the web tension, ST is the surface traction on the roll and S is the web speed. The coefficients a_{ij},b_i and c_1 are the parameters in the model. Their values are found by fitting the model to the measurement data by means of the least squares method. The value of the constant term c_1 is

immediately known to be zero, since the model should give zero Wound On Tension for zero input values.

The definition of Winding Force = Surface Traction – Web Tension and the Jorkama's winding theorem can be used to simplify the model to the Nip Induced Tension form

$$NIT = WOT - T = a_{11}NL^2 + a_{12}NL * WF + a_{13}NL * S + a_{21}WF^2 + a_{22}WF * S + a_{31}S^2 + b_1NL + b_2WF + b_3S \quad (98)$$

where WF is the Winding Force. Further simplification is achieved if the web speed quadratic and cross terms are left out, as the experimental evidence later on suggests. The reason for this is simple: it is difficult to wind with low nip loads and high speeds, because then the roll tends to become unstable in the lateral direction. So the measurement data would not contain such points. Also the dependence on web speed is smaller than on the other variables, so the non-linear speed related terms do not improve the model.

5.6.4 Design of Experiments

The measurement points were chosen according to the Central Composite Faced (CCF) design. In this design there are only three levels per factor. The measurement points lie on the corners of a hypercube and on the centres of the hypercube faces. There are also points in the centre of the hypercube. An example of the LWC paper experiment measurement points are in FIGURE 76.

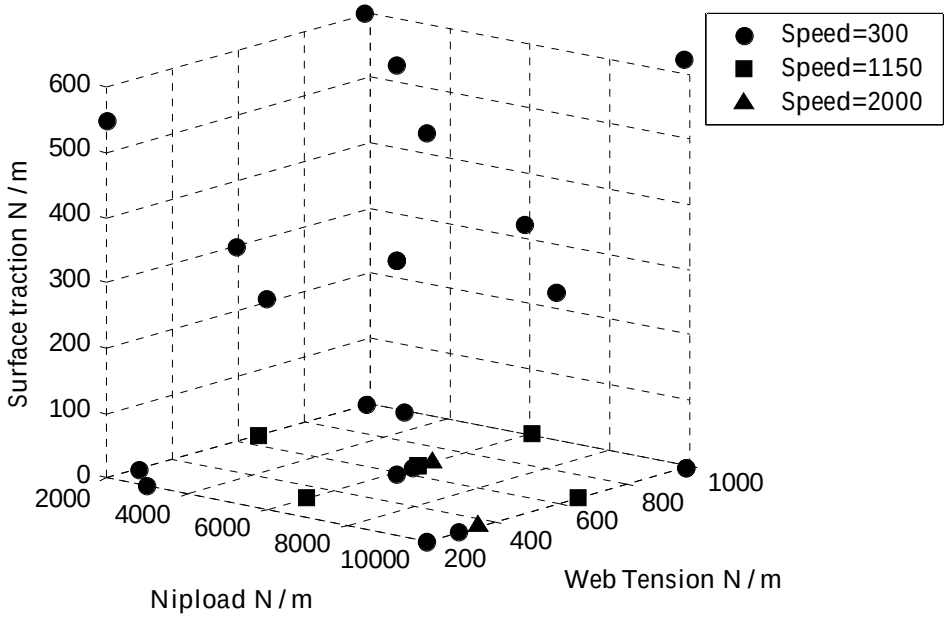

FIGURE 76 The measurement points in the Niploa-Tension-Surface Traction space. The web speed is the fourth factor, which is indicated with different markers. The number of measurement points is in this case 32, whereas CCF orthogonal design would contain 36 points for 4 factors. The condition number of the information matrix $X'X$ for the scaled and centered regressor matrix X is 2.91, so the design is not anymore orthogonal.

Not all the measurement points in the CCF design were possible to run. Especially many of the higher speed points had to be left out. Also some of the surface traction – nip load combinations are friction limited due to slippage. In spite of these limitations the more sophisticated D-optimal design methods were not used. The condition number for the Fisher's information matrix was in the range 2.9 to 5.4 in the four measurement series.

5.6.5 Centrifugal correction to the web tension measurement

At higher speeds the centrifugal acceleration at the web tension roller must be accounted for, FIGURE 77.

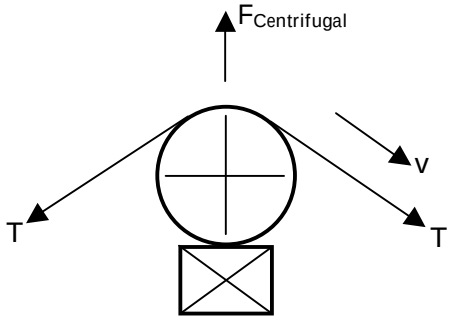

FIGURE 77 The centrifugal force relieves part of the force caused by the web tension on the web tension measurement roller.

The pressure *P* under the web wrap over the tension measurement roller on any surface element of area *dA* and mass *dm* is (the hoop pressure equation is used here)

$$P = \frac{T - \frac{dm}{dA} v^2}{R} = \frac{T - bv^2}{R} \tag{99}$$

where *R* is the roller radius, *v* is the web speed and *b* is the web basis weight. Since the force on the load cell is got as the integral of the (vector) pressure over the contact area, the measured web tension is the term bv^2 less than the true web tension. If the units of the basis weight are kg / m^2 and web speed m / s then the units of the correction term are N / m. When the drive system tension controller uses the uncorrected web tension measurement as its actual value, the true web tension will be correspondingly higher than the desired web tension. At 3000 m / min speed and 60 gsm basis weight the error is 150 N / m. At 1800 m / min the error is 54 N / m, so without a correction the true web tension would be 100 N / m higher at the higher running speed.

5.6.6 Other possible model outputs

The Wound On Tension is not the only conceivable output variable that can be chosen as the experimental nip model output variable. The measured web thickness in the roll or any other derived variable that relates to the roll hardness could do. The web thickness (or density) is not the best possible choice since it suffers from the calibration problem caused by the web caliper variations. When the measured web caliper is available, the radial strain is a better measure that accounts for the caliper changes:

$$\varepsilon_r = \frac{h}{h_0} - 1 \tag{100}$$

where h is the measured web thickness and h_0 is the web calliper. The web thickness measured by the density measurement is not exactly the true roll web thickness as mentioned earlier in the chapter covering the density measurement, but it is not far from the true value. And if only a measure of roll hardness is considered, the deviation from the true thickness does not matter.

Another choice for the output variable could also be the radial stress computed from the radial strain by means of the stress-strain curve. The stress or pressure is quite tangible measure of the roll hardness since it can also be directly measured with pull tabs and FSR's. And finally the stress can be transformed into the radial elastic modulus with the non-linear elastic modulus function:

$$E_r(\sigma_r) = C_0 + C_1\sigma_r + C_2\sigma_r^2 \tag{101}$$

The elastic modulus is a somewhat more abstract measure of roll hardness. However, it is also related to the visible roll hardness properties, like to the force needed to rotate the roll on the factory floor.

All these measures except the Wound On Tension can be directly computed from the measured web thickness or through the more strenuous way using the wound roll stress model. The more complicated method gives the correct form of stress and strain distributions inside the roll, and it also partitions the effect of speed into centrifugal and nip related terms. And the wound roll stress model is the only method, which can account for viscoelastic paper properties.

The Wound On Tension is however the "true" nip model output, because it is a direct result of the idealized winding nip effect. All the other roll hardness measures are only consequences of the WOT that was produced during winding. The WOT is measured in the same units as web tension and winding force, and its magnitude is close to them. Therefore the WOT is the preferred nip model output. The WOT is also directly related to the standard Cameron roll hardness test through the tangential elastic modulus.

5.7 Newsprint paper nip model measurement data

The data is compacted into "zero-dimensional" roll model, where each data row represents one complete winding run. The data is averaged over a diameter range in the roll, with beginning and end of the winding left out from the average. An example of a typical measurement run is shown in FIGURE 78.

There was no clear diameter dependence on the Wound On Tension curves as seen in FIGURE 79. The small increase/decrease of the WOT at acceleration and deceleration is perhaps due to the lacking inertia compensation in the Winding Force in the pilot winder.

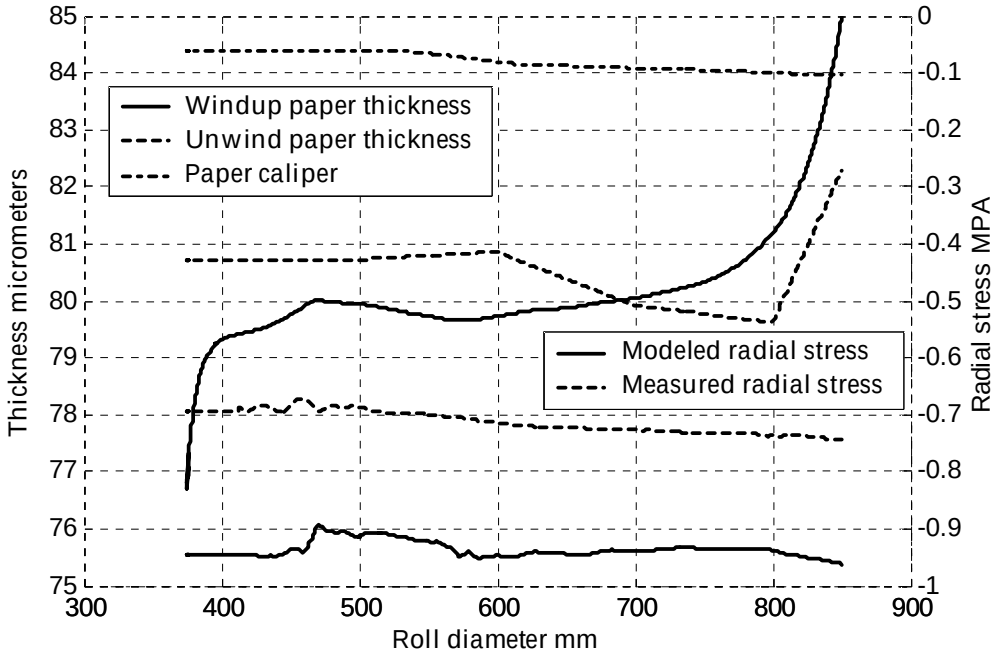

FIGURE 78 Newsprint paper measurement data. The averages for the model data are taken over the diameter range of 500 to 800 mm. There were 10 FSR pressure sensors in the roll at 5 different radial locations in pairs, on each sides of the roll. The measured pressure line is the average of the sensors on both sides of the roll.

Table 7 Newsprint paper properties. The paper calliper is h, the basis weight is b, the radial elastic modulus parameters C_0,C_1,C_2, the paper to paper friction coefficient μ_{PP}, the paper to drum friction coefficient μ_{PD} and the tangential elastic modulus parameters E_{t0} and E_{t1}. The Poisson ratios were set to zero.

h, mm	C_0, MPa	C_1	C_2, 1/MPa	E_{t0}, MPa	E_{t1}	b g/m^2	μ_{PP}	μ_{PD}
0.0848	0.674	-35.2	-22.6	5800	111	55	0.35	0.34

The Newsprint paper parameter values are shown in Table 7. The paper calliper value is not actually used anywhere in the computations, since the actual calliper is measured by means of the preceding reverse run before every measurement run, as seen in FIGURE 78. The total stress version of the wound roll stress model was used with the logarithmic stress strain curves both in

radial and tangential directions. The data was run with the steel (hard) winding drum. The wound roll stress model did not compensate for viscoelasticity. The measured radial stress (column 2 in Table 8) was used to check the validity and accuracy of the model stress output, see FIGURE 80. The radial stress measured with the FSR s is obviously less accurate and reliable measure of the roll hardness than the results obtained by means of the density measurement and the wound roll stress model. However, the correlation between the measured and model stresses is quite good. In order to reach this result the FSR s had to be recalibrated after the runs due to the soft paper as described earlier.

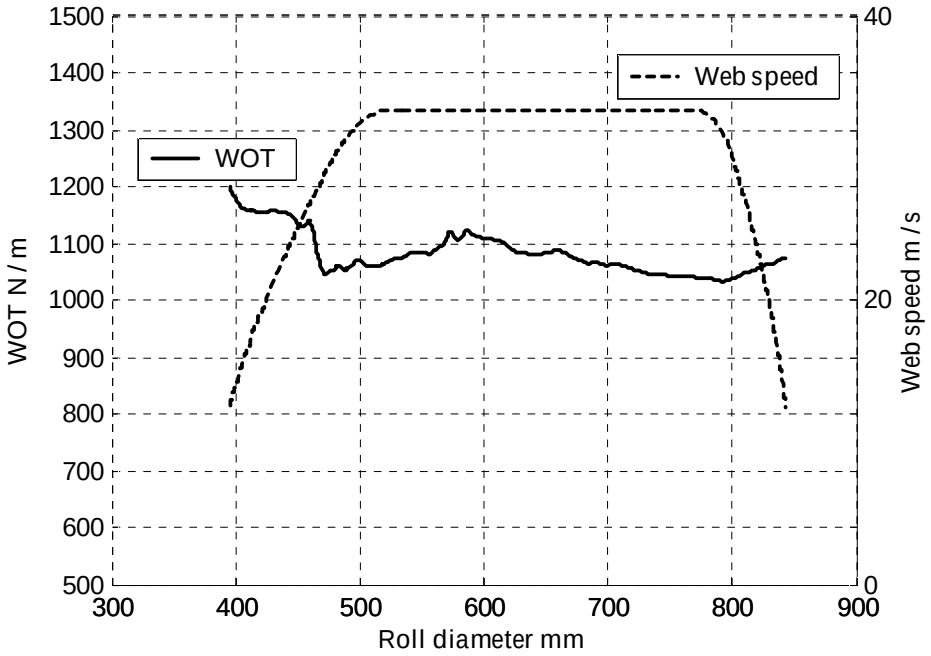

FIGURE 79 The Wound On Tension and web speed curves from the same run as in FIGURE 78. There is a slight dependence of WOT on speed or acceleration.

Table 8 Newsprint paper measurement data from 32 test winding runs. The data is sorted according to ascending Wound On Tension. The pilot winder was equipped with the steel winding drum. Viscoelasticity is not modelled in the data. The columns and their units are: σ_r,model = radial stress in MPa computed from the wound roll stress model, σ_r,meas. = measured radial stress in MPa with the FSR s, WOT = computed Wound On Tension in N / m, NL = nip load in N / m, T = web tension in N / m, ST = surface traction in N / m, S = web speed in m / s, h = web calliper in mm, ε = radial strain and E_r = radial elastic modulus in MPa.

σ_r,model	σ_r,meas.	WOT	NL	T	ST	S	h	ε	E_r
-0.08	0.05	349	1998	205	0	12.1	83.9	-0.05	3.4
-0.09	0.03	358	2000	198	0	5.0	84.2	-0.05	3.5
-0.10	-0.04	410	1991	511	0	19.2	84.4	-0.05	4.1
-0.10	-0.02	412	1996	844	0	33.2	84.0	-0.05	3.9
-0.14	-0.10	467	2000	787	0	5.0	84.2	-0.06	5.3
-0.18	-0.13	593	4991	217	0	19.2	83.7	-0.07	6.2
-0.25	-0.26	722	4998	398	0	10.0	85.1	-0.08	8.1
-0.26	-0.29	733	4999	398	0	10.0	85.1	-0.08	8.2
-0.26	-0.26	737	4998	398	0	10.0	85.0	-0.08	8.3

-0.25	-0.21	745	4994	550	0	33.2	83.7	-0.08	8.0
-0.27	-0.25	749	4991	511	0	19.2	84.0	-0.08	8.5
-0.27	-0.27	750	4998	398	0	10.0	85.0	-0.08	8.5
-0.28	-0.20	765	4991	511	0	19.2	83.9	-0.08	8.7
-0.28	-0.28	770	4990	511	0	19.2	84.5	-0.08	8.7
-0.30	-0.28	786	5000	492	0	5.0	84.3	-0.08	9.2
-0.27	-0.23	816	7990	256	0	33.3	84.2	-0.08	8.5
-0.32	-0.32	847	8000	198	0	5.0	84.5	-0.08	9.5
-0.35	-0.36	852	4992	805	0	19.2	83.7	-0.09	10.2
-0.32	-0.38	874	4991	198	300	5.0	84.4	-0.08	9.6
-0.38	-0.44	931	7990	511	0	19.2	83.8	-0.09	10.7
-0.36	-0.39	941	4992	198	600	5.0	84.3	-0.09	10.4
-0.53	-0.55	1122	8000	787	0	5.0	84.1	-0.10	13.0
-0.50	-0.47	1125	7990	845	0	33.2	84.2	-0.10	12.6
-0.57	-0.51	1180	4993	786	300	5.0	84.3	-0.11	13.4
-0.55	-0.44	1192	6493	491	300	5.0	84.4	-0.10	13.2
-0.56	-0.52	1264	7991	198	625	5.0	84.9	-0.10	13.3
-0.63	-0.56	1285	4993	786	566	5.0	85.1	-0.11	13.9
-0.62	-0.53	1307	6492	492	600	5.0	84.3	-0.11	13.8
-0.70	-0.68	1394	7992	786	300	5.0	84.5	-0.11	14.3
-0.82	-0.81	1576	7991	786	625	5.0	85.0	-0.12	14.3

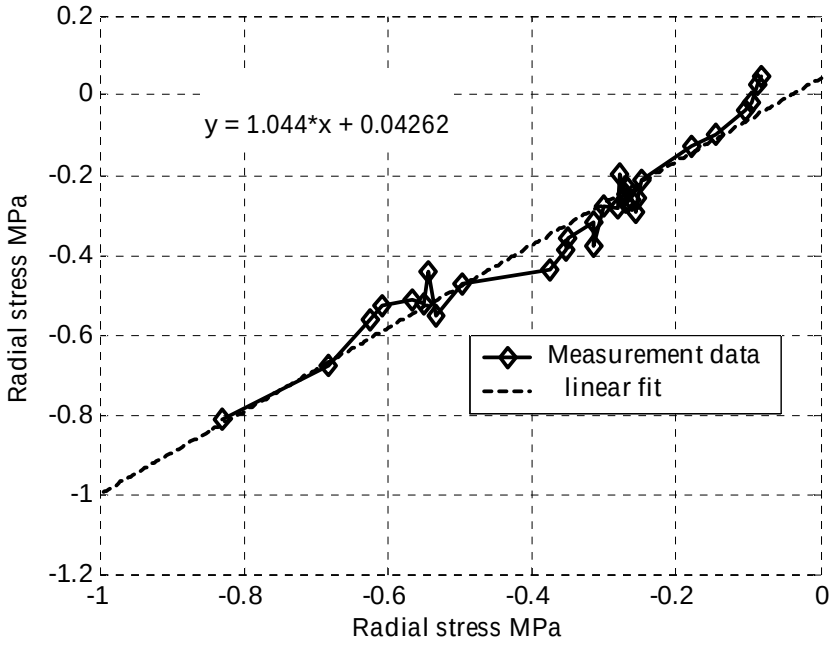

FIGURE 80 Correlation between the radial stress computed from the wound roll stress model (x-axis) and the radial stress measured with the FSR's (y-axis). The data is taken from Table 8.

The "H"-type Flexiforce sensors seem to be too crude to measure the lowest pressures correctly in FIGURE 80. There is always variation in the sensor readings between the radial locations and the sides of the roll as seen in FIGURE 78. This variation is caused by hardness and thickness variations in the paper web itself, and it causes randomness to the measurements. The more

sensors are used, the better average pressure is measured. The sensing area of the sensor is quite small increasing the possibility that the sensor can be placed on a local hard or soft spot.

The importance of measuring the paper calliper for every measurement run is evident in FIGURE 81. The Newsprint paper is soft and has high viscoelasticity and so it looses considerably thickness on every run. If this would not be compensated, the wound roll stress model would give false results. The viscoelasticity shows up also during pauses in the run series. Normally 2-4 measurement runs could be done per day. If there is a break of several days or perhaps just a weekend, the paper regains some of its bulk while it is left alone in the roll.

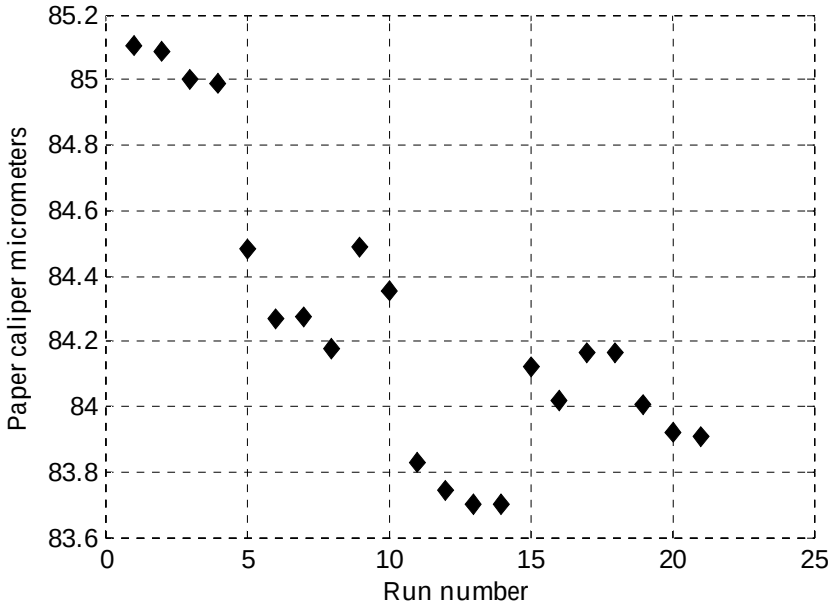

FIGURE 81 The loss of bulk during the measurement run series. The figure shows the measured average paper calliper in the 21 first runs (the roll is the same). The points were the calliper increases mark pause in the test run.

The stress-strain dependence is seen in FIGURE 82. It follows the stress-strain curve measured in the stack testing machine "Computed stress". The small deviation is due to the difference of the web thickness that the density measurement gives compared to the true web thickness inside the roll. The pressure in the tightest roll was a decade greater than the pressure in the softest roll, which still was a roll, not a pile of paper. The highest stress is yet well under one megapascal. The range of strain is from less than 5% up to 12%. The range of the Wound On Tension is from 349 N/m up to 1576 N/m. The "normal" Newsprint paper roll pressure of 0.5 MPa is reached at about 1100 N/m WOT. The radial modulus varied from 3.4 MPa to 14.3 MPa, and the value at 0.5 MPa pressure was 12.6 MPa, where the strain was 10%.

5.7.1 Newsprint paper measurement data run with resilient winding drum

The measurement series was run with the same paper but instead of the hard steel winding drum a soft covered resilient winding drum was used. The maximum WOT is slightly higher than with the hard winding drum due to the higher maximum nip load used (10000 versus 8000 N/m). The paper parameters were otherwise the same as for the hard winding drum runs except for the paper to drum friction coefficient μ_{PD}, which was now 0.49.

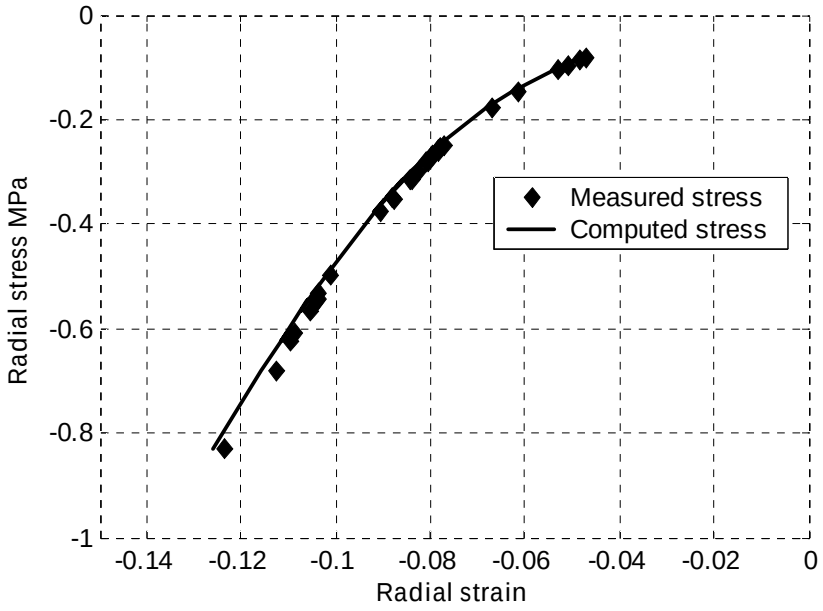

FIGURE 82 The stress-strain curve from the Newsprint measurement data.

Table 9 Newsprint measurement data from the 27 winding runs with the resilient winding drum. The data is sorted to ascending WOT.

σ_r,model	σ_r,meas	WOT	NL	T	ST	S	h	ε	E_r
-0.08	-0.11	345	2000	198	0	5.0	82.2	-0.05	3.5
-0.17	-0.22	507	2000	786	0	5.0	83.1	-0.07	5.9
-0.16	-0.17	524	1990	510	0	19.2	82.3	-0.06	5.7
-0.17	-0.19	541	1992	510	0	19.2	82.4	-0.07	5.9
-0.17	-0.23	559	1990	198	325	5.0	82.6	-0.07	6.1
-0.19	-0.25	602	1994	843	0	32.8	82.4	-0.07	6.5
-0.26	-0.30	677	1989	786	325	5.0	82.9	-0.08	8.4
-0.33	-0.44	846	5988	509	0	19.2	82.7	-0.09	9.8
-0.36	-0.28	886	5996	510	0	19.2	82.5	-0.09	10.3
-0.35	-0.39	887	5989	198	325	5.0	82.6	-0.09	10.2
-0.36	-0.43	888	6000	491	0	5.0	83.3	-0.09	10.5
-0.37	-0.50	908	5996	510	0	19.2	82.4	-0.09	10.6
-0.35	-0.44	914	5985	548	0	32.7	82.5	-0.09	10.3
-0.43	-0.36	970	5991	804	0	19.2	82.7	-0.10	11.6
-0.37	-0.47	980	9988	254	0	32.7	82.5	-0.09	10.5
-0.42	-0.37	1028	9990	216	0	19.2	82.8	-0.09	11.5
-0.44	-0.33	1053	10001	198	0	5.0	82.9	-0.10	11.9
-0.48	-0.48	1096	5990	198	625	5.0	82.8	-0.10	12.3
-0.53	-0.55	1103	5989	786	325	5.0	83.0	-0.10	13.0

-0.51	-0.46	1140	9991	510	0	19.2	82.7	-0.10	12.8
-0.59	-0.64	1191	10000	786	0	5.0	82.5	-0.11	13.6
-0.59	-0.57	1244	9991	841	0	32.4	82.5	-0.11	13.6
-0.61	-0.51	1308	9989	198	325	5.0	83.3	-0.11	13.7
-0.69	-0.64	1334	5985	786	599	5.0	83.6	-0.11	14.2
-0.66	-0.69	1385	9986	198	625	5.0	82.7	-0.11	14.1
-0.83	-0.88	1547	9989	786	325	5.0	83.3	-0.12	14.3
-0.88	-0.81	1622	9986	786	625	5.0	83.1	-0.13	14.1

The correlation between the measured and computed stresses are not as good as with the hard winding drum, see FIGURE 83. The reason for this is the difficulty of calibrating the sensors for the paper. There were two sets of sensors used in the run series, and calibration drift over time caused problems.

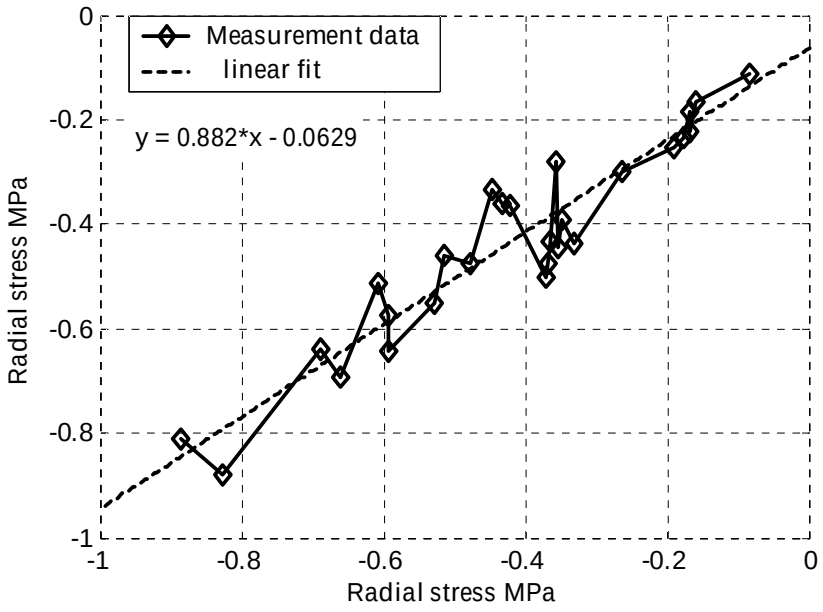

FIGURE 83 Correlation between the radial stress computed from the wound roll stress model (x-axis) and the radial stress measured with the FSR's (y-axis). The data is taken from Table 9.

The calliper loss in the course of the measurement run series is again shown in FIGURE 84. Again the paper regains part of its lost bulk, if the roll is not wound for several days. The decrease in calliper from run to run is larger when the roll was wound tight in the preceding run. The total decrease in thickness over the 2x(32+27)=118 runs were almost 3 micrometers from the original 85 micrometers = 3.5 %.

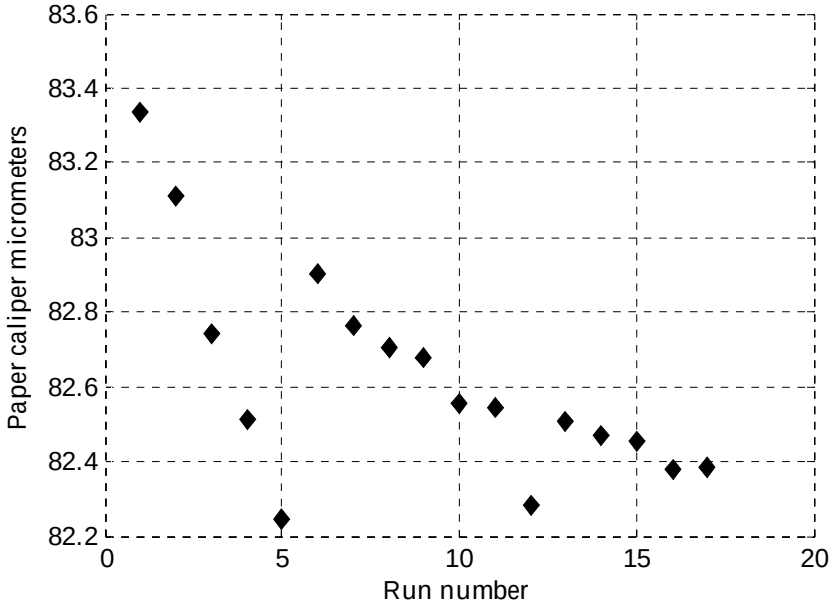

FIGURE 84 The loss of bulk during the measurement run series. The figure shows the measured average paper calliper in the 17 first runs (the roll is the same). The points were the calliper increases mark pause in the test run.

5.8 Newsprint paper response surface nip models

The Response Surface Method model was fitted to the previous measurement data with the Matlab™ Statistics Toolbox function Regress. The model is full quadratic to nip load, web tension and surface traction but only linear to speed. The constant term is zero. The model parameters are shown in Table 10 for both the direct WOT model and for the NIT model. All the quadratic term coefficients are negative, indicating that the WOT curve bends downwards when nip load, tension or surface traction increases, which is reasonable. The linear term coefficients are positive except for speed, meaning that increase in speed decreases WOT. Speed increase of 10 m / s decreases WOT 20 – 30 N / m.

Table 10 The Response Surface model parameters to the Newsprint paper nip model data for hard winding drum. The WOT model was fitted to the data directly and the NIT model according to the NIT model *WOT-T=NIT(T,WF)*, where *WF* is the Winding Force = Surface Traction – Web Tension. The terms in the table are: NL = nip load, T = web tension, ST = surface traction and S = web speed.

	NL^2	NLxT	NLxST	T^2	TxST	ST^2	NL	T	ST	S
WOT model	-7.88e-06	4.13e-05	4.04e-05	-0.000180	0.000220	-0.000817	0.153	0.339	0.779	-2.05
NIT model	-6.46e-06	1.67e-05	-1.67e-05	-0.000125	0.000250	-0.000125	0.158	0.373	0.627	-3.82

The goodness of fit is shown in FIGURE 85. The difference between the modelled and measured WOT is shown along with the 95% confidence limits of the residuals. The direct WOT model fitted slightly better to the data, the maximum residual was then –44 N / m for the 593 N / m WOT and RMS residual was 21.8 N / m and $R^2_{adjusted}$ 0.993. The maximum residual for the NIT model

was then –82 N / m for the 847 N / m WOT and RMS residual was 40.5 N / m and $R^2_{adjusted}$ 0.980.

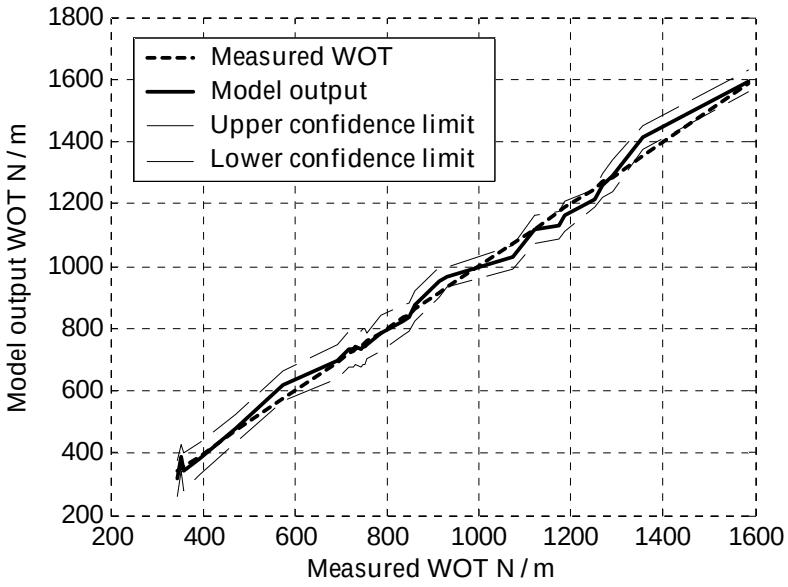

FIGURE 85 The Response Surface model fit to the measurement data.

The linear term coefficients give 160 N / m increase in WOT for 1000 N / m increase in nip loading, 34 – 37 N / m increase in WOT for 100 N / m increase in web tension and 78 – 63 N / m increase in WOT for 100 N / m increase in surface traction.

5.8.1 Nip model parameters for the resilient winding drum

The fit to the measurement data for the resilient winding drum was not as good as for the hard winding drum, even though the reason for this is not evident in the measurement data.

Table 11 The Response Surface model parameters for the resilient winding drum.

	NL^2	NLxT	NLxST	T^2	TxST	ST^2	NL	T	ST	S
WOT model	-3.33e-06	7.96e-06	3.36e-05	-0.000463	3.34e-05	-0.000380	0.118	0.755	0.579	0.688
NIT model	-3.78e-06	-6.98e-06	6.98e-06	-9.33e-05	0.000187	-9.33e-05	0.133	0.466	0.534	0.805

The direct WOT model fitted again slightly better to the data, the maximum residual was then -69 N / m for the 980 N / m WOT and RMS residual was 38.0 N / m and $R^2_{adjusted}$ 0.979. The maximum residual for the NIT model was then 100 N / m for the 1547 N / m WOT and RMS residual was 46.0 N / m and $R^2_{adjusted}$ 0.975.

The linear term coefficients give 118 - 133 N / m increase in WOT for 1000 N / m increase in nip loading, 76 – 47 N / m increase in WOT for 100 N / m increase in web tension and 58 –53 N / m increase in WOT for 100 N / m increase in surface traction. The decrease in WOT for increasing speed is now practically

zero. The web tension seems to have larger effect in WOT and nip load smaller effect than with hard winding drum.

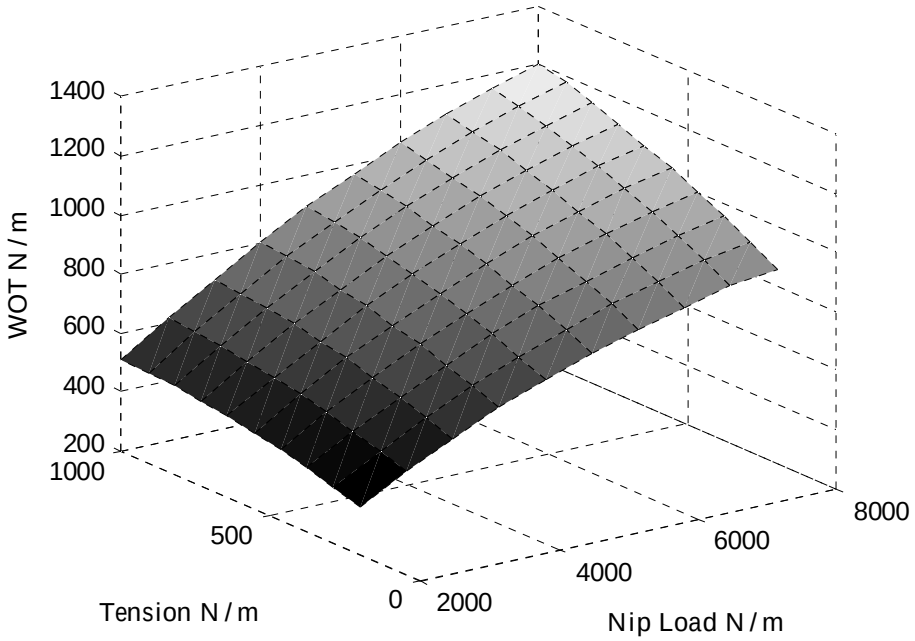

FIGURE 86 The Response Surface Model for the Newsprint paper nip model with hard winding drum. The model is drawn as a function of nip load and web tension and at zero surface traction and web speed.

5.8.2 Comparison of the hard and resilient winding drum nip models for Newsprint paper

The comparison was done at different web tension and surface traction levels and as a function of the nip load. The curves for zero surface traction are shown in FIGURE 87. The hard winding drum produces slightly more WOT at lower nip loads, but at over 6000 – 8000 N / m nip loads the resilient winding drum gives more WOT. The WOT curve for hard winding drum saturates at lower nip loads and the maximum WOT remains lower than for the resilient winding drum. Exceptionally at low nip loads and high web tensions the soft covered drum produces more WOT than the steel drum. The effect of surface traction is seen in FIGURE 88. The surface traction increases more WOT for hard than resilient winding drum and the saturation at high nip loads for hard winding drum seem to occur later.

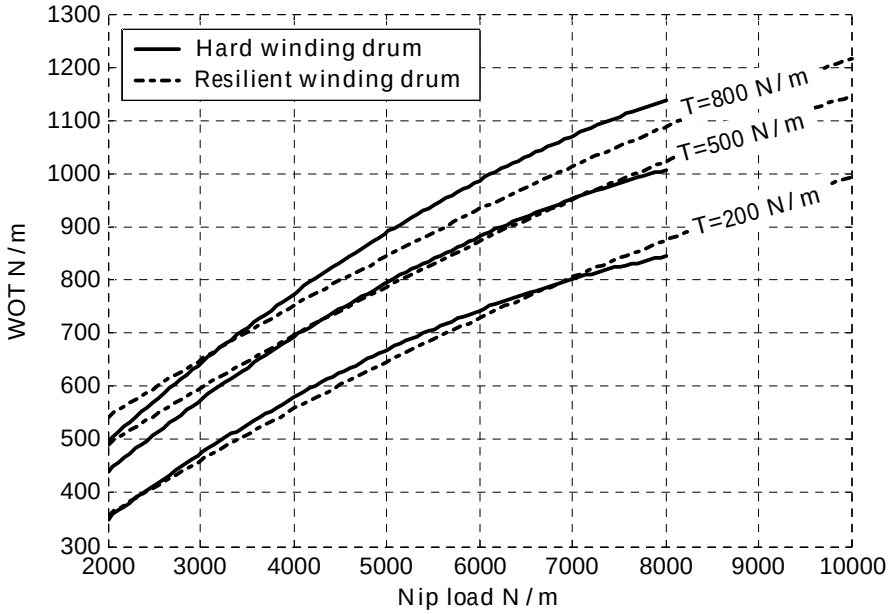

FIGURE 87 Comparison of the WOT produced by the hard and resilient winding drums. The curves are drawn for three different web tensions and zero surface traction.

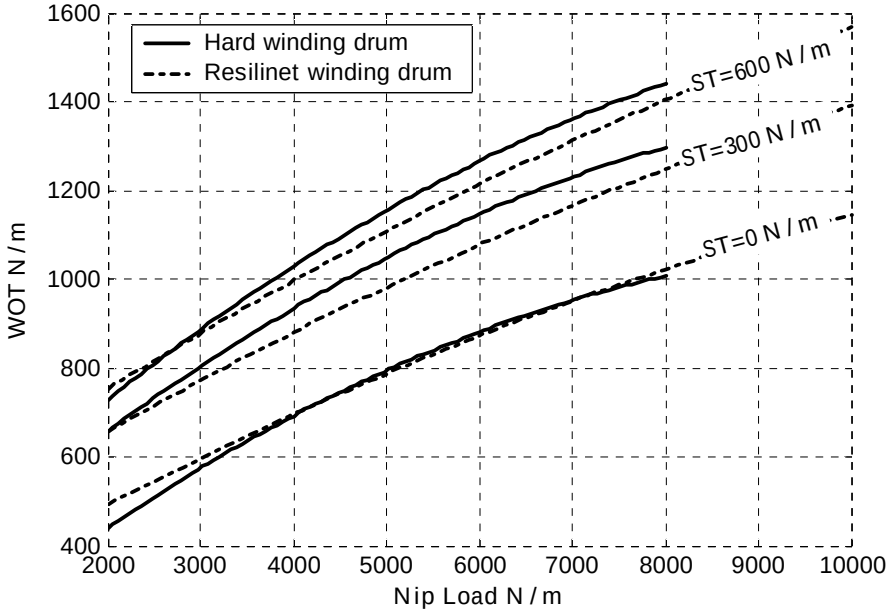

FIGURE 88 Comparison of the WOT produced by the hard and resilient winding drums. The curves are drawn for three different surface tractions and web tension was kept at 500 N / m.

5.9 LWC paper nip model measurement data

The LWC paper is much harder in the radial direction (z-direction in the stack) than the Newsprint paper, and this results higher radial pressures in the roll. Also the radial deformations are smaller than with the Newsprint paper. Even though the larger pressure range improves pressure measurement resolution, there is more variation in the pressure values between different measurement

positions in the roll. This variation is due to the thickness and hardness variations in the LWC paper. Also the higher nip pressure causes more pressure sensor wear and failures and worse measurement accuracy. The smaller radial strain range also causes worse density measurement resolution, which degrades measurement accuracy. However, it was possible to measure the nip model data with reasonable accuracy.

Table 12 LWC paper properties. The paper calliper is h, the basis weight is b, the radial elastic modulus parameters C_0,C_1,C_2, the paper to paper friction coefficient μ_{PP}, the paper to drum friction coefficient μ_{PD} and the tangential elastic modulus parameters E_{t0} and E_{t1}. The Poisson ratios were set to zero.

h, mm	C_0, MPa	C_1	C_2, 1/MPa	E_{t0}, MPa	E_{t1}	b g/m^2	μ_{PP}	μ_{PD}
0.0503	1.38	-68.5	-17.6	8730	76.5	57	0.25	0.34

The measurement data is in Table 13. Even though the range of WOT is close to the range for the Newsprint paper, from less than 500 N/m up to 1600 N/m, the range of pressures go up to 2.5 MPa compared to Newsprint paper's less than 1 MPa. The range of radial strain is from 4.5 to 8.5 %, which is less than 2 micrometers in paper thickness. The approximate median value for WOT is at 1100 N/m and 1.5 MPa pressure, three times higher than for Newsprint. The 1 MPa pressure is crossed at about 800 N/m WOT.

Table 13 LWC paper measurement data from 22 test winding runs. The data is sorted according to ascending Wound On Tension. The pilot winder was equipped with the steel winding drum. Viscoelasticity is not modelled in the data. The columns and their units are: σ_r,model = radial stress in MPa computed from the wound roll stress model, σ_r,meas. = measured radial stress in MPa with the FSR's, WOT = computed Wound On Tension in N/m, NL = nip load in N/m, T = web tension in N/m, ST = surface traction in N/m, S = web speed in m/s, h = web calliper in mm, ε = radial strain and E_r = radial elastic modulus in MPa.

σ_r,model	σ_r,meas	WOT	NL	T	ST	S	h	ε	E_r
-0.42	-0.33	480	1999	305	0	13.3	50.30	-0.045	26.8
-0.57	-0.47	559	1999	648	0	13.3	50.33	-0.050	34.7
-0.69	-0.64	612	2001	992	0	13.3	50.24	-0.053	40.0
-0.79	-0.66	716	4999	305	0	13.3	50.33	-0.056	44.3
-0.91	-0.74	757	2995	296	325	5.0	50.41	-0.058	49.0
-1.10	-0.74	840	2999	640	325	5.0	50.46	-0.061	55.3
-1.08	-1.12	850	5002	648	0	13.3	50.24	-0.062	54.7
-1.07	-1.03	862	8000	305	0	13.3	50.35	-0.061	54.6
-1.08	-1.03	865	7001	403	0	13.3	50.20	-0.062	54.6
-1.23	-1.26	896	5001	648	0	13.3	50.28	-0.063	58.9
-1.14	-0.95	909	4992	701	0	33.3	50.21	-0.062	56.6
-1.24	-1.16	910	5001	649	0	13.3	50.38	-0.064	59.1
-1.26	-1.22	915	5000	640	0	5.0	50.21	-0.064	59.7
-1.56	-1.65	1058	7999	648	0	13.3	50.31	-0.069	65.4
-1.67	-1.71	1072	5003	992	0	13.3	50.27	-0.070	66.5
-1.52	-1.39	1095	7996	296	325	5.0	50.51	-0.068	64.7
-1.55	-1.09	1096	7996	296	625	5.0	50.41	-0.069	65.2

-1.72	-1.59	1119	4995	640	555	5.0	50.54	-0.070	67.0
-1.92	-1.38	1218	7996	640	325	5.0	50.54	-0.073	67.9
-2.02	-2.15	1244	8001	991	0	13.3	50.27	-0.076	67.8
-2.22	-1.62	1341	5500	983	595	5.0	50.51	-0.078	66.5
-2.69	-2.31	1606	7999	983	625	5.0	50.46	-0.085	63.3

5.9.1 LWC paper measurement data run with resilient winding drum

The measurement data for the resilient winding drum in Table 14 shows lower WOT values than with the hard winding drum. The maximum nip load used was again higher, 10000 instead of 8000 N/m. The paper parameters were otherwise the same as for the hard winding drum runs except for the paper to drum friction coefficient μ_{PD}, which was now 0.37.

Table 14 LWC measurement data from the 22 winding runs with the resilient winding drum. The data is sorted to ascending WOT.

σ_r,model	σ_r,meas.	WOT	NL	T	ST	S	h	ε	E_r
-0.07	0.02	193	1999	659	0	19.2	51.16	-0.039	6.2
-0.22	-0.19	308	2000	982	0	5.0	51.31	-0.052	17.0
-0.69	-0.59	662	5997	316	0	19.2	51.38	-0.068	40.0
-0.70	0.00	677	1997	198	550	5.0	51.88	-0.068	40.4
-0.84	-0.79	725	6004	659	0	19.2	51.05	-0.071	43.4
-0.84	-0.70	730	6007	658	0	19.1	51.29	-0.071	43.3
-0.78	-0.79	730	5993	701	0	33.3	51.28	-0.070	42.1
-0.88	-0.76	735	6000	639	0	5.0	51.42	-0.072	43.9
-0.91	-0.98	762	5998	659	0	19.2	51.54	-0.073	44.3
-1.03	-1.05	800	6002	1001	0	19.0	51.24	-0.075	44.9
-0.93	-1.07	842	9993	358	0	33.3	51.10	-0.073	44.4
-1.08	0.00	849	1994	982	600	5.0	52.00	-0.076	44.8
-1.16	0.00	915	5995	590	325	5.0	51.66	-0.078	44.3
-1.22	-1.10	949	10008	656	0	18.8	51.20	-0.080	43.5
-1.27	0.00	1004	5997	590	325	5.0	51.89	-0.081	42.9
-1.31	0.00	1018	5997	590	325	5.0	51.88	-0.081	42.9
-1.54	-1.53	1117	10001	982	0	5.0	51.44	-0.087	42.9
-1.52	0.00	1128	5995	982	325	5.0	52.15	-0.086	42.9
-1.51	-1.12	1147	9993	1044	0	33.3	51.34	-0.086	42.9
-1.53	0.00	1211	5996	590	624	5.0	52.00	-0.087	42.9
-1.56	0.00	1257	9998	198	625	5.0	52.16	-0.088	42.9
-1.88	0.00	1562	9992	982	625	5.0	52.00	-0.101	42.9

The caliper loss of the LWC paper is shown in FIGURE 89. The LWC paper has lost only 0.5 micrometers of the original paper thickness in the 2x13=26 runs.

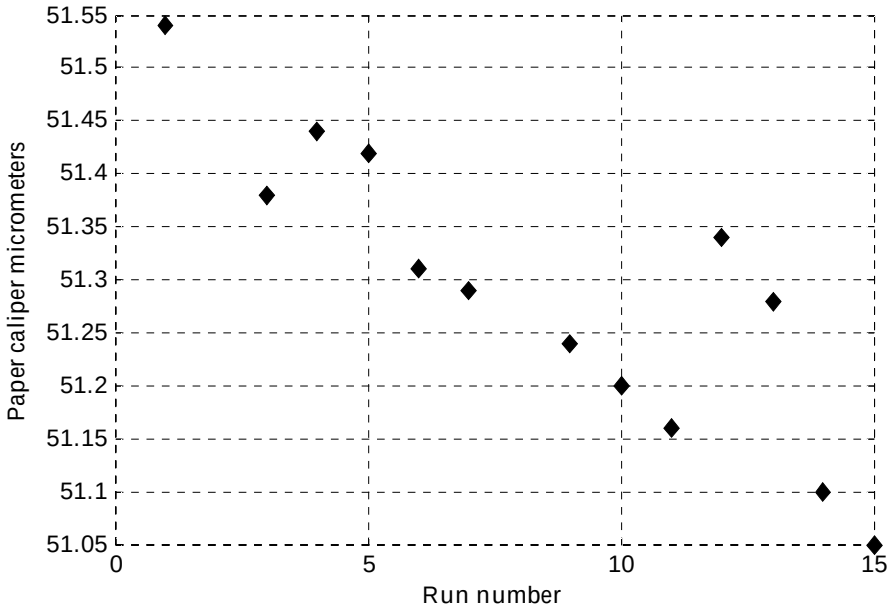

FIGURE 89 The loss of bulk during the measurement run series. The figure shows the measured average paper calliper in the 13 first runs (the roll is the same). The points where the calliper increases mark pause in the test run.

The radial strains in the Table 14 for the resilient winding drum are larger than the strains for the hard winding drum because there were two rolls used, one for the hard winding drum runs and another for the resilient winding drum runs. The paper was the same in the rolls, and they were even taken from the same production set. However, the cross machine thickness variation causes differences in the paper properties. The stress strain curves were measured for both of the rolls to compensate the differences.

5.10 LWC paper response surface nip models

The nip model parameters are shown in Table 15 for hard winding drum. The speed dependence is practically zero for both model versions. The linear term coefficients give 160 – 180 N / m increase in WOT for 1000 N / m increase in nip load, 28 – 40 N / m increase in WOT for 100 N / m increase in web tension and 60 – 63 N / m increase in WOT for 100 N / m increase in surface traction.

Table 15 The Response Surface model parameters to the LWC paper nip model data for hard winding drum. The WOT model was fitted to the data directly and the NIT model according to the NIT model *WOT-T=NIT(T,WF)*, where *WF* is the Winding Force = Surface Traction – Web Tension. The terms in the table are: NL = nip load, T = web tension, ST = surface traction and S = web speed.

	NL^2	NLxT	NLxST	T^2	TxST	ST^2	NL	T	ST	S
WOTmodel	-1.23E-05	4.56E-05	3.73E-05	-5.01E-05	1.13E-04	-8.23E-04	1.79E-01	2.82E-01	6.30E-01	1.76E-01
NITmodel	-8.53E-06	2.74E-05	-2.74E-05	-7.69E-05	1.54E-04	-7.69E-05	1.57E-01	3.97E-01	6.03E-01	1.29E-02

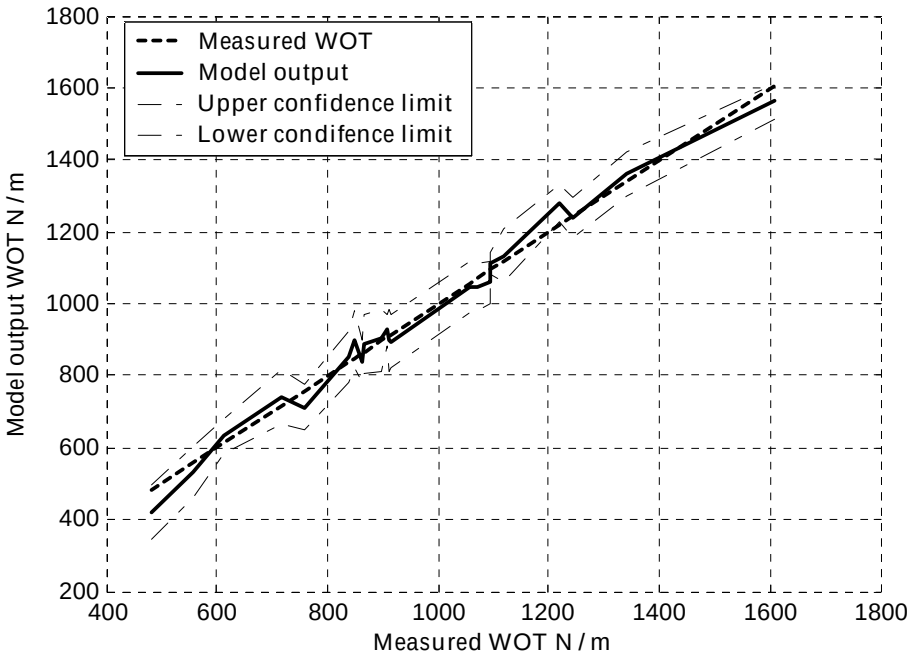

FIGURE 90 The Response Surface model fit to the measurement data.

The goodness of fit is shown in FIGURE 90. The maximum residual for the WOT model was 60 N / m at 480 N / m WOT (and for 1218 N / m WOT), the RMS residual was 30.5 N / m and $R^2_{adjusted}$ was 0.976. The maximum residual for the NIT model was 77 N / m for 1095 N / m WOT, the RMS residual was 40.0 N / m and $R^2_{adjusted}$ was 0.968. Again the normal model gave a slightly better fit to the data than the NIT model.

5.10.1 Nip model parameters for the resilient winding drum

The nip model parameters are shown in Table 16. The resilient winding drum gave still quite small dependence on speed, 10 m / s increase in speed decreases WOT only by 10 – 20 N / m. The linear term coefficients for give 130 – 170 N / m increase in WOT for 1000 N / m increase in nip load and 85 – 96 N / m increase in WOT for 100 N / m increase in surface traction. The effect of web tension is almost vanishing. The WOT model version has even negative coefficient for the web tension linear term, but it is compensated by the quadratic term.

Table 16 The Response Surface model parameters for the resilient winding drum.

	NL^2	NLxT	NLxST	T^2	TxST	ST^2	NL	T	ST	S
WOTmodel	-8.62E-06	3.46E-05	-2.17E-05	3.06E-04	1.47E-04	-7.45E-05	1.73E-01	-3.77E-01	8.52E-01	-1.13E+00
NITmodel	-5.44E-06	3.61E-05	-3.61E-05	-3.24E-05	6.48E-05	-3.24E-05	1.34E-01	4.03E-02	9.60E-01	-2.08E+00

5.10.2 Comparison of the hard and resilient winding drum nip models for LWC paper

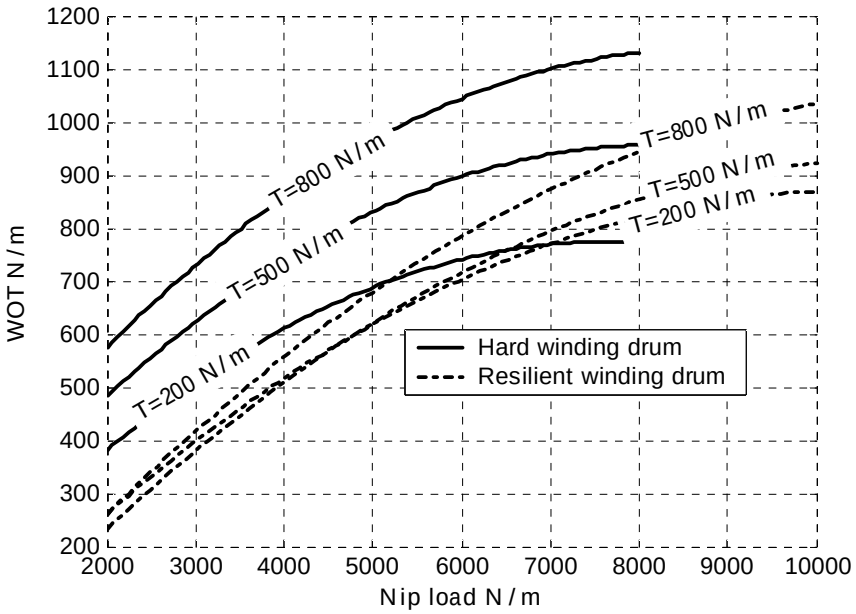

FIGURE 91 Comparison of the WOT produced by the hard and resilient winding drums. The curves are drawn for three different web tensions and zero surface traction.

The result of the comparison for the hard and resilient winding drum for the LWC paper is shown in FIGURE 91 and FIGURE 92. The effect of the nip load on the WOT saturated for the hard winding drum at about 8000 N / m nip load and larger nip loads would not produce any more WOT, the same result as with the Newsprint paper. The web tension has much larger effect on WOT for the hard winding drum, but the surface traction has on the other hand larger effect for the resilient winding drum.

The effect of surface traction saturates quickly for the hard winding drum, and there is not much more WOT gained between 300 and 600 N / m surface traction especially for low nip loads. On the other hand for the resilient winding drum, the surface traction increase from 300 to 600 gives almost as much more WOT as the increase from 0 to 300 N / m.

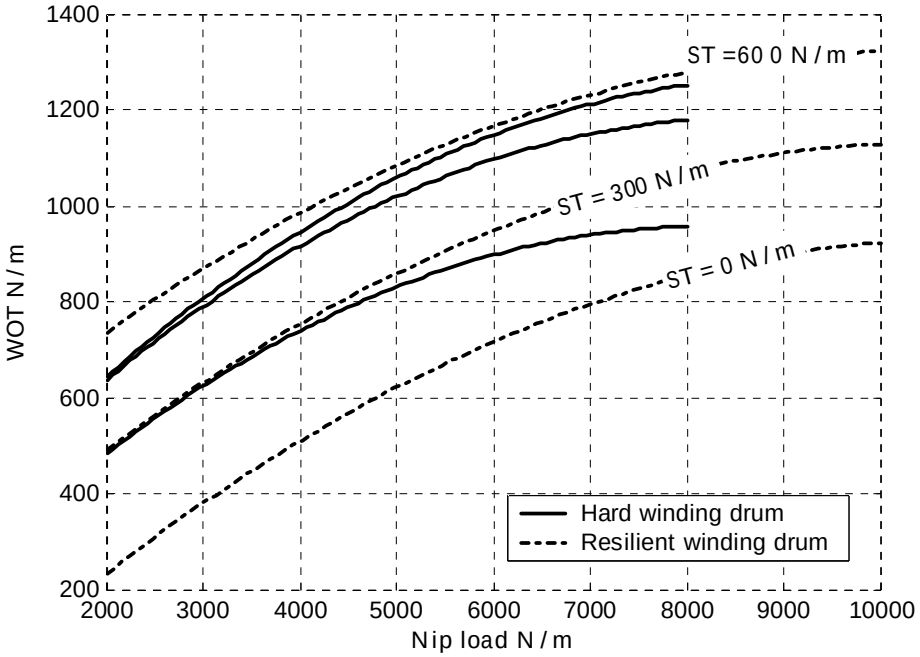

FIGURE 92 Comparison of the WOT produced by the hard and resilient winding drums. The curves are drawn for three different surface tractions and web tension was kept at 500 N / m.

5.11 Viscoelasticity in winding nip modeling

The effect of viscoelasticity on the Wound On Tension measurement and modeling was tested with the Newsprint paper and hard winding drum. The Newsprint was chosen, since it is more viscoelastic than the LWC paper. The Newsprint paper is uncalendered and bulky, and it has retained its deformation capacity better than the LWC paper. The z-direction viscoelasticity in the Newsprint paper was modeled with two time constants of 180 and 4300 seconds, the first accounting for 0.51% strain and the other for 0.46% strain. The faster time constant is much less than the winding time in the pilot winder, so the layers deeper inside the roll have relaxed this time constant already before the pressures are measured from the roll. The MD viscoelasticity was also modeled with two time constants of 14 and 369 seconds and the strain is 0.015% as a sum for both time constants together.

The viscoelastic relaxation has very small effect on the modeled radial pressures and Wound On Tensions for the Newsprint paper. The result is shown in a compact form in FIGURE 93, which shows the radial stress and strain curves as a function of the WOT. The WOT values are also taken from both versions. The effect of the winding time viscoelastic relaxation can be seen to be negligible. Also the effect on the computed WOT values is very small. The relaxation of course depends on the winding time and thus the winding speed. The winding time varied from 240 seconds to 1600 seconds.

However, the viscoelasticity do show up as a pressure drop over longer periods of time. The roll was run with 5000 N / m nip load, 400 N / m web

tension and with 600 m/min web speed, which produced 750 N/m WOT. The winding time was 830 seconds. After the winding the pressures were measured. Then the roll was left alone for 17 hours and the pressures were measured again. The resulting pressure relaxation is seen in FIGURE 94.

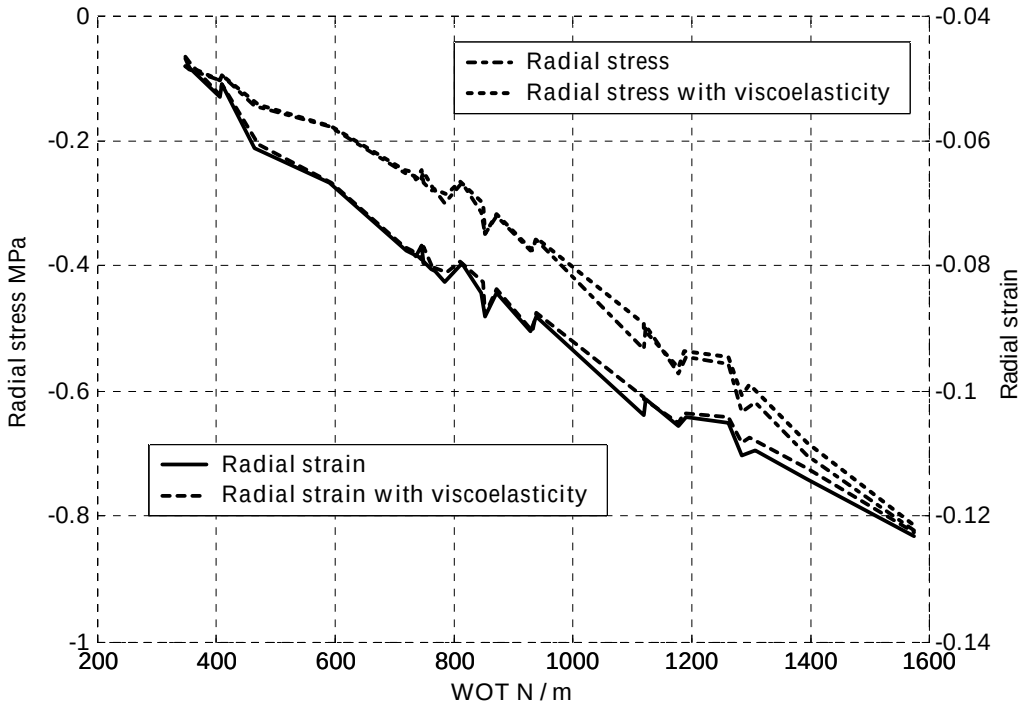

FIGURE 93 Comparison of the radial stresses, radial strains and Wound On Tensions measured for Newsprint paper with viscoelasticity modelled in the wound roll stress model and without it.

The average pressures after the winding were 0.260 MPa from the model and 0.269 MPa from the measurements. After 17 hours relaxation time the pressures had dropped to 0.202 MPa from the model and 0.228 from the measurements. The relative relaxation was then 22.3% in the model pressures and 15.2% in the measured pressures. The model overestimates the relaxation, which is perhaps caused by inaccurate viscoelastic parameters. The parameters were measured only over 2 hours period in the stack testing machine, which might be too short time to measure the long term behaviour correctly. Another explanation can be temperature or humidity changes in the pilot plant in the night. This was quite a loose roll and the pressure was only half of the 0.5 MPa level that can be considered as normally tight roll. At higher pressures the relaxation will be larger.

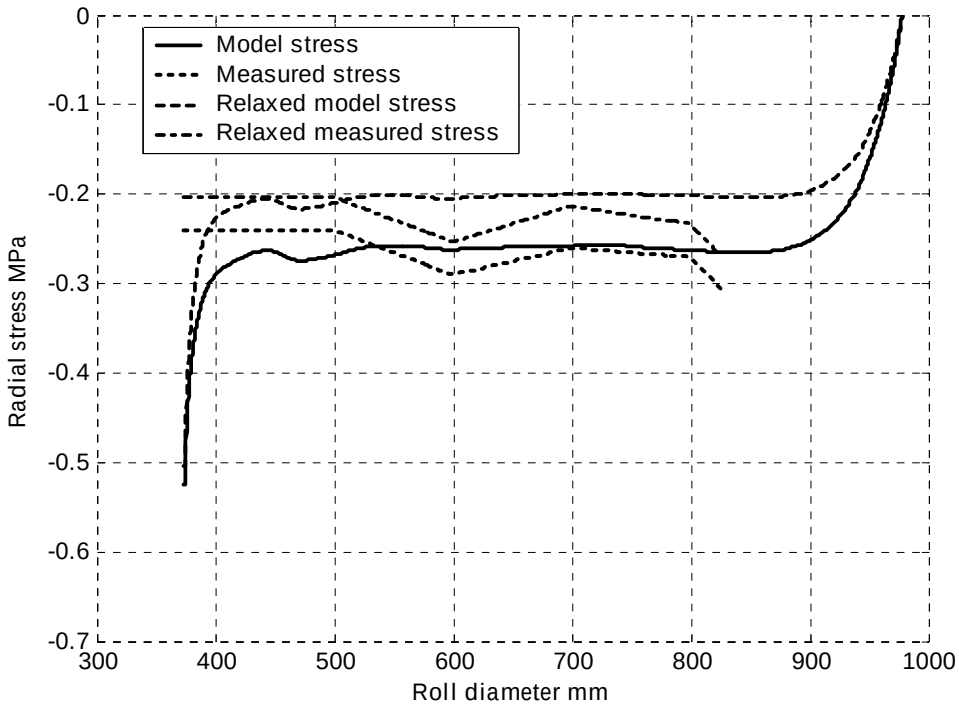

FIGURE 94 Pressure relaxation in the Newsprint paper roll in 17 hours.

5.12 Comparison of the Newsprint paper nip model to the Good's measurement data

The hard winding drum nip model for the Newsprint model output were compared to the WOT measurement data by Good, FIGURE 71, even though the paper properties differ from each other in Table 6 and Table 7. The result of the comparison is drawn in FIGURE 95. The values are close to each other at low nip loads, but at higher nip loads the measured values remain at much lower WOT levels than the model values. Both the model and the measurement data have similar dependence on web tension. The measurement data in Table 8 has the lowest nip loads at 2000 N/m, so the nip model is an extrapolation below the 2000 N/m nip load level.

5.13 Validation of the measurement data and the wound roll stress model

The validation data was run in the reverse running mode, which is pure centre winding and the Wound On Tension is equal to the web tension. Winding speed was 300 m/min. The roll was wound four times with different web tensions of 400, 500, 600 and 700 N/m. The pressure in the roll was measured after every run with 10 FSR sensors at five radial locations. The result is seen in FIGURE 96.

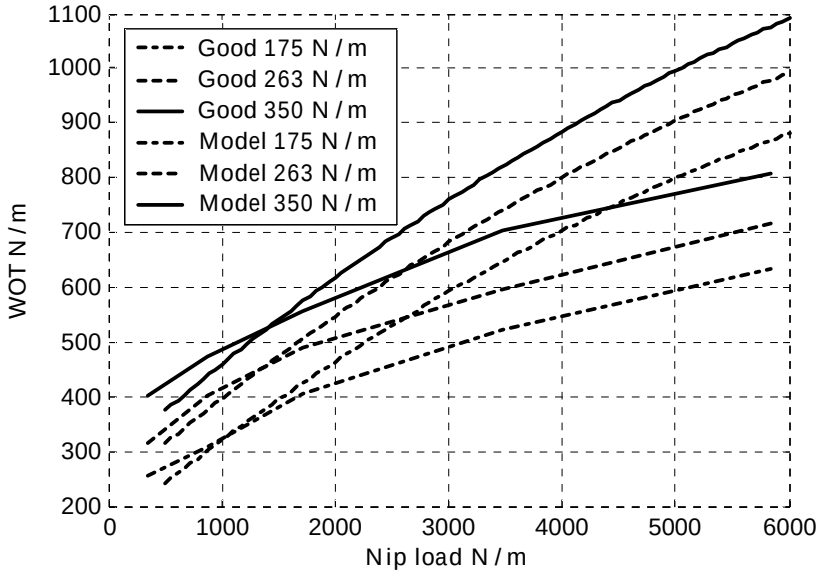

FIGURE 95 Comparison of the measurement data for centre wound Newsprint (Good et al. 1999) and the Newsprint paper nip model output. The lines are drawn with three web tension values and over a range of nip load.

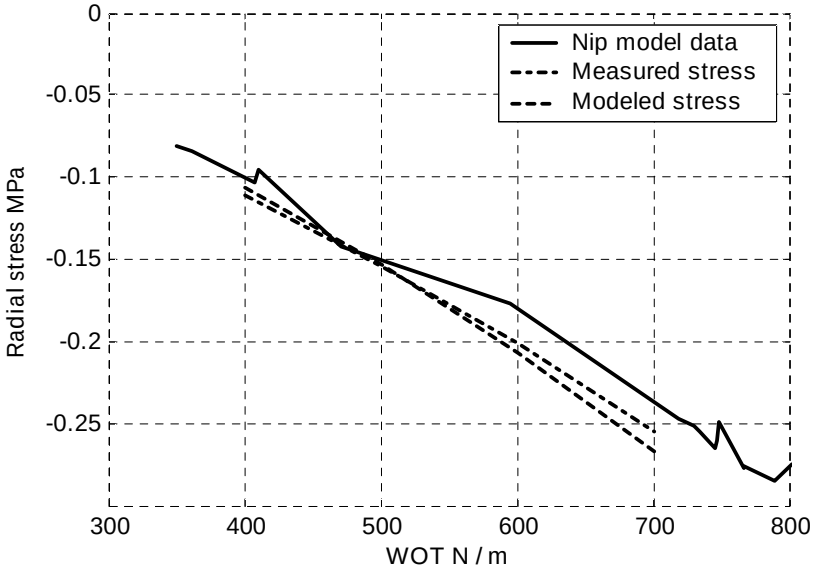

FIGURE 96 Validation measurement data for the Newsprint paper. The nip model data is taken from Table 8 from the modelled stress column.

The modeled stress was simulated with the total stress wound roll model with tension loss in the outer web layer. The small deviation of the nip model data from the other lines at 600 and 700 N / m WOT can be explained by the higher running speed at these measurement points.

The measurement data does support the Jorkama's winding theorem (Jorkama 2001), even though the NIT model fit was not as good as the WOT model fit. The NIT model predicts that for constant winding force and nip load web tension increase causes equal increase in WOT, which is approximately true.

6 NEW PARADIGM FOR WINDING CONTROL

The traditional trial and error winding control tuning is based on empirical knowledge on how the winding parameters affect the roll tightness, what are the "good" value limits for them and how to avoid roll defects and maintain winder runnability. The feedback from the tuning trials is slow and laborious using for example Smith needle or Cameron test (Roisum 1990).

The methods and tools presented in the previous chapters are useful new tools in winding control tuning. The wound roll stress and nip models can be used in the off-line what-if control design to predict the Wound On Tension and roll stresses. The wound roll stress model can then be directly used to simulate the winding with the newly created reference value curves. The nip model in its input-output inverted form is a component in on-line winder control. The new way of winding control allows the conventional three winding parameters to be replaced by only one reference value curve that better describes the roll tightness. Finally when the measured web calliper is available, the wound roll stress model can be used to refine the measured web thickness in the roll to the actual roll stresses and Wound On Tension. This makes up a "long loop" winding control, where the outcome of the previous run can be used to fine tune the next run and iteratively find an optimum control setting.

The next chapters will outline a procedure for winder control tuning using the new tools. Finally some winding experiment results are presented that demonstrate the methods.

6.1 The inverted nip model

The experimental nip model was a function of four variables, the nip load, web tension, winding force and web speed, and the output was the Wound On Tension. The model output can also be fitted to the radial pressure. The simplest way to do this is to fit a polynomial curve between the WOT and pressure data columns.

The nip model can be used to control design if it can be inverted, that is the Wound On Tension must be the input value and the nip load, web tension and winding force the outputs. The inverted model is by no means unambiguous, the winding parameters for a certain WOT value can be chosen from an infinite set of values. The quadratic response surface model equation was

$$\begin{aligned} WOT = {} & a_{11}NL^2 + a_{12}NL*T + a_{13}NL*ST + a_{14}NL*S + a_{21}T^2 + \\ & a_{22}T*ST + a_{23}T*S + a_{31}ST^2 + a_{32}ST*S + a_{41}S^2 + \\ & b_1NL + b_2T + b_3ST + b_4S + c_1 \end{aligned} \quad (102)$$

where NL is the nip load, ST is the surface traction, T is the web tension and S the web speed. This equation can be easily solved for any of the three winding parameters and a certain WOT value. The solution values can be plotted in the (NL,T,ST) space (speed would be the fourth space coordinate, but only three dimensional plot is comfortable to visualize).

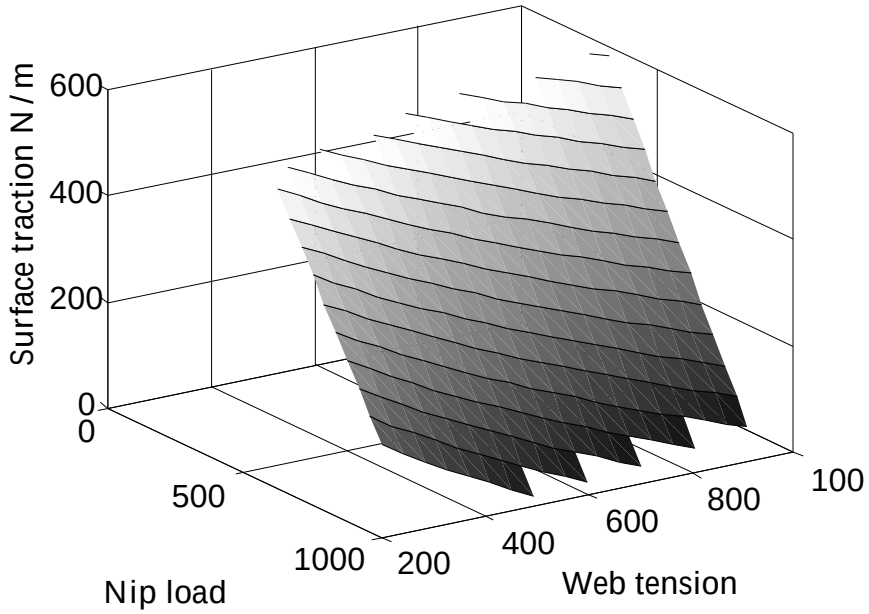

FIGURE 97 The inverted nip model plot for Wound On Tension = 1000 N / m. The plot edges are serrated due to coarse plot grid.

The surface plot in FIGURE 97 contains all the (NL,T,ST) points that give 1000 N / m WOT for 10 m / s speed, limited inside the cube of the plot. Any of the points is valid for use in the winder control to produce the 1000 N / m WOT. However, it would be advantageous to use a point close to the centre of the plot surface, as far away from the limitation cube edges as possible. This choice would give reference values that are reasonably valued and give space for possible control changes.

The limits that define the plot cube need not to be fixed, but they could be changed during winding. The cube can also shrink to a plane or even to a line if the minimum and maximum limits are set equal. In this case there would be a

great chance that no solution points exist. This would anyhow be useful if for example the web tension would be left for the winder operator to choose and only nip load and winding force would be solved from the desired WOT. Then the web tension limits are set equal to the tension set value. The winder speed is in all cases open for changes during winding.

The limits set for the winding parameters can be more versatile than simple minimum and maximum, although variable. One example of a more complicated condition is the friction limit for the winding force. The winding force cannot exceed the static friction limit

$$WF_{\max} = \mu \times NL \tag{103}$$

where μ is the paper to drum cover friction coefficient. The friction limit must hold not only for the winding drum but the other drum also used to produce the winding force. The nip load in this other nip can be different from the winding drum nip load.

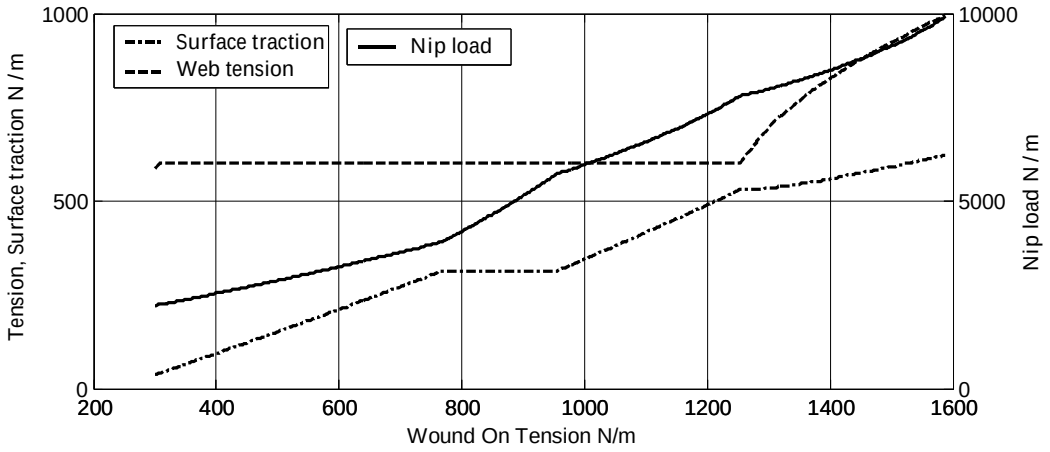

FIGURE 98 Winder reference values computed from the inverted nip model as functions of the Wound On Tension.

The winding parameter values resulting from the inverted nip model are drawn in FIGURE 98. The winding speed was kept at zero m/s in this example. As can be seen from the drawing, the web tension is constant, 600 N/m, up to 1250 N/m WOT, and increases only then. The algorithm for the inverted nip model was written to keep the web tension constant as long as possible. The priority for changing the values was selected as nip load first, then winding force and the web tension only if necessary. Web tension and winding force are kept in the middle of the limiting values as long as possible. All the three winding parameters hit the limits at the same points, at the WOT minimum/maximum.

6.1.1 The speed correction

The winding speed did not affect much the WOT produced in the winding nip, as the coefficient for speed in the experimental nip models was small. This holds at least up to 2000 m / min speeds. However, the roll does become looser even though the WOT would be same but speed higher. This is due to the centrifugal forces pulling the web layers outwards (and perhaps air penetrating the roll loosens it too). The effect of these forces is the same as if the roll would be wound with a lower effective *WOT'*:

$$WOT' = WOT - br_{out}r\omega^2 \approx WOT - bv^2 \tag{104}$$

where v is the web "speed" in the roll at the layer's radius and b is the basis weight. This in not the same speed than the speed the layer entered the roll. Even though the centrifugal forces disappear when the winder eventually stops, the roll will remain looser than it would be if it would be imaginary wound at zero speed. This is explained by the fact that the intermediate roll radii r_{out} will be larger than without the centrifugal forces. The magnitude of the winding speed loosening effect on radial pressure and paper thickness was tested with simulation on the 57 gsm LWC paper. The WOT for the wound roll stress model was adjusted until the radial pressure would be the same as with zero speed. This was repeated for several WOT and speed values. The plateau area for radial pressure is rather long even at high speeds, and the adjustment can be done for single diameter point.

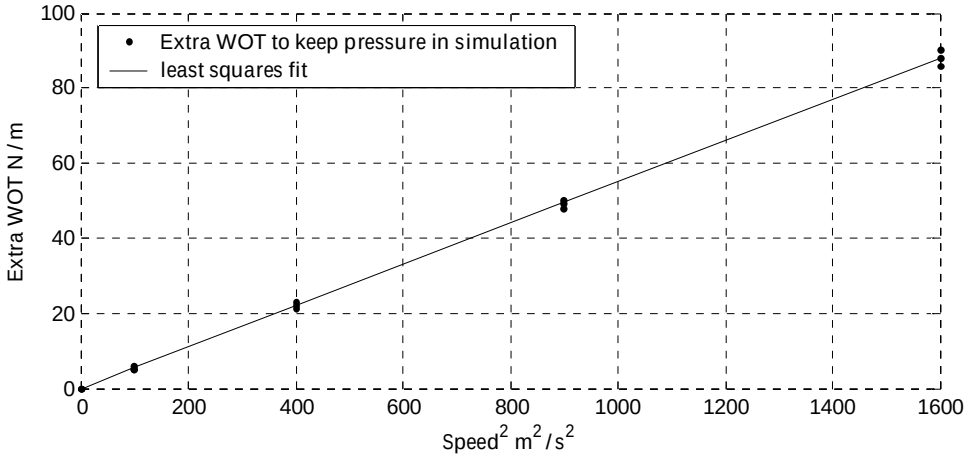

FIGURE 99 The dots show values of extra WOT to keep the zero speed radial pressure at speeds of 10, 20, 30 and 40 m / s and WOT levels of 400, 600 and 800 N / m.

The least squares fit in FIGURE 99 give the coefficient for the correction term b_{fit} = 54.87 g / m^2, lower than the correct 57 g / m^2. However, the correction is very close to the centrifugal correction term for the web tension measurement. If the winder web tension measurement is not corrected for centrifugal forces, the winder automatically compensates the centrifugal loosening of the roll.

6.2 Off line winder control tuning

The first step in the winding tuning is to define the desired roll tightness profile as a function of the roll diameter. The tightness is most explicitly expressed in terms of the Wound On Tension or the radial pressure. The radial strain could be the third choice for tightness measure, but the two others are more directly related to the conventional tightness indicators, like the Cameron test and the Smith needle. The choice of appropriate tightness profile for a particular web and roll type is beyond the scope of this work (Blaedel 1974, Frye 1989). Usually the roll is made tighter at the bottom with monotonically decreasing tightness towards the increasing diameter. Simple criteria for choosing the proper tightness are for example the torque capacity and the telescoping limit. Both give a lower limit based on static paper to paper friction which can sustain the accelerating centre torque or the weight of the roll without slippage. Absolute maximum limits are set at the tensile strength or under it if permanent deformations should be avoided.

The next step in the tuning procedure is to create the winder reference value curves by means of the inverted nip model. This includes choosing the proper limits of the reference values and the preferable winding speed and other set values based on paper properties, winder condition and capacity need and other factors affecting winder runnability.

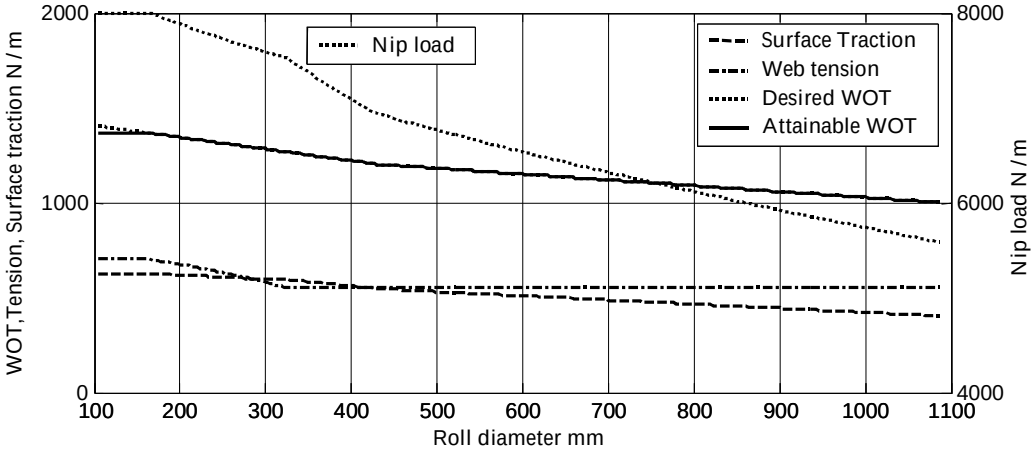

FIGURE 100 Example of the winder reference value curves created by means of the inverted nip model.

An example of the reference values is drawn in FIGURE 100. The desired WOT is defined with two line segments, starting with 1400 N / m at the core and ending at 1000 N / m at 1080 mm diameter. The limits for web tension was set at 400 and 700 N / m and the maximum nip load at 8000 N / m. The planned winding speed was 40 m / s. The maximum WOT possible with these limitations was 1366 N / m, which falls just short of the desired WOT at the beginning of winding. If this is not satisfactory, the limits should be raised. This would in any case be a rather tight roll. The wound roll stress model can be run with the WOT curve just created to see the roll stresses in more detail. The radial stress predicted by the inverted nip model and the simulated radial stress are drawn in FIGURE 101. The simulated radial stress correctly drops to zero at roll

surface and increases near the core. The simulation can be completed by means of the viscoelastic relaxation model to see how much the roll will loose its pressure over long period of time.

6.3 On-line winding control

The conventional way of winding control is to store the designed reference value curves for nip load, web tension and winding force to the winder control system for use during winding. The winder operator possibly can do run time modifications to the stored values, but no automatic adjustment is available.

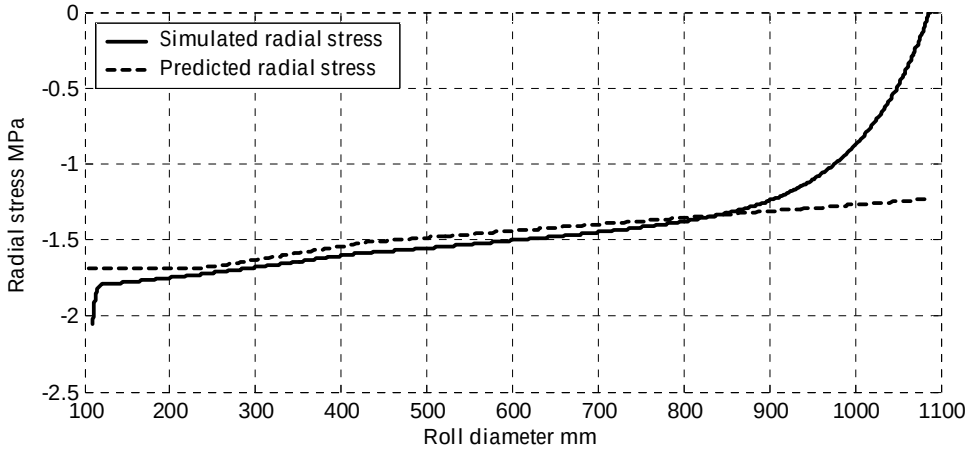

FIGURE 101 Simulated radial stress and predicted radial stress by the nip model.

The inverted nip model is useful also as an on-line winding control tool. Instead of using the stored nip load, web tension and winding force reference curves for winding, the designed Wound On Tension (or radial pressure) curve is the only predetermined reference value. The other reference values are computed run-time by means of the inverted nip model and the WOT curve. This makes it possible to try to adjust to changes during winding.

6.3.1 Simulated winding example

The following data simulates an actual winding run with the previously designed roll tightness WOT curve to clarify how the new winding control method would work in practise.

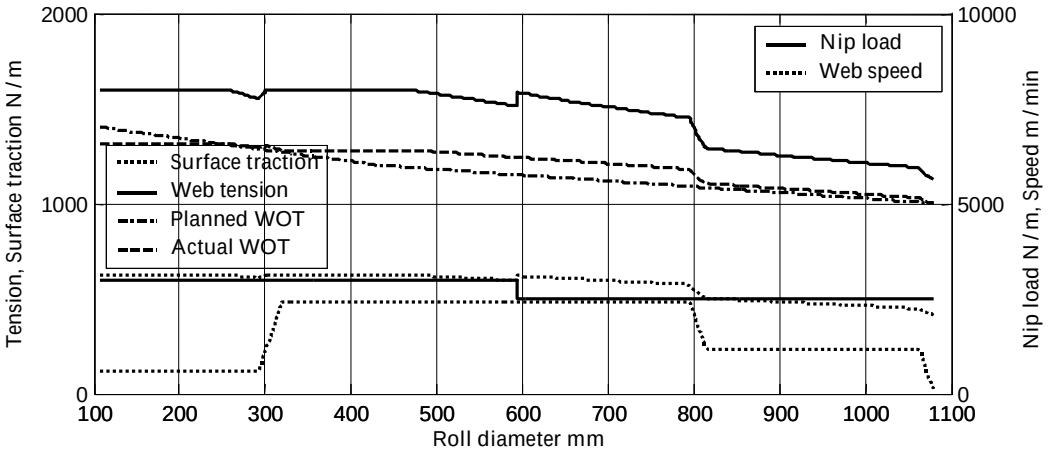

FIGURE 102 Computed winding reference values in a simulated winding.

The simulated winding was run with the planned WOT as target, but instead of using the planned web tension curve, the manually selected web tension set value was used. The winding speed related loosening compensation modified the planned WOT curve according to the actual speed. The winding was started at 10 m / s, at the 300 mm diameter speed was increased to 40 m / s and again decelerated to 20 m / s at 800 mm diameter. The web tension was first 600 N / m but was reduced to 500 N / m at 600 mm diameter. Due to the constant web tension the desired WOT was achieved only just before the 500 mm roll diameter. After this point the proper WOT could be maintained and web tension and speed changes were possible to compensate by adjusting nip load and winding force.

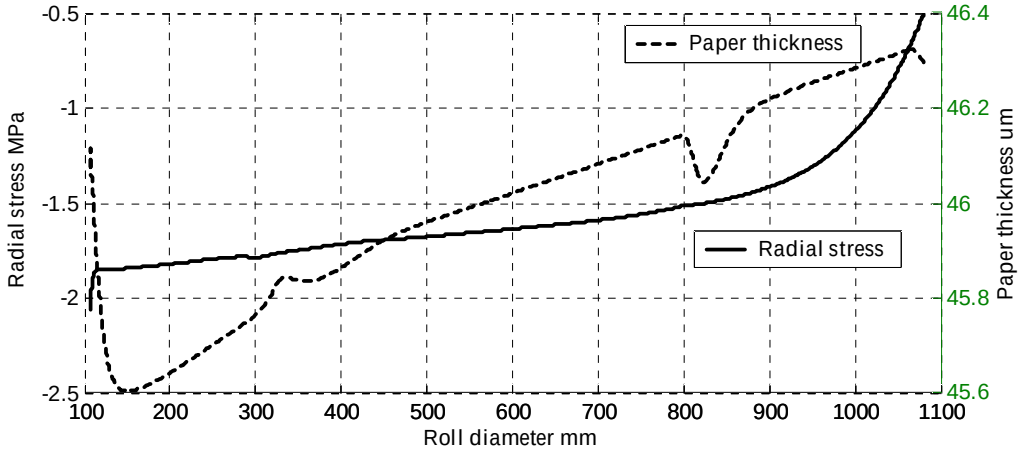

FIGURE 103 Simulated radial pressure and paper thickness curves.

The actual measured paper thickness curve in the roll as measured by the density measurement is shown in FIGURE 103. The thickness is increasing towards increasing diameter due to the tapered WOT curve. The radial stress curve in the same picture shows similar trend.

In an actual winding run the measured thickness can be used in the computation of the actual Wound On Tension curve, if the measured web calliper is available. This is later demonstrated in the winding trials data.

6.4 Winding geometries

The previously described winding procedure assumes that the winder reference values are not practically limited by the winder structure. This is only true in a special single drum winder type, where the accumulating roll mass is relieved by core support and the winding force is produced by means of surface traction. If the winding force is generated by centre torque at the roll core, then for example 600 N/m winding force at 1000 mm roll diameter requires oversized 300 Nm/m motors in each winding station.

The conventional two-drum winder type can easily produce the required winding force but has severe disability to maintain the correct nip loading at large roll diameters. This can be partly relieved in the modified two-drum type, either by pressurized air support between the winding drums or by some other means.

How these limitations affect the design of the winding control scheme in light of the new winding tools will be described. However, since no measurements and trials were done with a two-drum pilot winder, the results are only extrapolations of the findings made with the single drum winder. The uncertainty affects only the numerical accuracy of the analysis, not its general validity.

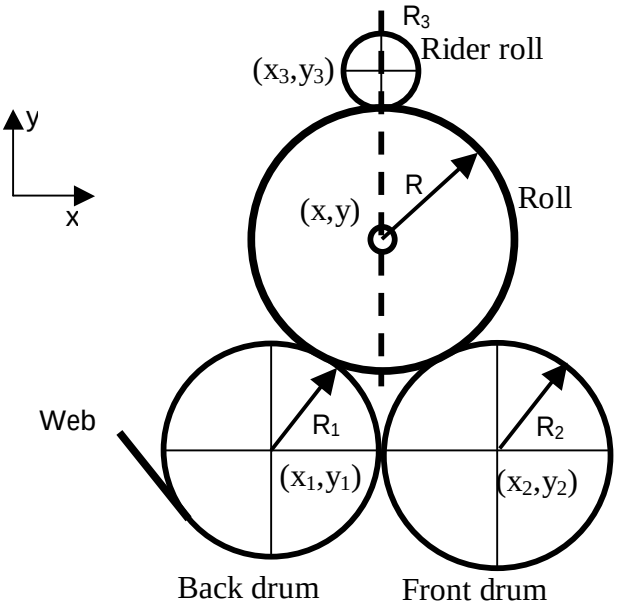

FIGURE 104 A two-drum winder configuration.

6.4.1 Two-drum winder geometry

The geometry of a two-drum winder is depicted in FIGURE 104 with the drum and roll coordinates and radii shown. The original basic form of this winding configuration was symmetric with respect to the line passing through the rider roll and roll centre points as the drum radii were equal. Modern winders display a variety of modified geometries, and even variable geometries were the rider roll is not the only moving drum. The line on which the rider roll is sliding can also be inclined and need not to pass through the gap of the drums. The common element in all these winders is that the roll is supported or loaded by three nips.

The roll radius and its centre coordinates can be solved when the rider roll position is measured from the following three simultaneous equations:

$$\begin{aligned} (x-x_1)^2+(y-y_1)^2-(R+R_1)^2&=0\\ (x-x_2)^2+(y-y_2)^2-(R+R_2)^2&=0\\ (x-x_3)^2+(y-y_3)^2-(R+R_3)^2&=0 \end{aligned} \tag{105}$$

where x,y are the roll centre coordinates, x_1,y_1 are the back drum centre coordinates, x_2,y_2 are front drum centre coordinates and x_3,y_3 are the rider roll centre coordinates. The respective roll and drum radii are R,R_1,R_2 and R_3. The solution can be found by means of crude algebra, even though the famous Greek mathematician Apollonius of Perga living in 3rd century B.C. solved it with compass and ruler. In general there exists eight circles tangent to three given circles, all solutions to (105).

When all the centre coordinates are known, the equilibrium of all the forces acting on the roll can be solved. The forces include the drum support reactions F_1 and F_2, the rider roll load F_3 and the gravitational force G. The drum support forces and the rider roll load point from the respective drum centre to the roll centre. The winding force appears as two forces tangent to the roll periphery and of equal magnitude T_1 and T_2. The winding force is defined here as the static surface traction T_2 of the front drum. The winding force is positive when it would cause the winder to accelerate (if T_1 would not be present). The torques of the forces T_1 and T_2 acting on the roll cancel each other and their directions are perpendicular to the lines connecting the drum centres to the roll centre. The inertia torque needed for acceleration and deceleration is brought to the roll through the front drum and appears as a tangential force T_a at the front drum nip. The web tension does not appear in the roll equilibrium.

$$\begin{aligned} F_1\cos(\theta_1)+F_2\cos(\theta_2)+F_3\cos(\theta_3)-T_1\sin(\theta_1)-T_2\sin(\theta_2)-T_a\sin(\theta_2)&=0\\ F_1\sin(\theta_1)+F_2\sin(\theta_2)+F_3\sin(\theta_3)+T_1\cos(\theta_1)+T_2\cos(\theta_2)+T_a\cos(\theta_2)&=G \end{aligned} \tag{106}$$

where θ_1, θ_2 and θ_3 are the direction angles of the forces. If other support forces are present, they must be added to the above equilibrium equations. The equilibrium equations can be solved for the drum support forces if the rider roll load is given or the rider roll load can be the other unknown and the back drum load known.

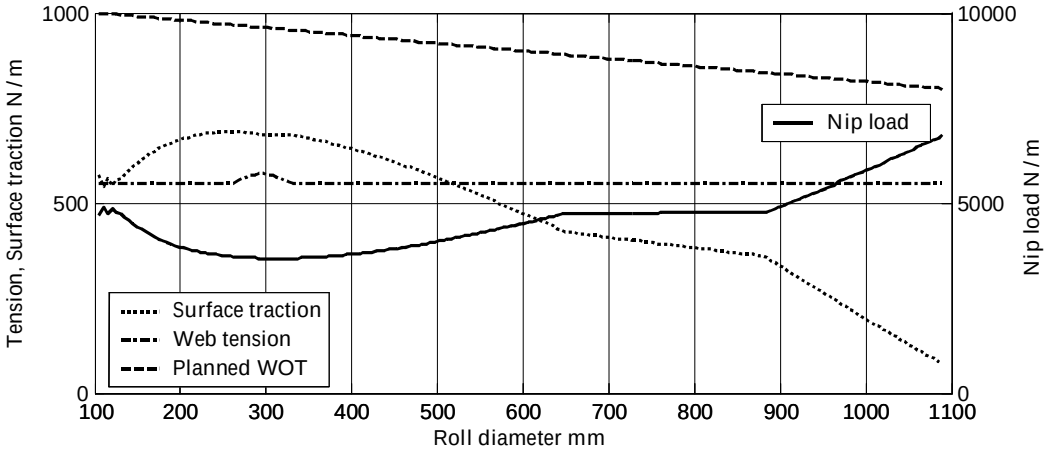

FIGURE 105 Two-drum winder planned reference values.

6.4.2 Two-drum winder control tuning

An example of the tuning of a two-drum winder control reference values according to the geometry in FIGURE 104 is shown in FIGURE 105. The planned Wound On Tension was 1000 N / m at the core and 800 N / m at 1080 mm roll diameter. The roll density is 1250 kg / m^2. The different geometry in this winder compared to the single drum winder limits the way that nip loading can be used for WOT control. The general trend in the back drum nip load is increasing rather than decreasing as in the example in FIGURE 100. The lower nip load up to 600 mm diameter is due to the upper rider roll load limit and after 900 mm diameter the rider roll load has reached its minimum.

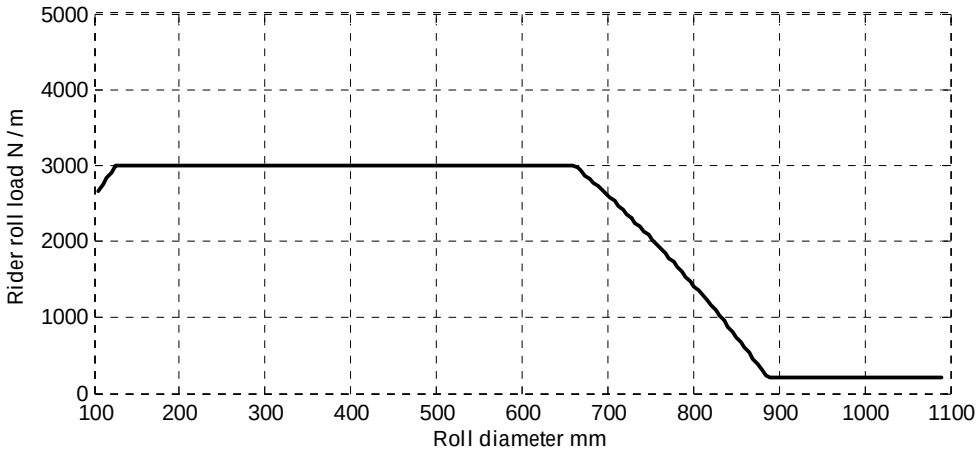

FIGURE 106 Rider roll load of a two-drum winder.

The corresponding rider roll load is drawn FIGURE 106. The force equilibrium was solved for the planned back drum nip load, but the rider roll load high limit was set to 3000 N / m and low limit to 200 N / m. Although the nip load could be freely chosen only between 660 to 890 mm roll diameter, the planned WOT could be attained everywhere. This was even possible with a

constant web tension reference, except for a small pump near the 300 mm diameter. The winding force was the most important winding tool.

The design situation can be much more complex than in this simple example for more asymmetric geometries and if extra support devices exist in the winder. The run-time adjustments by means of the inverted nip model apply here as well as for the single drum winder. The effect of the inertia forces on the nip loads is compensated to keep the back drum nip load at the target value during deceleration. The WOT measurement with the density measurement and the measured web calliper can be also done.

6.5 Winding experiments with the inverted nip model

The accuracy of the inverted nip model was tested with trial runs in the pilot winder. The winder was the same single drum winder that was used in the nip model measurements. The resilient winding drum was used. Both Newsprint and LWC paper was used in the trials.

The Newsprint paper roll was run with radial the stress reference value curve. The winding was started with tight winding, which gradually stepwise decreased. The target radial stress was –0.7 MPa at the start of winding and lowered to –0.4 MPa with 0.1 MPa steps. The winding speed was 300 m/min. The Wound On Tension and radial stress curves are drawn in FIGURE 107. The planned WOT curve was derived from the radial stress target curve through the experimental nip model. The actual WOT and stress curves were measured with the density measurement and the wound roll stress model. The web calliper was measured from the preceding reversed winding.

Both the WOT and radial stress values followed reasonably well the target value. In the beginning at around 300 mm diameter the nip produced about 100 N/m more WOT than required, but at the larger diameters the actual value tended to go under the target. The actual radial stress was within 0.1 MPa from the target value.

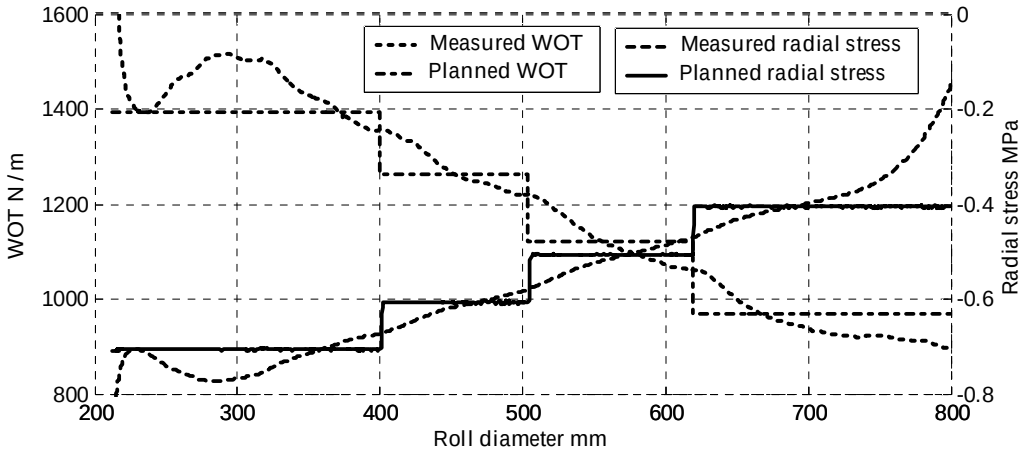

FIGURE 107 Newsprint paper trial run with radial pressure target.

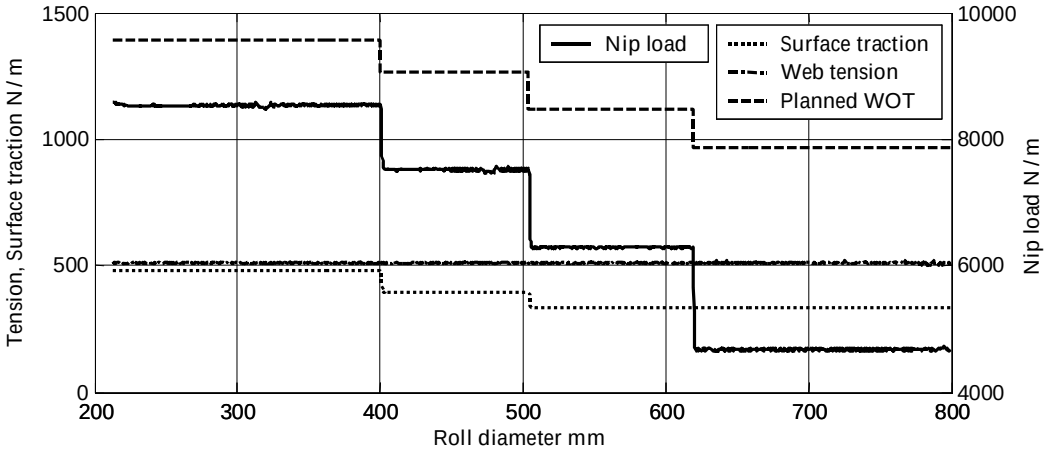

FIGURE 108 The reference value curves resulting from the radial stress target value.

The nip load, web tension and surface traction reference value curves of the Newsprint paper trial run are drawn in FIGURE 108. The inverted nip model did not change the web tension at all, it was kept at the constant 500 N / m value throughout the whole winding. Also the surface traction was changed very moderately, the steps were under 100 N / m and in the last pressure drop the surface traction remained constant. The nip load was the main winding control tool. The nip load at the –0.7 MPa target was about 8500 N / m and dropped finally at the –0.4 MPa target to 4700 N / m. The resilient winding drum made it possible to use high nip loads without fear of too high nip pressure that could damage the paper. The limits for the nip load were set to 2000 and 10000 N / m, but the nip load could have been limited to lower values, in which case the winding force would be used to produce more WOT.

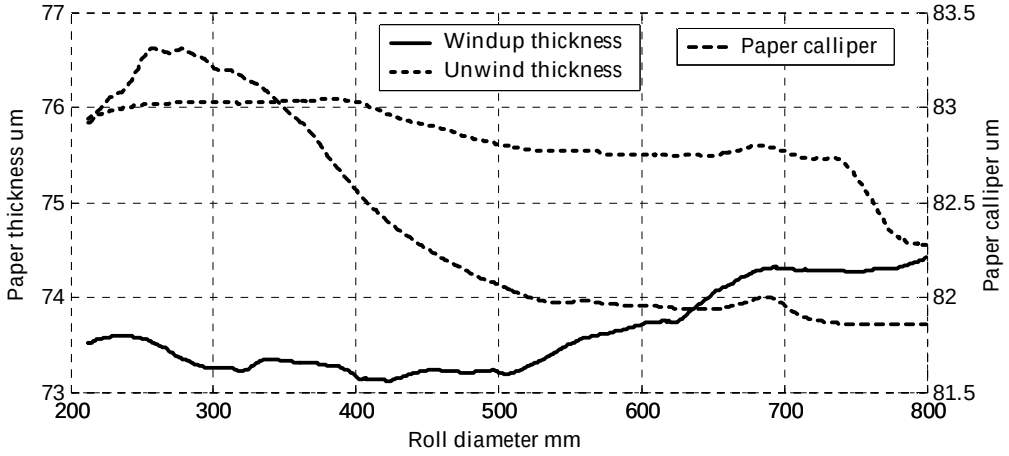

FIGURE 109 The measured paper thickness and calliper curves.

The paper thickness curves in FIGURE 109 measured by the density measurement show that the winder could press the paper thinner at the roll bottom under 500 mm roll diameter. The paper calliper is on the contrary over 1 μm thicker at the beginning than at the roll surface. The windup thickness curve

cannot be used alone to measure the true roll tightness due to the large calliper variations even within this relatively short stretch of paper. The unwind paper thickness measurement is also not enough to replace the calliper measurement, since the unknown tightness profile in the unwind roll has modulated that measurement.

The LWC paper roll was first run with a constant nip load of 6000 N / m, 500 N / m web tension, 325 N / m surface traction and 300 m / min web speed up to 1150 mm diameter. These reference values should produce 960 N / m Wound On Tension according to the nip model. The result is drawn in FIGURE 110.

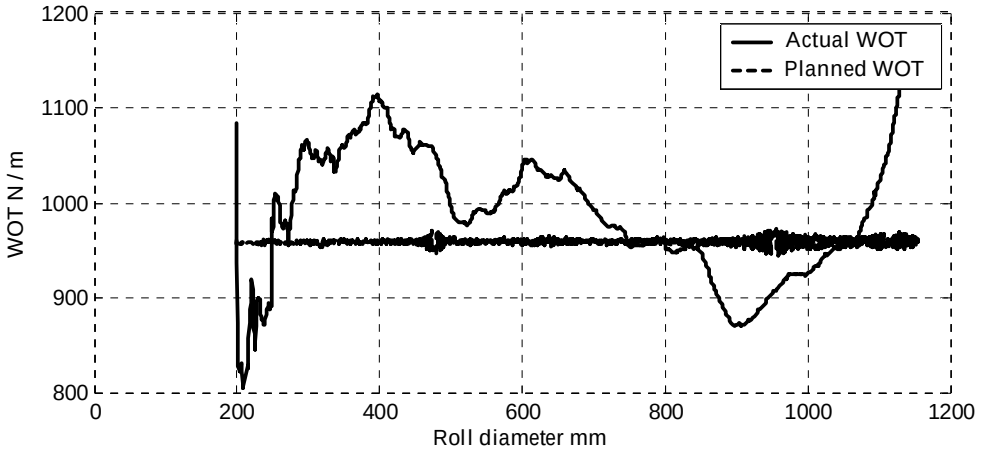

FIGURE 110 LWC paper roll run Wound On Tension curves.

The actual measured WOT curve is more than 100 N / m higher at the beginning of the winding, but drops below it at larger diameters. At the roll surface the actual WOT raises again, but this is somewhat in error since the calliper measurement ended at the 1088 mm roll diameter. The average measured WOT is though 990 N / m, only 3% over the predicted WOT. This example demonstrates that the values in the experimental nip model were averages over the whole roll, and that there are local variations in the produced WOT in the roll. This variation is partly artificial due to the alignment problems between the calliper and thickness measurements. The filtering delays in the measurements are fitted to each other by doing the density measurement for the reversed run backwards in time. However, there seems to be a general trend that the WOT is decreasing during winding even with constant winding parameters.

As with the Newsprint paper roll, also the LWC paper test roll had large calliper variations, FIGURE 111. The calliper was rather constant up to 850 mm diameter, but after that varied within almost 1 μm, which is quite much for a 50 μm paper.

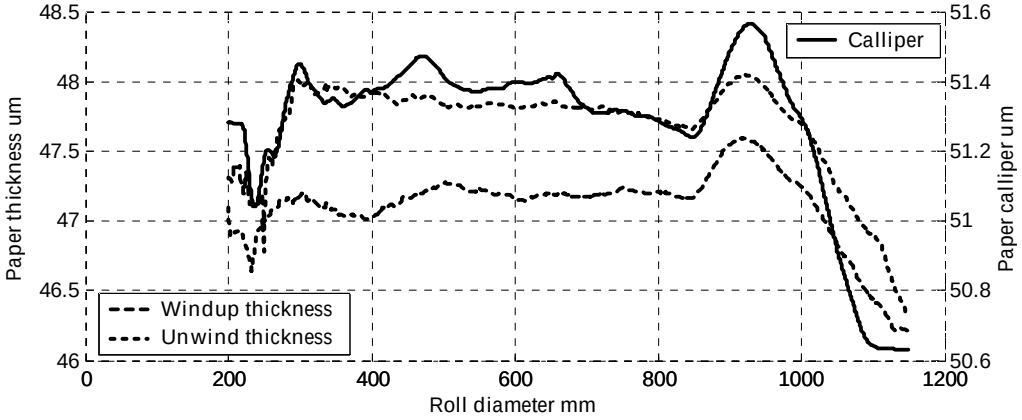

FIGURE 111 Paper thickness and calliper in the LWC paper winding.

Next the roll was run with evenly decreasing radial stress reference curve. The stress reference started with –1.5 MPa at 200 mm diameter and decreased to –0.8 MPa at 1200 mm diameter. The resulting actual and reference radial stress and WOT curves are drawn in FIGURE 112. This time the actual WOT exceeded the target maximally almost 400 N / m at the 355 diameter. This caused 0.4 MPa overshoot in the actual radial stress. The winder followed its reference values well, and there exists no immediate explanation for the excessive WOT. After 750 mm roll diameter the actual WOT followed well the planned WOT. This time the roll had its bottom and surface flipped as compared the run in FIGURE 110 (this happens every time when the roll is taken out from the winder between runs). The 355 mm diameter corresponds to 1230 mm diameter in FIGURE 110.

The next trial run simulated a "bad" winding, with radial stress reference starting at –1.5 MPa at 200 mm diameter, decreasing to –0.86 MPa at 800 mm diameter and increasing again to –1.5 MPa at 1200 mm diameter. This corresponds to a two-drum winding, where the uncontrollably increasing nip loading causes the roll surface to become tighter than the interior.

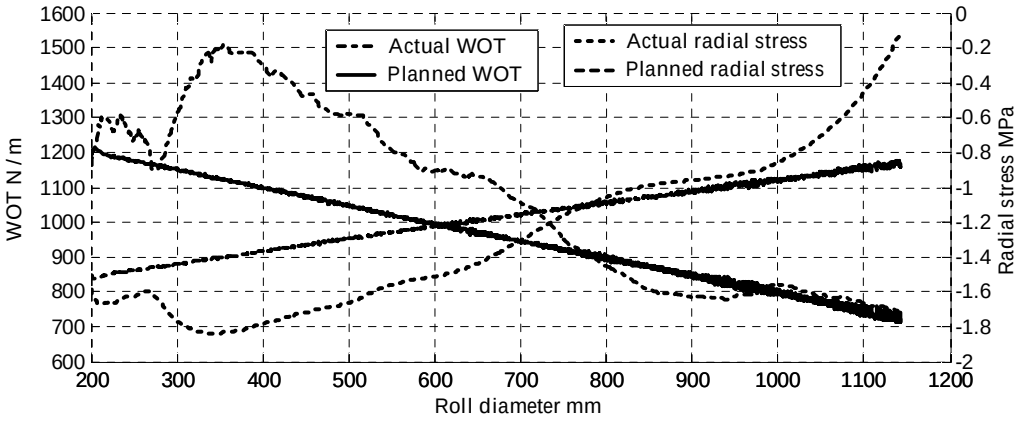

FIGURE 112 LWC paper run WOT and radial stress curves with decreasing stress reference.

This time the actual WOT followed the target WOT within 100 N / m and the error in radial stress was maximum 0.2 MPa at 800 mm roll diameter, except for the soft start at the very beginning. The increasing WOT after 800 mm diameter did not cause much tighter roll surface layer, at least not in terms of stresses. The relatively hard LWC paper has in any case long decreasing stress surface layer. Softer paper grades would be more vulnerable to sharp WOT and stress changes.

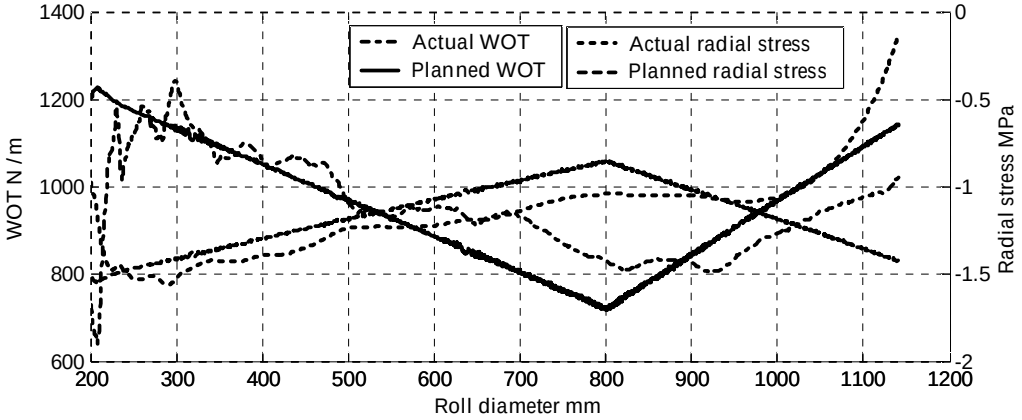

FIGURE 113 LWC paper run WOT and radial stress curves with sagged stress reference.

6.6 Discussion on the new methodology of winding tuning

The new methods presented for tuning winding controls, as an off-line procedure as well as on-line control and measurement system, improve the efficiency of the tuning work. The inverted nip model simplifies the planning of the winder reference values, as the three (four if speed is included) reference value curves are replaced by only one, either Wound On Tension or radial stress. Both are direct measures of roll tightness. The tuning work can be done by a person skilled on generic winding technology and roll properties and not on the specific features of the winder at hand. The point of view of the work can be shifted from the winder peculiarities to the end user need of roll quality. The simplification in the tuning work is even more prominent in the two-drum winder, where the winding geometry is more complicated than in single drum winders.

The output of the inverted nip model is not unambiguous. This gives freedom in the control design to choose the reference values so that they not only produce the correct WOT and satisfy the limits but also optimize the winding. This includes defect free roll quality and optimal winder runnability. Both tasks can be automated when the winder and web properties are known. Some responsibility can also be left for the winder operator, like adjusting the limits at run-time or even manual control of some of the references.

The inverted nip model winder control also allows responding to run-time web speed and tension alternations from the planned values. This is especially beneficial in a multi-station winder where every winding station can be individually adjusted.

When the measured web caliper is available at the winder the result of the winding can be checked by direct on-line measurement. This is the same measurement method that was used to gather the data for the nip model, the WOT measurement based on the density measurement and the wound roll stress model. The density measurement in its basic form was not able to display the true tightness of the roll, but augmented with the caliper and stress model can do it.

The accuracy of the open loop winding control by means of the inverted nip model depends on the accuracy of the nip model when paper properties and winding conditions vary. The winding trials demonstrated that the true WOT can be 10-50% in error occasionally. The strain stress curves are rather easy to measure but the nip model itself takes tens of winding trials at the pilot winder to recalibrate.

The next chapter will introduce a more exact if not accurate method of winding control, the closed loop winding based on the measured paper thickness. It allows winding the paper to an exact radial strain value. It also uses the inverted nip model as a system component, but its accuracy is not hampered by a moderate inaccuracy of the nip model.

7 CLOSED LOOP WINDING CONTROL

The only on-line measurement available from the outcome of the winding process is the web thickness or density measurement. The radial pressure can be only measured indirectly during winding by means of the density measurement and the stress strain relationship. If the Wound On Tension could be measured directly, it would be another candidate for the feedback variable. The practical control loop for the roll tightness control has to be based on the density measurement.

The system components of the winding process are shown in FIGURE 114.

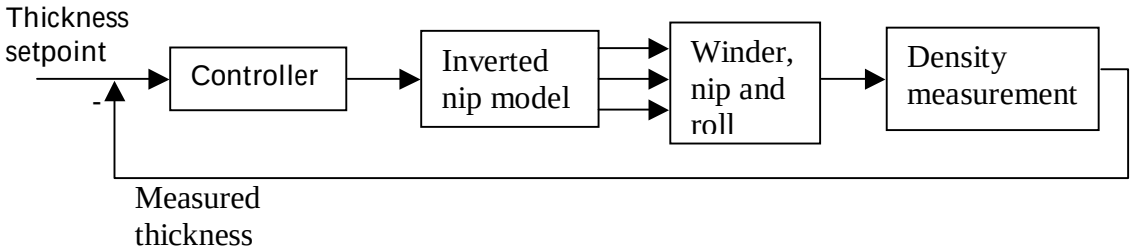

FIGURE 114 Closed loop winding process components.

The controller input is the difference of the thickness set point and the measured thickness and the output is the Wound On Tension. The WOT is converted into the nip load, web tension and winding force references by means of the inverted nip model. The references from the nip model command the winder control system. The density measurement reads the roll diameter and web length values from the winder control system and produces the actual web thickness for the controller.

Both the wound roll stress model and the experiments tell that the static relationship from the Wound On Tension to the web thickness in the roll is linear, that is the steady state response can be explained by a simple static gain. This is possible since the inverted nip model hides the nonlinearities from the

winder reference values to the wound roll. The density measurement is basically a linear filter with unity gain.

The dynamic response is dominated by the density measurement, the winder control system and its actuators are much faster than the density measurement. The nip response apparently does have some slow dynamics that is very difficult to measure and identify accurately. This behavior is probably responsible for the alleged nip tendency to make tight winding after softer winding and vice versa. The web caliper variations and viscoelastic paper properties make it difficult to observe accurately small and fast responses of the winding process.

Winding can be naturally modeled as a discrete time process since no changes occur in the roll (if the viscoelastic relaxation is forgotten) if no new laps are wound onto the roll. The sampling is best done at every roll revolution so that the resulting discrete time dynamic models are more time-invariant as the roll diameter increases during winding. This means sampling at uneven time and web length intervals even at constant web speed. The dynamic winding model is not necessarily time invariant, for example the recursive least squares algorithm used in the density measurement is time varying if the forgetting factor λ is adjusted during winding.

There is no earlier published work on closed loop winding control before this work. The interest in the closed loop winding control is not so much in its practical applications but it is a way to show the performance of the nip and winding models and the density measurement. The following analysis will focus on the basic aspects of the winding process models and a few control principles.

7.1 Static response

The static response can be found from the previous nip model measurement data for the Newsprint and LWC, Tables 3,4,8 and 9. The paper thickness in the tables as a function of the Wound On Tension is drawn in FIGURE 115. The linear fit lines are also drawn. The coefficient K_d from the WOT to the web thickness are -0.00434 μm / N*m for Newsprint and -0.00157 μm / N*m for LWC paper. The LWC is almost three times harder than the Newsprint paper. Much of the deviation of the measurement values from the least squares lines can be explained by the different winding speeds that was used in different runs. The winding speed was found to be almost negligible in the nip model. But even though speed has no effect on the Wound On Tension it does have effect on the roll tightness and on the web thickness.

7.2 Winding simulation

The winding simulation can be done according to the system configuration in FIGURE 114, when the roll is replaced with the stress model and the nip with the nip model. If the winder reference values are of no interest, the nip models

can be omitted. The density measurement is done exactly as in real winding, and the diameter and length values are obtained from the roll model. The model can be also run in open loop mode, when the feedback loop is cut off.

Since the wound roll model naturally updates its outputs at every lap added to the roll, the simulation proceeds in the discrete time accordingly. No continuous time numerical differential equation solvers are needed. The only continuous time effect, the viscoelastic pressure relaxation, can be simulated with the viscoelastic roll model between every discrete time step as earlier described. Winding speed and its decreasing effect on the roll tightness due to the centrifugal forces is also included in the simulation if the web basis weight is set properly.

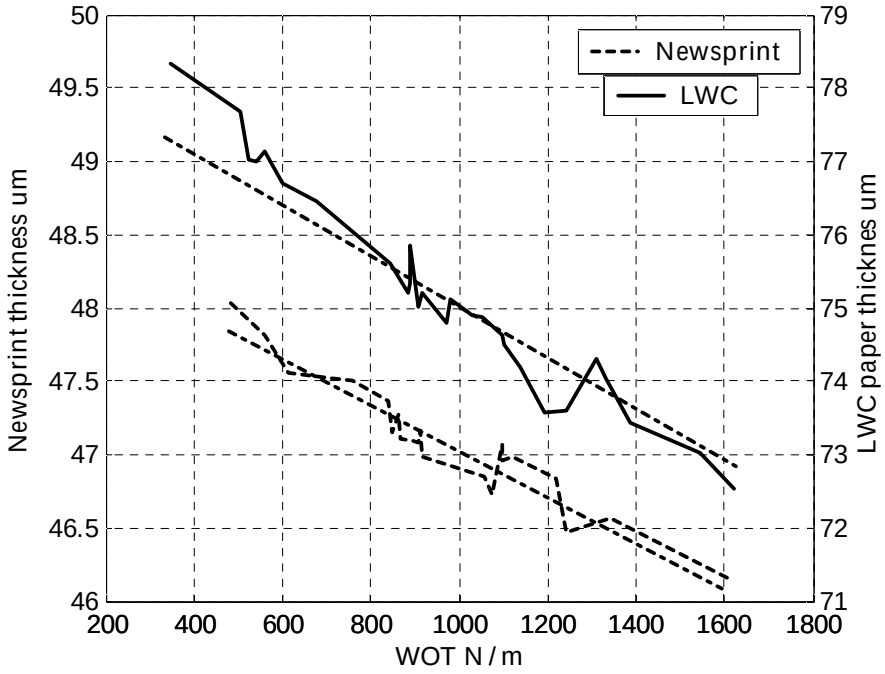

FIGURE 115 Newsprint and LWC paper thickness in the roll under various Wound On Tension values. Linear least squares fit lines are drawn in dash dotted pen.

7.3 Dynamic response

Since the density measurement is the slowest component in the winding process, its dynamic response will be analyzed in detail. The two density measurement versions presented earlier differ in their dynamic responses. The conventional pulse density measurement is a finite impulse response (FIR) type filter, which has finite duration step response. The other version that is used in this work, the recursive least squares algorithm, is more like infinite impulse response (IIR) type filter. However, it is not time invariant system and not even a linear system.

The usual textbook version of the recursive time-variant least squares algorithm is (Johansson 1993):

$$\hat{\theta}_k = \hat{\theta}_{k-1} + P_k\phi_k\left(y_k - \phi_k^T\hat{\theta}_{k-1}\right) = \left(I - P_k\phi_k\phi_k^T\right)\hat{\theta}_{k-1} + P_k\phi_k y_k$$
$$P_k = \frac{1}{\lambda}\left(P_{k-1} - \frac{P_{k-1}\phi_k\phi_k^T P_{k-1}}{\lambda + \phi_k^T P_{k-1}\phi_k}\right) \quad (107)$$

The first equation above can be seen as a time varying linear system equation in state space format, when y_k is the input variable and $\hat{\theta}_k$ is the state vector. When the measured web length and roll diameter values L_k and D_k are inserted in these equations they are written as

$$\hat{\theta}_k = \begin{bmatrix} \hat{h}_k \\ \hat{D}_{0,k}^2 \end{bmatrix}$$
$$\phi_k = \begin{bmatrix} L_k \\ 1 \end{bmatrix}, y_k = D_k^2$$
$$P_k = \begin{bmatrix} p_{11} & p_{12} \\ p_{12} & p_{22} \end{bmatrix} = \frac{1}{\sum_i \lambda^{k-i}\sum_i \lambda^{k-i}L_i^2 - \left(\sum_i \lambda^{k-i}L_i\right)^2}\begin{bmatrix} \sum_i \lambda^{k-i} & -\sum_i \lambda^{k-i}L_i \\ -\sum_i \lambda^{k-i}L_i & \sum_i \lambda^{k-i}L_i^2 \end{bmatrix} \quad (108)$$
$$I - P_k\phi_k\phi_k^T = \begin{bmatrix} 1-(p_{11}L_k + p_{12})L_k & -(p_{11}L_k + p_{12}) \\ -(p_{12}L_k + p_{22}) & 1-(p_{12}L_k + p_{22}) \end{bmatrix}$$
$$P_k\phi_k = \begin{bmatrix} p_{11}L_k + p_{12} \\ p_{12}L_k + p_{22} \end{bmatrix}$$

where $\hat{h}_k$ is the estimated web thickness. The input variable can be written as a function of the "true" web thickness h_k as

$$D_k = D_{k-1} + 2h_k \quad (109)$$

and these can be combined to the non-linear time varying difference system:

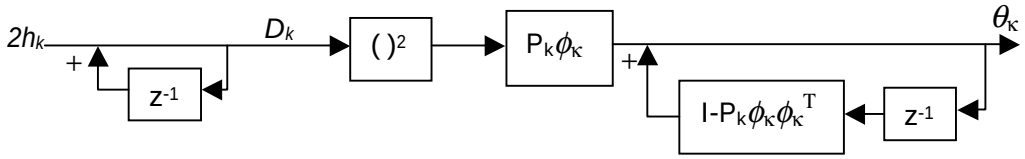

FIGURE 116 The time varying least squares algorithm system diagram.

The time response of the least squares algorithm is actually time invariant after the initial transient, if the forgetting factor λ is constant. The above nonlinear system could be linearized and simplified for the controller design, but it could be more useful to fit a simple linear transfer function to the simulated response. This can be done for example with the help of the Matlab System Identification Toolbox function ARX.

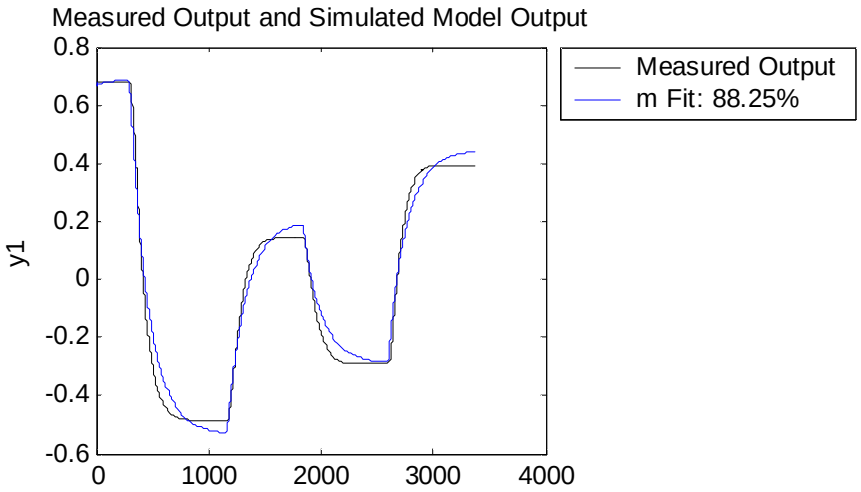

FIGURE 117 Web thickness in a simulated winding run (Measured Output) and the second order ARX model output fitted to it.

The simulation data in FIGURE 117 was run with "buffer length" 50 which gives forgetting factor λ=49/50=0.98. The fitted second order transfer function has poles at 0.994 and –0.0703.

Better fit can be achieved with manual trial and error method. The fit for the transfer function

$$\left(\frac{1-a}{1-az^{-1}}\right)^2 \tag{110}$$

is very good over wider range of the forgetting factor values when the value for the pole *a* is chosen with the heuristic formula

$$\begin{aligned} a &= \frac{b-1}{b} \\ b &= bl \times \left(1 - 0.2\frac{bl}{250}\right) \end{aligned} \tag{111}$$

where *bl* is the "buffer length" parameter for the density measurement. The fit of the first order transfer function is also quite good:

$$\frac{1-\sqrt{a}}{1-\sqrt{a}z^{-1}} \tag{112}$$

The comparison of the first and second order model step responses to the simulation step response can be seen in FIGURE 118. Especially the second order model fit is much better than could be achieved with the Matlab fit. There is a certain difference in these model and simulation responses when the value of the forgetting factor λ is changed during the winding simulation.

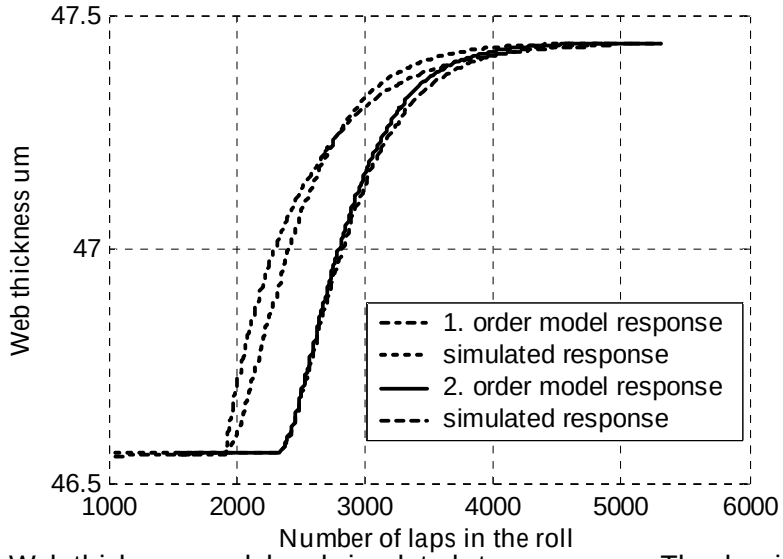

FIGURE 118 Web thickness model and simulated step responses. The density measurement buffer length was 250.

The time varying least squares algorithm minimizes the modified least squares performance criterion (Johansson 1993):

$$J\left(\hat{\theta}_k\right)=\sum_{i=1}^{k}\lambda^{k-i}\left(y_i-\phi_i^T\hat{\theta}_k\right)^2=\sum_{i=1}^{k}\left(\lambda^{\frac{k-i}{2}}y_i-\lambda^{\frac{k-i}{2}}\phi_i^T\hat{\theta}_k\right)^2 \tag{113}$$

which can be geometrically interpreted as if the data points have been moved towards the origin by multiplying them with the factor $\lambda^{(k-i)/2}$. The closer the points are to the origin, the less weight they have to the least squares result.

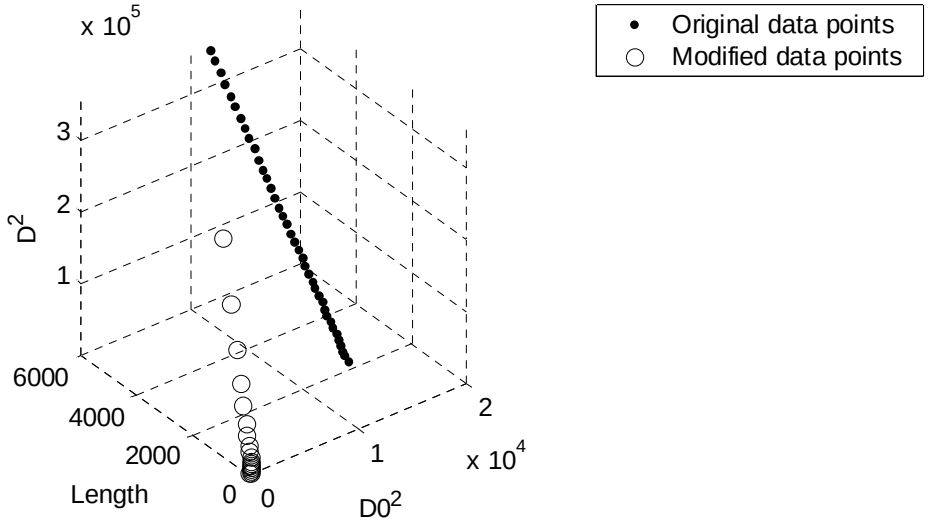

FIGURE 119 Time varying least squares data weighting

The effect of the weighting on the data points is seen in FIGURE 119, where only every 100th data point is drawn from the previous simulation data.

Even though the forgetting factor is a number close to one, repeating multiplication quickly moves the older data points to the origin. If the value of the forgetting factor is changed during simulation, its old values still affect the least squares outcome, in contrary what happens with the simple transfer function model, if its poles are moved. The least squares algorithm never completely forgets its past history, even though practically it does when enough time has elapsed. There is also inherent weighting in benefit of those points that are farther away from the origin in the unmodified data. In the windup data, the larger its length and diameter values are the later they are sampled, but in the unwind data the diameter values are decreasing. The automatic forgetting factor adjustment based on the confidence limit compensates for this by increasing or decreasing the buffer length during winding.

7.4 The density controller

The criteria for the choice of the density or thickness controller are on the other hand smoothness of its output and the steady state error. The relative weight on these determines the "gain" of the controller. Some kind of gain scheduling would be preferable based on for example the density measurement forgetting factor, which mostly determines the slowest time constant of the overall system.

The response of the controller must be moderate and avoid too large and sharp WOT changes. Otherwise roll defects, like crepe wrinkles, CD sheet offsets, starring and even web breaks can occur. Since the winding process itself is not an integrating process, the controller should include an integrator to make the steady state error zero.

The variations in the paper caliper are about the same magnitude than the difference in the web thickness of the loosest and tightest roll achievable with the normal range of the winding parameter values. If the density controller set value would be held constant during winding it would mean large variations in tightness. The winding must be based on measured paper caliper and the controller set value is the caliper minus some offset, for the printing paper this is about 3-8 μm. The accuracy of the measured caliper is crucial in order to have smooth thickness control. If the caliper is erroneous or delayed by excessive filtering, it may cause large fluctuations in the true reference value to the controller. This makes it difficult to find out if the controller is performing badly or if the reason for unsteady response is due to the reference value fluctuations.

7.4.1 The PI controller

The natural choice for the controller is the basic PI controller type. It easy to tune, it is quite robust due to its simplicity and it has the integrating action. The derivative term is not justified since the variations in the caliper would cause fluctuations in the WOT output that should be avoided.

The program structure for the PI controller was taken from (Åström & Hägglund, 1995), which contains some useful features like the integrator anti-windup and smooth parameter changes.

The tuning of the PI controller was chosen to be pole placement based on the simple first order system model. The transfer function of the discrete time PI controller with unity sample interval is

$$K\left(1+\frac{1}{T_i}\frac{1}{z-1}\right) \tag{114}$$

where K is the controller gain and T_i is the integration time. The desired closed loop poles are a complex pole pair with the characteristic polynomial as

$$z^2 - 2X\cos(Y)z + X^2 \tag{115}$$

where the complex pole pair is $X(\cos(Y)+-\sin(Y)I)$. If the winding model static gain is K_d, the controller parameters are found by setting the closed loop characteristic polynomial coefficients equal to the desired closed loop polynomial coefficients:

$$\begin{aligned} K &= \frac{\sqrt{a}-X^2}{\left(1-\sqrt{a}\right)X^2K_d} \\ T_i &= \frac{\sqrt{a}-X^2}{\sqrt{a}\left(X^2-2X\cos(Y)+1\right)} \end{aligned} \tag{116}$$

where a is the parameter of the first order model fitted to winding simulation data.

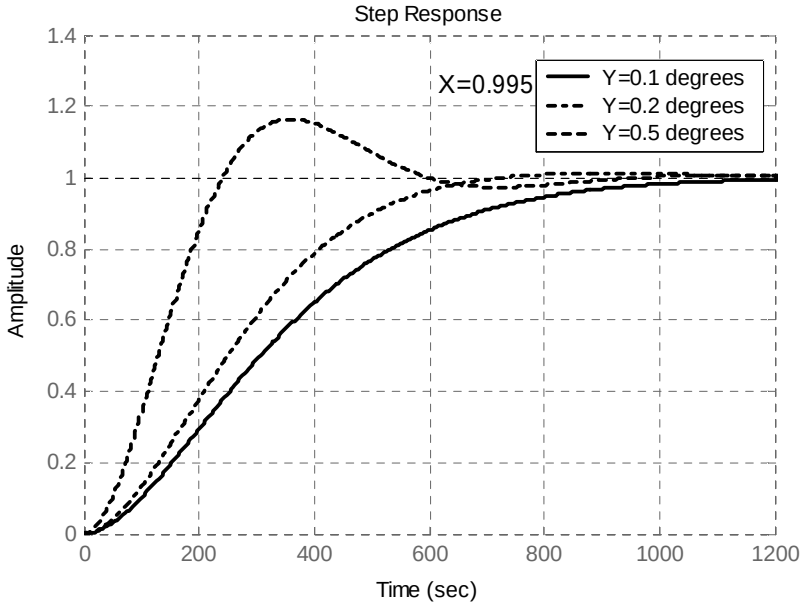

FIGURE 120 Second order system step responses with different damping values.

Practical values for the desired pole parameters were found to be *X=0.995* and *Y=0.09*⁰ for smooth but quick closed loop response in simulations and both in winding trials, see FIGURE 120 and FIGURE 121. Since the parameter *a* depends on the density measurement forgetting factor λ, the PI controller autotuning by pole placement is also adaptive tuning.

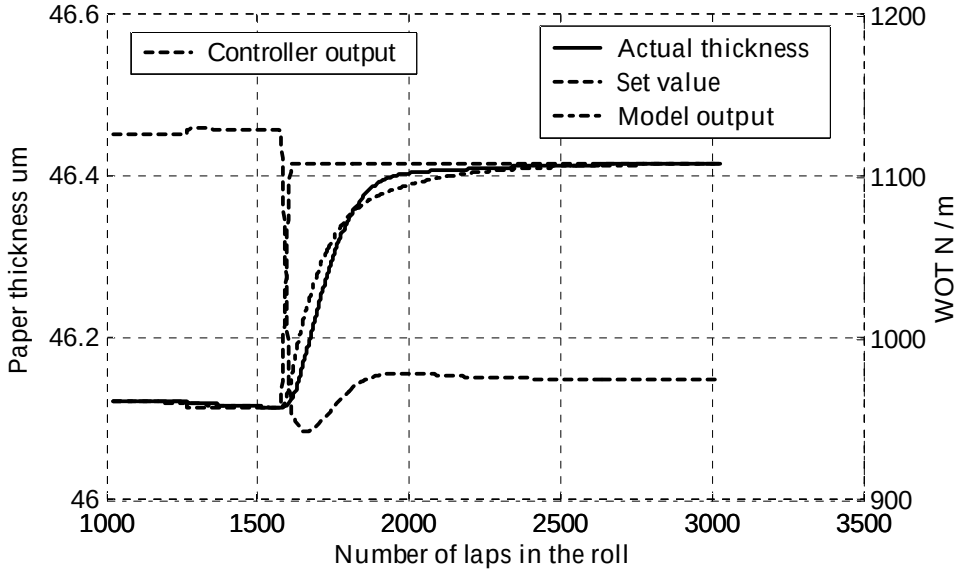

FIGURE 121 Performance of the PI controller in simulation. The model output refers to the first order transfer function used to tune the controller.

As can be seen in FIGURE 121 the first order model fitted to the simulated winding data is not perfectly following the simulation output, which causes robustness problems. The settling time is about 1000 roll revolutions, as was expected. The performance can be made faster with feed forward or set point weighting (Åström & Hägglund, 1995). The feed forward is computed by dividing the set value by the static system gain. The effect of the feed forward in the PI controller performance is simulated in FIGURE 122. The response is now faster than without the feed forward, but the actual value makes a large overshoot. The controller's output without feed forward makes very smooth transient with small overshoot, which is optimal with respect to the requirements of clean winding.

7.4.2 The state variable feedback controller

The state feedback controller or regulator is able to move the closed loop poles to any desired location. It is a useful tool for stabilizing an unstable plant. When the system is given in the state space format

$$x_{k+1} = Ax_k + Bu_k \tag{117}$$

then the feedback $u_k=-Kx_k$ allows the closed loop system $x_{k+1}=(A-BK)x_k$ characteristic polynomial roots to be moved anywhere. The program to do this can be written directly by solving the algebra or by using the Matlab Control System Toolbox function PLACE, which has better numerical properties. If the full state is not measured directly but only the output $y_k=Cx_k$, then the state estimator is needed:

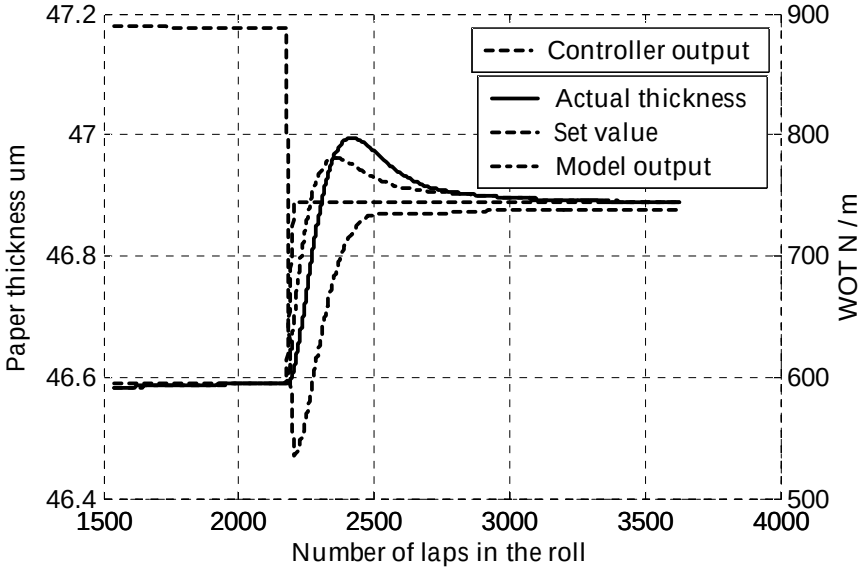

FIGURE 122 PI controller performance in simulation with feed forward

$$\hat{x}_{k+1} = (A - LC)x_k + Ly_k \tag{118}$$

The state estimator can be tuned similarly to the state feedback with pole placement and the function PLACE. The estimator poles should be faster than the closed loop poles (smaller absolute value) for good performance.

The state estimator – state feedback can be slightly modified to give it two important properties with respect to steady state error and input-output mapping. Normally the closed loop input value would be the same as it was for the open loop system, which in this case is the Wound On Tension. To be able to control the web thickness directly the input can be moved to the state estimator input:

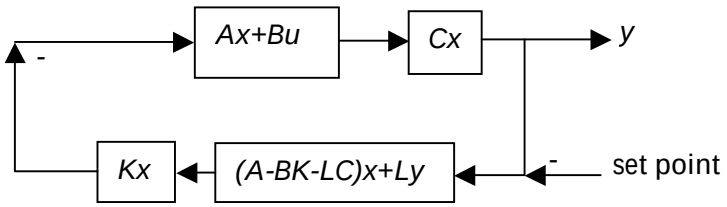

Figure 123 State feedback and state estimator controller configuration

The modified closed loop system and the original system still have their poles in the same locations. The other requirement is to have zero steady state error. This can be achieved by cascading the open loop system with an integrator, and doing the state feedback and the state estimator tuning on this augmented system.

7.4.3 The LQR tuning of the state feedback controller

Even though the pole placement tuning for the state estimator – state feedback is straightforward, the number of tuning parameters is quite high already for 3x3 system. There are three estimator and three closed loop poles or complex pole pairs, six parameters in total. The LQR tuning is a way to be able to handle the tuning with less parameters. The steady state linear quadratic regulator minimizes the following performance criterion with the constant gain state feedback:

$$J(u) = \sum_{i=1}^{\infty} x_i^T Q x_i + u_i^T R u_i \tag{119}$$

where Q and R are weighting matrices, which now replace the poles as tuning parameters (Lewis and Syrmos, 1995). The state feedback gain vector K is derived from the solution matrix S of the infinite time algebraic Riccati equation:

$$\begin{aligned} S &= A^T\left(S - SB\left(B^T SB + R\right)^{-1} B^T S\right)A + Q \\ K &= \left(B^T SB + R\right)^{-1} B^T SA \end{aligned} \tag{120}$$

and again the Matlab Control System Toolbox helps with the function DARE to solve the Riccati equation. The LQR tuning can be adequately handled with only one parameter $q>0$ if R is set to one and $Q=qI$. The extra benefit of the LQR tuning is that it is guaranteed to be stable (if the system model is accurate enough) and it has good robustness (Lewis and Syrmos, 1995). The state estimator can be tuned similarly by means of the DARE function when A is replaced by A^T, B is replaced by C^T and $L=K^T$. However, it is advantageous to utilize the knowledge of the main process noise, which in this case is the web calliper variation. This leads to a modified optimal state estimator, the steady state Kalman estimator. The LQR controller – Kalman estimator pair is called the LQG controller. With the process noise input, the system equations become:

$$\begin{aligned} x_{k+1} &= Ax_k + Bu_k + Gw_k \\ y_k &= Cx_k + v_k \end{aligned} \tag{121}$$

where w_k is the process noise and v_k is the measurement noise. The process noise should have as many components as the state vector has so that the coefficient matrix G would be square, but we have knowledge on only one

noise source. So we must set all other columns of *G* to zero except the one corresponding to the web thickness. The nonzero column is then *B/Kd*. The tuning parameters *Q* and *R* get statistical interpretation in the Kalman filter framework, $Q=E(ww^T)$ and $R=E(vv^T)$. They meaning is that the less we can trust the measurements (large *R*), the more we have to run the estimator "open loop". On the other hand the more the process noise disturbs the true state (large *Q*), the more we have to rely on the measurement. With other words with high measurement noise the filtering becomes tighter.

The steady state Kalman filter tuning is as simple as the LQR tuning with the DARE function, now the parameter matrix *Q* is replaced by GQG^T.

7.4.4 LQG design for the second order system model

Now the LQG design equations will be written for the simple second order system model transfer function previously fitted to the winding simulation data. The system model is first augmented with the pure integrator and converted to state space format:

$$\begin{aligned} x_{k+1} &= \begin{bmatrix} 2a & -a^2 & 0 \\ 1 & 0 & 0 \\ 2a & -a^2 & 1 \end{bmatrix} x_k + K_d \begin{bmatrix} (1-a)^2 \\ 0 \\ (1-a)^2 \end{bmatrix} u_k + \begin{bmatrix} (1-a)^2 & 0 & 0 \\ 0 & 0 & 0 \\ (1-a)^2 & 0 & 0 \end{bmatrix} w_k \\ y_k &= \begin{bmatrix} 0 & 0 & 1 \end{bmatrix} x_k + v_k \end{aligned} \tag{122}$$

where *a* is the system model double pole. It was computed from the density measurement forgetting factor, which makes this adaptive design.

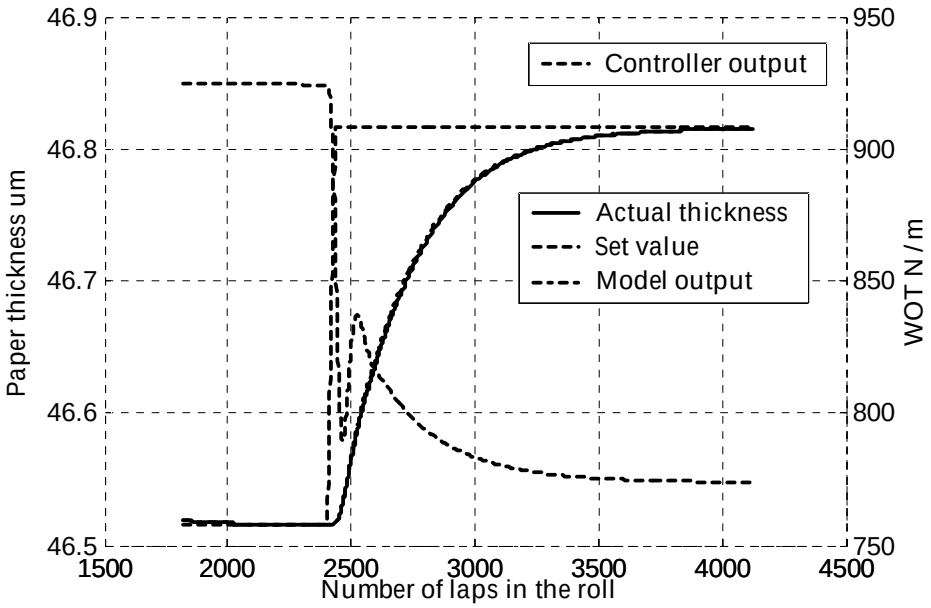

FIGURE 124 LQG controller step response in simulation. Tuning was done for the second order system model.

Strictly speaking the LQG design is only valid for time invariant systems, but intuitively we should have "nearly" optimal design anyway. The design requires that the plant is controllable and detectable, which can be checked by testing the ranks of the controllability and observability matrices:

$$\begin{aligned} Rank\left(\begin{bmatrix} B & AB & A^2B \end{bmatrix}\right) &= Rank\left(K_d(1-a)^2 \begin{bmatrix} 1 & 2a & 3a^2 \\ 0 & 1 & 2a \\ 1 & 2a+1 & 3a^2+2a+1 \end{bmatrix} \right) = 3 \\ Rank\left(\begin{bmatrix} C \\ CA \\ CA^2 \end{bmatrix}\right) &= Rank\left(\begin{bmatrix} 0 & 0 & 1 \\ 2a & -a^2 & -a^2 \\ 3a^2+2a & -2a^3-a^2 & 1 \end{bmatrix}\right) = 3 \end{aligned} \tag{123}$$

The LQG controller response in FIGURE 124 is otherwise very good except for the controller output swing just after the step input. The density measurement buffer length was kept at 100 and the controller tuning parameters were q=3, r=1 and the Kalman estimator used the same tuning values. The resulting closed loop poles were at 0.98797, 0.99088 and 0.99707 and the estimator poles at 0.94195 and 0.97053*(0.999+-0.0506i). The controller is slightly slower than the PI controller with the pole placement tuning. The model output and the simulated web thickness fit perfectly.

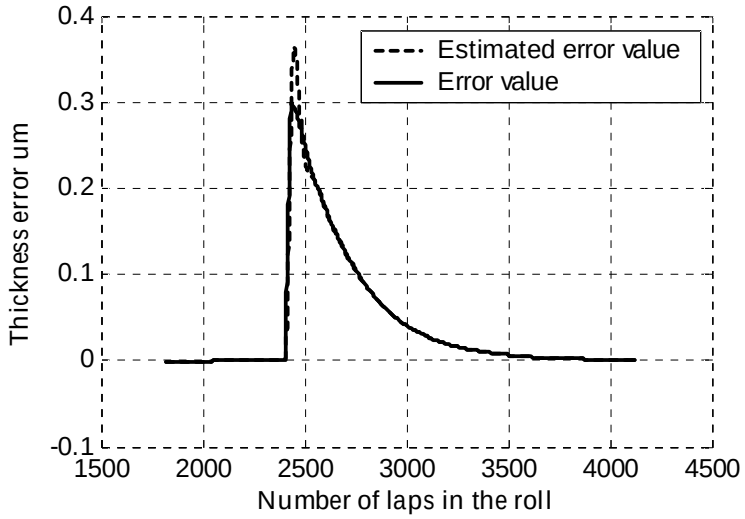

FIGURE 125 Estimated and true error values in the simulation of FIGURE 124.

The Kalman filter performance can be seen in FIGURE 125. The estimated error value is the third component of the estimated state vector. They fit very well except for the sharp overshoot of the estimation.

7.4.5 LQG design for the first order system model

The design is otherwise the same as previous but now there are only two state variables. The system in the state space format is now:

$$\begin{aligned} x_{k+1} &= \begin{bmatrix} \sqrt{a} & 0 \\ \sqrt{a} & 1 \end{bmatrix} x_k + Kd \begin{bmatrix} 1-\sqrt{a} \\ 1-\sqrt{a} \end{bmatrix} u_k + \begin{bmatrix} 1-\sqrt{a} & 0 \\ 1-\sqrt{a} & 0 \end{bmatrix} w_k \\ y_k &= \begin{bmatrix} 0 & 1 \end{bmatrix} x_k + v_k \end{aligned} \tag{124}$$

The controllability and observability matrices have always full rank:

$$\begin{aligned} Rank([B \quad AB]) &= Rank\left(K_d \left(1-\sqrt{a}\right) \begin{bmatrix} 1 & \sqrt{a} \\ 1 & \sqrt{a+1} \end{bmatrix} \right) = 2 \\ Rank\left(\begin{bmatrix} C \\ CA \end{bmatrix} \right) &= Rank\left(\begin{bmatrix} 0 & 1 \\ \sqrt{a} & 1 \end{bmatrix} \right) = 2 \end{aligned} \tag{125}$$

The closed loop step response is seen in FIGURE 126. The controller and the estimator were both tuned with parameters *q*=5 and *r*=1. The closed loop poles were placed at 0.99588*(1+-0.00146i) and the estimator poles at 0.92473*(0.997+--0.0778i). The controller output response is excellent with no overshoot, and there is also no overshoot in the actual value. The response is a bit slow, so possibly the *q*-parameter could have been greater, but the winding trials will show the true performance.

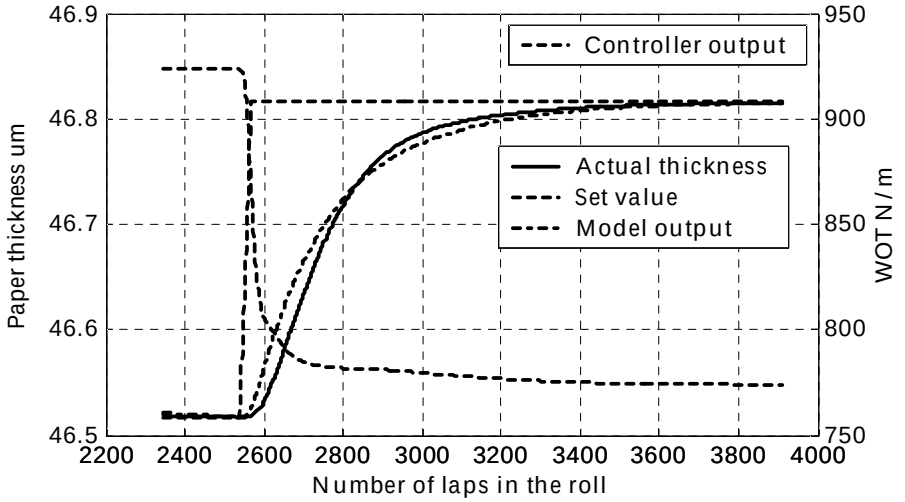

FIGURE 126 LQG controller step response in simulation. Tuning was for the first order system model.

The state estimator outputs in FIGURE 127 reveal an interesting feature in this LQG controller. The estimator performance is good, the fit between the estimated and true error value is good. But the first component in the estimated state vector is the derivative of the error value, as is expected, since the system is made of an integrator cascaded with a first order filter. The controller output is $k_1x_1+k_2x_2$, which is the weighted sum of the error value and its derivative. But

these are fed into the integrator, and the output of the integrator will be the weighted sum of the error value and its integral. That is the LQG controller together with the integrator form a PI-controller, whose input is filtered by the state estimator.

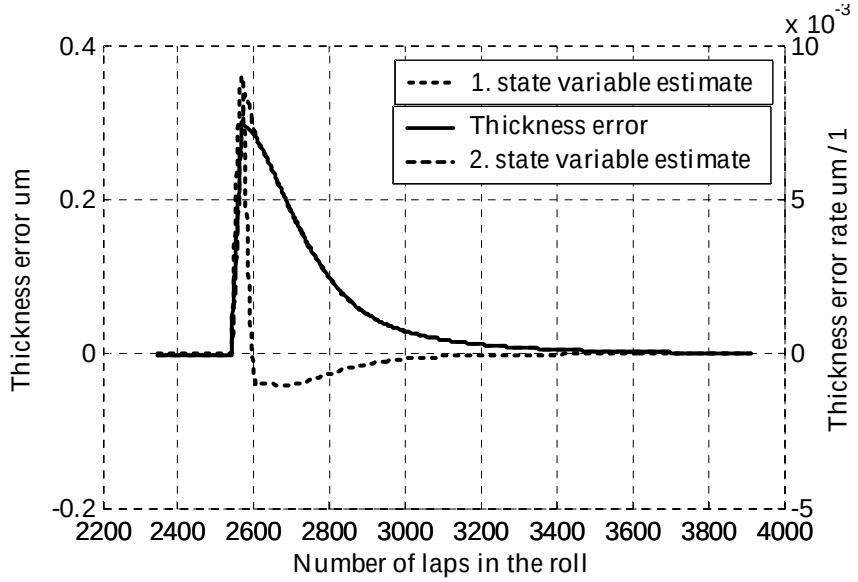

FIGURE 127 State estimator output variables and the error value of the simulation in FIGURE 126.

7.4.6 LQR tuning for the PI controller

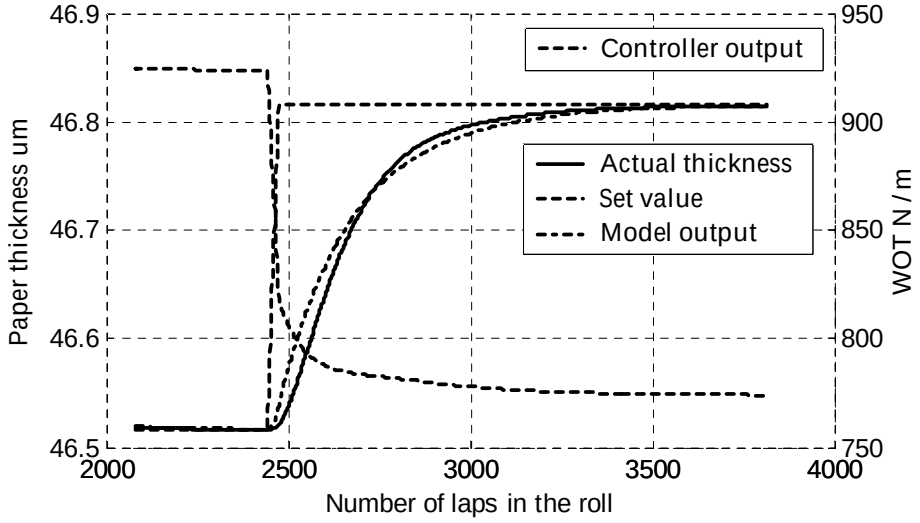

FIGURE 128 Step response of LQR tuned PI controller

The LQG design in the previous chapter was seen to be equal to a PI controller. The design can be simplified by omitting the state estimator, since both of the state variables can be measured. The resulting LQR controller is an alternate form for the PI controller. Another choice is to use the standard PI controller and set its parameters to $K=k_1$ and $Ti=k_1/k_2$ and $[k_1\ k_2]$ is the regulator gain

vector. The step response of the resulting PI controller is drawn in FIGURE 128. The difference to the LQG controller is very small as it should be.

7.5 Closed loop winding trials

The closed loop winding trials were run with the resilient winding drum, mostly with the LWC paper. The LWC paper is seen to be more difficult to control accurately due to its higher radial elastic modulus. The thickness measurement resolution is poorer and the relative calliper variation is greater than with the Newsprint paper. All the four controller types presented in the previous chapter, the PI controller tuned with pole placement, the LQG controllers tuned with the second and third order system models and the PI controller tuned with the LQR method were tested. The tuning parameter values were the same as in the simulations. The controllers had all three winding parameters, nip load, winding force and web tension available for the Wound On Tension control through the inverted nip model. The winding speed was 300 m / min in all trials, simply to make the monitoring of the runs easier. The control priority was that nip load would be changed first, winding force next and web tension only if the two others would be close to their limits. The winding parameter limits were set to 2000 and 10000 N / m for nip load, 200 and 1000 N / m for web tension and 0 to 625 N / m for surface traction. The friction limit for the surface traction was 0.2 x nip load. High values for the nip load were possible to use because of the properties of the resilient winding drum. The actual WOT was computed back from the winding parameters by means of the normal nip model.

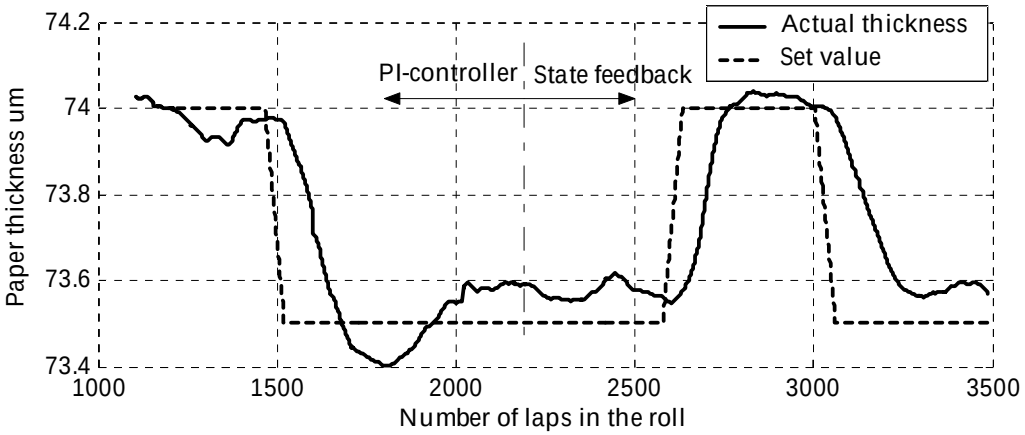

FIGURE 129 Closed loop Newsprint paper winding with PI and state feedback controllers

Handling of the initial transient is a difficult problem for winding controllers. Firstly the density measurement must itself settle to the correct thickness value. This transient can be prolonged due to bad diameter measurement values at winding start. Secondly the controller itself must be properly initialised to avoid excessive transient. Most importantly the integration memory must be set according to the manual mode WOT before the

controller is set to automatic mode. Also the state estimator must have passed its initial transient.

7.5.1 Newsprint paper trials

The Newsprint paper roll was run with both the PI controller that was tuned by pole placement and with the state feedback controller that was based on the first order system model. The controller type was changed on the fly in the middle of the run. The controller set value was kept constant except for few step changes of 0.5 μm during the winding.

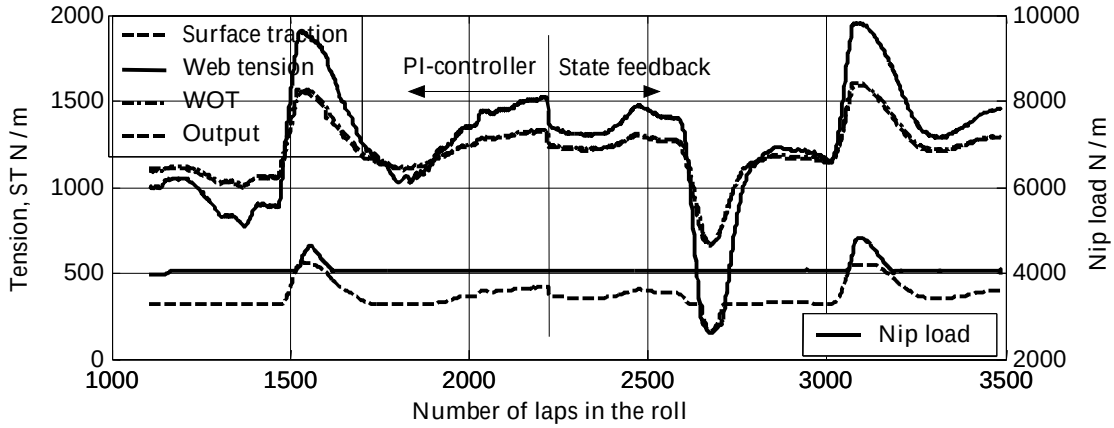

FIGURE 130 Controller output and the winding parameters in the trial of the previous picture.

The winding results in FIGURE 129 and in FIGURE 130 show that both controller types worked reasonably well. The error value varied in between +- 0.1 μm. The responses following the step changes in the set value were quite fast compared to the simulation results. The swings in the nip load due to these step changes were large, lowest nip load was about 3000 N/m and highest nearly 10000 N/m. The controllers needed to change the web tension only at the lowering step changes, and even then only 160-200 N/m above the normal 500 N/m level. Winding force changed also moderately. The highest WOT values were nearly 1600 N/m and the lowest less than 700 N/m. The controller output and the actual WOT are very close to each other, no controller saturation occurred and the winder followed the controller commands closely. The winder tension reference handling causes a small delay. Since the thickness reference value was constant and didn't account for the paper calliper variations, the controller output and error value variations were larger than would have been otherwise. There is no sign of controller induced oscillations in the web thickness, but the variations are caused by the changes in the web calliper.

7.5.2 LWC paper trials

The LWC paper roll available for the trials was much larger than the Newsprint roll, so longer runs made possible to try more versatile reference value curves.

The large calliper variations in the roll made it practically impossible to run with constant set value for the controller, so the calliper offset based reference value was used.

The PI controller performance is seen in FIGURE 131. The controller was tuned with pole placement as earlier. The reference value to the controller followed the measured paper calliper minus some offset. The offset was changed three times by 0.5 μm during winding. At the end of the winding the calliper measurement had ended and the winding continued with constant reference value. The controller performed very well and could easily keep the error value well under 50 nm (nanometers) except for the step transients.

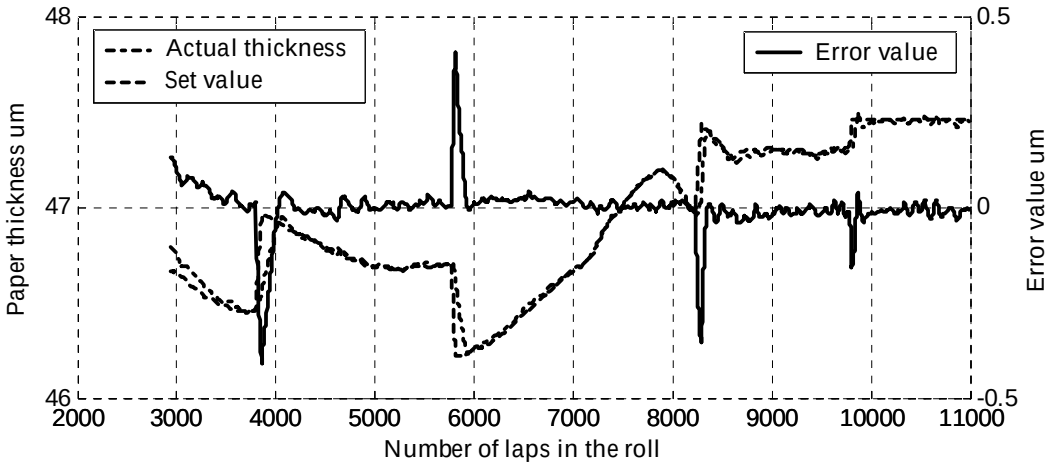

FIGURE 131 LWC paper closed loop winding with PI controller

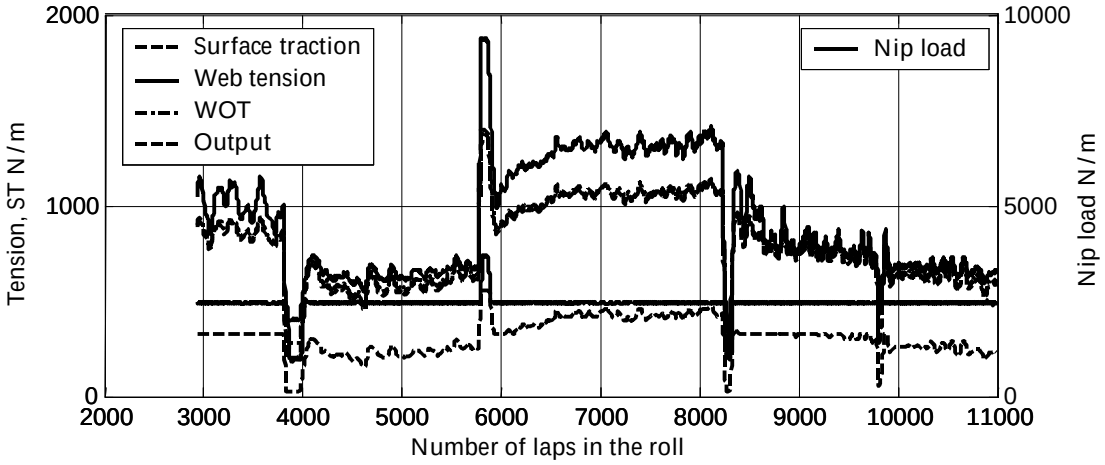

FIGURE 132 Controller output and the winding parameters in the trial of the previous picture.

The PI controller used the winding parameters much the same way as with the Newsprint paper, FIGURE 132. The controller output has hit the limits, 1400 N/m maximum and 200 N/m minimum, WOT values at the step transients. Also the winder didn t produce quite the maximum and minimum

WOT s due to its other limitations. There can be seen a drop of WOT at around 6000 laps just after the step change to tighter winding, which can be a proof that the nip makes tight winding after softer winding by itself.

The LQG controller s performance was not satisfactory when it was tuned to the second order system model, FIGURE 133. The tuning parameter q was decreased to 2, but still there were clear oscillations in the controller output. With even lower tuning values the controller became slow and didn t follow the reference value well. There was no evident reason found for this poorer performance especially when this controller tuning worked well in the simulations.

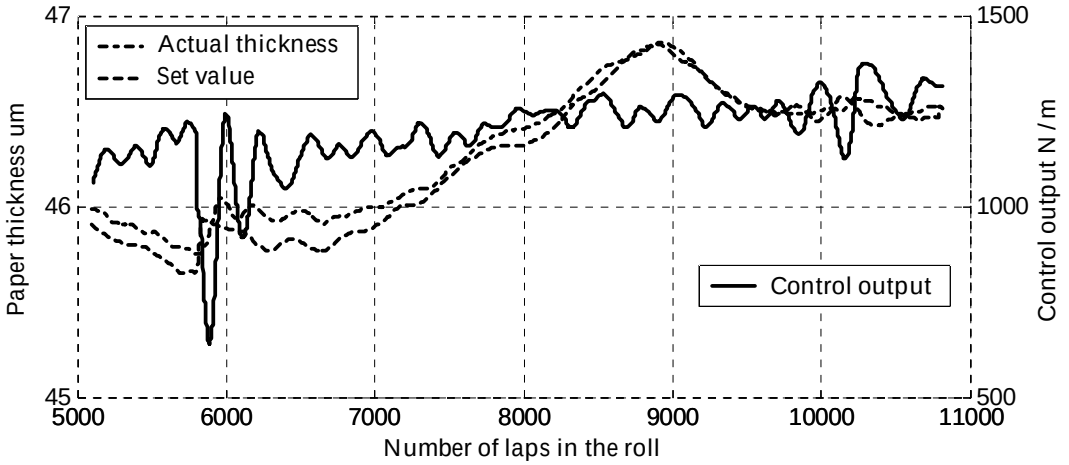

FIGURE 133 LQG controller performance tuned with the second order system model.

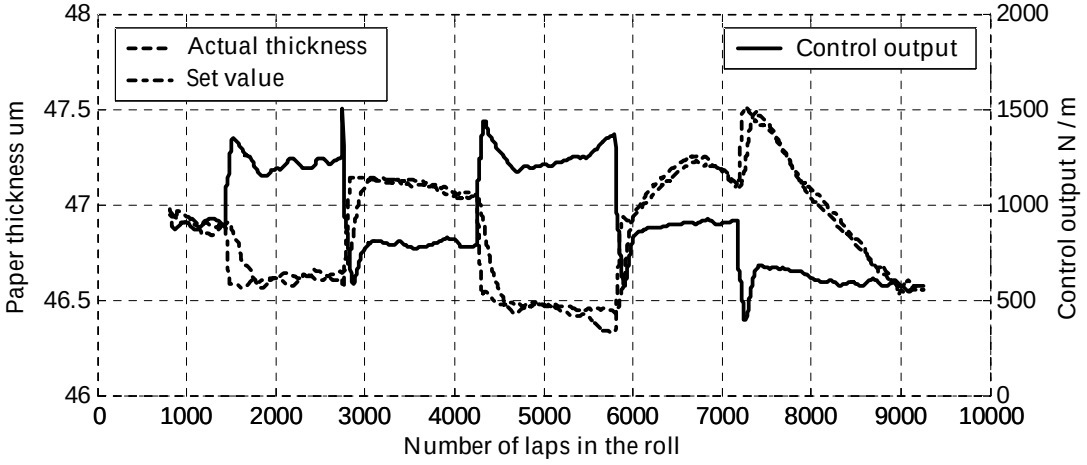

FIGURE 134 LQG controller performance tuned with the first order system model.

On the other hand the LQG controller that was tuned with the first order system model worked well, FIGURE 134. It was clearly slower than the PI controller with the tuning value q=5, as would be expected since the closed loop poles had larger absolute values.

The PI controller tuned with the LQR design worked similarly to the LQG controller that was tuned with the first order system model, a result that would be expected, since the two designs are equal except for the state estimator. The PI controller could be more robust due to the simpler structure. This time there were no step changes made on the set value, but the reference value was linearly modified so that the winding was 0.3 μm tighter in thickness at the beginning than at the 1200 mm roll diameter. The result is drawn in FIGURE 135 and in FIGURE 136. Now the controller lowered its output WOT from about 1000 N / m at the beginning to the 600 N / m in the end. To do this it didn t have to change the web tension at all and also the surface traction was changed moderately. The nip load was decreased from 6000 N / m down to 3000 N / m. The slower controller could keep the absolute error value under 0.1 μm and most of the time under 50 nanometers.

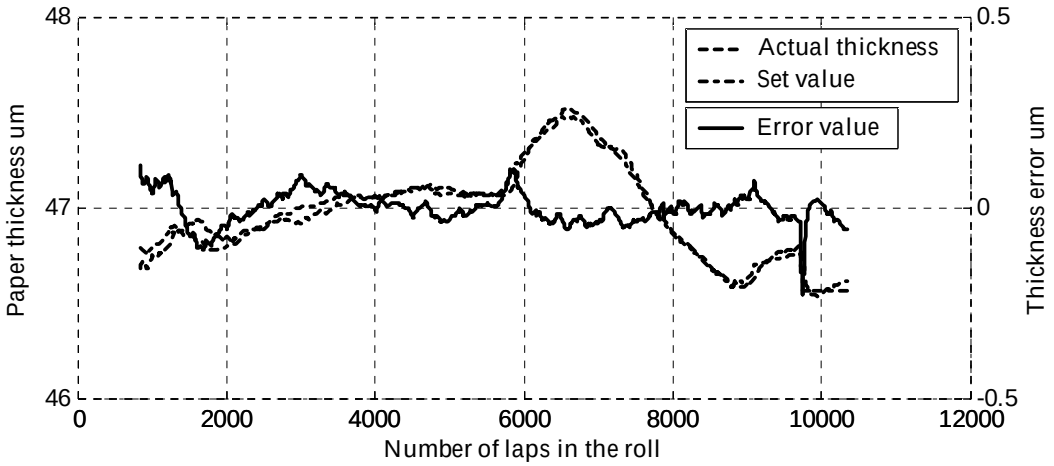

FIGURE 135 PI controller performance with LQR tuning

7.6 Discussion on the closed loop winding

The results in the previous chapters show that winding on measured thickness feedback is possible without causing severe problems on winder runnability or roll structure. The controller is possible to design and tune so that it handles the winder reference values smoothly and still can keep the desired paper thickness.

These results have been got on a single drum winder with roll support at the core. The limited possibility of controlling the nip loading at large roll diameters in two drum winders can make it impossible to wind closed loop. The closed loop winding would be the most exact way of winding. In multi station winders every roll would be wound exactly to the correct tightness. Even though the web calliper or tension would vary in the cross machine direction, the controllers would change the winder reference values to make every roll equally tight. This of course presumes accurate web calliper data to

be available at the winder, both in the cross and machine directions over the whole jumbo roll.

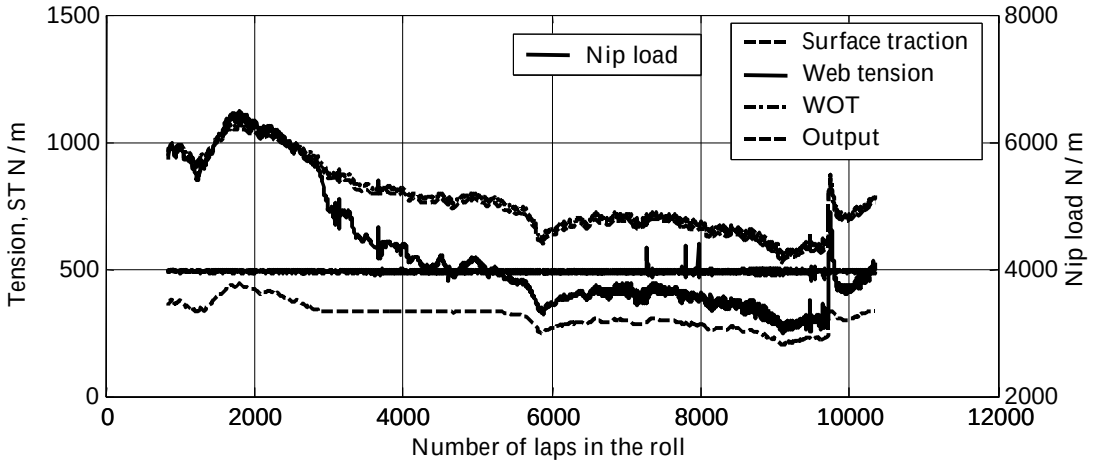

FIGURE 136 Controller output and the winding parameters in the trial of the previous picture.

The density measurement and the inverted nip model have proved their capabilities as components in the closed loop winding control. The accuracy and reliability of the density measurement is good even in following the fast step changes of the thickness reference in the trials. It can response within 250 wound laps to 0.5 μm thickness changes and keep the 95% confidence limit of the measurement within 5 to 10 nanometers. The control error is possible to keep under 50 nanometers, but if moderate winding parameter changes are desired, 0.1 μm control error has to be accepted. The accuracy of the inverted nip model and the web calliper measurement based on the wound roll stress model were also more than enough for the control purposes.

8 CONCLUSIONS

The vital parts of automatic winding tightness control are the inverted nip model and the density measurement. The web calliper measurement is also needed to be able to control the z-direction strain instead of sheer web thickness in the roll. At least the paper materials tested in the work had large calliper variations over the length of one roll. These calliper variations would make constant thickness control alone useless.

The experimental nip model could be based solely on the measured web thickness or strain data. The stresses need not to appear in the model. The winding control would then be roll deformation control without dealing with the web and roll stresses. Even though this would only be a partial view of winding, it would be a realistic one, since the density measurement is the only on-line roll tightness measurement proven to be accurate.

The radial direction web strain in the roll can be linked to the stresses by means of the z-direction stress-strain or elastic modulus curves measured in the stack testing machine on a paper sample. The radial interlayer stress so derived is an approximation of the true plateau area stress. It is not correct near the core or the roll surface. The radial modulus depends on the strain or stress for the nonlinearly elastic paper material, and is another indicator of roll tightness or hardness.

There exist a practical limitation in using the wound roll stress model in actual winding control. The experimental nip model, density measurement and the controller implementations are relatively simple programs with light CPU demand. They can be easily run in real time in the winder PLC or DCS control system. The wound roll stress model is a complicated program with heavy CPU load. However, the wound roll stress model is unavoidably needed to convert the measured web thickness to the Wound On Tension and the correct radial and tangential roll stresses. The web calliper measurement method presented in the thesis also depends on the wound roll stress model. And viscoelasticity and centrifugal forces can only be correctly handled by means of the wound roll stress model.

The Wound On Tension is a comprehensible roll tightness measure. It can be directly compared to the web tension and in nipless centrewinding the Wound On Tension equals the web tension. The standard Cameron gap test is directly linked to the Wound On Tension through the web tangential elastic modulus. The absolute upper limit of the Wound On Tension is the tensile strength of the web material. The Wound On Tension is also the input variable of the normal wound roll stress model, which together with the nip model comprises a winding simulation system.

It must be kept in mind that the density measurement is the original source of data and all other derived variables, Wound On Tension and the roll stresses, are got from the idealized models. The nip model assumes that all tension changes in the winding process occur in the winding nip and the outermost web layer. The material models have been obtained from small paper samples even though there is known elastic and thickness variations throughout the roll. Even the density measurement is based on an idealization that it measures the web thickness but in reality it measures the radial deformations. The wound roll stress model is a valuable aid in giving more insight how much these idealizations and deviations affect the measurement results. For example the model predicts the difference between the true web thickness in the roll and the thickness that can be measured by the density measurement.

This work is based on a more solid experimental ground than the earlier works (Roisum 1990) and (Good et al. 1999), since it combines two independent measurements, the density measurement and the radial stress measurement by means of the force sensitive resistors. The computed pressure can be validated with the directly measured pressure. The pressure measurement was shown to be more inaccurate and unreliable than the density measurement. Another improvement is the indirect web calliper measurement, which compensates not only the calliper variations within the roll but also the bulk loss from run to run.

The closed loop winding tightness control based on the density measurement and the inverted nip model was shown to be possible and even feasible for paper mill use. The method was validated with laboratory winder trials, but practical application requires separate web calliper measurement to be available. It is not clear whether the present commercial web calliper measurement systems are accurate enough for the winding control purpose. The inverted nip model was shown to be a useful tool in winding tuning and control even without closed loop control. And if the measured web calliper is available, the density measurement and the wound roll stress model will provide the Wound On Tension as the actual roll tightness measure.

REFERENCES

Austrel, P-E., 1997, "Modeling of Elasticity and Damping for Filled Elastomers", Doctoral Thesis, Lund University.

Benson, R. C. , December 1995, "A Nonlinear Wound Roll Model Allowing for Large Deformation", Journal of Applied Mechanics, Vol. 62, Transactions of the ASME, pp. 853-859.

Bindyck, R., Rubinfeld, D., "Econometric Models and Economic Forecasts"

Blaedel, K. L., 1974, "A Design Approach to Winding a Roll of Paper", Doctoral Thesis, University of Wisconsin-Madison.

Burns, S. J., Meehan, R. R., Lambropoulos, J. C., 1999, "Strain-based formulas for stresses in profiled center-wound rolls", Tappi Journal, Vol. 82: No 7, pp. 159-167.

Debesis, W., R., Burns, S., J., 2003, "Comparison of Stresses in Center-Wound Rolls from Two Linear Elastic Models", Journal of Applied Mechanics, Vol. 70.

Frye, K. G., 1989, "Runnability in the Pressroom", TAPPI Finishing and Converting Proceedings.

Fikes, M., W., R., 1990, "The Use of Force Sensing Resistors to Measure Radial Interlayer Pressures in Wound Rolls", M. S. Thesis, Oklahoma State University.

Good, J. K. and Pfeiffer, J. D., 1992, "Tension Losses during Centerwinding", TAPPI Finishing and Converting Conference.

Good, J. K. and Wu, Z., Dec. 1993, "The Mechanism of Nip-Induced Tension in Wound Rolls", J. Appl. Mech.-Trans. ASME, Vol. 60, pp. 942-947.

Good, J.,K., Hartwig, J. and Markum, R., 1999, "A Comparison of Center and Surface Winding using the Wound-In-Tension Method", Proceedings of the Fifth International Conference on Web Handling, Oklahoma.

Good, J.,K., 2001, "Modeling Nip Induced Tension in Wound Rolls", Proceedings of the Sixth International Conference on Web Handling, Oklahoma.

Güldenberg, B., 2000, “Einfluss der Nipinduzierten Effekte auf den Wickelprozess von Papier ”, Dissertation, Ruhr-Universitat Bochum.

Güldenberg, B., Welp, E., G., 2001, “Nipwirkung in Walzenwicklern – Experimentelle Beobachtung und theoretische Modellierung ”, Das Papier, No. 4, pp. 50-57.

Hakiel, Z., May 1987, “Nonlinear Model for Wound Roll Stresses ”, Tappi Journal, Vol. 70, No. 5, pp. 113-117.

Ilomäki, M., 2004, “Application of Fracture Mechanics in Analyzing Delamination of Cyclically Loaded Paperboard Core ”, Dissertation, University of Oulu.

Jorkama, M., von Hertzen, R., 1999, ”Contact Mechanical Approach to the Winding Nip ”, Proceedings of the Fifth International Conference on Web Handling, Oklahoma.

Jorkama, M., “Contact Mechanical Model for Winding Nip ”, 2001, Acta Polyt. Scan., Me 146, The Finnish Academies of Technology.

Jorkama, M., von Hertzen, R., 2001, ”Development of Web Tension in a Winding Nip ”, Proceedings of the Sixth International Conference on Web Handling, Oklahoma.

Jorkama, M., von Hertzen, R., 2002, ”The Mechanism of Nip-Induced Tension in Winding ”, Journal of Pulp and Paper Science, Vol. 28, No. 8, pp. 280-284.

Johansson, Rolf., 1993, “System Modelling and Identification ”, Prentice-Hall, Inc.

Lee, Y., M., Wickert, J., A., March 2002, “Stress Field in Finite Width Axisymmetric Wound Rolls ”, Transactions of the ASME, Vol. 69, pp. 130-138.

Lewis, F., L., Syrmos, V., L., 1995, “Optimal Control ”, John Wiley & Sons, Inc..

Li, S., Cao, J., 2001, “A Study on the Stress Distribution in Coil Wrapping and its Effect on Final Coil Deformation ”, Department of Mechanical Engineering, Northwestern University, Illinois.

Lif, J., 2003, “Analysis of the Time and Humidity-Dependent Mechanical Behaviour of Paper Webs at Offset Printing Press Conditions ”, Doctoral Thesis, Royal Institute of Technology, Stockholm.

Komulainen, P., 1982, "Roll Quality Measurement and Control", Paper Finishing and Converting Conference Proceedings, TAPPI PRESS, Atlanta, pp. 87-92.

Olsen, J. E., 1996, "Theoretical Analysis of Winding Mechanics", Doctoral Thesis, Norwegian Institute of Technology.

Persson, K., 1991, "Material model for paper, experimental and theoretical aspects", Diploma report, Lund Institute of Technology.

Pfeiffer, J., D., 1966, "Internal Pressures in a Wound Roll of Paper", TAPPI Journal, Vol. 49, No. 8, pp. 342-347.

Pfeiffer, J. D., Aug. 1968, "Mechanics of a Rolling Nip on Paper Webs", TAPPI Journal, Vol. 51, No. 8, pp. 77-85.

Pfeiffer, J. D., Feb. 1977, "Nip Forces and Their Effect on Wound-In Tension", TAPPI Journal, Vol. 60, No. 2, pp. 115-117.

Pfeiffer, J. D., March 1977, "Wound-off Tension Measurement in Paper Rolls", TAPPI Journal, Vol. 60, No. 3, pp. 106-108.

Pfeiffer, J., D., 1996, "Using Paper Compressibility Measurements to Enhance Roll Quality", TAPPI Finishing and Converting Conference.

Piper, 1995, "A Nonlinear Model to Calculate the Stressed State of a Center-Wound Roll, 3th International Web Handling Conference, Oklahoma State University.

Qualls, W. R., May 1995, "Hygrothermomechanical Characterization of Centerwound Rolls", Ph. D. Dissertation, Oklahoma State University.

Roisum, D., May 1990, "The Measurement of Web Stresses during Roll Winding", Doctoral Thesis, Oklahoma State University.

Willett, M. S., and Poesch, W. L., 1988, "Determining the Stress Distributions in Wound Reels of Magnetic Tape Using a Nonlinear Finite-Difference Approach", ASME Journal of Applied Mechanics, Vol. 55, pp. 365-371.

Åström, K., Hägglund, T., 1995, "PID Controllers, Theory, Design and Tuning", Instrument Society of America.

HELSINKI UNIVERSITY OF TECHNOLOGY CONTROL ENGINEERING LABORATORY

Editor: H. Koivo

Report 133 Hyötyniemi, H.
On the Universality and Undecidability in Dynamic Systems. December 2002.

Report 134 Elmusrati, M. S., Koivo, H. N.
Radio Resource Scheduling in Wireless Communication Systems. January 2003.

Report 135 Blomqvist, E.
Security in Sensor Networks. February 2003.

Report 136 Zenger, K.
Modelling, Analysis and Controller Design of Time-Variable Flow Processes. March 2003.

Report 137 Hasu, V.
Adaptive Beamforming and Power Control in Wireless Communication Systems. August 2003.

Report 138 Haavisto, O., Hyötyniemi, H.
Simulation Tool of a Biped Walking Robot Model. March 2004.

Report 139 Halmevaara, K., Hyötyniemi, H.
Process Performance Optimization Using Iterative Regression Tuning. April 2004.

Report 140 Viitamäki, P.
Hybrid Modeling of Paper Machine Grade Changes. May 2004.

Report 141 Pöyhönen, S.
Support Vector Machine Based Classification in Condition Monitoring of Induction Motors. June 2004.

Report 142 Elmusrati, M. S.
Radio Resource Scheduling and Smart Antennas in Cellular CDMA Communication Systems. August 2004.

Report 143 Tenno, A.
Modelling and Evaluation of Valve-Regulated Lead-Acid Batteries. September 2004.

Report 144 Hyötyniemi, H.
Hebbian Neuron Grids: System Theoretic Approach. September 2004.

Report 145 Hyötyniemi, H. (ed.)
Complex Systems: Science at the Edge of Chaos - Collected papers of the Spring 2003 postgraduate seminar. October 2004.

Report 146 Paanasalo, J.
Modelling and Control of Printing Paper Surface Winding. June 2005.

ISBN 951-22-7749-2

ISSN 0356-0872

Picaset Oy, Helsinki 2005